





This is to certify that the  
thesis entitled


UPPER PALEOZOIC STRATIGRAPHIC HISTORY AND  
PROVENANCE OF THE FAREWELL TERRANE, SW  
ALASKA

presented by

MATTHEW A. MALKOWSKI

has been accepted towards fulfillment  
of the requirements for the

M.S. degree in GEOLOGICAL SCIENCES

  
Major Professor's Signature

08/26/10

Date

*MSU is an Affirmative Action/Equal Opportunity Employer*

LIBRARY  
Michigan State  
University



**PLACE IN RETURN BOX** to remove this checkout from your record.  
**TO AVOID FINES** return on or before date due.  
**MAY BE RECALLED** with earlier due date if requested.

DATE DUE	DATE DUE	DATE DUE



UPPER PALEOZOIC STRATIGRAPHIC HISTORY AND PROVENANCE OF THE  
FAREWELL TERRANE, SW ALASKA

By

Matthew A. Malkowski

A THESIS

Submitted to  
Michigan State University  
in partial fulfillment of the requirements  
for the degree of

MASTER OF SCIENCE

Geological Sciences

2010



## ABSTRACT

### UPPER PALEOZOIC STRATIGRAPHIC HISTORY AND PROVENANCE OF THE FAREWELL TERRANE, SW ALASKA

By

Matthew A. Malkowski

The Farewell terrane, in southwest Alaska, is predominantly located in the western Alaska Range, but crops out as far north as the Kuskokwim Mountains and represents one of the largest exotic terranes in the North American Cordillera. Exposed both north and south of the Denali fault, the Farewell terrane contains three somewhat distinct stratigraphic successions: 1) Neoproterozoic–Devonian carbonate rocks of the Nixon Fork subterrane, 2) Cambrian–Devonian carbonate and siliciclastic strata of the Dillinger subterrane, and 3) Devonian–Jurassic(?) siliciclastic strata of the Mystic subterrane. This investigation aims to constrain the upper Paleozoic tectonic evolution of the Farewell terrane through sedimentologic interpretations and measured stratigraphy as well as by utilizing combined provenance techniques of sandstone modal compositions and U–Pb detrital zircon geochronology.

Measured stratigraphy and sedimentologic analyses of upper Paleozoic (Mississippian–Permian) siliciclastic strata from the Mystic subterrane suggest a submarine basin-floor turbidite fan depositional environment. Modal composition trends reveal pervasive occurrences of lithic volcanic and sedimentary grains reflecting contributions from a magmatic arc to a recycled orogen source. U-Pb detrital zircon age peaks from the newly defined Mystic Pass formation reveals four trends in age spectra: 2000–1800 Ma, 465–405 Ma, 365–315 Ma, and 305–290 Ma. These trends correlate with both Siberian and North American magmatic source areas.



## ACKNOWLEDGMENTS

I offer my sincerest gratitude to my advisor, Dr. Brian A. Hampton, whose guidance and support helped make all of this possible. I am also grateful to my other committee members for their time and effort in preparation of this manuscript and suggestions throughout this study. More specifically I express my appreciation to: Brian Hampton for providing me with the knowledge, resources, and liberty to develop as a geologist and researcher; Professor Kaz Fujita for his endless academic support, and willingness to help with all aspects related to my pursuit of a graduate degree; Dwight Bradley for his wealth of knowledge on the regional geology and generous logistical support for field work in Alaska; and Duncan Sibley for his guidance in helping me improve my ability to develop scientific ideas and think critically. I would also like to express my gratitude to Dan Bradley whose field assistance was an essential part of this project's success. I thank Julie Dumoulin, Robert Blodgett, Maurice Colpron, for helpful research discussions and George Gehrels, Alex Pullen, and Ian Drost for lab support.

Special thanks to the Geological Society of America, the American Association of Petroleum Geologists, Shell Oil Company, and Michigan State University for critical financial support, which allowed me to conduct field work and sample analyses as well as provide funding for travel to national meetings and conferences.

I am thankful to my friends and colleagues for their invaluable companionship including Bethany Sala, Brad Priebe, Larry Besaw, Ben Johnson, Phil Toutant, and Chad Babcock. Finally, I thank my parents for supporting my academic goals during my six years at Michigan State University.



## TABLE OF CONTENTS

LIST OF TABLES.....	v
LIST OF FIGURES.....	vi
CHAPTER 1: INTRODUCTION AND BACKGROUND.....	1
1.1 Introduction.....	1
1.2 Geologic Background.....	3
1.3 Previous Work.....	6
1.4 Research Questions.....	11
1.5 General Methods.....	13
1.6 Summary.....	15
1.7 References.....	17
CHAPTER 2: SEDIMENTOLOGY, STRATIGRAPHY, AND DEPOSITIONAL SETTING OF THE MYSTIC PASS FORMATION.....	20
2.1 Introduction.....	20
2.2 Stratigraphic Overview of the Mystic Subterrane.....	23
2.3 Mystic Pass Formation.....	28
2.4 Facies Associations.....	32
2.5 Depositional Setting.....	41
2.6 Discussion.....	43
2.7 Conclusions.....	45
2.8 References.....	47
CHAPTER 3: PROVENANCE OF THE MYSTIC PASS FORMATION.....	50
3.1 Introduction.....	50
3.2 Previous Work.....	53
3.3 Sandstone Petrography.....	53
3.4 U–Pb Detrital Zircon Analysis.....	61
3.5 Discussion.....	83
3.6 Conclusions.....	88
3.7 References.....	91
CHAPTER 4: CONCLUSIONS.....	99
APPENDICES	
A. Measured stratigraphic section of the Mystic Pass formation.....	102
B. Raw point-count data.....	117
C. Analytical results of U–Pb detrital zircon isotope ratios and age data.....	119
D. Mystic subterrane at Sheep Creek, eastern McGrath quadrangle.....	130
E. Analytical results of U–Pb detrital zircon data (Sheep Creek Fm.).....	136
F. Measured stratigraphic section of the Sheep Creek Fm.....	140

## LIST OF TABLES

Table 2.1	Summary of facies classifications and interpretations for the Mystic Pass formation.....	37
Table 2.2	Summary of descriptions and interpretations of facies associations for the Mystic Pass formation.....	38
Table 3.1	Summary of parameters for sandstone point counts.....	56
Table 3.2	Recalculated modal point-count percentage data for sandstone samples of the Mystic Pass formation.....	57
Table B1	Raw point-count data from sandstone of the Mystic Pass formation.....	118
Table C1	Analytical results of U-Pb detrital zircon isotope ratios and age data from the Mystic Pass formation.....	120
Table E1	Analytical results of U-Pb detrital zircon isotope ratios and age data from the Sheep Creek Formation.....	137

## LIST OF FIGURES

Figure 1.1	Generalized geologic map showing the regional area of interest and the distribution of exposed portions of the Farewell terrane.....	2
Figure 1.2	Three-part stratigraphy of the Farewell terrane.....	4
Figure 1.3	Generalized stratigraphic sections of the Farewell terrane from areas that contain correlative Mystic subterrane strata.....	7
Figure 1.4	Early Carboniferous paleogeographic reconstruction showing the distribution of major tectonic elements.....	8
Figure 1.5	Geologic map showing the field area (Mystic Pass) in the western Alaska Range.....	14
Figure 2.1	Generalized geologic map showing the regional area of interest and the distribution of exposed portions of the Farewell terrane.....	21
Figure 2.2	Three-part stratigraphy of the Farewell terrane.....	22
Figure 2.3	Generalized stratigraphic sections of the Farewell terrane from areas that contain correlative Mystic subterrane strata.....	24
Figure 2.4	Simplified stratigraphy of known units from Mystic subterrane exposures in the western Talkeetna Quadrangle, SW Alaska.....	26
Figure 2.5	Geologic map showing the field area (Mystic Pass) in the western Alaska Range.....	29
Figure 2.6	Measured stratigraphy of the Mystic Pass formation.....	30
Figure 2.7	Regional exposures of the Mystic Pass formation.....	31
Figure 2.8	Outcrop photos of the Mystic Pass formation I.....	33
Figure 2.9	Outcrop photos of the Mystic Pass formation II.....	34
Figure 2.10	Outcrop photos of the Mystic Pass formation III.....	35
Figure 2.11	Depositional setting for the Mystic Pass formation.....	42

Figure 3.1	Generalized geologic map showing the regional area of interest and the distribution of exposed portions of the Farewell terrane.....	52
Figure 3.2	Geologic map showing the field area (Mystic Pass) in the western Alaska Range.....	54
Figure 3.3	Sandstone petrography of the Mystic Pass formation.....	58
Figure 3.4	Average modal composition of all sandstone samples from the Mystic Pass formation.....	59
Figure 3.5	Sandstone modal compositions I.....	60
Figure 3.6	Sandstone modal compositions II.....	62
Figure 3.7	U–Pb Concordia diagrams of single detrital zircon grains from three samples of sandstone from the Mystic Pass formation.....	67
Figure 3.8	Detrital zircon age spectra from the Mystic Pass formation (this study).....	68
Figure 3.9	Normalized relative probability plots showing the distribution of detrital zircon ages from three sandstone samples of the Mystic Pass formation.....	69
Figure 3.10	Detrital zircon age spectra from previous work on Mystic subterranean strata.....	72
Figure 3.11	Summary of all detrital zircon ages from Mystic subterranean strata.....	73
Figure 3.12	Plot of U/Th versus age for all three detrital zircon samples from the Mystic Pass formation.....	74
Figure 3.13	Unrestored map showing the modern locations of relevant sources and tectonic elements discussed in the text.....	77
Figure 3.14	Summary of potential Phanerozoic source areas.....	80
Figure 3.15	Early Carboniferous paleogeographic reconstruction showing the distribution of major tectonic elements.....	90
Figure A1	Measured stratigraphic section of the Mystic Pass formation.....	103



Figure D1	Generalized geologic map showing the regional area of interest and the distribution of exposed portions of the Farewell terrane.....	133
Figure D2	Geologic map showing the field area (Sheep Creek) in the eastern McGrath quad.....	134
Figure D3	Detrital zircon age spectra from Mystic subterrane strata map unit (PDs) in the eastern McGrath quadrangle.....	135
Figure F1	Measured stratigraphic section of the Sheep Creek Formation.....	141

## **CHAPTER 1: INTRODUCTION AND BACKGROUND**

### **1.1 INTRODUCTION**

Nearly the entire western margin of North America, from Mexico to the North Slope of Alaska, represents a collisional zone comprised of fault-bounded geologic fragments with distinct geologic histories. These fragments are most commonly referred to as tectonostratigraphic terranes (Coney et al., 1980; Jones et al., 1982; Howell et al., 1985; Plafker and Berg, 1994; Dickinson, 2004). Although this margin has been heavily studied, the timing and nature in which each of these terranes has accreted as well as their tectonic evolution prior to accretion remains a subject of debate. Furthermore, the Mesozoic and Cenozoic accretionary history of southern Alaska has received a considerable amount of recent study (e.g. Trop and Ridgway, 2007; Perry et al., 2009; Hampton et al., 2010), however the Paleozoic is poorly constrained.

Southern Alaska is one of the more understudied portions of the Cordilleran accretionary margin as bedrock exposures are in remote areas and it is home to the highest topography in North America. Thus, several fundamental questions remain regarding the tectonic evolution of this region. And while it is widely accepted that many of the terranes that make up southern Alaska were in proximity to western North America by the mid-Mesozoic (Plafker and Berg, 1994; Dickinson, 2004; Trop and Ridgway, 2007), little is known about the pre-Mesozoic accretionary history of this margin. Such is the case for the Farewell terrane in south-central Alaska (Figure 1.1), which consists of Neoproterozoic to Jurassic-age rocks including a thick (~3-4 km) succession of upper Paleozoic siliciclastic strata. These strata have been interpreted to include foreland

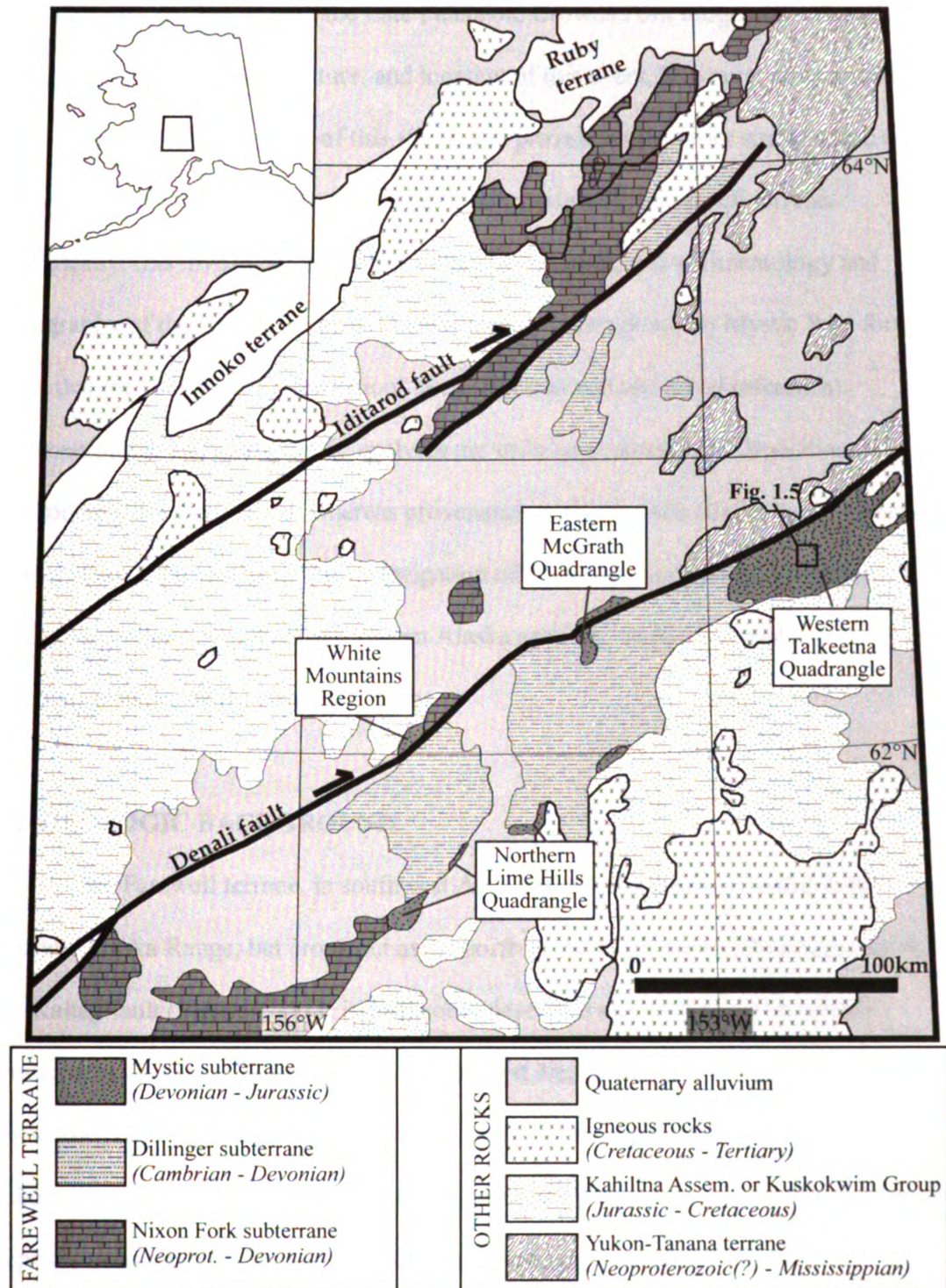


**Figure 1.1.** Generalized geologic map showing the regional area of interest and the distribution of exposed portions of the Farewell terrane. The majority of Farewell exposures are in the Alaska Range south of the Denali fault, but crop out as far North as the Kuskokwim Mountains north of the Iditarod fault. Note the small box in the western Talkeetna quad. shows the field area in Figure 1.5. Modified from Bradley et al., 2003.

basin deposits associated with the Late Paleozoic Browns Fork orogen (Bradley et al., 2003). The precise timing, nature, and location of this event, however, remain unknown.

The primary objective of this study is to provide a first-order stratigraphic and provenance constraint for Paleozoic siliciclastic strata of the Farewell terrane. Specifically, this investigation focuses on the provenance, and sedimentology and stratigraphy of the upper Paleozoic (Mississippian–Pennsylvanian) Mystic Pass formation (note that the “Mystic Pass formation” is an informal and unofficial reference). Sedimentologic and stratigraphic analyses are utilized to constrain a depositional environment for these strata, whereas provenance analyses were conducted to determine source areas. The results of this investigation offer initial constraint on the upper Paleozoic tectonic evolution of southern Alaska and bear on pre-accretionary paleogeographies of the Farewell terrane.

## **1.2 GEOLOGIC BACKGROUND**

The Farewell terrane, in southwest Alaska, is predominantly located in the western Alaska Range, but crops out as far north as the Kuskokwim Mountains, south of the Kaltag fault (Figure 1.1). It is commonly described as containing a three-part stratigraphy (Figure 1.2) that consists of: 1) latest Neoproterozoic through lower Paleozoic (Devonian) shallow-marine, mainly carbonate strata of the Nixon Fork subterrane, 2) lower Paleozoic (Cambrian–Devonian) interbedded submarine fan turbidite deposits and carbonate units of the Dillinger subterrane, and 3) upper Paleozoic (Devonian–Permian) to lower Mesozoic (Jurassic) siliciclastic strata of the Mystic subterrane. Alternatively, Decker et al., 1994 described the Nixon Fork and Dillinger



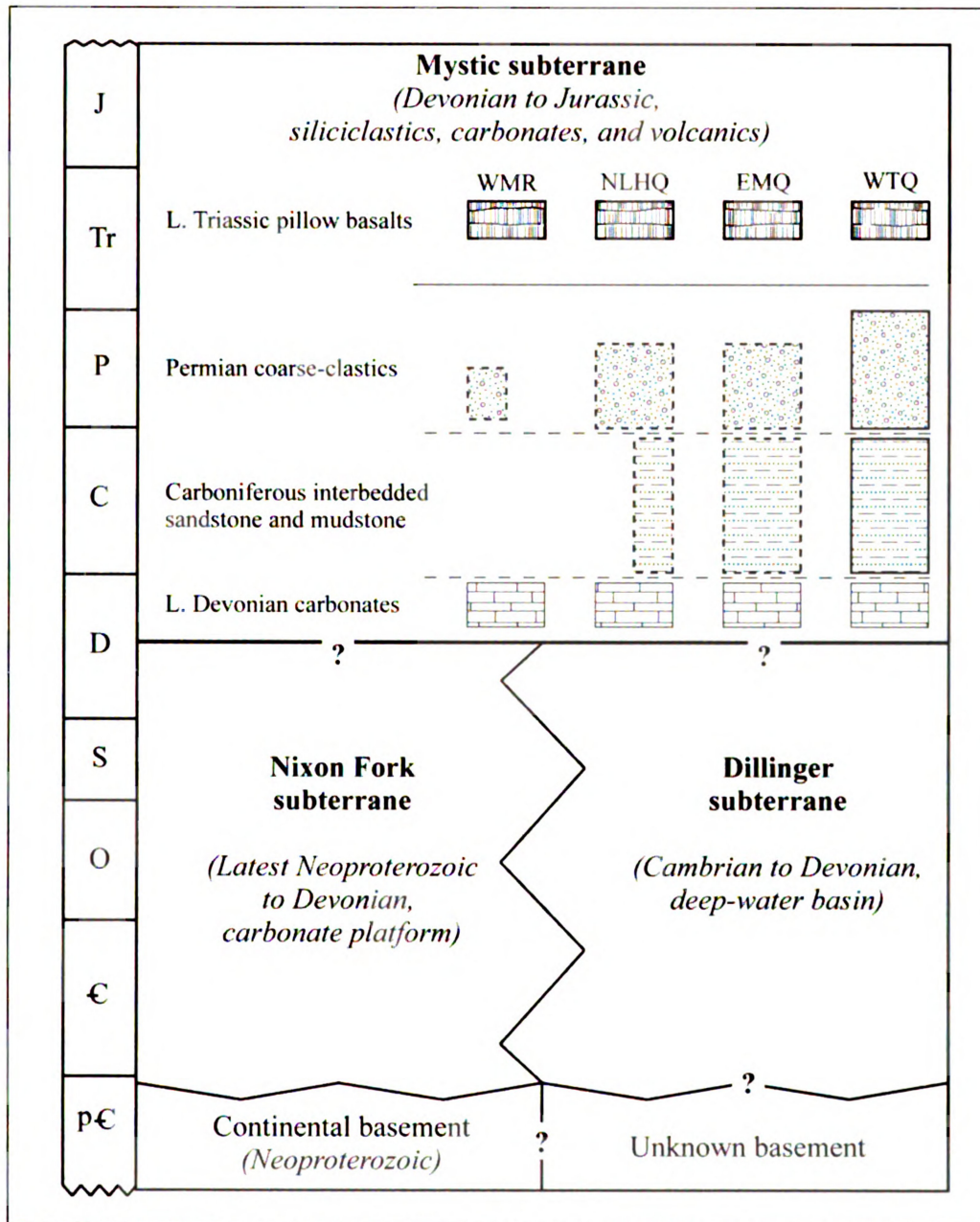


**Figure 1.2.** Three-part stratigraphy of the Farewell terrane. Simplified overview of the schematic relationships between different lithologies and components of the Farewell terrane. Dotted lines surrounding stratigraphic units indicate poorly documented thickness and lateral extents. Contacts between each unit are unknown. WMR- White Mountains Region, NLHQ- northern Lime Hills quadrangle, EMQ- eastern McGrath quadrangle, WTQ- western Talkeetna quadrangle.

subterrane as being lateral facies variations and referred to them together as the White Mountains sequence, and the Mystic subterrane is described as the Mystic sequence. Although these two nomenclatures are not mutually exclusive, the remainder of this paper will follow the subterrane nomenclature described by the former. This investigation focuses on the mid to upper Paleozoic siliciclastic strata exposed in the Mystic subterrane (Figure 1.1 and 1.2).

The Mystic subterrane contains a range of lithologies, but most notably includes two siliciclastic units whose stratigraphic relationship has not been confirmed. The first is a >1500-m-thick Permian-aged succession of sandstone, conglomerate, and fossil-leaf bearing siltstone collectively referred to as the Mt. Dall conglomerate, which outcrops as a broad syncline in the Mt. Dall region. The second is a structurally imbricated succession of Mississippian–Pennsylvanian siliciclastic strata (herein unofficially referred to as the Mystic Pass formation), and is the most extensive unit mapped within the Mystic subterrane. These strata are described as a thick, structurally deformed flysch-like sequence containing thick lenses of pebble- to cobble-conglomerate with clasts of limestone and black cherty argillite (Reed and Nelson, 1980). Given their chronologic and lithologic associations, it is likely that these units are closely related and may represent temporal variations of the same (foreland?) basin (Bradley et al., 2003). However, the structural disparities between the broadly folded Mt. Dall conglomerate and the isoclinally folded Mystic Pass formation complicate the nature of their relationship. The focus of this study is on the upper Paleozoic siliciclastic strata of the Mystic Pass formation. While these strata have received some previous work in the form of regional mapping, general lithologic descriptions, and isolated geochronology (Reed and Nelson,

1980; Jones et al., 1983; Bradley et al., 2007) this is the first investigation aimed at integrating the sedimentology, stratigraphy, and provenance of the Mystic Pass formation.

These upper Paleozoic siliciclastic strata of the Mystic subterrane are most widespread in the western Alaska Range (Talkeetna quadrangle) south of the Denali Fault (Figure 1.3), but potentially correlative rocks are also sporadically mapped in other regions of southwest and central Alaska. These exposures include the Farewell-Sheep Creek region (eastern McGrath quadrangle), White Mountains (western McGrath quadrangle), and four additional mapped exposures in the Lime Hills quadrangle (Figure 1.1). Although these units are all mapped as potentially belonging to the Mystic subterrane, stratigraphic differences are noted in the White Mountains region and the western Lime Hills quadrangle (Figure 1.3).

### **1.3 PREVIOUS WORK**

With the exception of several regional mapping projects and isolated studies (Reed and Nelson, 1980; Bundtzen et al., 1997; Bradley et al., 2003 and 2007; Sunderlin 2008), very little previous work has been carried out which focuses on the stratigraphic history and provenance of the Farewell terrane. Based on findings from previous studies, three models have been proposed to explain the stratigraphic history and/or tectonic evolution of the Farewell terrane and its relationship with the North American Cordillera. As reference for the following models, refer to Figure 1.4 for a paleographic reconstruction of where primary tectonic elements were located during the mid Paleozoic (Early Carboniferous).

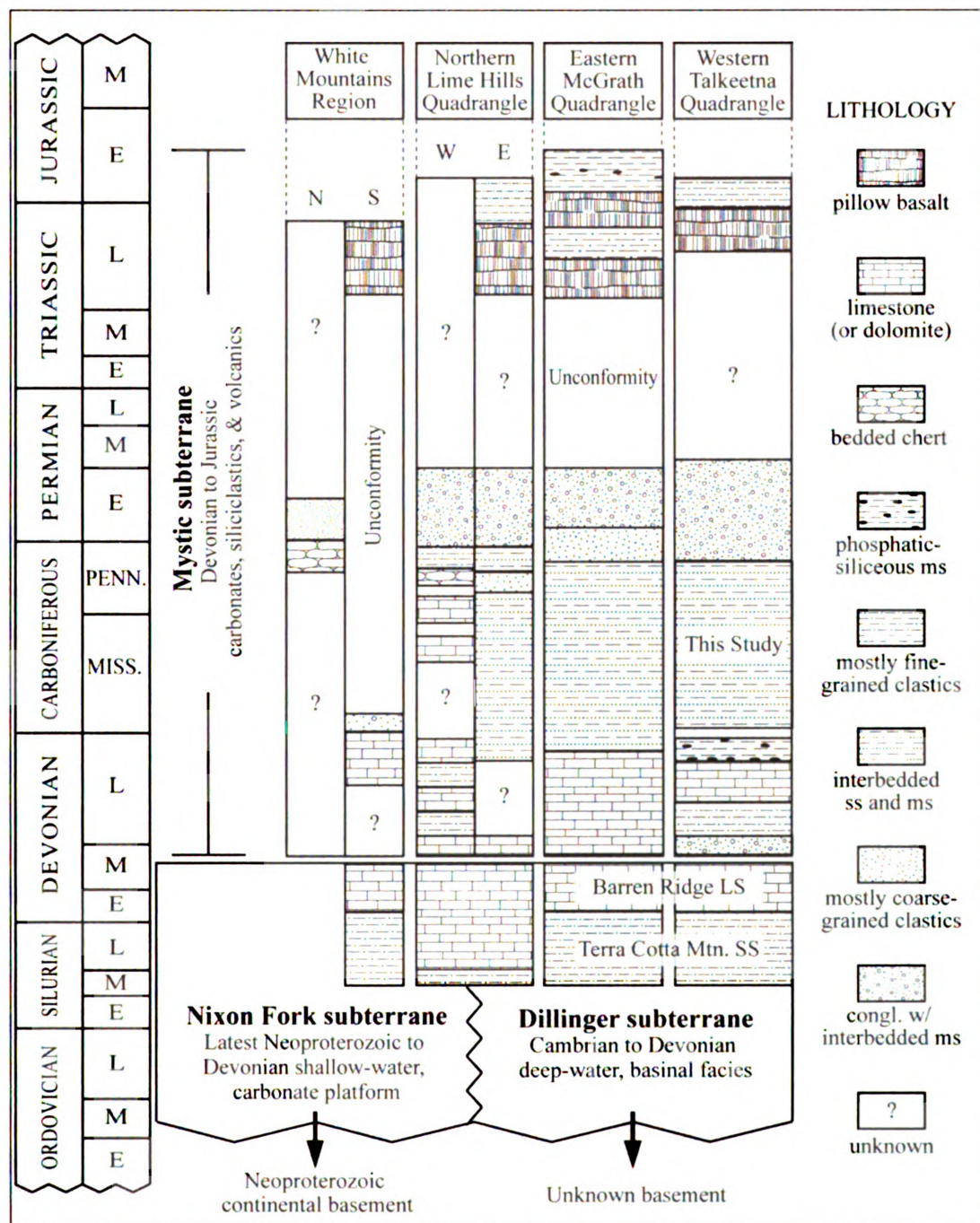


**Figure 1.3.** Generalized stratigraphic sections of the Farewell terrane from areas that contain correlative Mystic subterrane strata. Exact ages and stratigraphic thicknesses are not precise as age control is sparse for a majority of the documented strata. Also, the nature of the contact between Mystic subterrane strata and the underlying Nixon Fork and Dillinger subterrane has been documented as both stratigraphic and unconformable. Due to the lack of age constraint and field work in these areas, there are several unknown time gaps they may or may not be represented in different regions of the Farewell terrane. See Figure 1.1 for locations of documented stratigraphy.





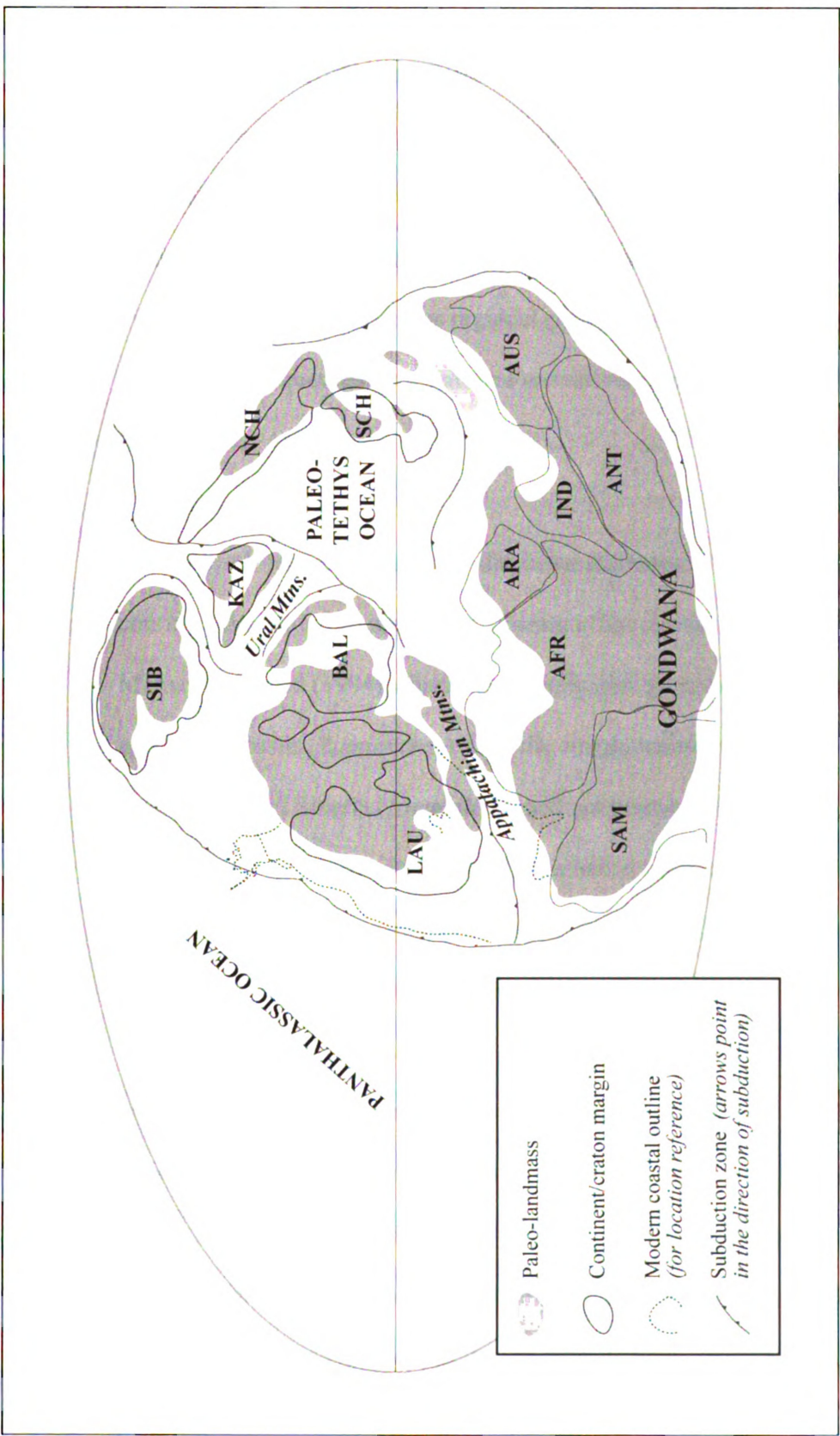


**Figure 1.4.** Early Carboniferous paleogeographic reconstruction showing the distribution of major tectonic elements. This sets the stage for upper Paleozoic events associated with Farewell terrane. AFR-Africa, ANT-Anarctica, ARA-Arabia, AUS-Australia, BAL-Baltica, IND-India, KAZ-Kazakhstan, LAU-Laurentia, NCH-North China, SAM-South America, SCH-South China, SIB-Siberia. Modified from Scotese (2002).

1. The Farewell terrane represents a displaced fragment of the Paleozoic continental margin of North America (Jones et al., 1982; Decker et al., 1994). This suggests that upper Paleozoic siliciclastic strata present within the Farewell terrane would be a result of exhumation and deposition that occurred in proximity to the North American margin. Decker et al. (1994) highlight the evidence for this hypothesis as regional correlations in unconformity ages and stratigraphic sequences between the Farewell terrane and northern Alaska and the Canadian Arctic.
  
2. The Farewell terrane represents a displaced fragment of the Siberian continental margin. Evidence for Siberian affinities was first proposed by Mamay and Reed (1984) where they highlighted the presence of Permian-aged plant fossils (*Zamiopteris*) from the conglomerate of Mt. Dall, which are characteristic of Siberia (Angaraland) and not known to exist in North America. However, Sunderlin (2008) conducted further investigations on plant fossils from the conglomerate of Mt. Dall and concluded an overall mixed Siberian and Laurentian floral affinity. Paleontological studies by Blodgett et al. (2002) argue that several of the accreted Alaska terranes, including the Farewell terrane of southwest Alaska, the Arctic Alaska terrane of northern Alaska, the York terrane of northwest Alaska, the Livengood terrane of east-central Alaska, and Alexander terrane of southeast Alaska are rifted fragments of the Siberian platform. This work also suggests that these Alaskan terranes, as well as Baltica and Siberia, were all in close proximity

from Cambrian to Devonian time due to similar faunal affinities. Aside from the Siberian-aspect flora in the Mt. Dall conglomerate, there is little to no data available to test the hypothesis of a link between the Farewell terrane and Siberia during the upper Paleozoic (Mississippian–Permian).

3. The lower Paleozoic portion (Nixon Fork and Dillinger subterrane) of the Farewell represents a displaced fragment of a larger continental body (i.e., the Arctic Alaska–Chukotka Microplate) (Miller et al., 2006; Amato et al., 2009), and the upper Paleozoic portion (Mystic subterrane) are a result of exhumation and deposition that occurred proximal to Siberia. Dumoulin et al. (2002) demonstrate the occurrence of stratigraphic and faunal similarities between the lower Paleozoic carbonate units of the Farewell terrane and age-equivalent carbonate strata in the Brooks Range of northern Alaska, which diminish after Middle Devonian time. These findings suggest that during the early Paleozoic (Cambrian–Devonian) the Farewell terrane was in close proximity to Arctic Alaska and was likely part of a larger crustal platform fragment. Furthermore, Bradley et al. (2003) propose a previously unrecognized late Paleozoic orogeny (the Browns Fork Orogeny) associated with the Farewell terrane as part of a larger plate convergence zone from the Urals to an unspecified offshore region of the North American Cordillera.

In addition to the studies mentioned above, Bradley et al. (2007) conducted U-Pb detrital zircon geochronologic analyses on three samples from the Mystic subterrane, and

suggests that these data are consistent with the Farewell-Siberia connection suggested by previous studies (e.g., Blodgett et al., 2002; Dumoulin et al., 2002).

#### **1.4 RESEARCH QUESTIONS**

The purpose of this project is to provide the first detailed understanding of upper Paleozoic stratigraphy and provenance of the Mystic Pass formation from the Farewell terrane. This is needed to explain the timing, source, and nature of exhumation and sedimentation of thick successions of upper Paleozoic siliciclastic strata of the Mystic subterrane and thus constrain the upper Paleozoic tectonic history of the Farewell terrane. In doing so, this investigation aims to provide a first-order test of the following models/hypotheses:

1. Upper Paleozoic siliciclastic strata of the Mystic subterrane represent exhumation and sedimentation associated with tectonic interaction between the Farewell terrane (Nixon Fork and Dillinger subterrane) and the North American margin. This model is similar to that proposed by Jones et al. (1982), in that it would suggest the Farewell was in close proximity to North America during the upper Paleozoic. Modal compositions for this hypothesis would likely show a component of continental block detritus, but could also include magmatic arc and recycled orogen signatures as these elements are common along the edges of continents; however detrital grain ages would ideally match magmatic source ages from the North American margin and Laurentian craton.



2. Late Paleozoic siliciclastic strata of the Mystic subterrane represent exhumation and sedimentation associated with tectonic interactions involving an extension of the Uralian orogeny (as proposed by Bradley et al., 2003), the Siberian craton, or Baltica. This hypothesis would also help to explain the presence of Siberian-aspect fossils within these strata. This model could result in a range of modal compositions, which could include both cratonal sources and arc-derived detritus that has resulted from orogenesis.
  
3. Late Paleozoic siliciclastic strata of the Mystic subterrane represent exhumation and sedimentation associated with inter-oceanic tectonic development which could include arc-continent, arc-arc, or continent-continent interactions with the Farewell terrane and another regional terrane (i.e. the Alexander terrane) or island arc system. Provenance data supporting this model could include arc-related modal compositions and detrital zircon ages which match magmatic ages from other age-constrained Paleozoic terranes. Although this idea has not been clearly proposed in previous literature, it is feasible given that there are several other Paleozoic terranes (Arctic Alaska, Alexander, and York) described as being regionally proximal to the Farewell terrane (Blodgett et al., 2002; Dumoulin et al., 2002; Colpron and Nelson, 2009).

Most importantly, this investigation contributes new chronologic, stratigraphic, and provenance data from the Farewell terrane, which provides constraint on the upper Paleozoic tectonic development of this region.

## **1.5 GENERAL METHODS**

The Mystic subterrane is the ideal study location for addressing the research questions and hypotheses outlined above in that it contains abundant exposures of mid- to upper- Paleozoic siliciclastic sediments in southern Alaska. The fieldwork portion of this study consisted of geologic mapping, measuring stratigraphic sections, and sample collection of sandstone for petrographic and geochronologic analyses from the Mystic Pass formation at Mystic Pass in the western Talkeetna quadrangle in south-central Alaska (Figure 1.5). Documenting the sedimentology and stratigraphy of these areas provides a basis for evaluating depositional environments, basin setting, and tectonic history of the Mystic subterrane. This study presents measured stratigraphic section and sedimentary facies and architectural analyses to assess up-section (temporal) progressions in sedimentation and interpreting depositional process for constraining a depositional model for the Mystic Pass formation. This is discussed in Chapter 2.

A provenance analysis is used to determine the detrital source for strata of the Mystic Pass formation thus providing insight into what was being exhumed in proximity to the Farewell terrane during the upper Paleozoic. Sandstone modal compositions will provide a first-order constraint to the nature of the source rocks in the provenance terrane from which sandy detritus was derived (Dickinson et al., 1983). More specifically, this approach can help narrow down whether the Farewell terrane was in proximity to an

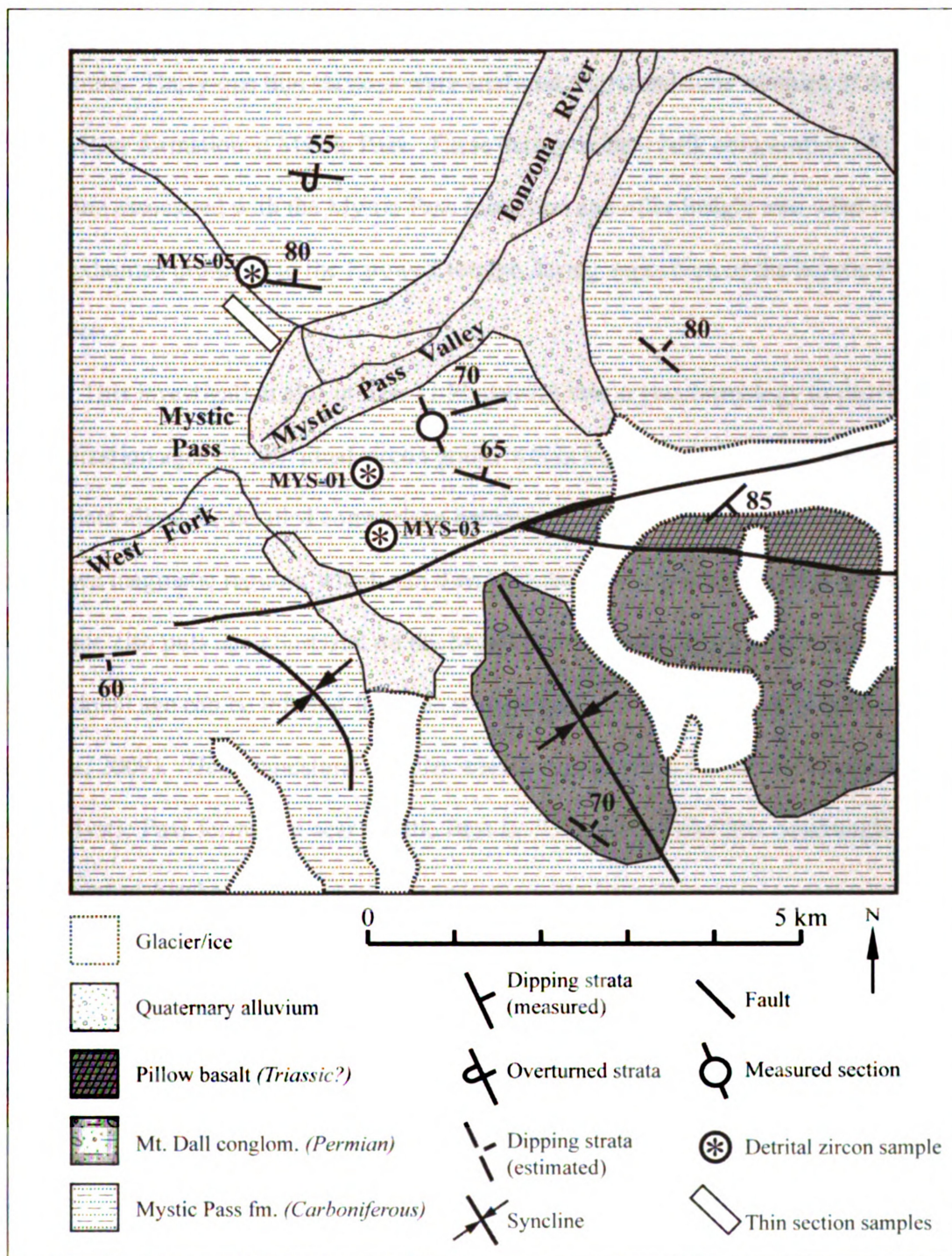


**Figure 1.5.** Geologic map showing the field area (Mystic Pass) in the western Alaska Range. This study is focused on the most prevalent map unit shown here, the Mystic Pass formation. Most thin section samples were collected where the white box is located with additional samples from detrital zircon and measured section localities. Circled asterisks show the general locations of where detrital zircon samples were collected along with their abbreviated sample name. Modified from Reed and Nelson, 1980.

island arc or a continental margin, for example, during the late Paleozoic development of these strata. Thirty-one thin sections were analyzed from sandstone samples of the Mystic Pass formation at Mystic Pass. These data provide a bulk composition of sandstone associated with the Mystic Pass formation and offer insight into what was being exhumed proximal to the Farewell terrane during deposition of the Mystic Pass formation.

This investigation also utilizes U-Pb detrital zircon geochronology to provide the crystallization ages of individual zircon grains within the siliciclastic units of study. These data allow for detailed comparison between the ages of detrital grains and the ages of known magmatic regions, which can then be evaluated as potential source areas. This technique also puts age-constraint on the Mystic Pass formation as a maximum depositional age can be inferred from the youngest grains in each sample (Dickinson and Gehrels, 2009). Three sandstone samples were collected for U-Pb detrital zircon analysis from Mystic Pass formation near Mystic Pass in the western Talkeetna quadrangle of south-central Alaska.

## **1.6 SUMMARY**

The following chapters discuss the stratigraphic history and provenance from the upper Paleozoic Mystic Pass formation of the Farewell terrane. Chapter 2 includes a stratigraphic overview of the Mystic subterrane as well as new sedimentologic and stratigraphic analyses of measured stratigraphy from the Mystic Pass formation. Chapter 3 focuses on the provenance of these strata and presents new data on modal compositions and U-Pb detrital zircon geochronology of the Mystic Pass formation. Together, these

data sets represent the first comprehensive analysis of sedimentology, stratigraphy, and provenance from the Mystic subterrane and provide first-order constraint on the tectonic evolution of Farewell terrane. Conclusions from this work are presented in Chapter 4.

## 1.7 REFERENCES

- Amato, J.M., Toro, J., Miller, E.L., Gehrels, G.E., Farmer, G.L., Gottlieb, E.S., Till, A.B., 2009, Late Proterozoic–Paleozoic evolution of the Arctic Alaska–Chukotka terrane based on U–Pb igneous and detrital zircon ages: Implications for Neoproterozoic paleogeographic reconstructions: *Geological Society of America Bulletin*, v. 121, p. 1219–1235, doi: 10.1130/B26510.1.
- Blodgett, R.B., Rohr, D.M., Boucot, A.J., 2002, Paleozoic links among some Alaskan accreted terranes and Siberia based on megafossils, *in* Miller, E.L., Grantz, A., and Klemperer, S.L., eds., *Tectonic evolution of the Bering Shelf–Chukchi Sea–Arctic Margin and adjacent landmasses*: Geological Society of America Special Paper 360, p. 273–280.
- Bradley, D.C., McClelland, W.C., Wooden, J.L., Till, A.B., Roeske, S.M., Miller, M.L., Karl, S.M., and Abbott, J.G., 2007, Detrital zircon geochronology of some Neoproterozoic to Triassic rocks in interior Alaska, *in* Ridgway, K.D., Trop, J.M., Glen, J.M.G., and O’Neill, J.M., eds., *Tectonic Growth of a Collisional Continental Margin: Crustal Evolution of Southern Alaska*: Geological Society of America Special Paper 431, doi: 10.1130/2007.2431(13).
- Bradley, D.C., Dumoulin, J., Layer, P., Sunderlin, D., Roeske, S., McClelland, W.C., Harris, A.G., Abbott, G., Bundtzen, T.K., and Kusky, T., 2003, Late Paleozoic orogeny in Alaska’s Farewell Terrane: *Tectonophysics*, v. 372, p. 23–40, doi: 10.1016/S0040-1951(03)00238-5.
- Bundtzen, T.K., Harris, E.E., Gilbert, W.G., 1997. Geologic map of the eastern half of the McGrath quadrangle, Alaska. Alaska Division of Geological and Geophysical Surveys Report of Investigations 97-14a, 38 pp., scale 1:125,000.
- Colpron, M., and Nelson, J.L., 2009, A Palaeozoic Northwest Passage: incursion of Caledonian, Baltican and Siberian terranes into eastern Panthalassa, and the early evolution of the North American Cordillera, *in* Cawood, P.A., and Kroner, A., eds., *Earth Accretionary Systems in Space and Time*. The Geological Society, London, Special Publications, 318, 273–307. doi: 10.1144/SP318.10.
- Coney, P.J., Jones, D.L., and Monger, J.W.H., 1980, Cordilleran suspect terranes: *Nature* 288, 320–33.
- Decker, J., Bergman, S.C., Blodgett, R.B., Box, S.E., Bundtzen, T.K., Clough, J.G., Coonrad, W.L., Gilbert, W.G., Miller, M.L., Murphy, J.M., Robinson, M.S., and Wallace, W.K., 1994, Geology of southwestern Alaska, *in*, Plafker, G., and Berg, H.C., eds., *The Geology of Alaska: Boulder, Colorado*, Geological Society of America, *Geology of North America*, v. G-1, p. 285–310.

- Dickinson, W.R., 2004, Evolution of the North American Cordillera, *Annual Review of Earth and Planetary Sciences*, vol. 32, pp.13–45.
- Dickinson, W.R., and Gehrels, G.E., 2009, Use of U–Pb ages of detrital zircons to infer maximum depositional ages of strata: A test against a Colorado Plateau Mesozoic database, *Earth and Planetary Science Letters* vol. 288, p. 115–125.
- Dumoulin, J.A., Harris, A.G., Gagiev, M., Bradley, D.C., and Repetski, J.E., 2002, Lithostratigraphic, conodont, and other faunal links between lower Paleozoic strata in northern and central Alaska and northeastern Russia, *in* Miller, E.L., Grantz, A., and Klemperer, S.L., eds., *Tectonic evolution of the Bering Shelf–Chukchi Sea–Arctic Margin and adjacent landmasses: Geological Society of America Special Paper 360*, p. 291–312.
- Hampton, B.A., Ridgway, K.D., and Gehrels, G.E., 2010, A detrital record of Mesozoic island arc accretion and exhumation in the North American Cordillera: U–Pb geochronology of the Kahiltna basin, southern Alaska: *Tectonics*, v. 29, doi: 10.1029/2009TC002544
- Howell, D.G., Jones, D.L., and Schrmer, E. R., 1985, Tectonostratigraphic terranes of the circum-Pacific region, *in* Howell, D. G., ed., *Tectonostratigraphic terranes of the circum-Pacific region: Circum-Pacific Council for Energy and Mineral Resources Earth Science Series*, no. 1, p. 3–30.
- Jones, D.L., and Silberling, N.J., 1979, Mesozoic stratigraphy; The key to tectonic analysis of southern and central Alaska: U.S. Geological Survey Open-File Report 79-1200, 41 p.
- Jones, D., Siberling, N.J., Gilbert, W.G., Coney, P.J., 1982, Character, distribution, and tectonic significance of accretionary terranes in the central Alaska Range, *Journal of Geophysical Research*, v. 87, p. 3709–3717.
- Mamay, S.H., and Reed, B.L., 1984, Permian plant megafossils from the conglomerate of Mount Dall, central Alaska Range, *in* Coonrad, W.L., and Elliott, R.L., eds., *The United States Geological Survey: Accomplishments during 1981: U.S. Geological Survey Circular 868*, p. 98–102.
- Miller, E.L., Toro, J., Gehrels, G., Amato, J.M., Prokopiev, A., Tuchkova, M.I., Vyacheslav, V.A., Dumitru, T.A., Moore, T.E., Cecile, M.P., 2006, New insights into Arctic paleogeography and tectonics from U–Pb detrital zircon geochronology: *Tectonics*, v. 25, TC3013, doi: 10.1029/2005TC001830.
- Perry, S.E., Garver, J.I., and Ridgway, K.D., 2009, Transport of the Yakutat terrane, southern Alaska: Evidence from sediment petrology and detrital zircon fission-track and U/Pb double dating: *Journal of Geology*, v. 117, p. 156–173.



- Plafker, G., and Berg, H.C., 1994, Overview of the geology and tectonic evolution of Alaska, *in* Plafker, G., and Berg, H.C., eds., The Geology of Alaska: Boulder, Colorado, Geological Society of America, Geology of North America, v. G-1, p. 989-1021.
- Reed, B.L., Nelson, S.W., 1980. Geologic map of the Talkeetna quadrangle, Alaska. U.S. Geological Survey Map I-1174, 15 p., scale 1:250,000.
- Ridgway, K.D., Trop, J.M., Nokleberg, W.J., Davidson, C.M., and Eastham, K.R., 2002, Mesozoic and Cenozoic tectonics of the eastern and central Alaska Range: Progressive basin development and deformation in a suture zone: Geological Society of America Bulletin, V. 114, p. 1480–1504.
- Trop, J.M., and Ridgway, K.D., 2007, Mesozoic and Cenozoic tectonic growth of southern Alaska: A sedimentary basin perspective, *in* Ridgway, K.D., Trop, J.M., Glen, J.M.G., and O'Neill, J.M., eds., Tectonic Growth of a Collisional Continental Margin: Crustal Evolution of Southern Alaska: Geological Society of America Special Paper 431, doi: 10.1130/2007.2431(13).
- Silberling, N.J., Jones, D.L., Monger, J.W., and Coney, P.J., 1992, Lithotectonic terrane map of the North American Cordillera: United States Geological Survey, Misc. Inv. Ser. Map I-2176
- Sunderlin, D., 2008, The flora, fauna, and sediments of the Mount Dall Conglomerate (Farewell Terrane, Alaska, USA), *in* Blodgett, R.B., and Stanley, G.D., Jr., eds., The terrane puzzle: New perspectives on paleontology and stratigraphy from the North American Cordillera: Geological Society of America Special Paper 442, p. 133–150, doi: 10.1130/2008.442(09).
- Wilson, F.H., Dover, J.H., Bradley, D.C., Weber, F.R., Bundtzen, T.K., Haeussler, P.J., 1998. Geologic map of central (interior) Alaska: U.S. Geological Survey Open-File Report 98-133, 64 p., 3 plates, scale 1:500,000 (also released as a CD-ROM).

## **CHAPTER 2: SEDIMENTOLOGY, STRATIGRAPHY, AND DEPOSITIONAL SETTING OF THE MYSTIC PASS FORMATION**

### **2.1 INTRODUCTION**

The North American Cordillera is one of the most extensively studied mountain belts in the world with much of this focus being on regions of contiguous U.S. and western Canada. However, southern Alaska is perhaps one of the more understudied portions of the Cordilleran accretionary margin as bedrock exposures are in remote areas and it is home to the highest topography in North America. Thus, several fundamental questions remain regarding the tectonic evolution of this region including the stratigraphic history and structural evolution of Triassic and older tectonostratigraphic terranes in southwest Alaska.

One of the more regionally extensive and least understood terranes in this region is the Farewell terrane (Figure 2.1). The Farewell consists of three subterrane: 1) the Nixon Fork subterrane consisting of latest Neoproterozoic through lower Paleozoic (Devonian) shallow-water, mainly carbonate strata, 2) the Dillinger subterrane, which consists of lower Paleozoic (Cambrian–Devonian) deep-water siliciclastic and carbonate units, and 3) the Mystic subterrane which contains upper Paleozoic (Devonian–Permian) to lower Mesozoic primarily siliciclastic strata (Figure 2.2). While previous studies have documented general lithologic descriptions and biostratigraphic age constraint, much of the basic sedimentology, stratigraphy, and structure remain unknown. An understanding of these fundamental aspects is an essential component for resolving the tectonic

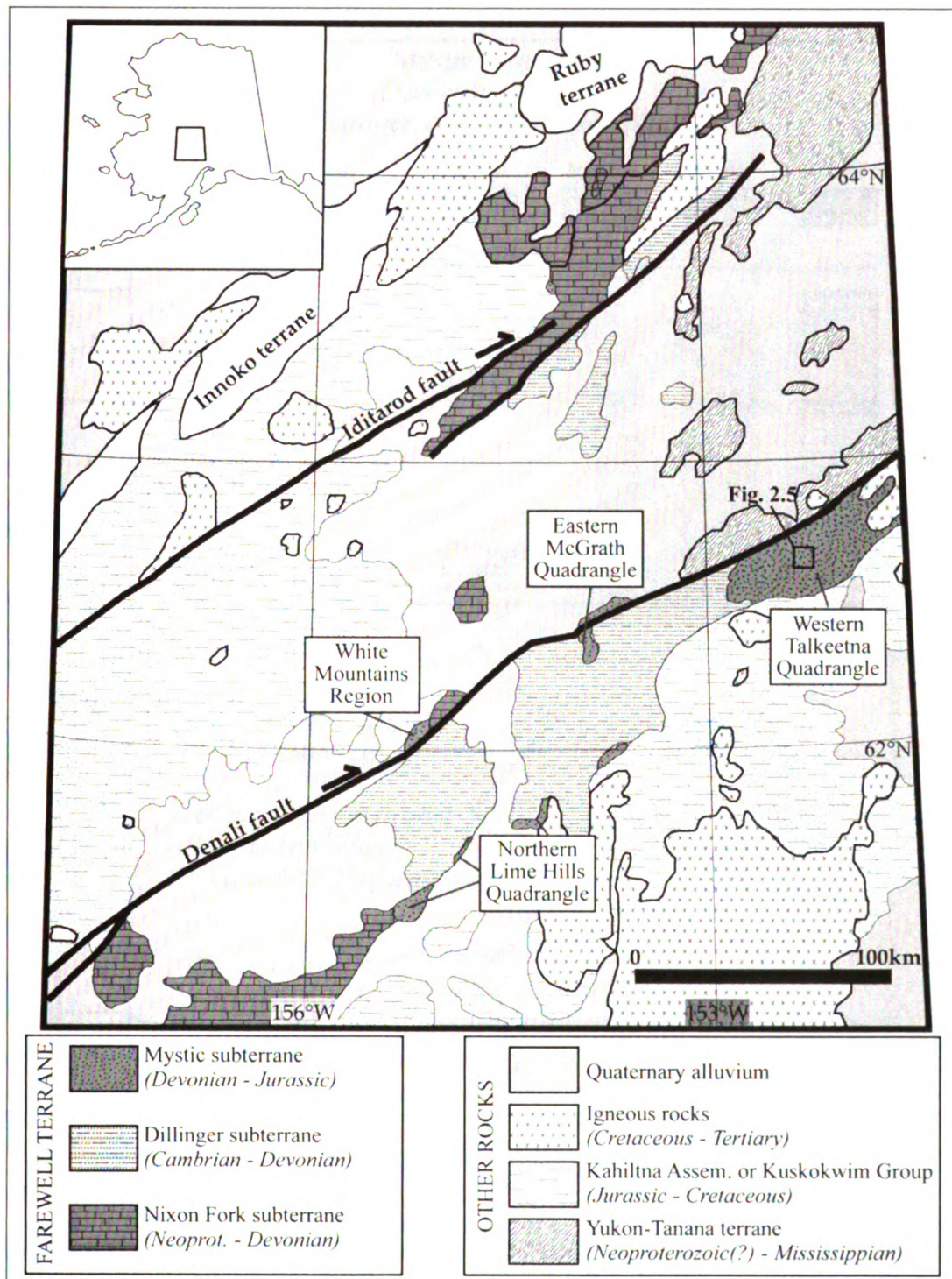


**Figure 2.1.** Generalized geologic map showing the regional area of interest and the distribution of exposed portions of the Farewell terrane. The majority of Farewell exposures are in the Alaska Range south of the Denali fault, but crop out as far North as the Kuskokwim Mountains north of the Iditarod fault. Note the small box in the western Talkeetna quad. shows the field area in Figure 2.5. Modified from Bradley et al., 2003.

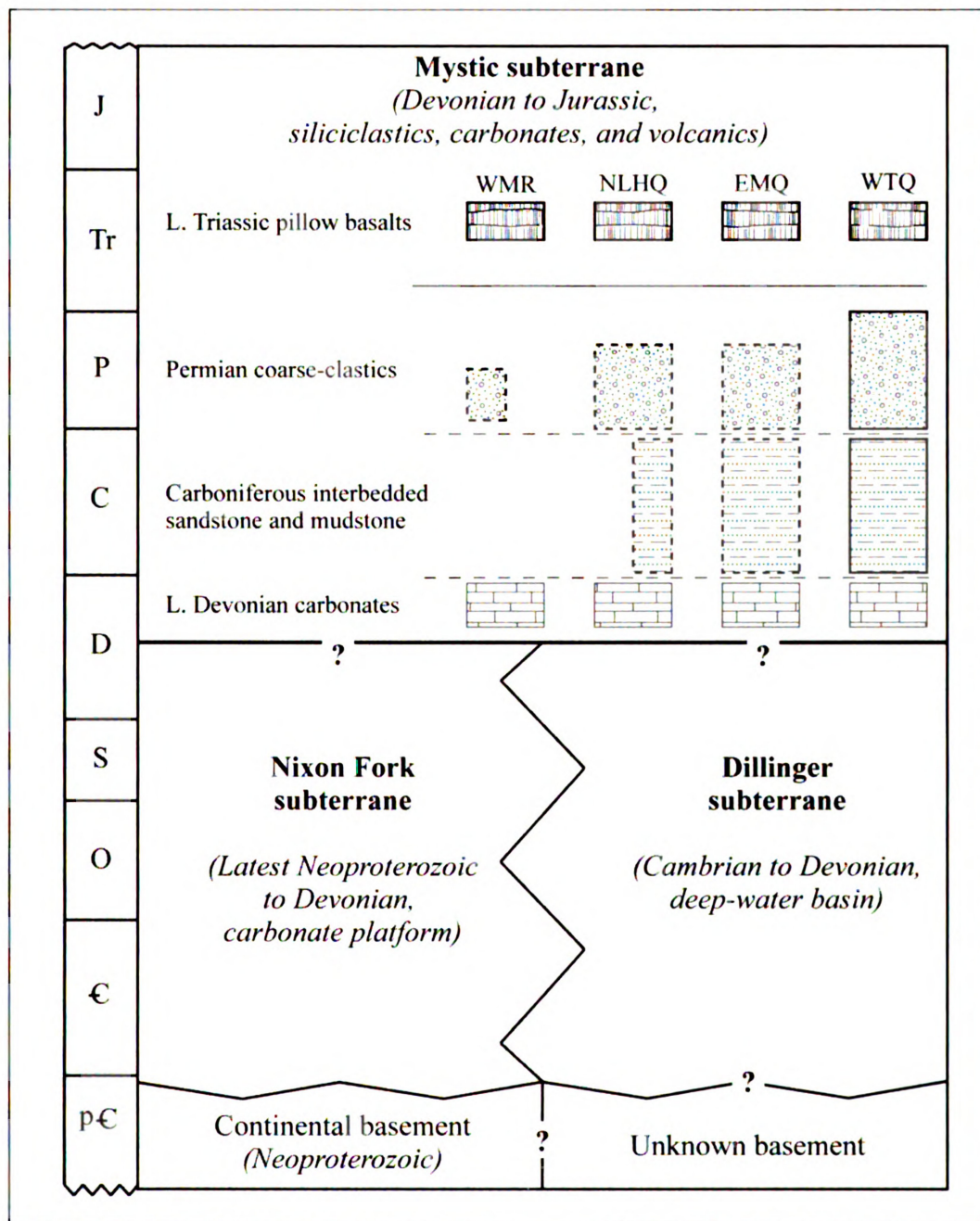


**Figure 2.2.** Three-part stratigraphy of the Farewell terrane. Simplified overview of the schematic relationships between different lithologies and components of the Farewell terrane. Dotted lines surrounding stratigraphic units indicate poorly documented thickness and lateral extents. Contacts between each unit are unknown. WMR- White Mountains Region, NLHQ- northern Lime Hills quadrangle, EMQ- eastern McGrath quadrangle, WTQ- western Talkeetna quadrangle.



evolution of the Farewell terrane, and the Paleozoic accretionary history of the northernmost portion of the North American Cordillera.

This study focuses on the stratigraphy of the Mystic subterrane and provides new sedimentologic and stratigraphic analyses of the upper Paleozoic (Mississippian–Permian) Mystic Pass formation from the Mystic Pass region of the western Alaska Range (Figure 2.1). A general stratigraphic overview of the Mystic subterrane indicates a combination of both marine and non-marine clastic deposition throughout much of the upper Paleozoic (Figure 2.3). Furthermore, measured stratigraphic section along with sedimentary facies and architecture analyses suggest that laterally extensive interbedded sandstone and mudstone of the Mystic Pass formation are likely part of turbiditic submarine fan depositional system and may record foreland basin deposition associated with upper Paleozoic orogenesis (Bradley et al., 2003).

## **2.2 STRATIGRAPHIC OVERVIEW OF THE MYSTIC SUBTERRANE**

Upper Paleozoic siliciclastic strata of the Mystic subterrane are most abundant in the western Alaska Range (Talkeetna quadrangle) south of the Denali Fault, but potentially correlative rocks are also sporadically mapped in other regions of southwest and central Alaska (Figure 2.1). In addition to the western Talkeetna quadrangle, primary exposures include the Farewell-Sheep Creek region (eastern McGrath quadrangle), the White Mountains region (western McGrath quadrangle), and four additional mapped exposures in the Lime Hills quadrangle (Figure 2.2). Although these units are all mapped as potentially correlating with the Mystic subterrane, stratigraphic differences are noted in the White Mountains region and the western Lime Hills

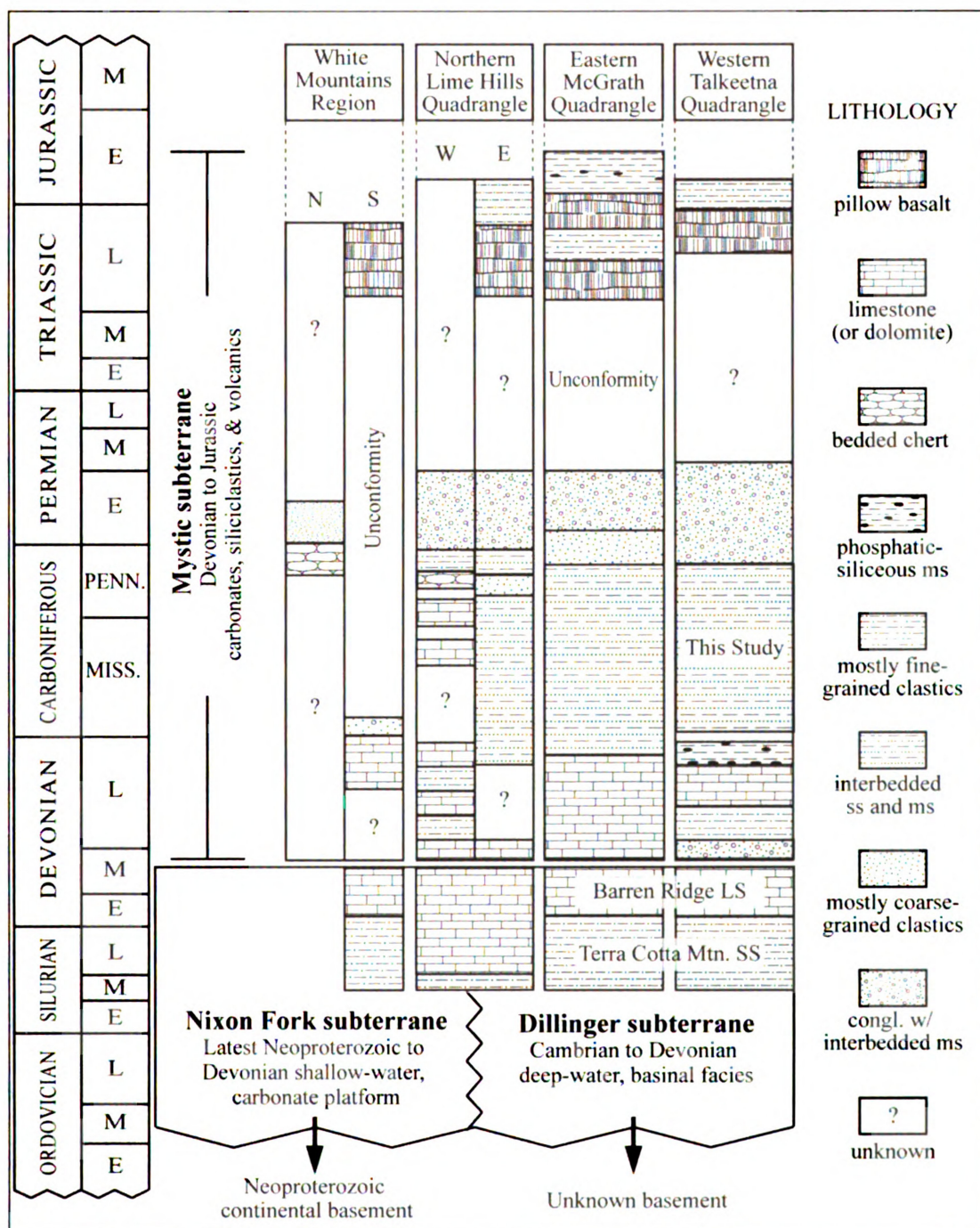


**Figure 2.3.** Generalized stratigraphic sections of the Farewell terrane from areas that contain correlative Mystic subterrane strata. Exact ages and stratigraphic thicknesses are not precise as age control is sparse for a majority of the documented strata. Also, the nature of the contact between Mystic subterrane strata and the underlying Nixon Fork and Dillinger subterrane has been documented as both stratigraphic and unconformable. Due to the lack of age constraint and field work in these areas, there are several unknown time gaps they may or may not be represented in different regions of the Farewell terrane. See Figure 2.1 for locations of documented stratigraphy.



quadrangle where Mississippian–Pennsylvanian siliciclastics are sparsely documented (Figure 2.3). The study area for this investigation concentrates primarily in the western Talkeetna quadrangle which contains the most extensive exposure of Mystic subterranean strata.

In the western Talkeetna Quadrangle the Mystic subterranean is locally underlain by carbonate and siliciclastic strata of the Dillinger subterranean (Figure 2.4). Decker et al. (1994) suggest a Middle Devonian angular unconformity as the contact between the Mystic and Dillinger subterraneans; however conformable relationships have also been reported (Blodgett and Gilbert, 1983 and Patton and others, 1984). The base of the Mystic subterranean strata is thought to be either a late Early Devonian (Emsian) limestone (Gilbert and Bundtzen, 1984; Blodgett and Gilbert, 1992; Blodgett et al., 2002) or a thin (~10 m) nonmarine redbed sequence consisting of sandstone & conglomerate with plant and coalified wood debris (Reed and Nelson, 1980). Basal units are overlain by a 125 – 250 m thick succession of sandstone, siltstone, and shale containing late Middle and early Late Devonian fauna. Upsection, is a reefoid limestone estimated at 60 to 90 meters thick, overlain by the so-called “blackball chert” containing radiolarians of Late Devonian age (Fammennian). Pillow basalts are interbedded within some of these Paleozoic strata and are of an unknown age, but inferred to be middle or late Paleozoic age (Reed and Nelson, 1980).

Overlying the Devonian strata of the Mystic subterranean are two key siliciclastic units, which are also the most relevant to this study. The first (and lower) is the Mystic Pass formation which is a 1 to 2 km thick (structural thickness) succession of Carboniferous interbedded sandstone and mudstone. Biostratigraphic age constraint

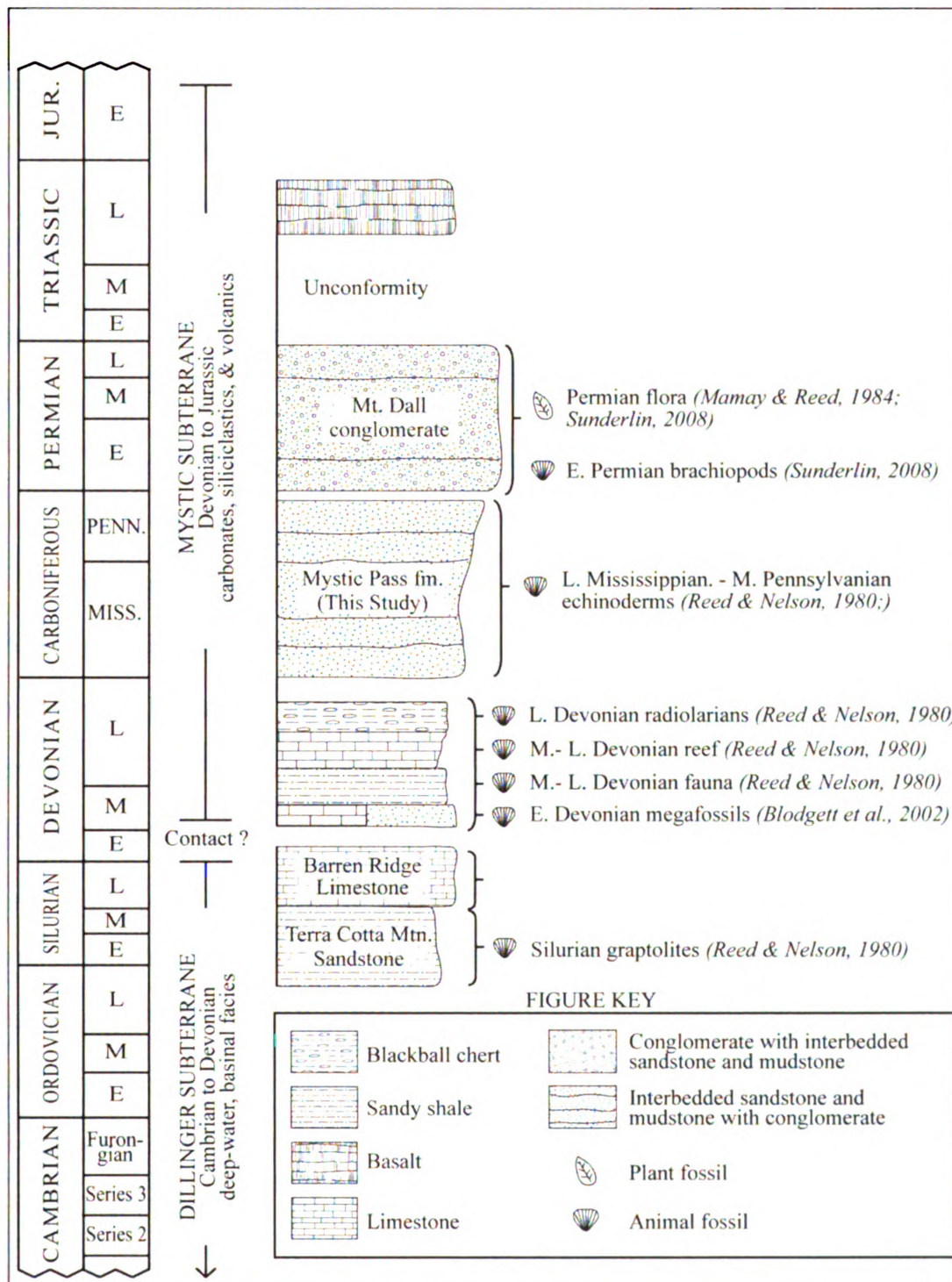


**Figure 2.4** Simplified stratigraphy of known units from Mystic subterrane exposures in the western Talkeetna quadrangle, SW Alaska. Both the Terra Cotta Mtn. Sandstone and the Barren Ridge Limestone belong to the Dillinger subterrane. This interpretation assigns a thin redbed sequence with coalified plant debris as the regional base of the Mystic subterrane. Contacts between all units are unknown. Stratigraphy from Reed and Nelson, 1980.

for this unit consists of late Mississippian echinoderms and middle Pennsylvanian echinoderms and foraminifers, (identified by A.K. Armstrong in Reed and Nelson, 1980). This structurally imbricated Mississippian–Pennsylvanian siliciclastic unit is the most extensive unit mapped within the Mystic subterrane. These strata are described as a thick, structurally deformed flysch-like sequence containing thick lenses of pebble- to cobble-conglomerate with clasts of limestone and black cherty argillite (Jones et al., 1982).

The second siliciclastic unit associated with the Mystic subterrane is a >1500-m-thick Permian-aged succession of sandstone, conglomerate, and fossil-leaf bearing siltstone referred to as the Mt. Dall conglomerate, which outcrops as a broad syncline. A Permian age for these strata is based on the presence of plant fossils (*Zamiopteris*) and brachiopods (Mamay and Reed, 1984; Sunderlin, 2008) as well as conglomerate clasts containing Pennsylvanian to Early Permian conodonts (Bradley et al., 2003). The Mt. Dall conglomerate is not a primary focus of this investigation, however previous work (Bradley et al., 2003; Sunderlin 2008) on these strata provide useful insight to the overall stratigraphic trends of the Mystic subterrane. Given the chronologic and lithologic relationships of the Mystic Pass formation and Mt. Dall conglomerate, it is possible that these units are closely related and represent temporal (and possibly spatial) variations of the same (foreland?) basin. It should be noted that with the exception of work by Sunderlin (2008) on the Mt. Dall conglomerate, there are no previously published measured stratigraphic sections which address up-section patterns in depositional processes associated with Farewell terrane strata. The following text focuses on new

sedimentologic and stratigraphic data from within the Mystic Pass formation as well as depositional and tectonic models interpreted from this work and previous studies.

### **2.3 MYSTIC PASS FORMATION:**

The Mystic Pass formation throughout the Alaska Range is extensively deformed and isoclinally folded in some locations, making this a difficult area to assess in a stratigraphic context. However, outcrops near Mystic Pass proper (study area) (Figure 2.5) are tilted (dipping SE), and stratigraphically continuous at ~100 m scale. The following documents a portion of the sedimentologic and stratigraphic characteristics of the Mystic Pass formation based on measured stratigraphic section (Figure 2.6) exposed at Mystic Pass proper. In addition to the descriptions documented in the context of a measured section, we also note some general sedimentological characteristics and several sedimentary features observed in the more structurally complicated exposures of the Mystic Pass formation.

#### **Regional Sedimentologic and Stratigraphic Trends**

The Mystic Pass formation is prevalent and well-exposed throughout this study's field area in the western Alaska Range (Figure 2.5). Regions west-northwest of Mystic Pass (Figure 2.7A) and south of the Denali fault include mostly strata of the Mystic Pass formation as well as finer-grained units of Paleozoic(?) phyllite (map unit Pzp of Reed and Nelson, 1980). Views to the southeast (Figure 2.7B) show potentially younger units including Triassic(?) pillow basalts and what may be the Mt. Dall conglomerate.



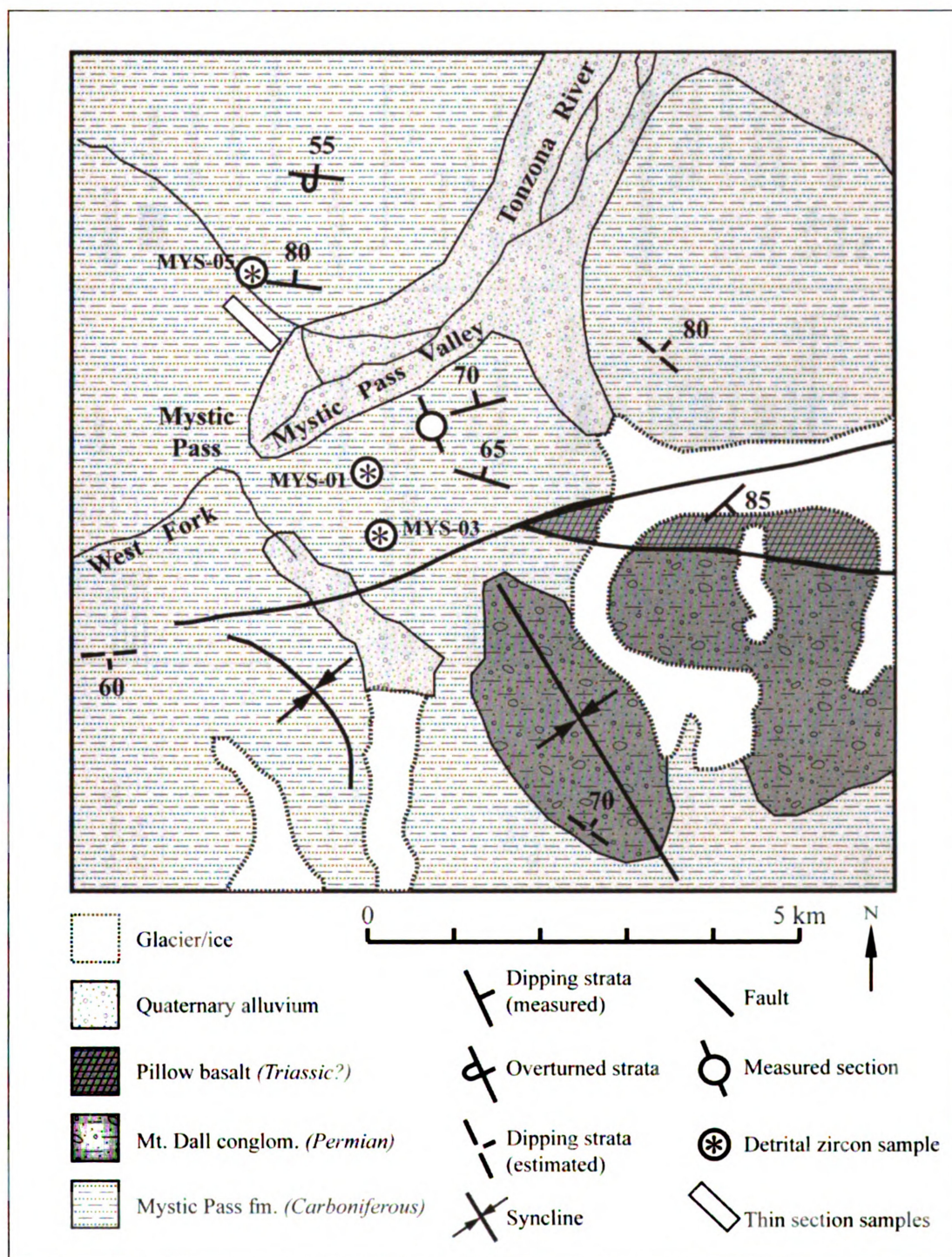


**Figure 2.5.** Geologic map showing the field area (Mystic Pass) in the western Alaska Range. This study is focused on the most prevalent map unit shown here, the Mystic Pass formation. Most thin section samples were collected where the white box is located with additional samples from detrital zircon and measured section localities. Circled asterisks show the general locations of where detrital zircon samples were collected along with their abbreviated sample name. Modified from Reed and Nelson, 1980.







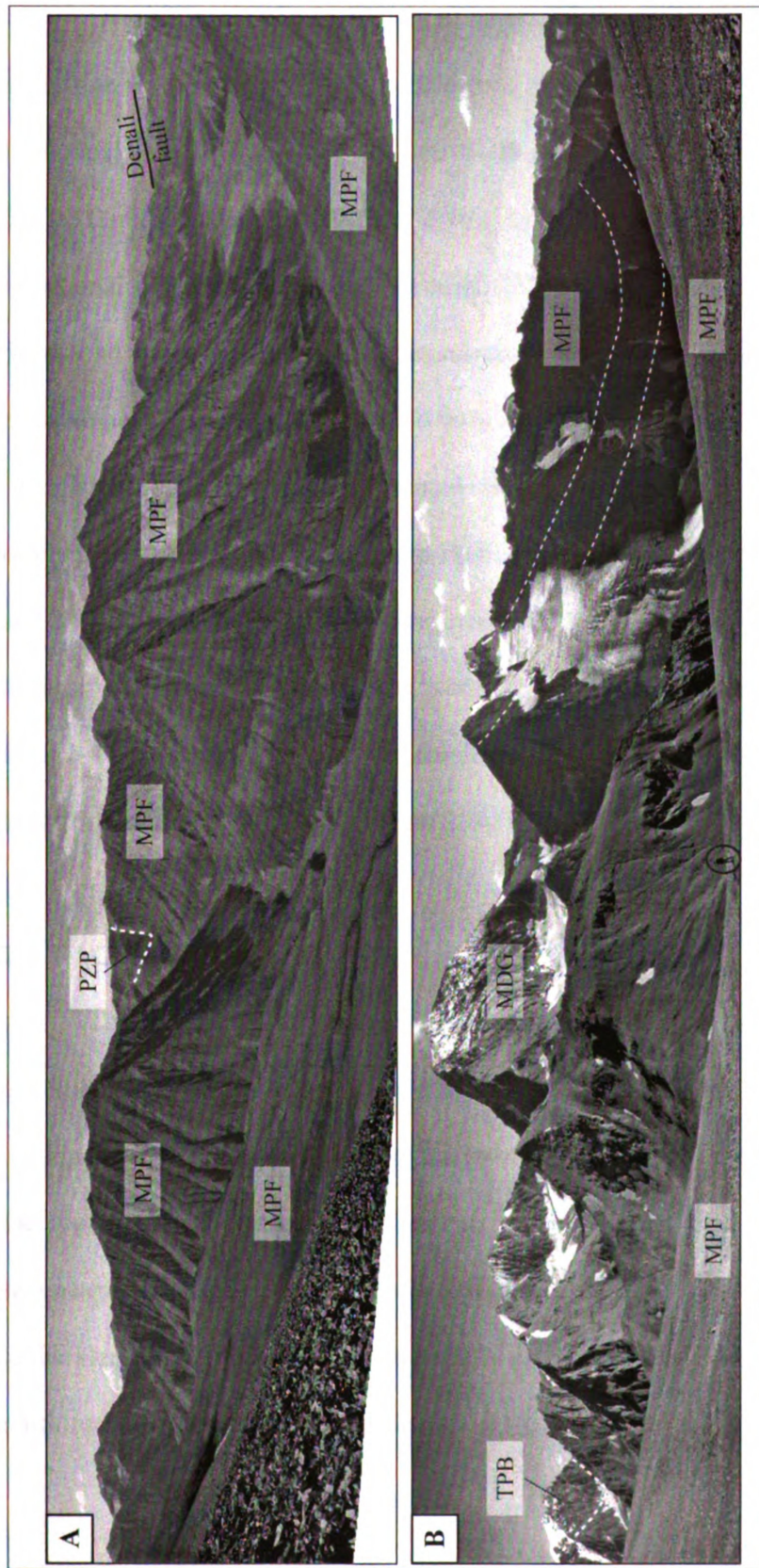


**Figure 2.7.** Regional exposures of the Mystic Pass formation. A) View to the north of the upper Paleozoic Mystic Pass formation (MPF) and Paleozoic(?) phyllite PZP (map unit Pzp of Reed and Nelson, 1980). Note the approximate location of the Denali fault for reference. B) View to the south of upper Paleozoic strata including the Mystic Pass formation, what may be the Mt. Dall conglomerate (MDG), and Triassic(?) pillow basalts (TPB). Note person for scale, circled. The interpretation of exposures of TPB and MDG are based on the location of mapped units by Reed and Nelson (1980).

Overall, strata consist largely of interbedded mudstone and fine- to coarse-grained sandstone with minor gravel- to pebble-conglomerate units (Figures 2.8, 2.9, and 2.10). Individual beds are laterally extensive (>100 m), exhibit tabular geometries, and are 0.02–3.0 m thick (Figures 2.9C and 2.10). Mudstone units display faint laminations, occasional flame structures, and are commonly bioturbated (Figures 2.8C and 2.10). Sandstone facies are characterized primarily by plane beds, ripple cross-stratification, and massive beds (Figure 2.8A). Graded beds are also common, but the nature of grading often is unconfirmed without additional up-indicators (Figure 2.8C). Flute casts are rarely present while mudstone rip-up clasts are common at the base of beds (Figures 2.8B and 2.9B). Both matrix- and clast-supported conglomerate occur sporadically throughout these strata (Figure 2.9A and 2.9D). Individual clasts are rounded to sub-rounded, range from 1–10 cm in diameter, and are dominated by red, black, and green chert, minor limestone, and rare sandstone (Figure 2.9D).

## **2.4 FACIES ASSOCIATIONS**

The sedimentology of upper Paleozoic siliciclastic strata at Mystic Pass is documented in a measured section shown in Figure 2.6. Overall, strata coarsen upward with increased occurrences of medium- to coarse-grained sandstone and conglomerate in the upper parts of the section. Facies classifications are based on the identification of seven separate sedimentary structures and facies (Table 2.1). Together, these facies led to the identification of two facies associations, which are attributed to medial and distal portions of an unconfined submarine fan environment. The sedimentologic descriptions



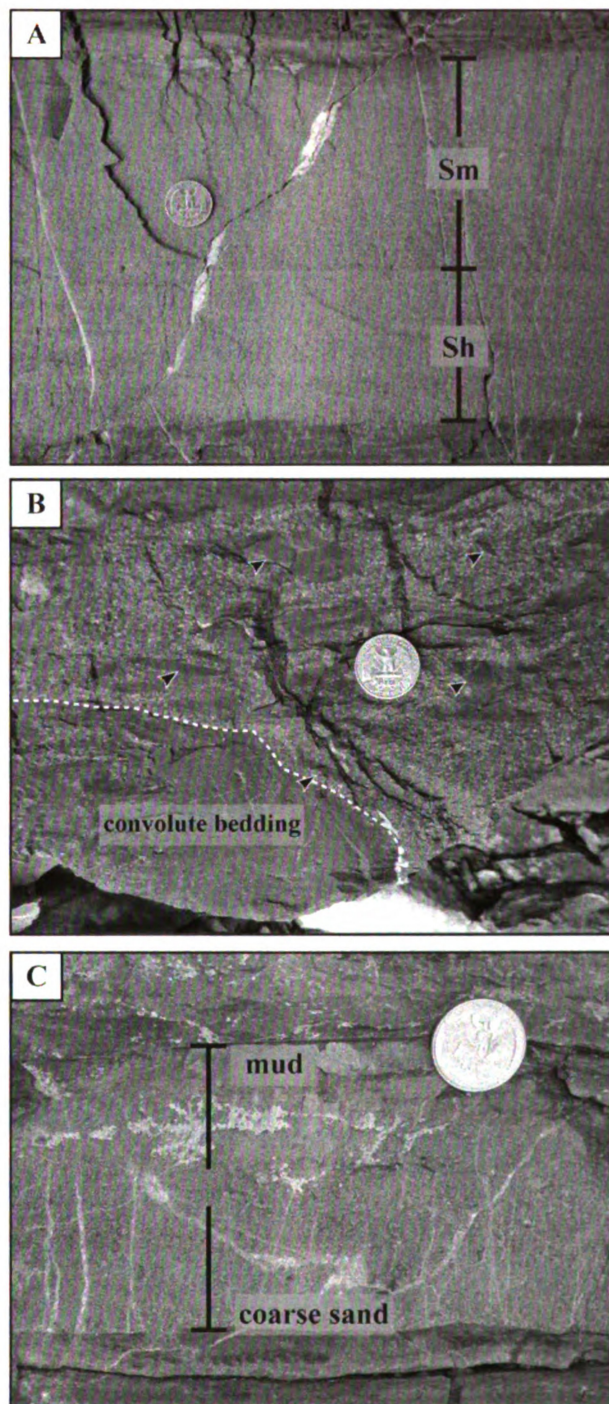


**Figure 2.8.** Outcrop photos of the Mystic Pass formation I. A) sandstone bed exhibiting both faint horizontal laminations (Sh) and massive bedding (Sm); B) mudstone rip-up clasts (arrows) and convolute bedding within a coarse sandstone bed and ; C) a fining upward (normally graded) sandstone bed deposited over a mudstone unit, which contains trace fossils (worm burrows). A U.S. quarter for scale in each photo.



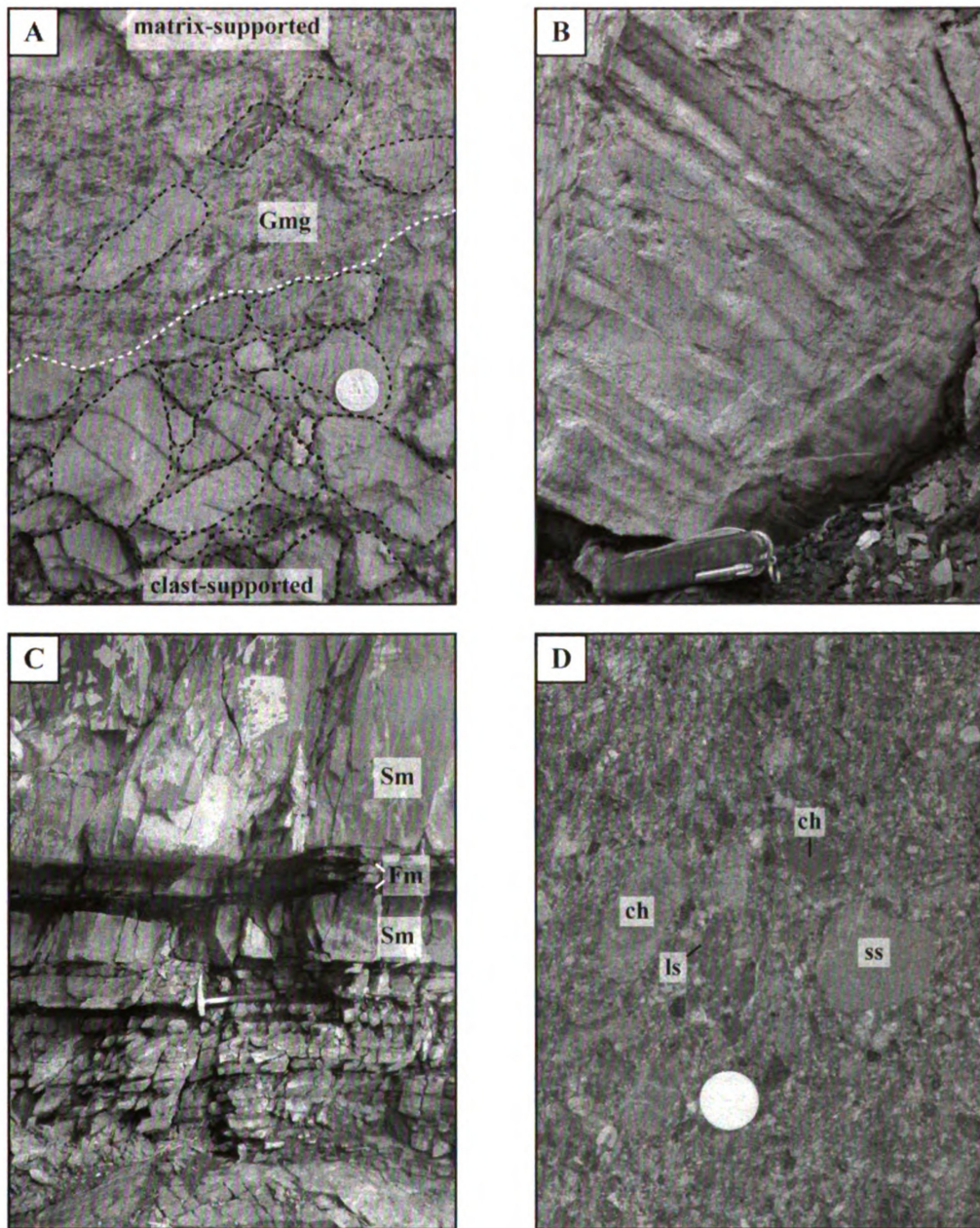


**Figure 2.9.** Outcrop photos of the Mystic Pass formation II. A) clast- to matrix-supported conglomerate (U.S. quarter for scale); B) flute casts at the base of a fine-grained sandstone bed (knife for scale); C) tabular bedding geometries of blocky, massive sandstone beds (Sm) and thin mudstone (Fm) beds (rock hammer for scale); D) mostly matrix-supported gravel- to pebble-conglomerate of mostly sedimentary (ch-chert, ss-sandstone, and ls-limestone) clasts.





**Figure 2.10.** Outcrop photos of the Mystic Pass formation III. A series of normally graded beds with medium-to coarse-grained sandstone fining upward to mudstone. As seen here, bed thicknesses were typically in the 4 to 8 cm range. Finer-grained sandstone and mudstone display faint ripple cross stratification (arrows).



and interpretations of facies associations and depositional systems are summarized in Table 2.2 and discussed in detail below.

### **Facies Association 1**

#### ***Description***

The lower ~90 meters of the measured section consists predominantly of interbedded fine-grained sandstone and mudstone with isolated occurrences of medium- to coarse-grained sandstone units. Bed thicknesses range from 2–15 cm, but typically average 4–7 cm and consistently exhibit tabular geometries (Figure 2.9). Individual beds are laterally extensive (>100 m) and commonly exhibit non-erosive basal contacts. Mudstone deposits are mostly massive (Fm) to finely laminated (Fl), and rarely display horizontal stratification (Sh) or ripple stratification (Sr) (Figure 2.9). Bioturbation and burrow structures are common in the thicker, more massive mudstone beds. Sandstone units are mostly massive (Sm) to horizontally stratified (Sh) (Figure 2.8). Normally graded beds occasionally occur in which grain sizes range from fine- to medium-grained sandstone (Figure 2.8 and 2.10).

#### ***Interpretation***

Sandstone and mudstone deposits of Facies Association 1 are interpreted to represent outer/distal portions of a submarine turbidite fan depositional environment. Thin, rhythmically interbedded sandstone and mudstone are due to deposition of sediment in turbidity currents and record reoccurring debris flow events. Laterally extensive, tabular bedding geometries are interpreted to result from debris flows being

<b>Table 2.1</b> Summary of facies classifications and interpretations for the Mystic Pass formation. Utilizing facies codes from Miall (1977).		
<i>Facies code</i>	<i>Sedimentary structures and facies</i>	<i>Interpretation</i>
<i>Fm</i>	<b>Massive (poorly laminated).</b> mudstone; occasional parallel laminations; bioturbation also sparsely present	Suspension settling after debris flow and waning turbidity currents
<i>Fl</i>	<b>Fine lamination.</b> mudstone; flat parallel laminaton; very small ripples	Suspension fallout/weak traction of turbidity currents
<i>Sm</i>	<b>Massive-structureless.</b> Fine- to coarse-grained sandstone; no grading or stratification	Sediment gravity flow deposits or sandy high-density turbidity currents
<i>Sr</i>	<b>Ripple cross-stratification.</b> Fine- to medium-grained sandstone; laminated symmetric and asymmetric geometry	Sedimentation during migration of current ripples; traction flow
<i>Sh</i>	<b>Horizontal stratification.</b> Very fine- to coarse-grained sandstone; normal grading;	Sedimentation under base flow conditions; traction carpets
<i>Gmm</i>	<b>Massive structureless.</b> Matrix-supported conglomerate; gravel- to cobble-sized clasts; weak to no grading	Plastic debris flow; high strength; viscous turbulent flow; high-density turbidity currents
<i>Gmg</i>	<b>Massive structureless.</b> Matrix- to clast-supported conglomerate; gravel- to cobble-sized clasts; gravel-rich deposits exhibit normal grading	Pseudoplastic debris flow; inertial bedload; turbulent flow; high-density turbidity currents

**Table 2.2** Summary of descriptions and interpretations of facies associations for the Mystic Pass formation.

<b><i>Facies Association 1 (FA 1)</i></b>	<b><i>Submarine Fan (Distal)</i></b>
Tabular, laterally extensive (>100m) deposits of interbedded grey sandstone, and mudstone; individual beds are 2 to 15 cm thick; non-erosive contacts at base of beds	Outer/distal portions of a submarine fan lobe; thin, rhythmically interbedded sandstone and mudstone are due to deposition of sediment in turbidity currents and record individual debris flow events; laterally extensive, tabular bedding geometries result from flows being unconfin ed
A. Mudstone. Finely laminated (Fl) and massive mudstone (Fm); worm burrows common in thicker, more massive deposits.	A. Suspension fallout (marine). Fl and Fm resulted from fallout of fine-grained material during and after the waning stages of a turbidity current; faint laminations correspond to weak traction; quiescent conditions allow for bioturbation of pelagic sediment
B. Sandstone. Horizontally stratified (Sh), massive, structureless (Sm) and occasionally normally graded fine- to medium-grained sandstone	B. Low density turbidity currents. Sm is due to sediment fallout from suspension during initial stages of debris flow deposition which lack coarse-grained material; Sh results from deposition by traction within turbidity currents
<b><i>Facies Association 2 (FA 2)</i></b>	<b><i>Submarine Fan (Medial)</i></b>
Tabular, laterally extensive (>100m) deposits of interbedded grey sandstone, and mudstone; individual beds are 2 to 15 cm thick; non-erosive contacts at base of beds	Medial/coarser portions of a submarine fan lobe; thin, rhythmically interbedded sandstone and mudstone are due to deposition of sediment in turbidity currents and record individual debris flow events; laterally extensive, tabular bedding geometries result from flows being unconfin ed
A. Mudstone. Finely laminated (Fl) and massive mudstone (Fm)	A. Suspension fallout (marine). Fl and Fm resulted from fallout of fine-grained material during and after the waning stages of a turbidity current; faint laminations correspond to weak traction
B. Sandstone. Horizontally stratified (Sh), ripple cross-stratified (Sr) massive, structureless (Sm) and occasionally normally graded fine- to medium-grained sandstone	B. Low density turbidity currents. Sm is due to sediment fallout from suspension during initial stages of debris flow deposition which lack coarse-grained material; Sh results from deposition by traction within turbidity currents; Sr reflects mixed processes of traction and suspension in upper flow conditions
C. Conglomerate. Mostly matrix-supported conglomerate with gravel- to pebble-sized clasts; gravel rich deposits commonly exhibit normal grading (Gmg); coarser, pebble-rich deposits were mostly massive showing very weak to no grading (Gmm)	C. High density turbidity currents or debris flows. Gmg results from suspension-dominated deposition of gravel-rich high density turbidity currents; Gmm is due to chaotic high-density debris flow deposits in pseudoplastic/viscous flow conditions

unconfined. Massive (Fm) mudstone units resulted from fallout of fine-grained material after the waning stages of a turbidity current as well as suspension settling of pelagic sediment during quiescent intervals (equivalent to Te of Bouma, 1962 and T7 and T8 of Stowe and Shanmugam, 1980). Finely laminated mudstone (Fl) deposits are associated with the waning stages of turbidity currents where weak traction is still present.

Sandstone units of Facies Association 1 are interpreted to represent deposition by low-density turbidity currents. Fine- to medium-grained massive sandstone (Sm) beds are interpreted to reflect sediment fallout from suspension during the initial stages of debris flow deposition in which coarser-grained material is absent (equivalent to Td facies of Bouma, 1962). Horizontally-laminated (Sh) beds are interpreted as transport and deposition by traction within turbidity currents (Bouma, 1962). The occasional presence of normally graded fine- to medium-grained sandstone is interpreted as fallout from suspension settling of progressively finer-grained material as turbidity currents lose their velocity. In summary, Facies Association 1 is represented by subaqueous debris flows demonstrating mostly processes of traction and suspension setting during and in between low-density turbidity currents (Lowe, 1982) in which Bouma facies Td-e are most prevalent (Bouma, 1962).

## **Facies Association 2**

### ***Description***

The second facies association is represented by the upper (~35 meters) portion of the section and continues with a succession of interbedded sandstone, mudstone, and minor conglomerate. Bed thicknesses are more variable and generally thicker (6 to 10

cm) on average than the lower portion but range from 2 cm to 15 cm and exhibit tabular geometries. Individual beds are laterally extensive (>100m) and exhibit non-erosive basal contacts. Mudstone deposits are mostly massive (Fm) however fine laminations (Fl) occur more frequently than in the lower part of the section. Bioturbation and burrow structures were not observed in this part of the section. Sandstone deposits are massive (Sm), horizontally stratified (Sh), and occasionally ripple cross-stratified (Sr) (Figures 2.8 and 2.10). Normally graded sandstone beds occur more frequently as this part of the section contains more abundant fine- to coarse-grained sandstone. Conglomeratic units are mostly matrix-supported with gravel- to pebble-sized clasts and gravel-rich deposits commonly exhibit normal grading (Gmg). Coarser, pebble-rich conglomerate units are mostly massive showing very weak to no grading (Gmm) (Figure 2.9).

### ***Interpretation***

Mudstone, sandstone, and minor conglomerate deposits of Facies Association 2 are interpreted to represent more proximal/medial portions of a submarine turbidite fan deposit. Similar to FA1, rhythmically interbedded mudstone, sandstone, and occasional conglomerate are the result of deposition in turbidity currents and record individual debris flow events. Tabular geometries of laterally extensive beds suggest that turbidity flows were largely unconfined. Finely-laminated mudstone (Fl) deposits are associated with the waning stages of turbidity currents whereas more massive mudstone (Fm) units are a result of suspension settling and deposition of pelagic sediment during quiescent intervals (equivalent to Te facies Bouma, 1962 and T7 and T8 of Stowe and Shanmugam, 1980). Massive sandstone beds are interpreted to reflect sediment fallout from

suspension during the initial stages of debris flow deposition from low density turbidity currents. Horizontally-stratified sandstone (Sh) units (plane beds) result from deposition by traction under low flow strength conditions within an upper flow regime (equivalent to Td facies of Bouma, 1962) whereas ripple cross-stratified beds (Sr) are interpreted to be the result of traction in lower flow conditions (equivalent to Tc facies of Bouma, 1962) (Simons and Richardson, 1961; Blatt et al., 1980). Both massive (Gmm) and normally graded (Gmg) Gravel- to pebble-conglomerate beds reflect high density turbidity currents (Lowe, 1982). Normally graded conglomerate (Gmg) and massive conglomerate (Gmm) are interpreted as chaotic high-density debris flow deposits in pseudoplastic/viscous flow conditions (Miall, 1978). The presence of slightly thicker and coarser sandstone beds in addition to the presence of gravel- to pebble-sized conglomerate are the best indication that these deposits are likely more proximal to the source than those of Facies Association 1.

## **2.5 DEPOSITIONAL SETTING**

Measured stratigraphy of the Mystic Pass formation is interpreted to represent the medial to distal portions of a base-of-slope, submarine fan environment (Figure 2.11). Sheet-like turbidite sandstones interbedded with structureless hemipelagic mudstones are characteristic of basin-floor fan deposits (e.g. Mutti, 1977; Ricci Lucchi, 1975; Walker et al., 1978; Posamentier and Allen, 1993). This includes deposition by a combination of low- to high-density sediment gravity flows associated with a submarine fan environment. The occurrence of both laminated mudstone, and horizontally-stratified



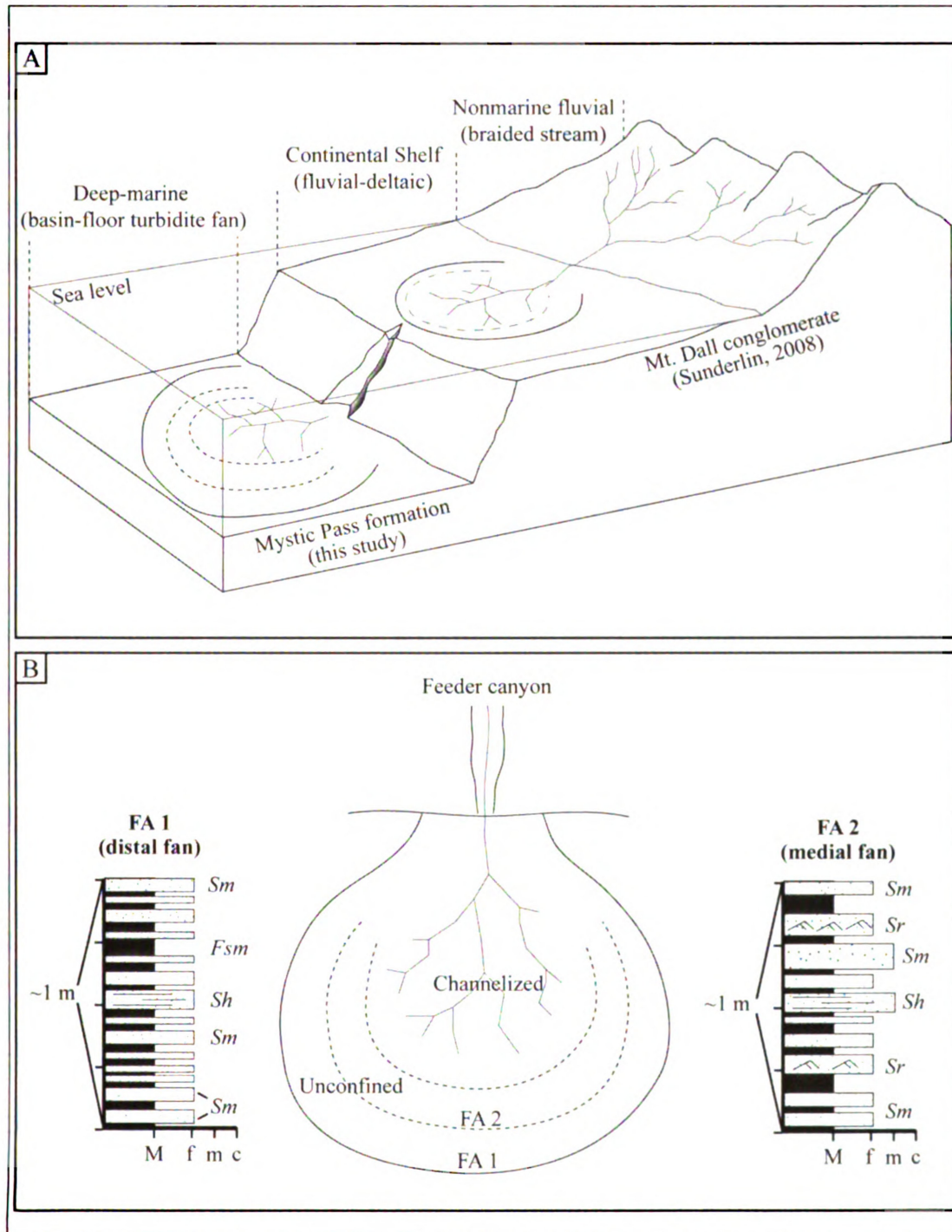


**Figure 2.11** Depositional setting for the Mystic Pass formation. A) Depositional environment schematic demonstrating the potential relationship between the Mystic Pass formation and the Mt. Dall conglomerate. B) Submarine turbidite fan model which highlights the facies associations assigned to measured stratigraphy from the Mystic Pass formation. In this model, both the medial and distal fan facies contain unconfined flows corresponding to the relatively thin, laterally extensive, and tabular beds of the Mystic Pass formation.

sandstone together with massive sandstone and minor ripple-cross-stratified sandstone suggests sediment distribution was influenced by both laminar and turbulent flow. Tabular beds marked by sharp non-erosive basal contacts support unconfined flow in the lower portions of sediment gravity flows. Massive mudstone and siltstone were likely associated with the waning stages of individual flow events (e.g., Ghibaudo, 1992). Convolute bedding is the result of post-depositional reorganization through dewatering and likely occurred in strata associated with high suspended sediment load during original deposition.

Measured stratigraphy from the Mystic Pass formation shows a general coarsening upward progression in which sandstone to mudstone ratios increase as sandstone beds are generally thicker and coarser, as does the presence of conglomerate. This could suggest an overall progradational package where younger and more proximal/medial parts of submarine fan systems successively prograded over older, more distal, finer-grained submarine fan deposits.

## **2.6 DISCUSSION**

A medial to distal fan depositional setting interpreted for the Mystic Pass formation is consistent with previous depositional environments interpreted for the Mt. Dall conglomerate (Sunderlin, 2008) as well as regional basin-scale interpretation to explain upper Paleozoic siliciclastic deposition of the Mystic subterrane (Bradley et al., 2003). Sunderlin (2008) also suggests that strata of Mt. Dall conglomerate were deposited in a fluvial, braided stream succession on the coastal margin of a developing foreland basin. Biostratigraphic age constraint on upper Paleozoic siliciclastic strata of

the Mystic subterrane assigns a Mississippian to Early Permian age for the Mystic Pass formation and a Permian age to the Mt. Dall conglomerate, and when considered together, the stratigraphy of these two units could reflect a coarsening upward progression of submarine turbidite deposits to shallow-marine or non-marine fluvial deposits. Based on these chronologic and stratigraphic relationships, it seems feasible to suggest that the depositional environments of both units represent temporal and or spatial progressions within the same basin.

Bradley et al. (2003) proposed that the Mt. Dall conglomerate represents a clastic wedge associated with foreland basin development during the Browns Fork orogeny. This interpretation is based on the presence of this fluvial clastic wedge (foreland) and coeval metamorphic ages from Farewell rocks in the Kuskokwim Mountains (hinterland) (Figure 1). Following the interpretation of Bradley et al. (2003), the Mystic Pass formation likely reflects deep marine deposition during earlier phases of foreland basin development association with the Browns Fork orogeny. This hypothesis could be tested by documenting the relationship (stratigraphic or structural) between the Mystic Pass formation and the Mt. Dall conglomerate as well as by obtaining additional age constraint on each unit.

Age equivalent (Mississippian–Permian) siliciclastic strata of the Mystic subterrane are sporadically documented throughout the Farewell terrane (Figures 2.1–2.3). Beyond lithologic similarities and sparse age correlations, it remains unknown as to whether or not these strata are related or if they are structurally bounded representing clastic wedges associated with independent orogenic events. Additional work is needed to determine the spatial relationship between various exposures of upper Paleozoic units

of the Farewell terrane, which bears significance on the overall tectonic evolution of this region.

It is important to note that a link between the Mt. Dall conglomerate and the Mystic Pass formation requires the assumption that they are stratigraphically continuous. Thus, future work should document the nature of the contact between these two units and determine their broader spatial and temporal extent as well as distinguish between how much of the exposed Mystic Pass formation is displaying structural thickness rather than stratigraphic thickness. Furthermore, an upper Paleozoic depositional and tectonic interpretation of the Farewell terrane could be greatly improved by documented the stratigraphic (or structural) relationship between units above and below the Mystic Pass formation.

## **2.7 CONCLUSIONS**

New sedimentologic and stratigraphic data including sedimentary facies from upper Paleozoic siliciclastic strata of the Mystic Pass formation suggest a submarine turbidite fan depositional environment. Modest temporal changes documented in measured stratigraphy likely reflect progradation and/or aggradation of a distal turbidite fan to that of a more proximal, medial fan depositional environment.

If stratigraphic relationships are assumed with the Mt. Dall conglomerate, the Mystic Pass formation can be interpreted to represent deep marine siliciclastic deposition during early foreland basin development of the Browns Fork orogeny (Bradley et al., 2003), and thus continues to coarsen up-section into the non-marine fluvial facies of the Mt. Dall conglomerate. Alternatively, if significant crustal/structural boundaries occur

between these two units, the Mystic Pass formation represents an independent siliciclastic wedge with unique tectonic affinities. Additional field studies are needed to document the relationship between the Mystic Pass formation and the Mt. Dall conglomerate as well as age equivalent siliciclastic strata exposed throughout the Farewell terrane.



## 2.8 REFERENCES

- Blatt, H., Middleton, G.V., and Murray, R., 1980, Origin of sedimentary rocks, 2<sup>nd</sup> ed.: Prentice-Hall, Englewood Cliffs, N.J., 782 p.
- Blodgett, R.B., and Gilbert, W.G., 1983, The Cheeneetnuk Limestone; A new Early(?) to Middle Devonian formation in the McGrath A-4 and A-5 Quadrangles, west-central Alaska: Alaska Division of Geological and Geophysical Surveys Professional Report 85, 6 p.
- Blodgett, R.B., and Gilbert, W.G., 1992, Paleogeographic relations of Lower and Middle Paleozoic strata of southwest and west-central Alaska: Geological Society of America Abstracts with Programs, v. 24, no. 5, p. 8.
- Blodgett, R.B., Rohr, D.M., Boucot, A.J., 2002, Paleozoic links among some Alaskan accreted terranes and Siberia based on megafossils, *in* Miller, E.L., Grantz, A., and Klemperer, S.L., eds., Tectonic evolution of the Bering Shelf–Chukchi Sea–Arctic Margin and adjacent landmasses: Geological Society of America Special Paper 360, p. 273–280.
- Bouma, A.H., 1962, Sedimentology of Some Flysch Deposits: Amsterdam, Elsevier, 168 p.
- Bradley, D.C., Dumoulin, J., Layer, P., Sunderlin, D., Roeske, S., McClelland, W.C., Harris, A.G., Abbott, G., Bundtzen, T.K., and Kusky, T., 2003, Late Paleozoic orogeny in Alaska's Farewell Terrane: Tectonophysics, v. 372, p. 23–40, doi: 10.1016/S0040-1951(03)00238-5.
- Bradley, D.C., McClelland, W.C., Wooden, J.L., Till, A.B., Roeske, S.M., Miller, M.L., Karl, S.M., and Abbott, J.G., 2007, Detrital zircon geochronology of some Neoproterozoic to Triassic rocks in interior Alaska, *in* Ridgway, K.D., Trop, J.M., Glen, J.M.G., and O'Neill, J.M., eds., Tectonic Growth of a Collisional Continental Margin: Crustal Evolution of Southern Alaska: Geological Society of America Special Paper 431, doi: 10.1130/2007.2431(13).
- Bundtzen, T.K., Harris, E.E., Gilbert, W.G., 1997. Geologic map of the eastern half of the McGrath quadrangle, Alaska. Alaska Division of Geological and Geophysical Surveys Report of Investigations 97-14a, 38 pp., scale 1:125,000.
- Dickinson, W.R., 2004, Evolution of the North American Cordillera, Annual Review of Earth and Planetary Sciences, vol. 32, pp.13–45.

- Dumoulin, J.A., Harris, A.G., Gagiev, M., Bradley, D.C., and Repetski, J.E., 2002, Lithostratigraphic, conodont, and other faunal links between lower Paleozoic strata in northern and central Alaska and northeastern Russia, *in* Miller, E.L., Grantz, A., and Klemperer, S.L., eds., Tectonic evolution of the Bering Shelf–Chukchi Sea–Arctic Margin and adjacent landmasses: Geological Society of America Special Paper 360, p. 291–312.
- Gilbert, W.G., and Bundtzen, T.K., 1984, Stratigraphic relationship between Dillinger and Mystic terranes, western Alaska Range, Alaska: Geological Society of America Abstracts with Programs, v. 16, no. 5, p. 286.
- Jones, D., Siberling, N.J., Gilbert, W.G., Coney, P.J., 1982, Character, distribution, and tectonic significance of accretionary terranes in the central Alaska Range, *Journal of Geophysical Research*, v. 87, p. 3709–3717.
- Lowe, D.R., 1982, Sediment gravity flows II: Depositional models with special reference to the deposits of high-density turbidity currents: *Journal of Sedimentary Petrology*, v. 52, p. 279–297.
- Mamay, S.H., and Reed, B.L., 1984, Permian plant megafossils from the conglomerate of Mount Dall, central Alaska Range, *in* Coonrad, W.L., and Elliott, R.L., eds., The United States Geological Survey: Accomplishments during 1981: U.S. Geological Survey Circular 868, p. 98–102.
- Miall, A.D., 1977, A review of the braided river depositional environment. *Earth-Science Review*, 13, 1–62.
- Miall, A.D., 1978, Lithofacies types and vertical profile models in braided river deposits: a summary, *in* Miall, A.D., eds., *Fluvial sedimentology*: Canadian Society of Petroleum Geology, Mem. 5, p. 597–604.
- Mutti, E., 1977, Distinctive thin-bedded turbidite facies and related depositional environments in the Eocene Hecho Group (South-central Pyrenees, Spain): *Sedimentology*, v. 24, p. 107–131.
- Patton, W.W., Jr., Moll, E.J., and King, H.H., 1984a, The Alaska mineral resource assessment program; Guide to information contained in the folio of geologic and mineral resource maps of the Medfra Quadrangle, Alaska: U.S. Geological Survey Circular 923, 11 p.
- Plafker, G., and Berg, H.C., 1994, Overview of the geology and tectonic evolution of Alaska, *in* Plafker, G., and Berg, H.C., eds., *The Geology of Alaska*: Boulder, Colorado, Geological Society of America, *Geology of North America*, v. G-1, p. 989–1021.

- Posamentier, H.W., and Allen, G.P., 1993, Variability of the sequence model: effects of local basin factors: *Sedimentary Geology*, v. 86, p. 91–109.
- Reed, B.L., Nelson, S.W., 1980. Geologic map of the Talkeetna quadrangle, Alaska. U.S. Geological Survey Map I-1174, 15 p., scale 1:250,000.
- Ricci Lucchi, F., 1975, Miocene paleogeography and basin analysis in the periadriatic Appenines, in Squyres, C., ed., *Geology of Italy: Tripoli, Libya, Petroleum Exploration Sociey of Libya*, p. 5–111.
- Simons, D.B., and Richardson, E.V., 1961, Forms of bed roughness in alluvial channels: *Am. Soc. Civil Engineers Proc., Jour. Hydraulics Div.*, v. 87 (HY3), p. 87–105.
- Stow, D.A.V., & Shanmugam, G. 1980. Sequence of structures in fine-grained turbidites: comparison of recent deep-sea and ancient flysch sediments. *Sedimentary Geology*, 25, 23–42.
- Sunderlin, D., 2008, The flora, fauna, and sediments of the Mount Dall Conglomerate (Farewell Terrane, Alaska, USA), in Blodgett, R.B., and Stanley, G.D., Jr., eds., *The terrane puzzle: New perspectives on paleontology and stratigraphy from the North American Cordillera: Geological Society of America Special Paper 442*, p. 133–150, doi: 10.1130/2008.442(09).
- Walker, R. G., 1978, Deep-water sandstone facies and ancient submarine fans: Models for exploration for stratigraphic traps: *American Association of Petroleum Geologists Bulletin*, v. 62, p. 932–966.
- Wilson, F.H., Dover, J.H., Bradley, D.C., Weber, F.R., Bundtzen, T.K., Haeussler, P.J., 1998. Geologic map of central (interior) Alaska: U.S. Geological Survey Open-File Report 98–133, 64 p., 3 plates, scale 1:500,000 (also released as a CD-ROM).

## **CHAPTER 3: PROVENANCE OF THE MYSTIC PASS FORMATION**

### **3.1 INTRODUCTION**

The addition of allochthonous material to a continental margin is one of the fundamental processes in the tectonic development of an orogenic belt. In many Cenezoic and even Mesozoic mountain belts the plate configuration driving orogenesis can often be directly observed along a continental margin. However, in the case of many Paleozoic orogenic belts (e.g. Appalachians, Urals), often the best remaining record of tectonic processes is preserved in the siliciclastic stratigraphy of sedimentary basins (e.g. Queenston and Catskill clastic wedges of the Appalachian orogen). Exhumation associated with accretionary events may be long-lived (>50 Myr) and result in thick successions of synorogenic clastic strata (>3 km) that record the provenance and depositional history of accretion through time. Recent advances in the application of U-Pb detrital zircon geochronology coupled with classic approaches in framework modal compositions provide a sensitive tool for understanding detrital contributions during accretionary events (e.g. Gehrels et al., 1995; DeGraaff-Surpless et al., 2003; Weislogal et al., 2006; Leier et al., 2007, Hampton et al., 2007; 2010). Comparing relative detrital contributions with known sources allows for a first order constraint on the provenance of a sedimentary basin.

An unresolved problem in the evolution of the North American Cordillera is the pre-Mesozoic accretionary history of tectonostratigraphic terranes along the continental margin of the northern Cordillera. One of the more regionally extensive and least understood of these terranes is the Farewell terrane in southwest and west-central Alaska

(Figure 3.1) which consists of: 1) latest Neoproterozoic through lower Paleozoic (Devonian) shallow-marine, mainly carbonate strata of the Nixon Fork subterrane, 2) lower Paleozoic (Cambrian–Devonian) interbedded submarine fan turbidite deposits and carbonate units of the Dillinger subterrane, and 3) upper Paleozoic (Devonian–Permian) to lower Mesozoic (Jurassic) siliciclastic strata of the Mystic subterrane. A key debate surrounding the tectonic evolution of the Farewell terrane is its origin and Paleozoic displacement history. A range of models have been proposed for the tectonic origin and paleogeographic evolution that include (1) the Farewell terrane represents a displaced fragment of the Paleozoic continental margin of North America (Jones et al., 1982; Decker et al., 1994), (2) the presence of Paleozoic flora and fauna of Siberian affinity indicate that the Farewell terrane represents a displaced (rifted) fragment of the Siberian platform (Blodgett et al., 2002), and (3) faunal and stratigraphic evidence suggests that the early Paleozoic development of the Farewell terrane may be linked with the Arctic Alaska–Chukotka microplate as they both contain a mix of Siberian and Laurentian fossils (Dumoulin et al., 2002).

This study focuses on the provenance of the upper Paleozoic siliciclastic strata from the Mystic subterrane to provide a first-order constraint on the upper Paleozoic displacement history of the Farewell terrane. New data from the Mystic Pass formation is provided by U-Pb detrital zircon geochronology as well as sandstone modal compositions from exposures in the Mystic Pass region of the western Alaska Range (Figure 3.1). These data allow for a comparison between the ages of detrital grains within the Mystic Pass formation and the ages of known magmatic bodies, which can then be evaluated as potential source areas.



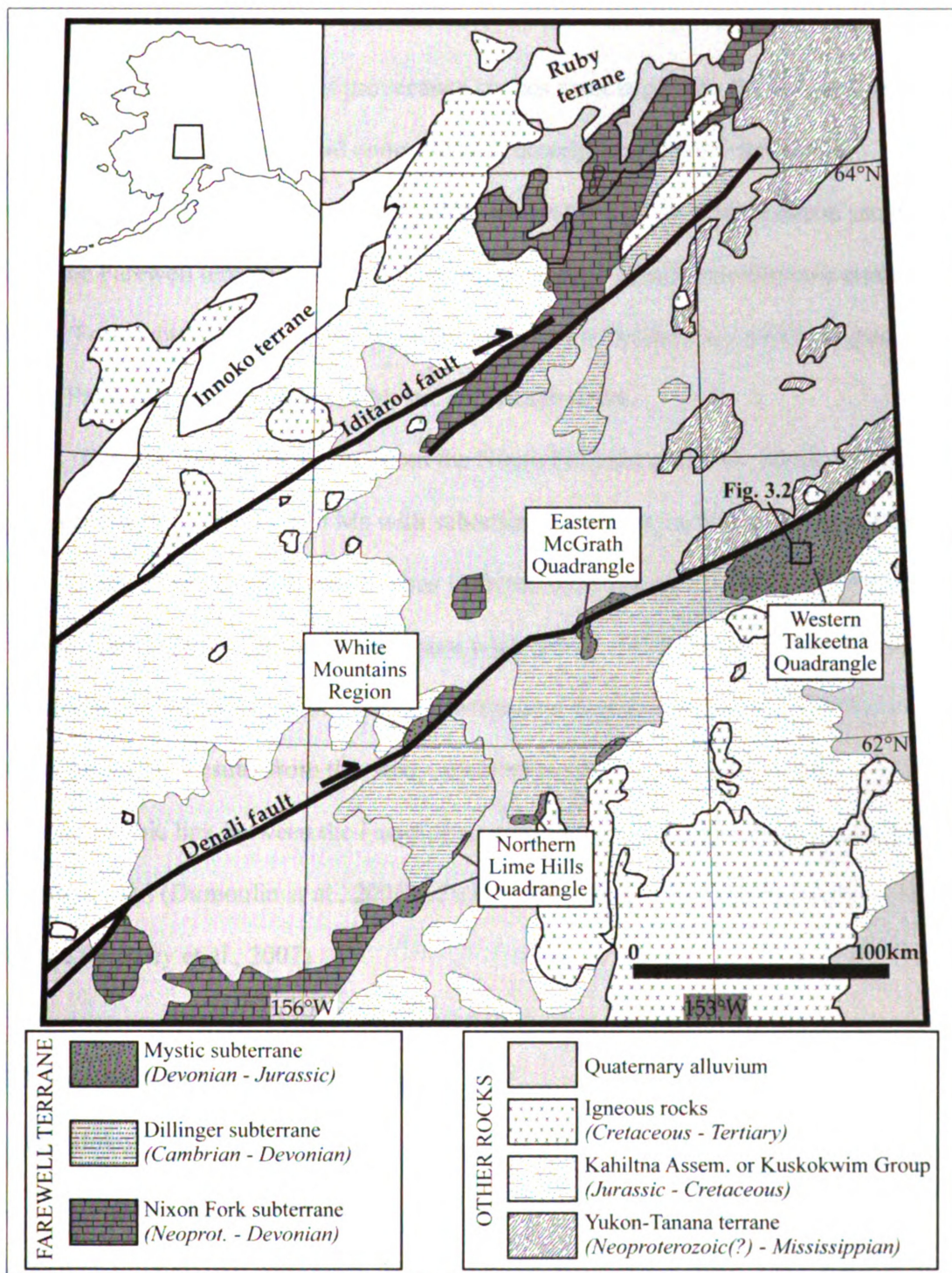


**Figure 3.1.** Generalized geologic map showing the regional area of interest and the distribution of exposed portions of the Farewell terrane. The majority of Farewell exposures are in the Alaska Range south of the Denali fault, but crop out as far North as the Kuskokwim Mountains north of the Iditarod fault. Note the small box in the western Talkeetna quad. shows the field area in Figure 3.2. Modified from Bradley et al., 2003.

### **3.2 PREVIOUS WORK**

To date, the majority of provenance studies associated with the Farewell terrane consist of general lithologic and compositional descriptions and detrital zircon geochronology. Bradley et al. (2007) published analyses of six detrital zircon samples from the Farewell terrane. Three of these samples were from Neoproterozoic strata of the Nixon Fork subterrane, and other three samples were collected from rocks mapped as being Paleozoic and belonging to Mystic subterrane strata.

Detrital zircon populations from the Nixon Fork samples were dominated by grains between ca. 1900–2100 Ma with subordinate peaks at ca. 900 Ma and ca. 1300 Ma. Age distributions of detrital zircons from the three younger samples thought to belong to the Mystic subterrane were more widespread. These samples were concluded to contain depositional ages of Triassic (interbedded ashfall tuff age), Carboniferous(?), and Silurian(?). Results from this study are cited as supporting evidence for a Neoproterozoic link between the Farewell terrane and Siberia and are said to strengthen the suggestion (Dumoulin et al., 2002) of a lower Paleozoic link with the Arctic Alaska terrane (Bradley et al., 2007).

### **3.3 SANDSTONE PETROGRAPHY**

#### **Methodology**

Standard petrographic thin sections were made from 31 medium-grained sandstone samples that were collected sporadically throughout the Mystic Pass formation (Figure 3.2). The thin sections were stained for potassium and calcium feldspar and point-counted using a modified Gazzi-Dickinson method (Dickinson, 1970; Ingersoll et



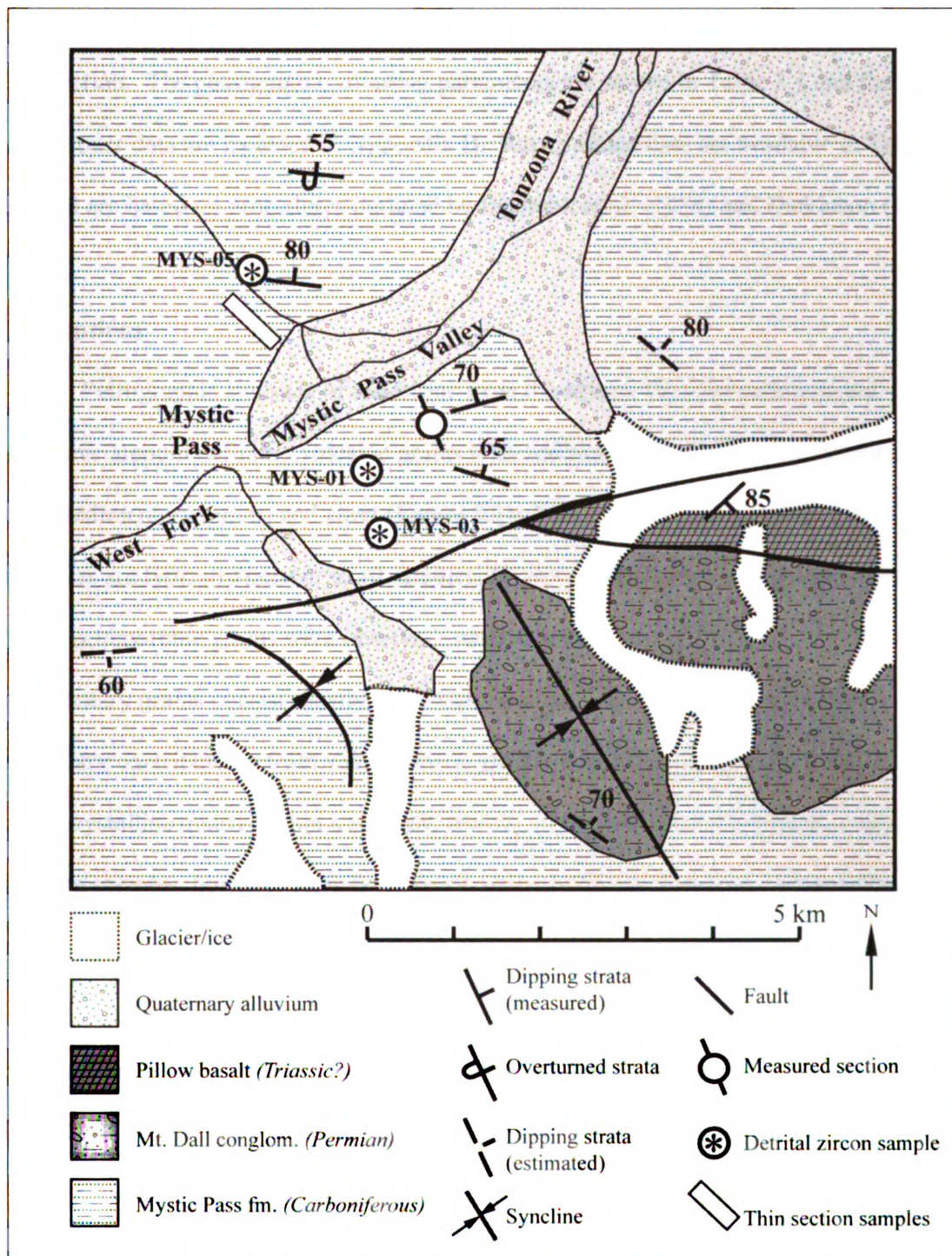


**Figure 3.2.** Geologic map showing the field area (Mystic Pass) in the western Alaska Range. This study is focused on the most prevalent map unit shown here, the Mystic Pass formation. Most thin section samples were collected where the white box is located with additional samples from detrital zircon and measured section localities. Circled asterisks show the general locations of where detrital zircon samples were collected along with their abbreviated sample name. Modified from Reed and Nelson, 1980.

al., 1984). Modal compositions were determined by indentifying 400 grains from each thin section. The petrographic counting parameters are shown in Table 3.1 and the raw point-count data are included in Appendix B. Recalculated data are available in Table 3.2 and are based on procedures outlined by Ingersoll et al. (1984) and Dickinson (1985).

## **Descriptions**

Petrographic analyses of sandstone from the Mystic Pass formation reveal pervasive amounts of lithic volcanic grains with additional significant contributions of lithic sedimentary grains, and chert (Figure 3.3). Mono- and polycrystalline quartz and feldspars are typically present in all samples, however only in minor amounts. Very few lithic metamorphic grains were observed, most of which are meta-chert. Lithic sedimentary grains consist mostly of fine-grained, argillaceous siliciclastics with secondary contributions from volcanoclastic grains, which commonly appear as monocrystalline quartz within a volcanic matrix. Low-grade metamorphism is apparent in some samples, however grain boundaries are identifiable. Figure 3.4 demonstrates the relative abundances of the average thin section sample from the Mystic Pass formation.

Modal compositions from the Mystic Pass formation are characterized predominantly by lithic grains and minor amounts of quartz and feldspar (Q-17%, F-2%, L-81%) (Figure 3.5A). The total quartz composition consists of monocrystalline quartz (Qm), polycrystalline quartz (Qp), and chert (C) with chert being the most common constituent. Feldspars are rare and consist mostly of plagioclase grains (P) with minor

**Table 3.1.** Summary of parameters for sandstone point counts.  
Note that the parameters shown above refer only to those grains identified. For example, mudstone and volcaniclastics were the only observed lithic sedimentary grains.

---

**- Quartz (Q) = Qm + Qp + chert**

-Monocrystalline quartz (Qm)

-Polycrystalline quartz (Qp)

-Chert (C)

**- Feldspar (F) = P + K**

-Plagioclase feldspar (P)

-Potassium feldspar (K)

**- Lithic fragments (L) = Ls + Lm + Lv**

-Lithic sedimentary (Ls)

-Mudstone (Lsm)

-Volcaniclastic (Lsvc)

-Lithic metamorphic (Lm)

-Lithic volcanic (Lv)

**Lt = Lv + Ls + Lm + Qp + chert**

---



**Table 3.2.** Recalculated modal point-count percentage data for sandstone samples of the Mystic Pass formation. All sample numbers beginning with “MYN” were collected northwest of the Mystic Pass valley, those beginning with MYS were collected with the measured section, and the last three samples shown above represent modal compositions of detrital zircon samples. See Figure 3.2 for sample locations.

Sample No	Q-F-L %			Qm-F-Lt %			Qm-P-K %			Lv-Lm-Ls %		
	Q	F	L	Qm	F	Lt	Qm	P	K	Lv	Lm	Ls
MYN 080709-01	4	1	94	0	1	98	25	25	50	96	0	4
MYN 080709-02	13	4	82	1	4	95	23	55	23	92	1	7
MYN 080709-03	12	6	82	1	6	93	18	46	36	96	0	4
MYN 080709-04	12	4	85	2	4	95	32	45	23	97	0	3
MYN 080709-05	9	6	85	2	6	92	28	38	34	94	0	6
MYN 080709-07	18	5	78	3	5	93	38	41	21	94	0	6
MYN 080709-08	10	4	86	3	4	94	42	23	35	92	0	8
MYN 080709-09	32	5	63	5	5	91	47	18	34	90	0	10
MYN 080709-10	20	2	79	3	2	96	63	38	0	77	0	23
MYN 080709-11	28	1	72	6	1	94	88	4	8	85	0	15
MYN 080709-12	26	1	73	4	1	95	75	25	0	84	3	13
MYN 080709-13	25	1	75	5	1	95	82	14	5	80	0	20
MYN 080709-15	14	1	85	2	1	97	64	7	29	73	1	26
MYN 080709-16	22	1	77	3	1	96	73	20	7	75	0	25
MYN 080709-17	24	0	76	3	0	97	92	8	0	72	0	28
MYN 080709-18	23	1	76	2	1	97	75	17	8	71	0	29
MYN 080709-19	31	1	68	5	1	94	83	4	13	77	0	23
MYN 080709-20	29	2	69	6	2	92	71	23	6	81	0	19
MYN 080709-21	18	4	79	6	4	90	60	30	10	81	0	19
MYN 080709-22	17	2	81	2	2	97	57	36	7	71	0	29
MYN 080709-23	18	3	79	6	3	91	69	14	17	77	0	23
MYN 080709-24	13	1	86	4	1	96	82	18	0	78	0	22
MYN 080709-25	11	3	87	3	3	95	50	25	25	82	0	18
MYN 080709-26	17	3	80	8	3	90	73	17	10	78	0	22
MYN 080709-28	15	1	84	5	1	94	78	9	13	75	0	25
MYS 080709-04	4	1	96	3	1	97	83	8	8	83	0	17
MYS 080709-07	12	1	88	3	1	96	81	19	0	75	0	25
MYS 080709-08	6	1	93	1	1	98	50	50	0	75	0	25
01 DZ	11	2	88	6	2	92	77	6	16	77	0	23
03 DZ	10	1	89	5	1	94	79	13	8	65	0	35
05 DZ	19	3	78	7	3	90	69	26	5	78	0	22

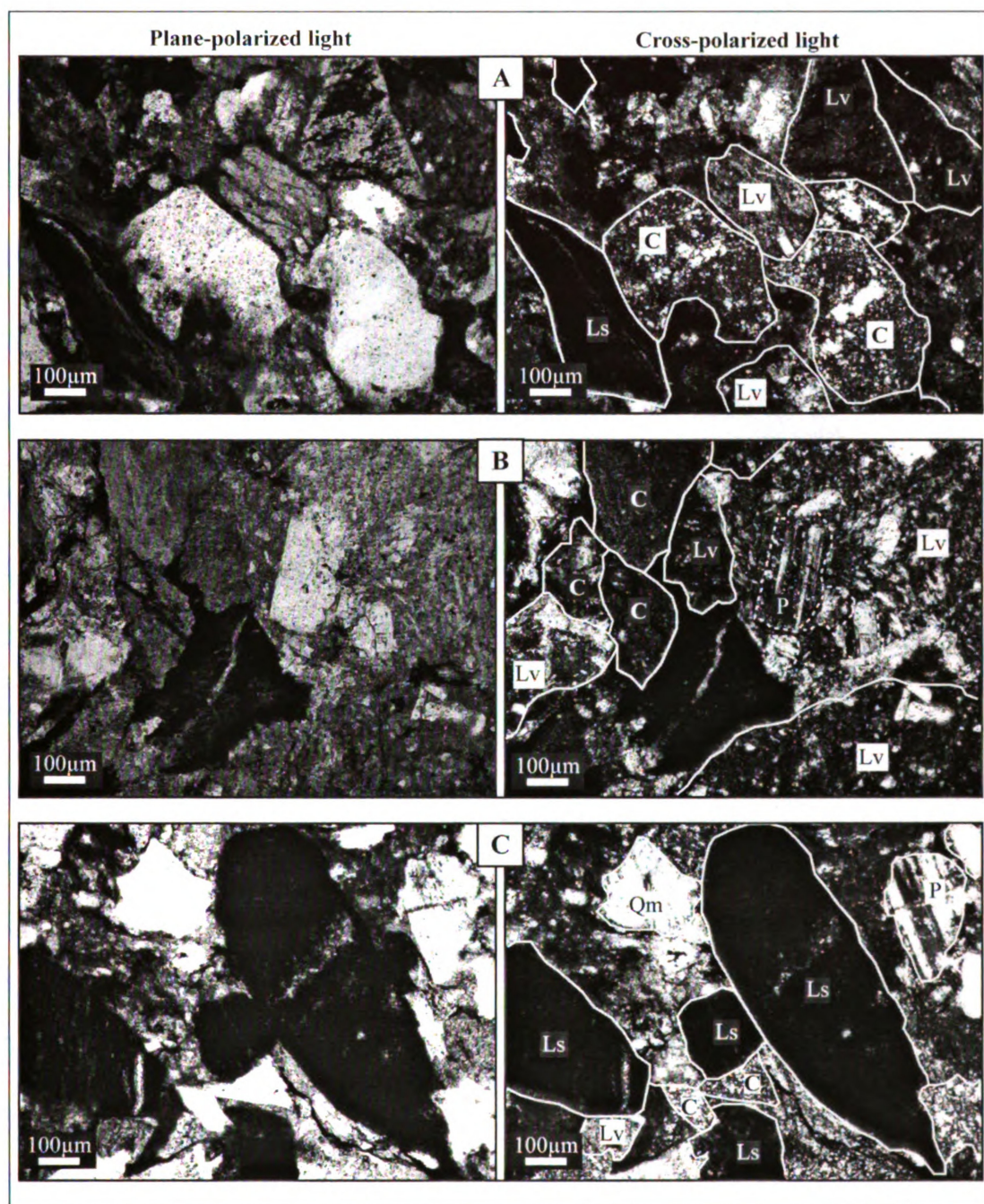


**Figure 3.3.** Sandstone petrography of the Mystic Pass formation. Photomicrographs are shown in both plain-polarized light (PPL) on the left and cross-polarized light (XPL) on the right. The scale bar is in the lower-left corner of each photo. (A) A characteristic sample showing the presence of lithic volcanic (Lv) and lithic sedimentary (Ls) grains, monocrystalline quartz (Qm), chert (C), and plagioclase (P), which are common in nearly all thin sections from the Mystic Pass formation. (B) Another sample demonstrating the abundance of lithic volcanic grains with subordinate lithic sedimentary grains. (C) A more sedimentary lithic rich sample exemplifying the fine-grained nature of lithic sedimentary grains and volcanic lithic grains; lithic volcanic grains, monocrystalline quartz, chert, and plagioclase are also seen in this sample.



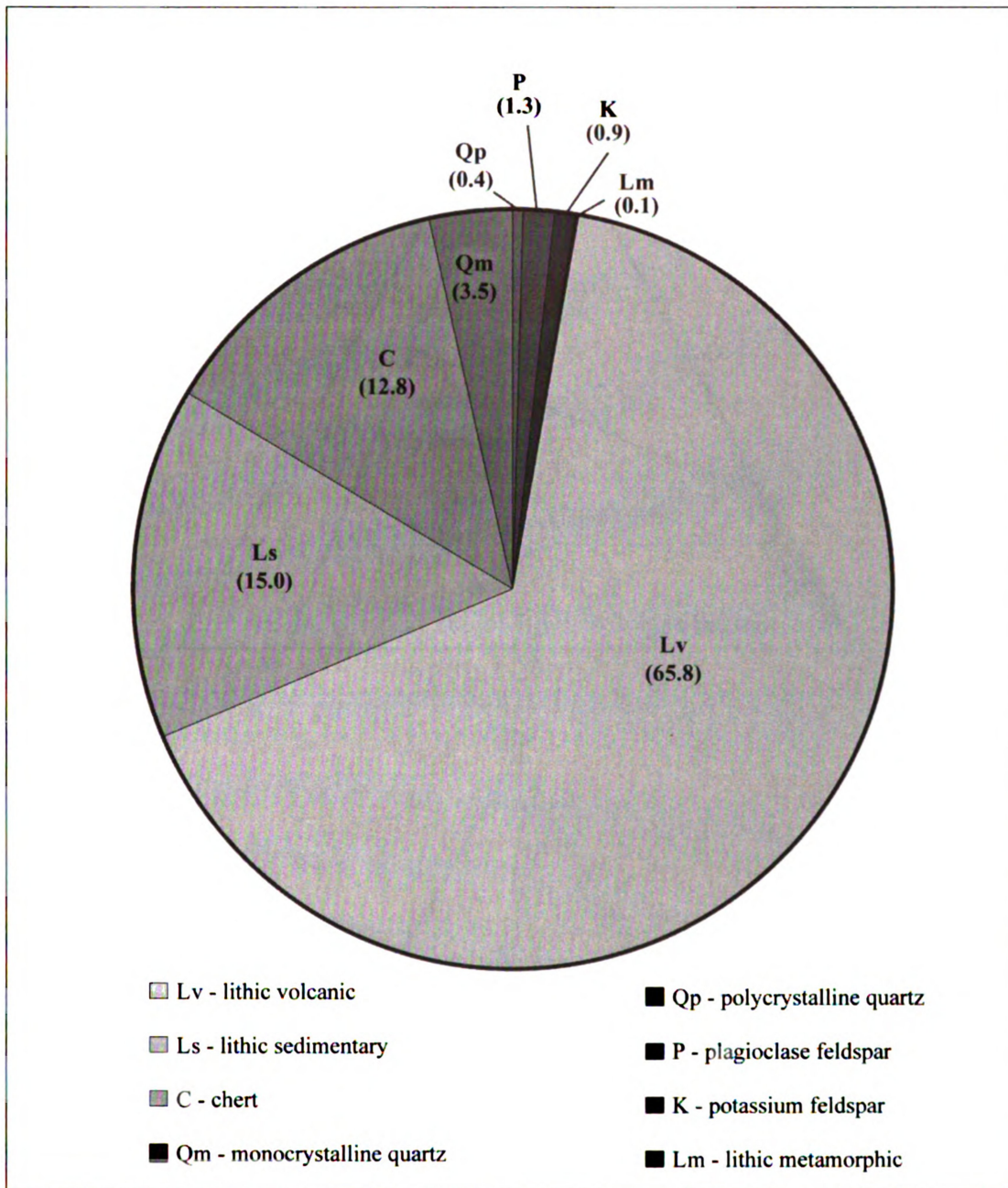


**Figure 3.4.** Average modal composition of all sandstone samples from the Mystic Pass formation.

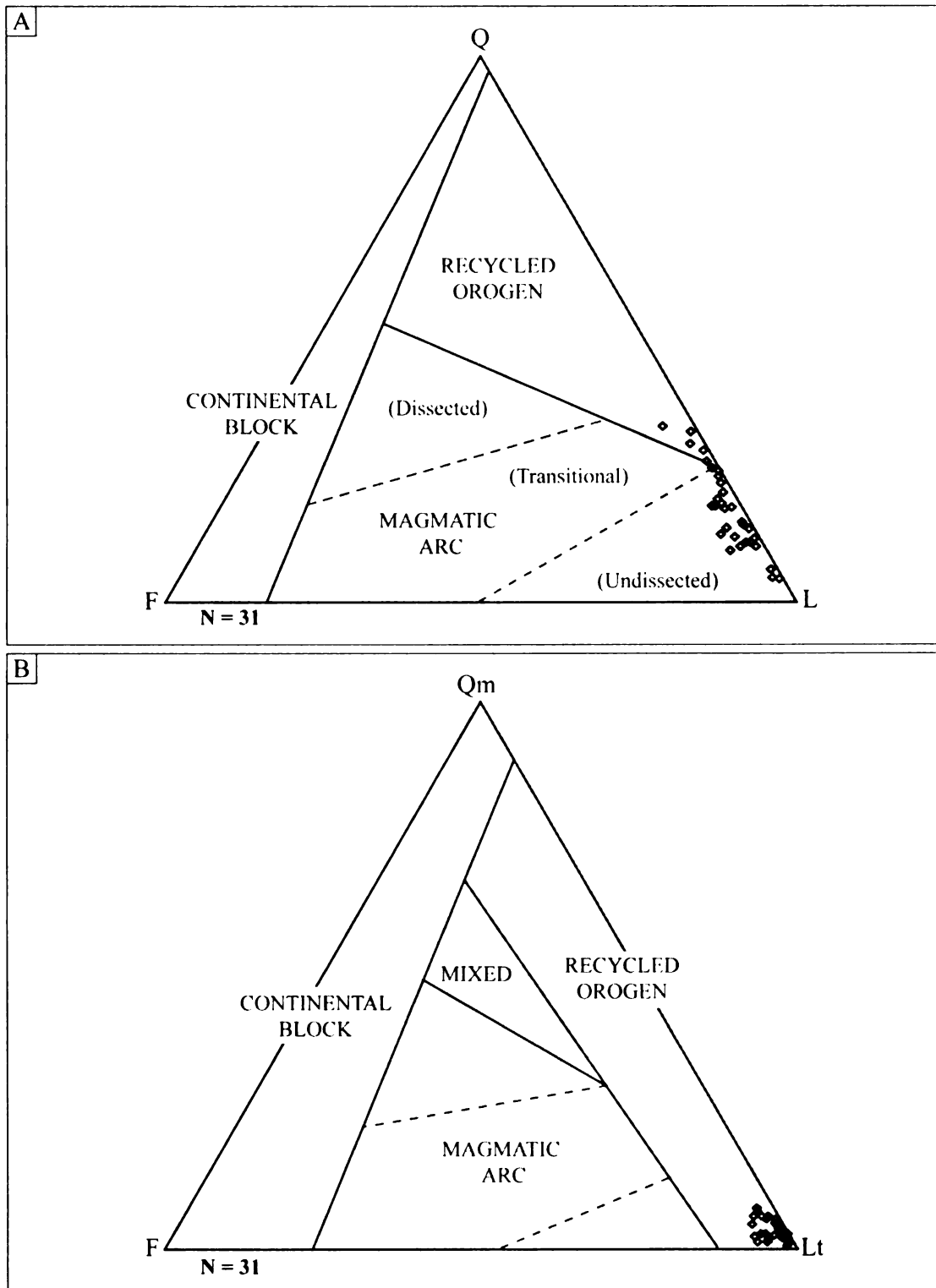


**Figure 3.5.** Sandstone modal compositions II. Relative abundances of framework grains from the Mystic Pass formation. See Table 2.1 for a summary of parameters and abbreviation symbols. Black diamonds denote sample locations. N - number of samples. Provenance fields are from Dickinson et al., 1983.

occurrences of potassium feldspar (K) (Qm-62%, P-23%, K-15%) (Figure 3.6A). Lithic grain populations are largely volcanic-derived (Lv) and also contain abundant portions of sedimentary grains (Ls) (Lv-81%, Lm-0%, Ls-19%) (Figure 3.6B).

### **Interpretation**

Comparing these data with the provenance fields of Dickinson et al. (1983), the composition of sandstone within the Mystic Pass formation is most similar to sandstone derived from an “arc-related” (undissected to transitional) “recycled orogen” (Figure 3.5). When comparing total quartz (Q), feldspars (F) and lithic fragments (L), the majority of the samples plot within the undissected magmatic arc provenance field (Figure 3.5A). However, a comparison between monocrystalline quartz (Qm), feldspars (F), and total lithic grains (Lt) shows that all samples plot within the recycled orogen provenance field (Figure 3.5B). In addition to the interpretations provided by these two provenance fields, the overall abundance of lithic volcanic grains (Lv) (Figure 3.4) suggests that the deposition system associated with the Mystic Pass formation was provided with significant proportions of arc-derived detritus, which likely indicates nearby exhumation of a magmatic arc.

### **3.4 U-Pb DETRITAL ZIRCON ANALYSIS**

Three sandstone samples were collected from exposures of upper Paleozoic strata of the Mystic subterrane for U-Pb detrital zircon analysis. All samples were collected from the Mystic Pass formation near Mystic Pass proper in the western Talkeetna



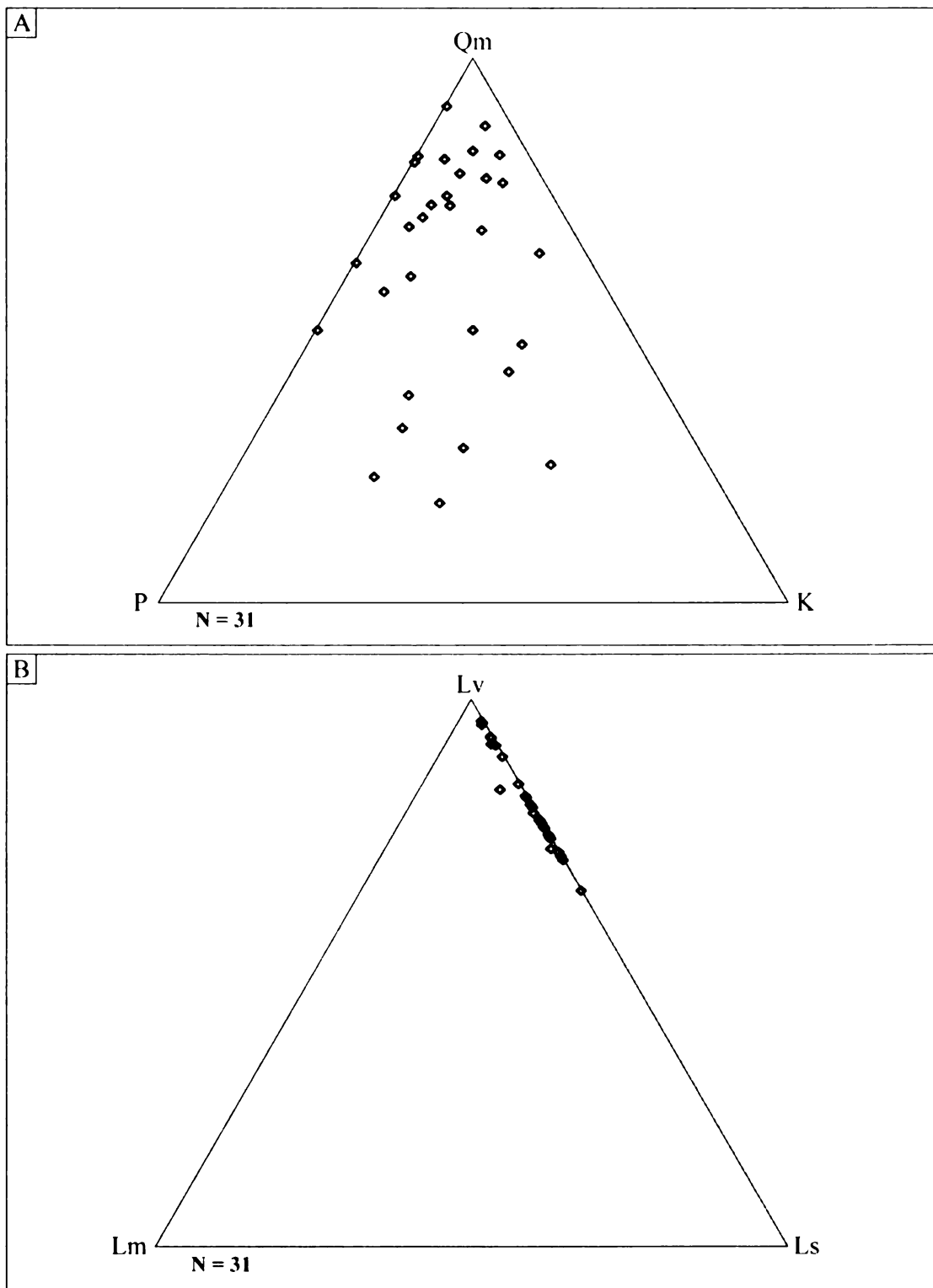


**Figure 3.6.** Sandstone modal compositions II. Relative abundances of framework grains from the Mystic Pass formation. See Table 2.1 for a summary of parameters and abbreviation symbols. Black diamonds denote sample locations. N - number of samples.

quadrangle in southwest Alaska (Figure 3.2). Brief descriptions of the sampled strata and specific locations are presented below.

### **Sample Location and Lithologic Summary**

**MYS 080209 – 01** (62° 38.495 N, 152° 29.788 W) – This sample was collected from a massive fine- to medium-grained sandstone bed approximately 1.25 m thick just south of the Mystic Pass valley (Figure 3.2).

**MYS 080309 – 03** (62° 38.216 N, 152° 29.777 W) – This was collected south of the Mystic Pass valley (Figure 3.2) from a small outcrop of interbedded fine-grained sandstone and mudstone.

**MYN 080709 – 05** (62° 39.573 N, 152° 31.560 W) – This fine- to medium-grained sandstone sample was collected north of Mystic Pass valley (Figure 3.2) and taken from a massive, tabular sandstone bed approximately 20 cm thick.

### **Methodology**

Zircon crystals were extracted by traditional methods of crushing and grinding, followed by separation with a Wilfley table, heavy liquids, and a Frantz magnetic separator. Samples were processed such that all zircons were retained in the final heavy mineral fraction. A large split of these grains (generally 1000-2000) was incorporated into a 1” epoxy mount together with fragments of a Sri Lanka standard zircon. The mounts were sanded down to a depth of ~20 microns, polished, imaged, and cleaned prior

to isotopic analysis.

U-Pb geochronology of zircons was conducted by laser ablation multicollector inductively coupled plasma mass spectrometry (LA-MC-ICPMS) at the Arizona LaserChron Center (Gehrels et al., 2006, 2008). The analyses involve ablation of zircon with a New Wave UP193HE Excimer laser (operating at a wavelength of 193 nm) using a spot diameter of 30 microns. The ablated material is carried in helium into the plasma source of a Nu HR ICPMS, which is equipped with a flight tube of sufficient width that U, Th, and Pb isotopes are measured simultaneously. All measurements are made in static mode, using Faraday detectors with 3e11 ohm resistors for  $^{238}\text{U}$ ,  $^{232}\text{Th}$ ,  $^{208}\text{Pb}$ - $^{206}\text{Pb}$ , and a discrete dynode ion counter for  $^{204}\text{Pb}$ . Ion yields are ~0.8 mv per ppm. Each analysis consists of one 12-second integration on peaks with the laser off (for backgrounds), 15 one-second integrations with the laser firing, and a 30 second delay to purge the previous sample and prepare for the next analysis. The ablation pit is ~15 microns in depth.

For each analysis, the errors in determining  $^{206}\text{Pb}/^{238}\text{U}$  and  $^{206}\text{Pb}/^{204}\text{Pb}$  result in a measurement error of ~1-2% (at 2-sigma level) in the  $^{206}\text{Pb}/^{238}\text{U}$  age. The errors in measurement of  $^{206}\text{Pb}/^{207}\text{Pb}$  and  $^{206}\text{Pb}/^{204}\text{Pb}$  also result in ~1-2% (at 2-sigma level) uncertainty in age for grains that are >1.0 Ga, but are substantially larger for younger grains due to low intensity of the  $^{207}\text{Pb}$  signal. For most analyses, the cross-over in precision of  $^{206}\text{Pb}/^{238}\text{U}$  and  $^{206}\text{Pb}/^{207}\text{Pb}$  ages occurs at ~1.0 Ga.

Common Pb correction is accomplished by using the measured  $^{204}\text{Pb}$  and assuming an initial Pb composition from Stacey and Kramers (1975) (with uncertainties of 1.0 for  $^{206}\text{Pb}/^{204}\text{Pb}$  and 0.3 for  $^{207}\text{Pb}/^{204}\text{Pb}$ ). Our measurement of  $^{204}\text{Pb}$  is unaffected by

the presence of  $^{204}\text{Hg}$  because backgrounds are measured on peaks (thereby subtracting any background  $^{204}\text{Hg}$  and  $^{204}\text{Pb}$ ), and because very little Hg is present in the argon gas (background  $^{204}\text{Hg} = \sim 300$  CPS).

Inter-element fractionation of Pb/U is generally  $\sim 5\%$ , whereas apparent fractionation of Pb isotopes is generally  $< 0.2\%$ . In-run analysis of fragments of a large zircon crystal (generally every fifth measurement) with known age of  $563.5 \pm 3.2$  Ma (2-sigma error) is used to correct for this fractionation. The uncertainty resulting from the calibration correction is generally 1-2% (2-sigma) for both  $^{206}\text{Pb}/^{207}\text{Pb}$  and  $^{206}\text{Pb}/^{238}\text{U}$  ages.

Concentrations of U and Th are calibrated relative to our Sri Lanka zircon, which contains  $\sim 518$  ppm of U and 68 ppm Th.

The analytical data are reported in Appendix C. Uncertainties shown in these tables are at the 1-sigma level, and include only measurement errors. Analyses that are  $> 30\%$  discordant (by comparison of  $^{206}\text{Pb}/^{238}\text{U}$  and  $^{206}\text{Pb}/^{207}\text{Pb}$  ages) or  $> 5\%$  reverse discordant are not considered further.

The resulting interpreted ages are shown on relative age-probability diagrams (from Ludwig, 2008). These diagrams show each age and its uncertainty (for measurement error only) as a normal distribution, and sum all ages from a sample into a single curve. Composite age probability plots are made from an in-house Excel program (available from [www.geo.arizona.edu/alc](http://www.geo.arizona.edu/alc)) that normalizes each curve according to the number of constituent analyses, such that each curve contains the same area, and then stacks the probability curves.

## U-Pb Age Distribution and Maximum Depositional Ages

Detrital zircon age data from the Mystic Pass formation consist of a total of 277 concordant to slightly discordant (Figure 3.7) Precambrian–Paleozoic age zircons with minor occurrences of Mesozoic age grains from one sample (Figure 3.8 and 3.9). Phanerozoic age grains (178 total) are most abundant (64%) and Precambrian age grains (99 total) are also common but with lesser abundance (36%). Of those Phanerozoic age grains, three reported Mesozoic ages (< 251 Ma) with the remaining 175 Phanerozoic grains being Paleozoic (540–251 Ma). The majority of Paleozoic age grains have ages that fall between 500 and 260 Ma with primary peak ranges of 465–405, 365–315, and 305–290 Ma. Most of the Precambrian age grains fall between 2.1 and 1.6 Ga with a primary peak range between 1.95 and 1.8 Ga. Age comparisons are based primarily on the geologic time scale of Gradstein et al. (2004).

For presenting the maximum depositional age (MDA) of each sample, three alternative measures are provided as outlined by Dickinson and Gehrels (2009). These include the youngest single grain, the youngest graphical age peak of a cluster of three or more grains, and a calculated weighted mean age (WMA) of the youngest cluster of three or more grains. Final interpretations of each sample's MDA will be based on the youngest graphical age peak of a cluster of three or more grains.

**MYS 080209–01** Sample *MYS 080209-01* is represented by 85 detrital zircon ages of which, 44% are Precambrian and 56% are Phanerozoic. The majority of Precambrian grains are present between ca. 2100–1700 Ma with a peak occurrence at 1879 Ma. All Phanerozoic age grains are Paleozoic with peaks occurring at 335, 351, 363, and 438 Ma. This sample's youngest detrital grain age is  $324 \pm 2$  Ma and the



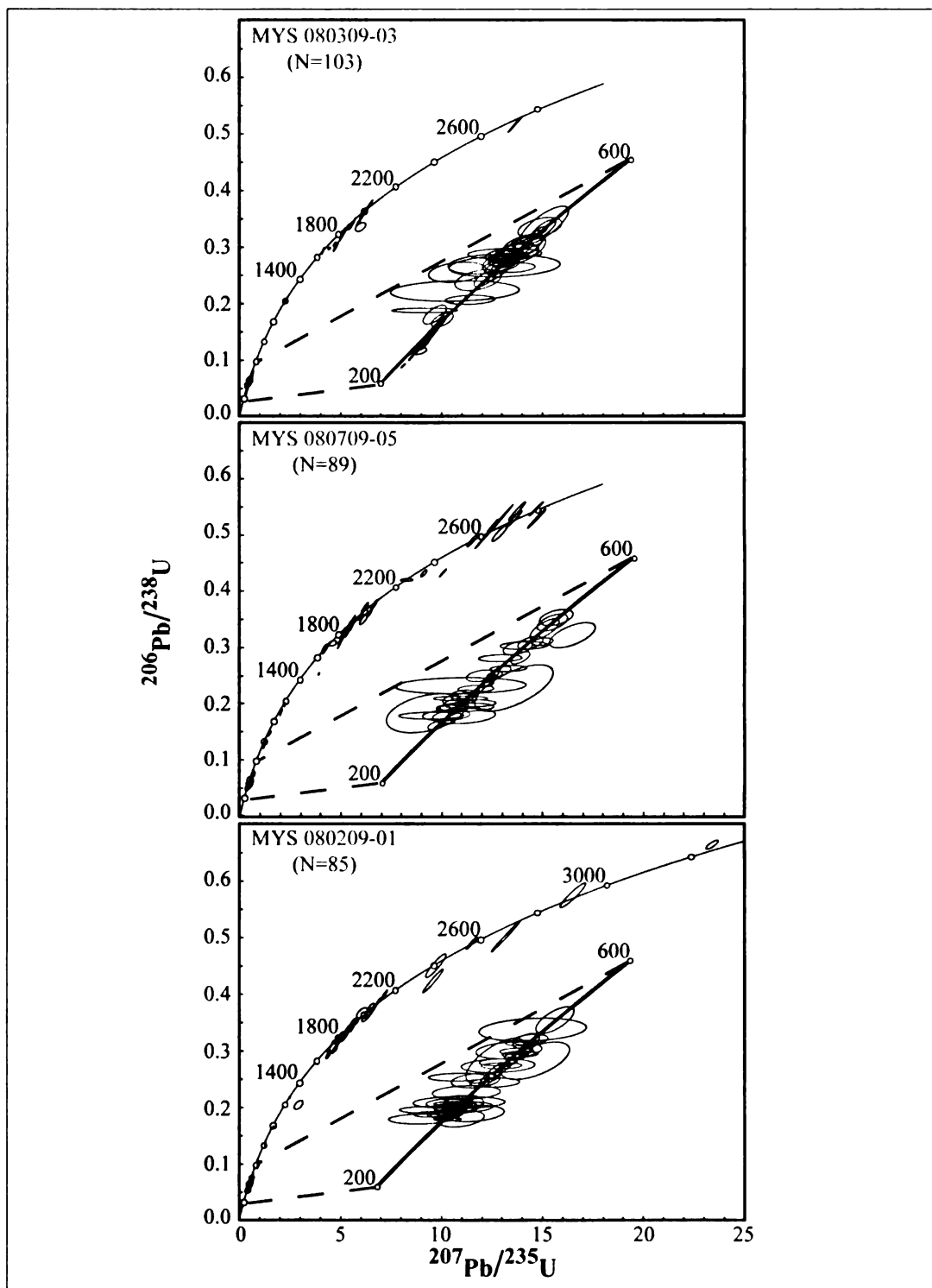


**Figure 3.7.** U-Pb concordia diagrams of single detrital zircon grains from three samples of sandstone from the Mystic Pass formation. Enlargements below each concordia curve show data for grains between 200 and 600 Ma. All data points are shown with 2-sigma error ellipses. Sample number and number of grains analyzed (N) are shown in boxes in the upper left corner of each plot.

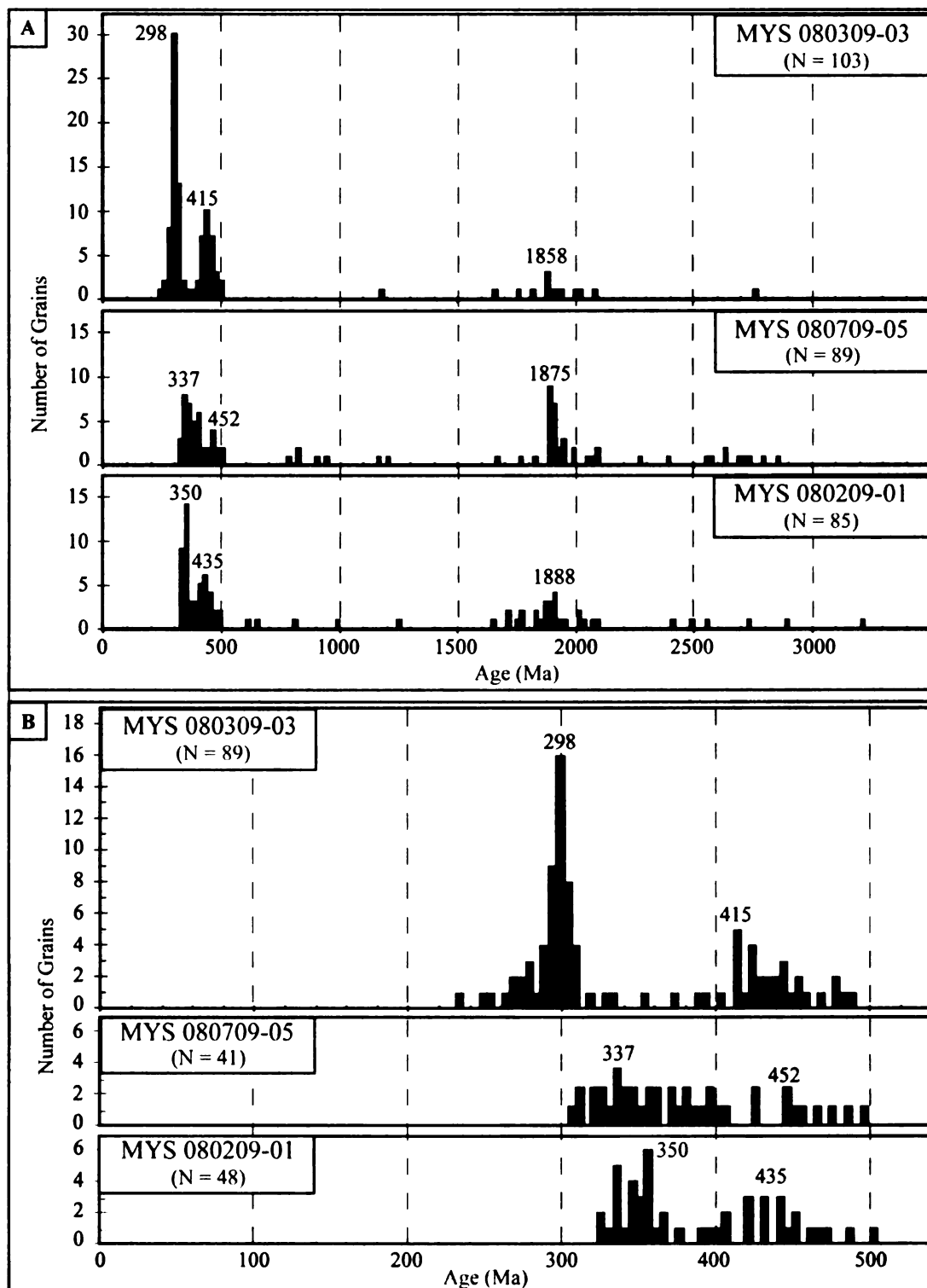


**Figure 3.8.** Detrital zircon age spectra from the Mystic Pass formation (this study). A) Histogram showing the distribution, in 20 million year bins, of ages for all grains analyzed for each sample. B) Histogram showing the distribution, in 5 million year bins, of Phanerozoic-age grains only.

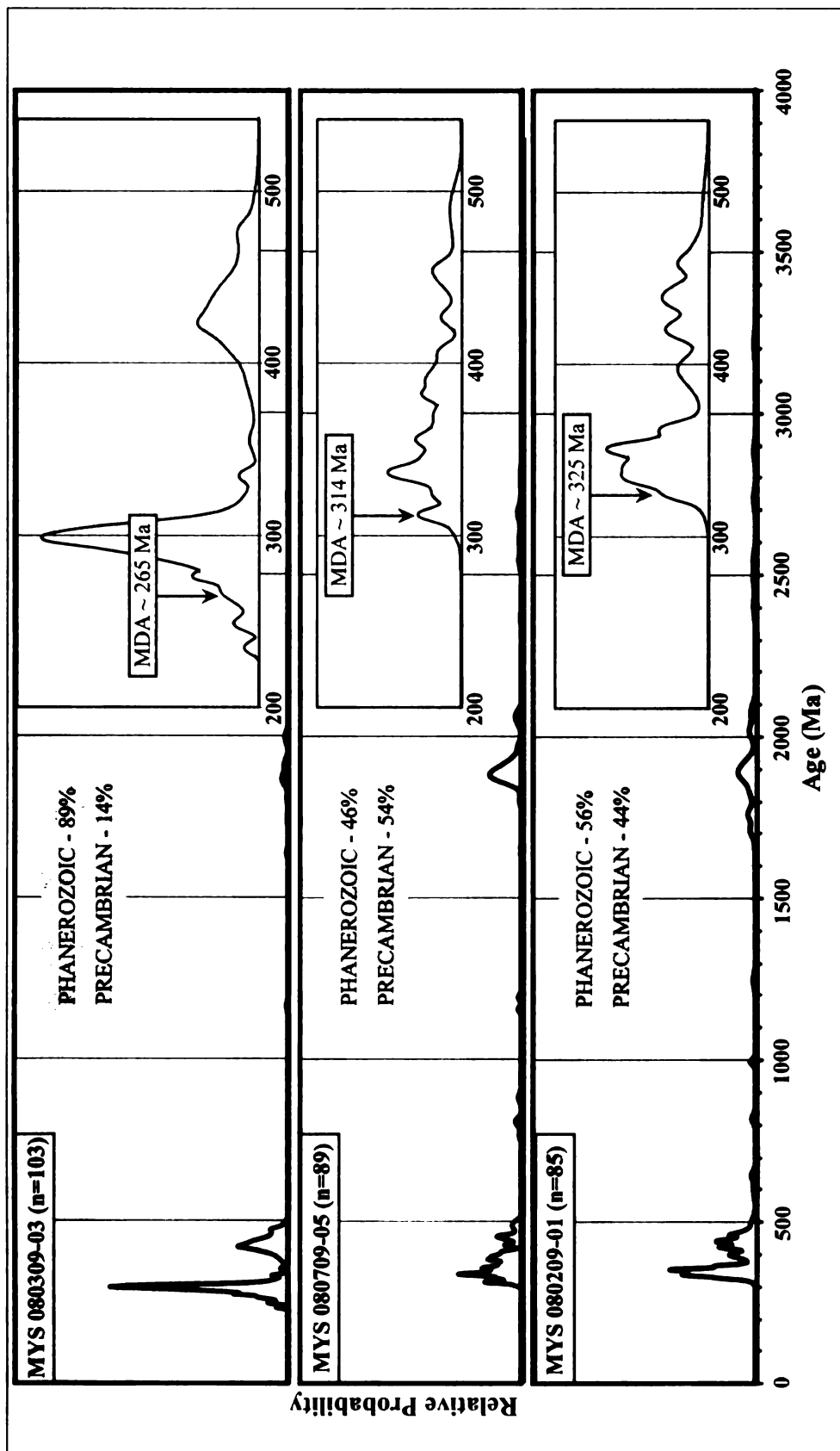


**Figure 3.9.** Normalized relative probability plots showing the distribution of detrital zircon ages from three sandstone samples of the Mystic Pass formation. The total number of grains analyzed was 277 of which 64% are Phanerozoic and 36% are Precambrian. Maximum deposition age (MDA) is determined by the youngest cluster of three or more overlapping and concordant analyses.

calculated weighted mean age is  $347.0 \pm 1.9$  Ma. The youngest age peak occurs at ca. 325 Ma.

**MYS 080309–03** Sample *MYS 080309-03* is represented by 103 detrital zircon grain ages with only 14% being Precambrian and 86% are Phanerozoic. Only 14 of 103 grains analyzed from this sample are Precambrian, which result in subtle peaks at 1865 and 2001 Ma. 86 of the 89 Phanerozoic age grains are Paleozoic while the remaining three youngest detrital grain ages ( $235 \pm 4$ ,  $248 \pm 3$ , and  $250 \pm 4$  Ma) are Mesozoic. Paleozoic age grains account for 84% of the analyses from this sample with the most prominent age peaks occurring at 275, 298, 424, and 473. The calculated weighted mean age is  $265.0 \pm 2.3$  Ma. The youngest age peak occurs at 249 Ma.

**MYS 080709–05** Sample *MYS 080709-05* is represented by 89 detrital zircon ages of which, 54% are Precambrian and 46% are Phanerozoic. The majority of Precambrian grains are present between ca. 2100–1800 Ma and display age peaks at 1895 and 1876 Ma. All Phanerozoic age grains are Paleozoic with peaks occurring at 338, 356, 389, and 453 Ma. This sample's youngest detrital grain age is  $307 \pm 7$  Ma and the calculated weighted mean age is  $333.1 \pm 2.5$  Ma with the youngest age peak occurring at 314 Ma.

Biostratigraphic age constraint for the Mystic Pass formation (map unit Pzus-Reed and Nelson, 1980) includes Late Mississippian echinoderms and Middle Pennsylvanian echinoderms and foraminifers (Reed and Nelson, 1980) collected from the western Talkeetna quadrangle. Maximum deposition ages are based on the youngest cluster of three or more overlapping and concordant analyses for samples *MYS 080209-01* and *MYS 080709-05* suggest Late Mississippian (~325 Ma) and Early Pennsylvanian

(~314 Ma) maximum deposition ages, respectively and are thus consistent with pre-existing biostratigraphic age constraints. Given that the three youngest grains from sample *MYS 080309-03* do not all overlap, they can be considered to be exhibiting lead loss. Thus the youngest cluster for this sample suggests a slightly younger maximum depositional age of Middle Permian (~265 Ma), which is only slightly younger than previous age constraint. However, if these ages are accurate, sample *MYS 080309-03* would reflect a Triassic maximum depositional age suggesting that the upper portions of the Mystic Pass formation is younger than previously reported. Also, it should be noted that detrital trends observed from this study are relatively similar to those seen in previous analyses (Bradley et al., 2007) of detrital zircons from the Mystic subterrane (Figure 3.10). In summary, maximum depositional ages provided by the youngest cluster of three or more analyses for the Mystic Pass Formation range from Late Mississippian (~325) to Middle Permian (~265) and are consistent to moderately younger than pre-existing biostratigraphic age constraints. Figure 3.11 shows a comprehensive histogram of all detrital zircon analyses from Mystic subterrane strata.

### **Provenance of Detrital Zircons**

Correlating the U-Pb ages of detrital zircons from the Mystic Pass formation with U-Pb ages of potential magmatic source areas serves as a valuable method for constraining the provenance of these strata. Relatively low uranium-thorium ratios of zircons (<10) from all three samples suggests that they reflect timing of magmatism and initial crystallization rather than thermal resetting from regional metamorphism (Figure 3.12). Detrital contributions of recycled zircon grains from Precambrian–



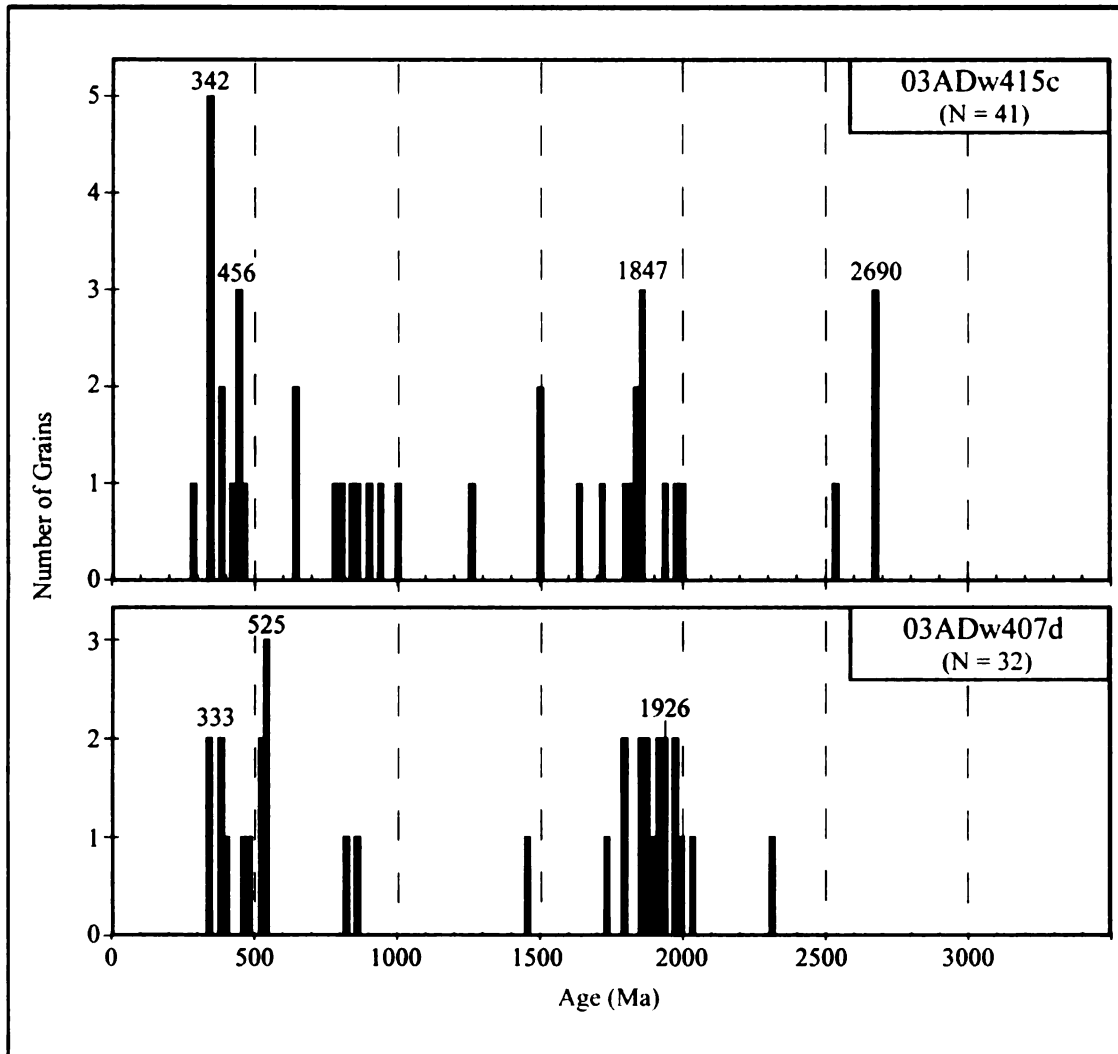


**Figure 3.10.** Detrital zircon age spectra from previous work on Mystic subterrane strata. Both samples were collected from map unit “Pzus” (Reed and Nelson, 1980) in the western Talkeetna quadrangle. The total, combined number of grains analyzed is 73. Data from Bradley et al. (2007).

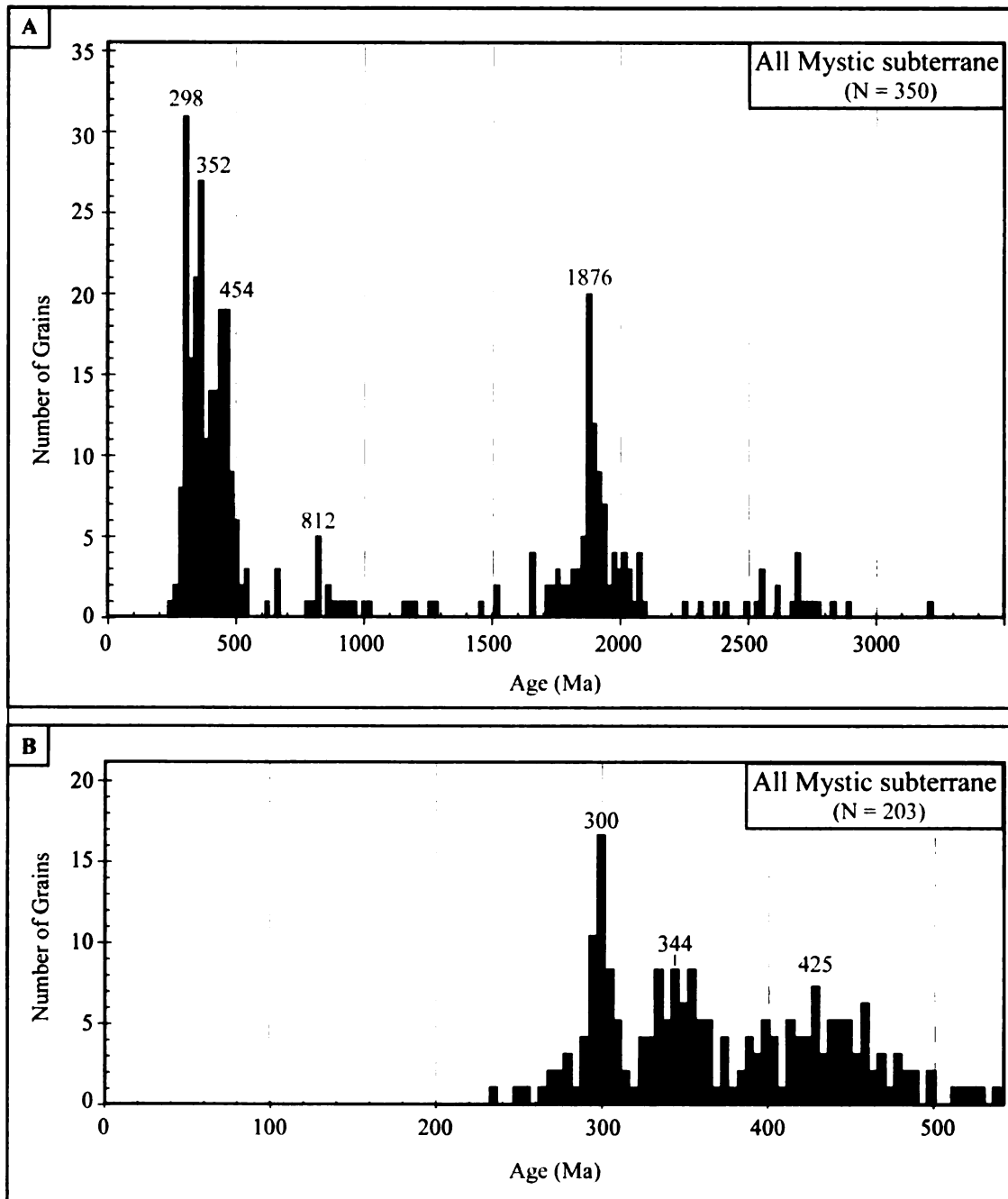


**Figure 3.11.** Summary of all detrital zircon ages from Mystic subterranean strata. Total number of grains from the Mystic subterranean is 350 of which 58% are Phanerozoic and 42% are Precambrian. A) Histogram showing the distribution, in 20 million year bins, of ages for all grains analyzed. B) Histogram showing the distribution, in 5 million year bins, of Phanerozoic-age grains only.

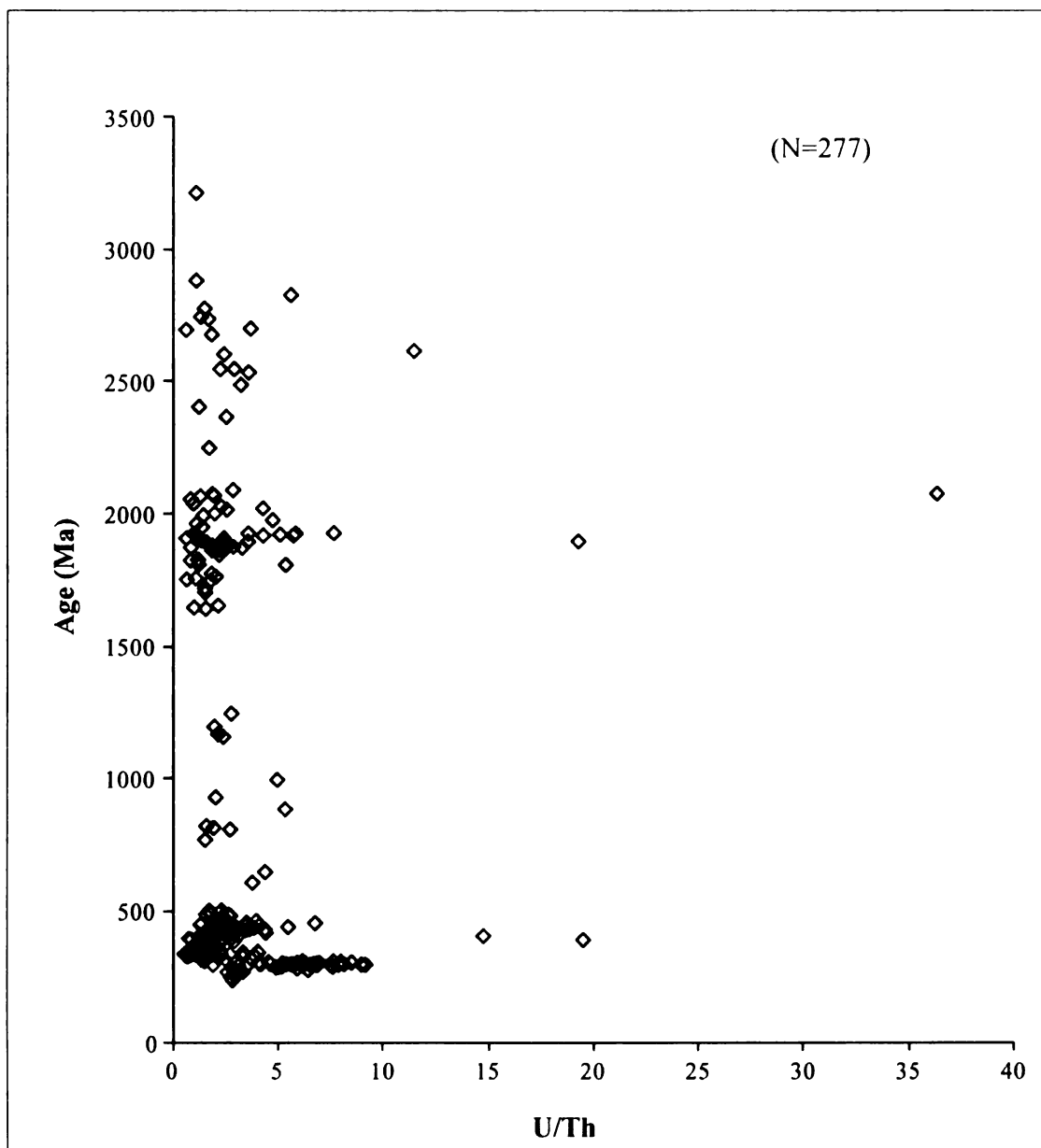


**Figure 3.12.** Plot of U/Th versus age of for all three detrital zircon samples from the Mystic Pass formation. Note that only 5 grains contain U/Th ratios greater than 10 indicating that detritus in the Mystic Pass formation was likely derived from an igneous rather than metamorphic source. N - number of samples.

Paleozoic sedimentary and metasedimentary sources likely make up a significant percentage of zircon grains. The following text outlines noteworthy magmatic source regions which may have contributed detritus to strata of the Mystic Pass formation.

Previous studies aimed at understanding the paleogeographic affinities of the Farewell terrane have suggested an Arctic origin (i.e., Decker et al., 1994; Blodgett et al., 2002; Dumoulin et al., 2002; Bradley et al., 2003, 2007; Colpron and Nelson, 2009). Thus an examination of potential source areas can likely be limited to Arctic-related sources and would ideally involve a comprehensive analysis of all known magmatic source areas in the northern hemisphere. However, given that there is no consensus on the displacement history of the Farewell terrane, and that there is a limited number of samples such an approach is exceptionally cumbersome and beyond the scope of this study. Nevertheless, the following provide a general summary of potential source areas and/or tectonic events responsible for providing detritus to the Mystic Pass formation which are either currently proximal to the Farewell terrane (i.e., Arctic Alaska and Yukon-Tanana terrane) or have been previously proposed to contain affinities with the Farewell terrane (i.e. Siberia - Uralian orogeny, Baltica - Caledonian orogeny, and other Cordilleran terranes – Alexander terrane).

### **Precambrian source areas**

Precambrian age grains account for approximately 36% of detrital zircons analyzed from the Mystic Pass formation in this study. The majority of these Precambrian grains (~66%) are between 2.1 and 1.7 Ga with all three samples containing only one major Precambrian age peak, which occurs between ca 1.95 and 1.8 Ga.

Therefore, a comparison between Precambrian trends in detrital zircons of the Mystic Pass Formation with potential magmatic source areas is focused on Paleoproterozoic magmatism between 2.0 and 1.8 Ga. It is important to note that zircons of this age are prevalent in several parts of the world including East Asia, South America, Laurentia, Australia, Africa, and Siberia (Condie, 2002; Condie et al., 2009; Safonova et al., 2010). This globally widespread presence of Paleoproterozoic granites between ca. 2.0–1.8 Ga has been suggested to reflect supercontinent assembly of Columbia (Rogers and Santosh, 2002), Nena (Rogers, 1996), or Nuna (Hoffman, 1997). A comprehensive analysis of all Paleoproterozoic source areas is beyond the scope of this study as only Arctic origins are proposed for the Farewell terrane. Thus the following comparison is limited mostly to those trends observed with regards to the Laurentian craton (North America) and the Siberian craton (Northeast Russia) (Figure 3.13).

***Northeast Russia (Siberian craton):*** The Siberian craton is located between the Ural Mountains and the Verkhoyansk fold and thrust belt (Figure 3.13) and serves as an important source for Paleoproterozoic zircons in northeast Russia. However broader Precambrian sources could also include the Baltic Shield (also referred to as the East European Craton – EEC), located west of the Urals (Figure 3.13). Detrital zircons from 5 modern major drainage basins in Russia which tap both the Siberian and Baltic cratons demonstrate a peak age occurrence, among others, between 2.0–1.8 Ga (Safonova et al., 2010). Furthermore, a study by Prokopyev et al. (2008) on detrital zircons from Pennsylvanian–Jurassic siliciclastic strata of the Verkhoyansk clastic wedge of Siberia reveals persistent contributions from Paleoproterozoic zircons between ca. 2.0–1.8 Ga,



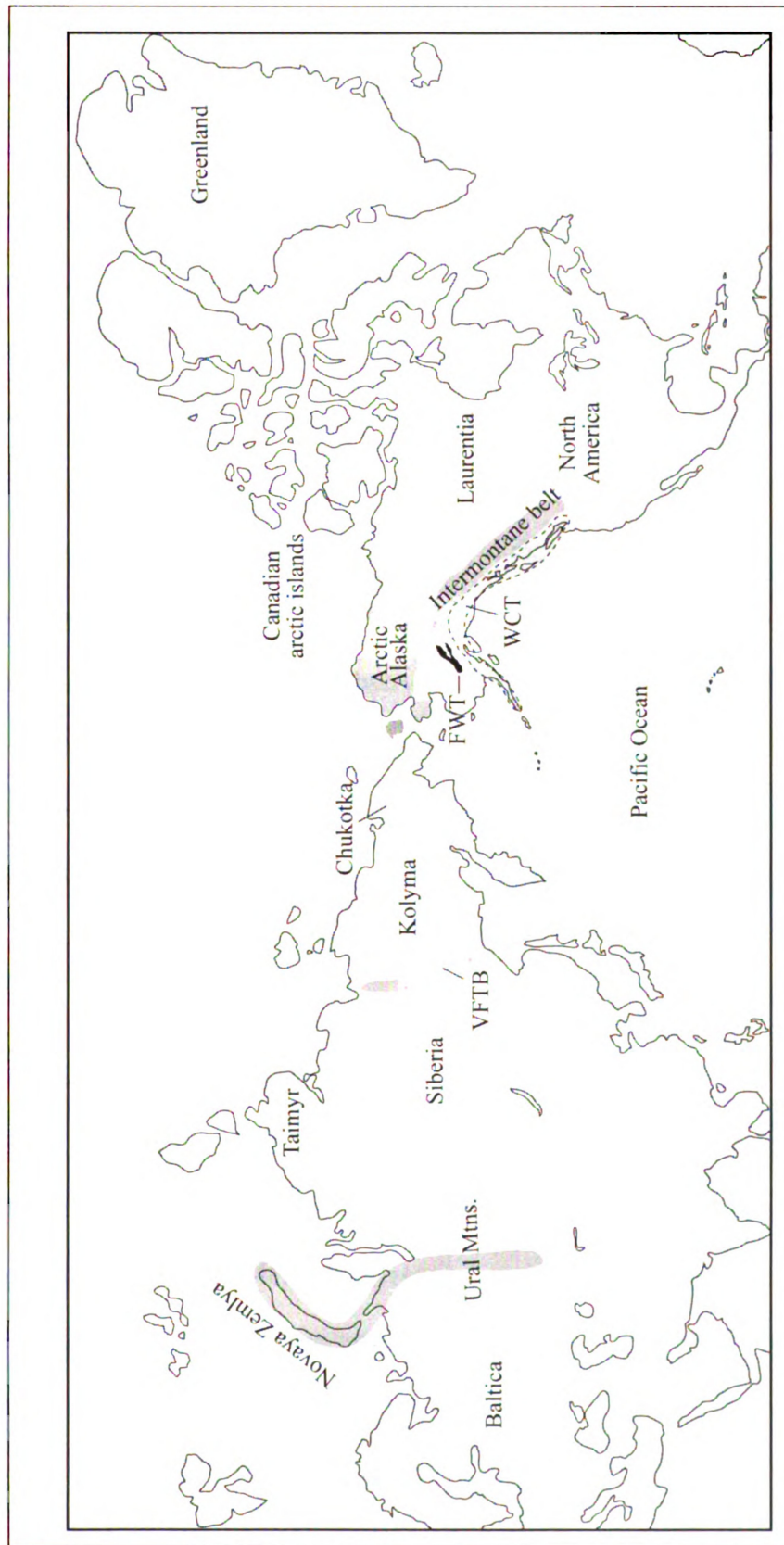


**Figure 3.13.** Unrestored map showing the modern locations of relevant sources and tectonic elements discussed in the text. Relevant portions of the Intermontane belt include the Yukon-Tanana terrane, and the Quesnellia - Slide Mountain terrane. Potential source areas from the Wrangellia composite terrane (WCT) include the Skolai arc and the Alexander terrane. FWT - Farewell bend, WCT - Wrangellia composite terrane, VFTB - Verkhoyansk fold and thrust belt

derived from the Siberian craton, indicating the availability of Siberian-derived detrital zircons in northeast Russia during the upper Paleozoic (Pennsylvanian–Permian). This study also reports a compilation of magmatic source areas from regions within and adjacent to the Siberian craton in which ~21 % of the zircon ages were within the 2.0–1.8 Ga age range.

***North America (Laurentian craton):*** Paleoproterozoic zircons between 2.0 and 1.8 Ga are prevalent in Laurentian igneous rocks and peak at approximately 1.9 Ga (Condie et al., 2009). Laurentian events contributing to the production of these zircons include the Wopmay, Penokean, Yavapai, Torngat, Cape Smith and Tans-Hudson orogens. This trend is even more commonly observed in detrital zircons from North American rocks, which peaks at ca. 1850 Ma (Condie et al., 2009). This is a characteristic trend observed in detrital zircons from miogeoclinal strata of British Columbia and Alaska (Gehrels et al., 1995) as well as in detrital zircons from Paleozoic strata of the Alexander terrane and east central Alaska (Gehrels et al., 1996; 1999).

### **Phanerozoic source areas**

Phanerozoic age grains make up the majority (64%) of detrital zircons from the Mystic Pass Formation and reflect three primary Paleozoic age peaks which comprise approximate ranges of 465–405 Ma (Middle Ordovician–Early Devonian), 365–315 Ma (Late Devonian–Early Pennsylvanian), and 305–290 Ma (Late Pennsylvanian–Early Permian). The following comparison of Paleozoic detrital trends with magmatic source areas includes much of the Arctic region as all previous studies of the Farewell terrane

have suggested an Arctic paleogeography for the Farewell terrane (e.g. Blodgett et al., 2002; Dumoulin et al., 2002; Bradley et al., 2003, 2007; Sunderlin, 2008, Colpron et al., 2009). Potential Phanerozoic sources are summarized in Figure 3.14.

***Yukon-Tanana Terrane (YTT):*** The Yukon-Tanana terrane is a northwest-southeast trending crustal fragment of pericratonic affinity that extends from the Alaska Range in east-central Alaska into the northern Canadian Cordillera in British Columbia. In general, its geology is described as a metamorphosed continental margin fragment, which was host to Upper Paleozoic (Devonian–Permian) magmatic arcs and back arcs (Nelson et al., 2006). Most of the magmatism associated with YTT is divided into a series of six cycles or time intervals, which mark major magmatic/tectonic events/cycles (Colpron et al., 2006; Piercey et al., 2006; and Nelson et al., 2006). Although magmatism is continuous from 390–253 Ma., peak intervals occur between 390–365, 365–357, 357–342, 342–314, 314–296, and 269–253 (see Nelson et al., 2006 for a summary of each cycle). Thus the YTT is a viable source option for Devonian–Permian age grains.

Other notable Paleozoic plutonic rocks in the northern Cordillera are those which are outboard of the Intermontane belt and include latest Neoproterozoic–Paleozoic sources associated with the so-called Wrangellia composite terrane (WCT). The Alexander terrane contains Permian–Triassic and Ordovician–Silurian plutonic suites with age ranges of ca. 280–220 Ma and ca. 480–410 Ma, respectively (Gehrels and Saleeby, 1987; Gehrels, 1990). Skolai arc in south and southeast Alaska and plutons on the Alexander terrane in southeast Alaska. Igneous age ranges for Skolai arc magmatism are between 285–320 Ma with a majority of ages around 310 Ma (Nokleberg et al., 1986;

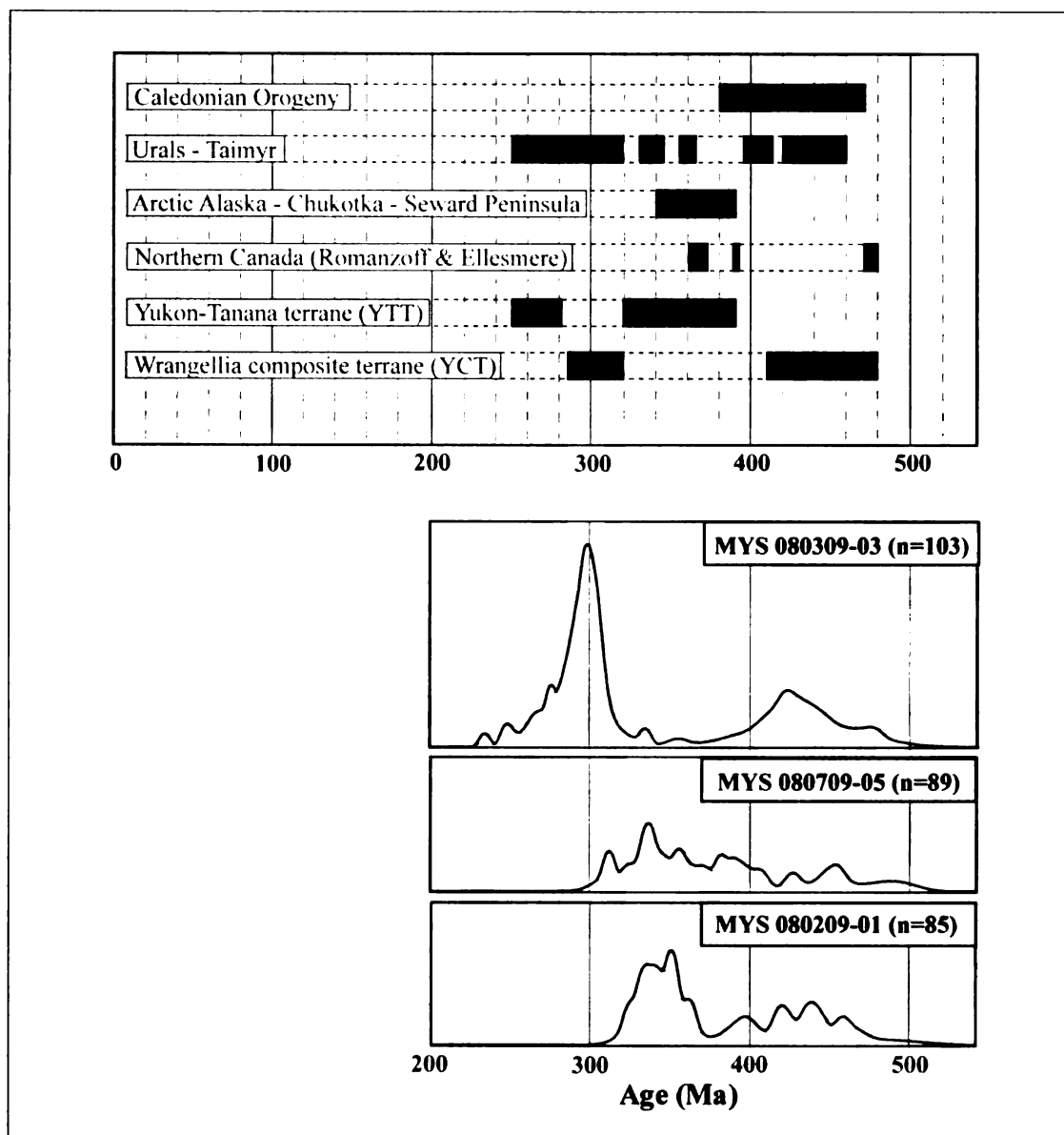


**Figure 3.14.** Summary of potential Phanerozoic source areas. Normalized relative probability plots of Phanerozoic detrital zircon ages from three sandstone samples of the Mystic Pass formation with potential source areas. Black bars represent durations of magmatism associated with each region or event. Older magmatism associated with Wrangellia composite terrane is from the Alexander terrane in southeast Alaska and the younger magmatic episode corresponds to the Skolai arc in southern Alaska.

Aleinikoff et al., 1988; Gardner et al., 1988; Beard and Barker, 1989; Plafker et al., 1989).

***Northern Canada and the Ellesmerian Orogeny:*** The Ellesmerian orogeny is proposed as a Middle Devonian to Early Mississippian event involving deformation of the Franklinian mobile belt of the northern and central Canadian Arctic Islands and northern Greenland (Trettin, 1991a). Evidence for tectonism and magmatism during this time is has been widely reported in circum-Arctic regions and is often attributed to the Ellesmerian orogeny. However, Rippington and Scott (2009) contend that there is still minimal concrete evidence to support the hypothesis of a Late Devonian to Early Carboniferous Orogen. Nevertheless, Devonian magmatism is recorded in the Cape Woods Pluton of the Arctic Islands with a cooling age of ca. 390 Ma, as well as in other smaller granitic bodies with an age of ca. 367 Ma (Trettin, 1991b). Early to Middle Ordovician granites are also reported along northern Ellesmere Island, which are suggested to be associated with the M'Clintock Orogeny (Trettin et al., 1987, and Trettin, 1991c). The Romanzof orogeny is an Early to Middle Devonian associated with deformation and widespread Late Devonian (375–362 Ma) granitic plutonism in northeast Alaska and northwest Canada (Lane, 2007).

***Caledonian – Appalachian Orogeny:*** Traditionally, regions assigned to the Caledonian orogeny included early Paleozoic areas of the British Isles and Scandinavia, but the “Caledonides” have also been extended to encompass all regions associated with orogenesis during the closure of the Iapetus Ocean which includes the Ordovician and

Silurian continental margins of Laurentia, Baltica, and Avalonia (McKerrow et al., 2000). The entire Caledonian orogeny covers a ~200 My (Cambrian–Devonian) time span, which includes numerous orogenic phases consisting initially of arc–arc or arc–continent collision followed by mostly continent–continent collisional events (Shelveian, Scandian, and Acadian) (McKerrow et al., 2000). The Ordovician Caledonian orogeny, which occurred between ca. 470–460 Ma, is referred to as the Grampian Phase (British Isles) or Taconian Phase (New England) (McKerrow et al., 2000). Late Caledonian granites associated with the Scandian phase record a span of magmatism from 435 to 380 Ma, which peaks at ~410 Ma (Atherton and Ghani, 2002).

Additional Scandian-phase granites associated with the East Greenland Caledonides cluster at ca. 430–420 Ma (Andersen et al., 1998; Kalsbeek et al., 1998) as well as Ar-Ar metamorphic cooling ages spanning 438–370 Ma (Dallmeyer et al., 1994; Dallmeyer & Strachan, 1994). Late Ordovician–Early Devonian (450–410 Ma) Caledonian deformation, metamorphism and magmatism is also preserved on Svalbard where several U-Pb zircon ages have been obtained (Johansson et al., 2005). Ordovician magmatism is present in central Norway where granite ages range from 477 to 430 Ma and may represent earlier, Taconic-phase, events of the Caledonian orogen (Yoshinobu, 2002).

***Arctic Alaska – Chukotka:*** Paleozoic plutons are present in northern Alaska along the Seward Peninsula and the Brooks Range. Miller et al. (2006) highlight evidence to suggest a larger, unified Arctic Alaska-Chukotka continental fragment. One of these points is the presence of a common suite of Devonian plutons in the Yukon, the Brooks



Range, Seward Peninsula and Chukotka, which together, range in age from 390 to 340 Ma (Kos'ko et al., 1993; Moore et al., 1994; Toro et al., 2002; Miller et al., 2006). More recent geochronologic work on metavolcanic rocks from the Seward Peninsula confirms this trend with ages of 391 Ma (Till et al., 2006), and age ranges between 403 and 378 Ma (Amato et al., 2009). It should also be noted that detrital zircon trends from strata affiliated with the Arctic Alaska–Chukotka microplate commonly display Neoproterozoic age peaks.

***Russia–Siberia (Urals and Taimyr Peninsula):*** The central and southern Urals of Russia contain abundant exposures of Paleozoic plutons which record one of the few remaining intact Pangean orogens, the Uralian orogeny (Brown et al., 2006). In recent years, there has been extensive geochronologic work aimed at constraining the timing of magmatic activity associated with Paleozoic Uralian orogenesis (Fershtater et al., 2007; 2009). Magmatism has been subdivided into the 6 major phases: 460–420, 415–395, 365–355, 345–330, 320–290, 290–250 (Fershtater et al., 2007). Age-equivalent (Permo-Carboniferous) granites and metamorphic rocks are also present along the Taimyr Peninsula in northern Russia and represent a continuation/extension of Uralian orogenesis (Zonenshain & Natapov 1989; Otto & Bailey 1995; Vernikovsky, 1996).

### **3.5 DISCUSSION**

Provenance trends from the Mystic Pass formation suggest diverse contributions of arc related and recycled orogen sources. Sandstone modal compositions from the Mystic Pass formation are dominated by lithic volcanic and sedimentary grains with subordinate occurrences of quartz suggesting nearby exhumation of an arc-related

recycled orogen source during deposition of these strata. These trends could support the hypothesis of a Late Paleozoic orogenic event (Browns Fork orogeny) proposed by Bradley et al. (2003) that included significant contributions from recycle orogen and magmatic arc sources. However, because there is no consensus on the displacement history of the Farewell terrane, and given its current location directly adjacent to continent scale strike-slip faults (e.g. Denali fault and Iditarod-Nixon Fork Fault), it is important to consider both local and regional magmatic arc source areas. The following text offers a general overview of local and regional arc and recycled orogen source areas that may have contributed detritus to the Mystic Pass formation.

Potential arc-related source areas, which are currently proximal to the Farewell terrane, include the Innoko, Ruby, and Yukon Tanana terranes. Patton et al. (1994) describes the Innoko terrane as consisting of two distinct assemblages: an oceanic assemblage of radiolarian chert with minor carbonates, basalt, and gabbro; and a volcanic arc-like assemblage of volcanoclastic rocks, cherty tuff, volcanic greywacke, argillite and diabase and gabbro intrusive rocks. These rocks are suggested to range in age from Late Devonian(?) to Early Cretaceous(?) (Patton et al., 1994), however there is insufficient age constraint to determine if the appropriate rocks of the Innoko terrane correlate with those of the Farewell. Additional arc and recycled orogen sources north of the Farewell terrane could also include Paleozoic units of the Ruby terrane. Those portions of the Yukon-Tanana terrane exposed in east-central Alaska consist primarily of greenschist to amphibolite grade metasedimentary and meta-igneous rocks of Proterozoic to Paleozoic protolith age (Dusel-Bacon et al., 2006). Thus the YTT remains a viable source for provided arc-derived detritus to siliciclastic rocks of the Mystic Pass Formation.

It is also important to consider contributions from arc and recycled orogen source areas that are outboard of the Farewell terrane in southern Alaska. The most notable being the Wrangellia composite terrane (WCT), which includes the Alexander terrane and the Skolai arc of the Wrangellia terrane. However, aside from these, many of the magmatic sources of the WCT including those that are proximal to the Farewell terrane postdate deposition of the Mystic Pass Formation.

Given that there is a range of paleogeographic models proposed for the Farewell terrane throughout the Paleozoic, one should ideally consider arc and recycled orogen sources beyond those which are currently proximal to the Farewell terrane. The following discusses Paleoproterozoic–Paleozoic detrital zircon trends from the Mystic Pass Formation to assess magmatic source areas from various arctic regions including magmatism affiliated with North America and Siberia.

U-Pb detrital zircon age peaks from the upper Paleozoic Mystic Pass Formation of the Farewell terrane in south-central Alaska display trends for 4 age ranges: ca. 2000–1800 Ma (Paleoproterozoic), 465–405 Ma (Middle Ordovician–Early Devonian), 365–315 Ma (Late Devonian–Early Pennsylvanian), and 305–290 Ma (Late Pennsylvanian–Early Permian). Comparing these trends with Arctic magmatism allows us to evaluate potential detrital source areas for upper Paleozoic strata of the Mystic Pass Formation. Based on geochronologic constraint and availability of data, this study examines magmatic provinces associated with the Siberian and Laurentian cratons, the Yukon-Tanana terrane, northern Canada and the Ellesmerian orogeny, the Caledonian orogeny, the Arctic Alaska – Chukotka microplate (including the Seward Peninsula), and Uralian orogeny (both in the Urals and Taimyr Peninsula) (Figure 3.13).

***Trend 1: ~2.0–1.8 Ga (Paleoproterozoic):*** Secondary Paleoproterozoic age peaks occurring between 2.0 and 1.8 Ga are present in all three detrital zircon samples from the Mystic Pass Formation. Both the Siberian and Laurentian cratons contain abundant igneous zircons of this age (Prokopiev et al., 2008; Condie et al., 2009; Safonova et al., 2010). Furthermore, this trend is commonly observed in detrital zircons from miogeoclinal strata in British Columbia and Alaska (Gehrels et al., 1995; 1996; 1999), in detrital zircons from the Verkhoyansk foreland basin of NE Russia (Figure 3.13) (Miller et al., 2006; Prokopiev et al., 2008) as well as in modern catchments of Russia (Safonova et al., 2010). This correlation could imply that the Mystic Pass Formation received detritus derived directly from a Siberian or Laurentian craton source, which might suggest that the Farewell terrane was in proximity to Siberia or North America during the upper Paleozoic. Alternatively, zircons of this age have been recycled and were derived from sedimentary or metasedimentary rocks which would suggest interactions between the Farewell well and something either along or outboard of a craton margin.

***Trend 2: ~465–405 Ma (Middle Ordovician–Early Devonian):*** Middle Ordovician–Early Devonian age peaks are present in all three samples from the Mystic Pass Formation. This trend is observed in other detrital zircon studies in the North American Cordillera and Arctic region (e.g. Gehrels et al., 1996; 1999; Miller et al., 2006; Amato et al., 2009). Possible sources for these grains include magmatism associated with the Caledonian orogeny and/or the Uralian orogeny. Silurian–Ordovician plutons are also

cited in association with Descon Formation of the Alexander terrane (Gehrels and Saleeby, 1987; Gehrels, 1990).

***Trend 3: ~365–315 Ma (Late Devonian–Early Pennsylvanian):*** Potential source areas for Late Devonian to Early Pennsylvanian detritus are prevalent within Arctic magmatic provinces. Plutonism associated with Uralian orogenesis, the Arctic Alaska – Chukotka microplate, and the Yukon – Tanana terrane all correlate with Farewell terrane detrital zircon peaks within this trend. Furthermore it has been postulated that Arctic Alaska and Chukotka were part of the same microcontinent during the Cambrian–Devonian (Dumoulin et al., 2002; Miller et al., 2002, 2006), and that the Farewell terrane was either proximal to or even part of the Arctic Alaska–Chukotka microplate (Dumoulin et al., 2002). Late Devonian granites associated with the Romanzof orogeny could also be considered as a source, but overall these age-ranges are far less compatible than those mentioned above.

***Trend 4: ~305–290 Ma (Late Pennsylvanian–Early Permian):*** A late Pennsylvanian–early Permian age peak is observed in one sample (MYS 080309-03). The Skolai arc of southern and southeastern Alaska and the Urals in Russia (Figure 3.13) contain documented igneous rocks of this age. Magmatism during this time is also documented in the Yukon-Tanana terrane, however few instances occur and this trend appears to line up with a significant decline in magmatism associated with YTT.

Needs a closing sentence here...

### 3.6 CONCLUSIONS:

Sandstone modal compositions from the Mystic Pass formation are dominated by lithic grains of mostly volcanic origin with secondary contributions of sedimentary grains and chert. Minor occurrences of mono and poly crystalline quartz and feldspars were observed (Qm-4%, F-2%, Lt-94%). These compositional trends suggest sandstone derivation from an arc-related (undissected to transitional) to recycled orogen source. Lithologically and chronologically feasible provenance regions currently proximal to the Farewell terrane include the Innoko and Ruby terranes to the north as well as the Yukon Tanana terrane, Skolai Arc, and Alexander terrane to the south.

U-Pb detrital zircon geochronology from the Mystic Pass formation contains age peaks at ca. 2000–1800 Ma (Paleoproterozoic), 465–405 Ma (Middle Ordovician–Early Devonian), 365–315 Ma (Late Devonian–Early Pennsylvanian), and 305–290 Ma (Late Pennsylvanian–Early Permian). North America (Laurentia) and northeast Russia (Siberia) both contain potential source areas with both magmatic and detrital age ranges between 2.0 and 1.8 Ga. Given the non-uniqueness of this trend, detrital zircons of this age are not sufficient for distinguishing between North American or Siberian provenance contributions for the Mystic Pass formation. The Arctic region contains compatible magmatic sources for all three Phanerozoic detrital zircon trends observed in Paleozoic strata of the Farewell terrane. A Middle Ordovician to Early Devonian detrital trend correlates well with magmatism associated with both Caledonian and Uralian orogenies as well as the Alexander terrane. Late Devonian to early Pennsylvanian detrital grains could be derived from plutons of the Arctic Alaska – Chukotka microplate, the Yukon-Tanana terrane, or the Urals. Finally, Late Pennsylvanian–Early Permian detrital zircons



may be limited to a Uralian orogenic source or the Skolai arc of southern Alaska as there is a paucity of other known Pennsylvanian–Permian magmatic ages from the Arctic region. Detrital zircon trends from upper Paleozoic stratigraphy of the Farewell terrane correlate with a range of Precambrian–Phanerozoic Arctic source areas indicating that the Farewell terrane was likely within or very near to the Uralian Seaway during the Paleozoic (Figure 3.15). Based on the lack of Neoproterozoic age zircons and “Baltic hump” (2.0–1.0 Ga) detrital signatures, much of the stratigraphy of the Mystic subterrane may have resulted from exhumation and deposition associated with orogenesis along the western margin of the Uralian Seaway.

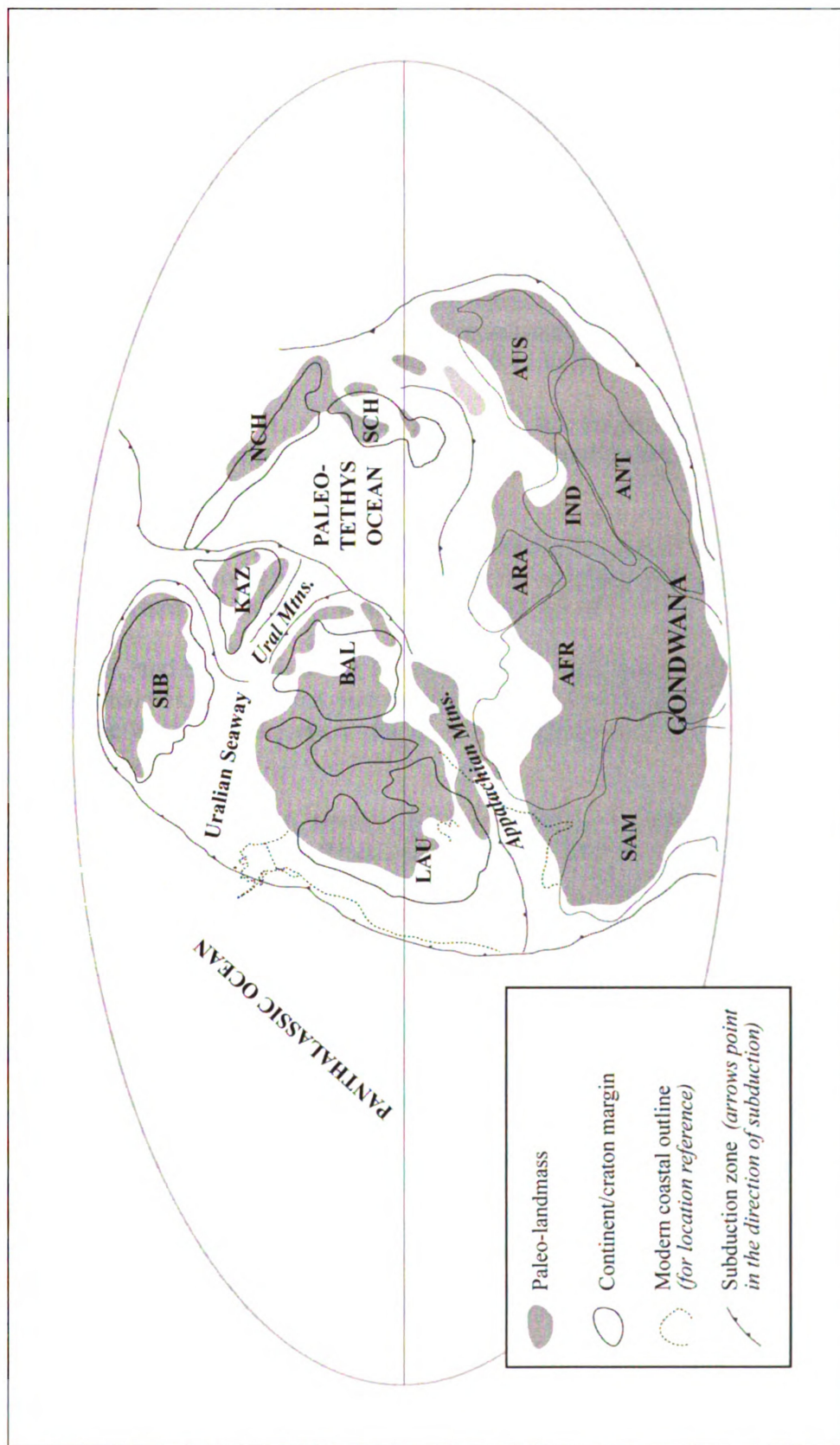


**Figure 3.15.** Early Carboniferous paleogeographic reconstruction showing the distribution of major tectonic elements. This sets the stage for upper Paleozoic events associated with Farewell terrane. AFR-Africa, ANT-Anarctica, ARA-Arabia, AUS-Australia, BAL-Baltica, IND-India, KAZ-Kazakhstan, LAU-Laurentia, NCH-North China, SAM-South America, SCH-South China, SIB-Siberia. Modified from Scotese, 2002.

### 3.7 REFERENCES

- Aleinikoff, J.N., Plafker, G., and Nokleberg, W.J., 1988, Middle Pennsylvanian plutonic rocks along the southern margin of Wrangellia, *in*, Hamilton, T.D., and Galloway, J.P., eds., The U.S. Geological Survey in Alaska: Accomplishments during 1987: U.S. Geological Survey Circular 1016, p. 110–113.
- Amato, J.M., Toro, J., Miller, E.L., Gehrels, G.E., Farmer, G.L., Gottlieb, E.S., Till, A.B., 2009, Late Proterozoic–Paleozoic evolution of the Arctic Alaska–Chukotka terrane based on U–Pb igneous and detrital zircon ages: Implications for Neoproterozoic paleogeographic reconstructions: Geological Society of America Bulletin, v. 121, p. 1219–1235, doi: 10.1130/B26510.1.
- Andresen, A., Hartz, E.H., and Vold, J., 1998, A late orogenic extensional origin for the intracrustal gneiss domes of the East Greenland Caledonides (72–74°N), Tectonophysics 285, 353–369.
- Atherton, M.P., and Ghani, A.A., 2002, Slab breakoff; a model for Caledonian, Late Granite syn-collisional magmatism in the orthotectonic (metamorphic) zone of Scotland and Donegal, Ireland, Lithos 62, 65–85,
- Beard, J.S., and Barker, F., 1989, Petrology and tectonic significance of gabbros, tonalities, shoshonites, and anorthosites in a late Paleozoic arc-root complex in the Wrangellia terrane, southern Alaska: The Journal of Geology, v. 97, p. 667–683.
- Blodgett, R.B., Rohr, D.M., Boucot, A.J., 2002, Paleozoic links among some Alaskan accreted terranes and Siberia based on megafossils, *in* Miller, E.L., Grantz, A., and Klemperer, S.L., eds., Tectonic evolution of the Bering Shelf–Chukchi Sea–Arctic Margin and adjacent landmasses: Geological Society of America Special Paper 360, p. 273–280.
- Bradley, D.C., McClelland, W.C., Wooden, J.L., Till, A.B., Roeske, S.M., Miller, M.L., Karl, S.M., and Abbott, J.G., 2007, Detrital zircon geochronology of some Neoproterozoic to Triassic rocks in interior Alaska, *in* Ridgway, K.D., Trop, J.M., Glen, J.M.G., and O’Neill, J.M., eds., Tectonic Growth of a Collisional Continental Margin: Crustal Evolution of Southern Alaska: Geological Society of America Special Paper 431, doi: 10.1130/2007.2431(13).
- Bradley, D.C., Dumoulin, J., Layer, P., Sunderlin, D., Roeske, S., McClelland, W.C., Harris, A.G., Abbott, G., Bundtzen, T.K., and Kusky, T., 2003, Late Paleozoic orogeny in Alaska’s Farewell Terrane: Tectonophysics, v. 372, p. 23–40, doi: 10.1016/S0040-1951(03)00238-5.

- Brown, D., Spadea, P., Puchkov, V., Alvarez-Marron, J., Herrington, R., Willner, A.P., Hetzel, R., Gorozhanina, Y., Juhlin, C., 2006, Arc–continent collision in the Southern Urals, *Earth-Science Reviews* 79, 261–287.
- Colpron, M., Nelson, J.L., and Murphy, D.C., 2006, A Tectonostratigraphic framework for the pericratonic terranes of the northern Canadian Cordillera, *in* Colpron, M. and Nelson, J.L., eds., *Paleozoic Evolution and Metallogeny of Pericratonic Terranes at the Ancient Pacific Margin of North America*, Canadian and Alaskan Cordillera: Geological Association of Canada, Special Paper 45, p. 1–23.
- Condie, K.C., 2002, Continental growth during a 1.9-Ga superplume event: *Journal of Geodynamics*, v. 34, p. 249–264
- Condie, K.C., Belousova, E., Griffin, W.L., Sircombe, K.N., 2009, Granitoid events in space and time: constraints from igneous and detrital zircon age spectra: *Gondwana Research*, v. 15, p. 228–242.
- Dallmeyer, R.D., and Strachan, R.A., 1994,  $^{40}\text{Ar}/^{39}\text{Ar}$  mineral age constraints on the timing of deformation and metamorphism, North-East Greenland Caledonides, *in* Higgins, A.K., (eds.) *Geology of North-East Greenland*, Rapp, Gronlands Geol. Unders., 162, 153–162.
- Dallmeyer, R.D., Strachan, R.A., and Henriksen, N., 1994,  $^{40}\text{Ar}/^{39}\text{Ar}$  mineral age record in NE Greenland: implications for tectonic evolution of the North Atlantic Caledonides, *J. Geol. Soc.* 151, 615–628.
- Decker, J., Bergman, S.C., Blodgett, R.B., Box, S.E., Bundtzen, T.K., Clough, J.G., Coonrad, W.L., Gilbert, W.G., Miller, M.L., Murphy, J.M., Robinson, M.S., and Wallace, W.K., 1994, Geology of southwestern Alaska, *in*, Plafker, G., and Berg, H.C., eds., *The Geology of Alaska: Boulder, Colorado*, Geological Society of America, *Geology of North America*, v. G-1, p. 285–310.
- DeGraaff-Surpless, K., Mahoney, J.B., Wooden, J.L., McWilliams, M.O., 2003, Lithofacies control in detrital zircon provenance studies: Insights from the Cretaceous Methow basin, southern Canadian Cordillera, *Geological Society of America Bulletin*, v. 115, p. 899–915.
- Dickinson, W.R., 1970, Interpreting provenance relations from detrital modes of greywacke and arkose: *Journal of Sedimentary Petrology*, v. 40, p. 395–707.
- Dickinson, W.R., Beard, L.S., Brakenridge, G.R., Erjavec, J.L., Ferguson, R.C., Inman, K.F., Knepp, R.A., Lindberg, F.A., and Ryberg, P.T., 1983, Provenance of North American Phanerozoic sandstones in relation to tectonic setting: *Geological Society of America Bulletin*, v. 94, p. 222–235.

- Dickinson, W.R., 1985, Interpreting provenance relations from detrital modes of sandstones, in, Zuffa, G.G., ed., *Provenance of Arenites*: Dordrecht, The Netherlands, Reidel, p. 333–361.
- Dickinson, W.R., 2004, Evolution of the North American Cordillera, *Annual Review of Earth and Planetary Sciences*, vol. 32, pp.13–45.
- Dickinson, W.R., and Gehrels, G.E., 2009, Use of U–Pb ages of detrital zircons to infer maximum depositional ages of strata: A test against a Colorado Plateau Mesozoic database, *Earth and Planetary Science Letters* vol. 288, p. 115–125.
- Dumoulin, J.A., Harris, A.G., Gagiev, M., Bradley, D.C., and Repetski, J.E., 2002, Lithostratigraphic, conodont, and other faunal links between lower Paleozoic strata in northern and central Alaska and northeastern Russia, *in* Miller, E.L., Grantz, A., and Klemperer, S.L., eds., *Tectonic evolution of the Bering Shelf–Chukchi Sea–Arctic Margin and adjacent landmasses*: Geological Society of America Special Paper 360, p. 291–312.
- Fershtater, G.B., Krasnobaev, A.A., Bea.F., Montero, P., Borodina, N.S., 2007, Geodynamic settings and history of the Paleozoic intrusive magmatism of the central and southern Urals: results of zircon dating, *Geotectonics*, Vol. 41, No. 6, pp. 465–486.
- Fershtater, G.B., Krasnobaev, A.A., Bea.F., Montero, P., Borodina, N.S., 2009, Intrusive magmatism during early evolutionary stages of the Ural Epiocceanic Orogen: U–Pb geochronology (LA ICP MS, NORDSIM, and SHRIMP II), geochemistry, and evolutionary tendencies, *Geochemistry International*, Vol. 47, No. 2, pp 143–162.
- Gardner, M.C., Bergman, S.C., Cushing, G.W., MacKevett, E.M., Jr., Plafker, G., Campbell, R.B., Dodds, C.J., McClelland, W.C., and Mueller, P.A., 1988, Pennsylvanian pluton stitching of Wrangellia and the Alexander terrane, Wrangell Mountains, Alaska: *Geology*, v. 16, p. 967–971.
- Gehrels, G.E., 1990, Late Proterozoic–Cambrian metamorphic basement of the Alexander terrane on Long and Dall Islands, southeast Alaska: *Geological Society of America Bulletin*, v. 102, p. 760–767, doi: 10.1130/0016-7606
- Gehrels, G.E., Saleeby, J.B., 1987, Geologic framework, tectonic evolution, and displacement history of the Alexander terrane: *Tectonics*, v. 6, p. 151–173.
- Gehrels, G.E., Butler, R.F., and Bazard, D.R., 1996, Detrital zircon geochronology of the Alexander terrane, southeastern Alaska: *Geological Society of America, Bulletin*, v. 108, p. 722–734.

- Gehrels, G.E., Johnsson, M.J., and Howell, D.G., 1999, Detrital zircon geochronology of the Adams Argillite and Nation River Formation, east-central Alaska, U.S., *Journal of Sedimentary Research*, Vol. 69, No. 1, pp. 135–144.
- Gehrels, G.E., Valencia, V., Pullen, A., 2006, Detrital zircon geochronology by Laser-Ablation Multicollector ICPMS at the Arizona LaserChron Center, in Loszewski, T., and Huff, W., eds., *Geochronology: Emerging Opportunities*, Paleontology Society Short Course: Paleontology Society Papers, v. 11, 10 p.
- Gehrels, G.E., Valencia, V., Ruiz, J., 2008, Enhanced precision, accuracy, efficiency, and spatial resolution of U-Pb ages by laser ablation–multicollector–inductively coupled plasma–mass spectrometry: *Geochemistry, Geophysics, Geosystems*, v. 9, Q03017, doi:10.1029/2007GC001805.
- Gradstein, F.M., Ogg, J.G., and Smith, A.G., 2004, *A Geologic Time Scale 2004*: Cambridge University Press, 589 p.
- Hampton, B.A., Ridgway, K.D., O'Neill, J.M., Gehrels, G.E., Schmidt, J., and Blodgett, R.B., 2007, Pre-, syn-, and post-collisional stratigraphic framework and provenance of Upper Triassic–Upper Cretaceous strata in the northwestern Talkeetna Mountains, Alaska, *in* Ridgway, K.D., Trop, J.M., Glen, J.M.G., and O'Neill, J.M., eds., *Tectonic Growth of a Collisional Continental Margin: Crustal Evolution of Southern Alaska*: Geological Society of America Special Paper 431.
- Hampton, B.A., Ridgway, K.D., and Gehrels, G.E., 2010, A detrital record of Mesozoic island arc accretion and exhumation in the North American Cordillera: U–Pb geochronology of the Kahiltna basin, southern Alaska: *Tectonics*, v. 29, doi: 10.1029/2009TC002544
- Hoffman, P. F., 1997, Tectonic genealogy of North America, *in*, Van der Pluijm, B. A. and Marshak, S. (eds) *Earth Structure: An Introduction to Structural Geology and Tectonics*. New York, McGraw-Hill, p. 459–464.
- Ingersoll, R.V., Ballard, T.F., Ford, R.L., Grimm, J.P., Pickle, J.D., and Sares, S.W., 1984, The effect of grain size on detrital modes: A test of the Gazzi-Dickinson point-counting method: *Journal of Sedimentary Petrology*, v. 54, p. 103–116.
- Johansson, A., Gee, D.G., Larionov, A.N., Ohta, Y., and Tebenkowsky, A.M., 2005, Grenvillian and Caledonian evolution of eastern Svalbard – A tale of two orogenies: *Terra Nova*, v. 17, p. 317–325, doi: 10.1111/j.1365-3121.2005.00616.x.
- Jones, D., Siberling, N.J., Gilbert, W.G., Coney, P.J., 1982, Character, distribution, and tectonic significance of accretionary terranes in the central Alaska Range, *Journal of Geophysical Research*, v. 87, p. 3709–3717.



- Kalsbeek, F., Nutman, A.P., and Jepsen, F., 1998, Granites in the Caledonian fold belt, East Greenland, in Frederiksen, K.S., and Thrane, K., (eds.) Symposium on Caledonian geology in East Greenland, Abstract Vol. Danmarks og Gronlands Geol. Unders. Rapp., pp. 43–44.
- Kos'ko, M.K., Cecile, M.P., Harrison, J.C., Ganelin, V.G., Khandoshko, N.V., and Lopatin, B.G., 1993, Geology of Wrangel Island, between Chukchi and East Siberian seas, northeastern Russia, Geological Survey of Canada Bulletin, v. 461, 101 pp.
- Lane, L.S., 2007, Devonian–Carboniferous paleogeography and orogenesis, northern Yukon and adjacent Arctic Alaska, Canadian Journal of Earth Sciences, 44, pp. 679–694.
- Leier, A.L., DeCelles, P.G., Kapp, P., and Gehrels, G.E., 2007, Lower Cretaceous strata in the Lhasa terrane, Tibet, with implications for understanding the early tectonic history of the Tibetan Plateau, Journal of Sedimentary Research, v. 77, p. 809–825.
- Ludwig, K.R., 2008, Isoplot 3.7. Berkeley Geochronology Center, Special Publication No. 4, 77 pp.
- McKerrow, W.S., Mac Niocaill, C., and Dewey, J.F., 2000, The Caledonian Orogeny redefined, Journal of the Geological Society, London, Vol. 157, pp. 1149–1154.
- Miller, E.L., Gelman, M., Parfenov, L., and Hourigan, J., 2002, Tectonic setting of Mesozoic magmatism: A comparison between northeastern Russia and the North American Cordillera, *in*, Miller, E.L., Grantz, A., and Klemperer, S.L., eds., Tectonic evolution of the Bering Shelf–Chukchi Sea–Arctic Margin and adjacent landmasses: Geological Society of America Special Paper 360, p. 333–358.
- Miller, E.L., Toro, J., Gehrels, G., Amato, J.M., Prokopiev, A., Tuchkova, M.I., Vyacheslav, V.A., Dumitru, T.A., Moore, T.E., Cecile, M.P., 2006, New insights into Arctic paleogeography and tectonics from U-Pb detrital zircon geochronology: Tectonics, v. 25, TC3013, doi: 10.1029/2005TC001830.
- Nelson, J.L., Colpron, M., Piercey, S.J., Dusel-Bacon, C., Murphy, D.C. and Roots, C.F., 2006, Paleozoic tectonic and metallogenic evolution of the pericratonic terranes *in* Yukon, northern British Columbia and eastern Alaska, *in* Colpron, M. and Nelson, J.L., eds., Paleozoic Evolution and Metallogeny of Pericratonic Terranes at the Ancient Pacific Margin of North America, Canadian and Alaskan Cordillera: Geological Association of Canada, Special Paper 45, p. 323–360.

- Nokleberg, W.J., Wade, W.M., Lange, I.M., and Plafker, G., 1986, Summary of geology of the Peninsular terrane, metamorphic complex of Gulkana River, and Wrangellia terrane, north-central and northwestern Gulkana Quadrangle, *in* Bartsch-Winkler, S., and Reed, K.M., eds., *Geologic Studies in Alaska*: U.S. Geological Survey Circular 978, p. 69–74.
- Otto, S.C., and Bailey, R.J., 1995, Tectonic evolution of the northern Ural Orogen, *Journal of the Geological Society*, London, 152, 903–906.
- Piercey, S.J., Nelson, J.L., Colpron, M., Dusel-Bacon, C., Roots, C.F., and Simard, R.-L., 2006, Paleozoic magmatism and crustal recycling along the ancient Pacific margin of North America, northern Cordillera, *in* Colpron, M. and Nelson, J.L., eds., *Paleozoic Evolution and Metallogeny of Pericratonic Terranes at the Ancient Pacific Margin of North America, Canadian and Alaskan Cordillera*: Geological Association of Canada, Special Paper 45, p. 281–322.
- Plafker, G., and Berg, H.C., 1994, Overview of the geology and tectonic evolution of Alaska, *in* Plafker, G., and Berg, H.C., eds., *The Geology of Alaska*: Boulder, Colorado, Geological Society of America, *Geology of North America*, v. G-1, p. 989–1021.
- Plafker, G., Nokleberg, W.J., and Lull, J.S., 1989, Bedrock geology and tectonic evolution of the Wrangellia, Peninsular, and Chugach terranes along the trans-Alaska crustal transect in the northern Chugach Mountains and southern Copper River basin: *Journal of Geophysical Research*, v. 94, p. 4255–4295.
- Prokopyev, A.V., Toro J., Miller, E.L., Gehrels, G.E., 2008, The paleo-Lena River–200 m.y. of transcontinental zircon transport in Siberia, *Geology*, v. 36, no. 9, p. 699–702.
- Ripington, S., and Scott, R., 2009, Ellesmerian tectonism: a critical appraisal from a circum-Arctic perspective, AAPG Search and Discovery Article #90096, AAPG 3-P Conference and Exhibition, Moscow, Russia.
- Rogers, J.J.W., 1996, A history of continents in the past three billion years: *The Journal of Geology*, v. 104, p. 91–107.
- Rogers, J.J.W., and Santosh M., 2002, Configuration of Columbia, a Mesoproterozoic supercontinent, *Gondwana Research*, v. 5, p. 5–22.
- Safonova, I., Maruyama, S., Hirata, T., Kon, Y., and Rino, S., 2010, LA ICP MS U-Pb ages of detrital zircons from Russia largest rivers: Implications for major granitoid events in Eurasia and global episodes of supercontinent formation: *Journal of Geodynamics*, article in press, doi: 10.1016/j.jog.2010.02.008.

- Soja, C.M., and Antoshkina, A.I., 1997, Coeval development of Silurian stromatolite reefs in Alaska and the Ural Mountains: Implications for paleogeography of the Alexander terrane, *Geology*, v. 25, no. 6, p. 539–542.
- Stacey, J.S., and Kramers, J.D., 1975, Approximation of terrestrial lead isotope evolution by a two-stage model: *Earth and Planetary Science Letters*, v. 26, p. 207–221.
- Till, A.B., Aleinikoff, J.N., Amato, J.M., and Harris, A.G., 2006, New paleontologic and geochronologic protolith ages for the paleo-continental margin of Arctic Alaska: *Geological Society of America Abstracts with Programs*, v. 38, no. 5, p. 13.
- Trettin, H.P., Parrish, R., and Loveridge, W.D., 1987, U-Pb age determinations of Proterozoic to Devonian rocks from northern Ellesmere Island, Arctic Canada; *Canadian Journal of Earth Sciences*, v. 24, p. 246–256.
- Trettin, H.P., 1991a, Introduction (Silurian–Early Carboniferous deformational phases and associated metamorphism and plutonism, Arctic Islands), *in* Trettin, H.P., ed., *Geology of the Innuitian Orogen and Arctic Platform of Canada and Greenland*: Boulder, Colorado, Geological Society of America, *Geology of North America*, v. E, p. 295.
- Trettin, H.P., 1991b, Late Silurian–Early Devonian deformation, metamorphism and granitic plutonism, Northern Ellesmere and Axel Heiberg Islands, *in* Trettin, H.P., ed., *Geology of the Innuitian Orogen and Arctic Platform of Canada and Greenland*: Boulder, Colorado, Geological Society of America, *Geology of North America*, v. E, p. 295–301.
- Trettin, H.P., 1991c, The Proterozoic to Late Silurian record of Pearya, *in* Trettin, H.P., ed., *Geology of the Innuitian Orogen and Arctic Platform of Canada and Greenland*: Boulder, Colorado, Geological Society of America, *Geology of North America*, v. E, p. 241–259.
- Vernikovsky, V.A., 1996, The geodynamic evolution of the Taimyr folded area, *Geology of the Pacific Ocean*, 12, 691–704.
- Weislogal, A.L., Graham, S.A., Chang, E.Z., Wooden, J.L., Gehrels, G.E., and Yang, H., 2006, Detrital zircon provenance of the Late Triassic Songpan-Ganzi complex: Sedimentary record of collision of the North and South China blocks, *Geology*, v. 34, p. 97–100.
- Yoshinobu, A.S., Barnes, C.G., Nordgulen, O., Prestvik, T., Fanning, M., and Pedersen, R.B., 2002, Ordovician magmatism, deformation, and exhumation in the Caledonides of central Norway: An orphan of the Taconic orogeny?, *Geology*, v. 30, no. 10, p. 883–886.

Zonenshain, L.P., and Natapov, L.M., 1989, Tectonic history of the Arctic region from the Ordovician through the Cretaceous, in Herman, Y., eds., *The Arctic Seas: Climatology, Oceanography, Geology, and Biology*, Van Nostrand Reinhold, New York, p. 829–862.

## **CHAPTER 4: CONCLUSIONS**

### **1. Upper Paleozoic (Mississippian–Permian) siliciclastic strata of the Mystic Pass**

Formation consist of interbedded mudstone and fine- to coarse-grained sandstone with occurrences of gravel- to pebble-conglomerate. Beds are laterally extensive (>100 m), exhibit tabular geometries, and range in thickness from 0.02–3.0 m. Mudstone units are mostly massive but occasionally exhibit faint horizontal laminations. Sandstone deposits are characterized by massive- to horizontally stratified beds, but occasionally display ripple cross stratification. Matrix- and clast-supported Conglomerate beds are commonly graded with clast compositions consisting mostly of red, black, and green chert, and subordinate occurrences of limestone and sandstone.

### **2. Sedimentary facies interpreted from measured stratigraphy of the Mystic Pass**

formation suggest a turbidite fan depositional environment. Following the interpretations of previous work and assuming stratigraphic continuity with the Mt. Dall conglomerate this interpretation suggests that the Mystic Pass formation may represent early stage foreland basin development associated with upper Paleozoic orogenesis. Alternatively these two siliciclastic units may be part of tectonically unrelated basins, and have simply been structurally juxtaposed into proximity with each other. Further work is needed to document the stratigraphic (or structural) relationship between units above (Mt. Dall conglomerate?) and below (Dillinger subterrane?) the Mystic Pass formation.

3. Sandstone modal compositions of the Mystic Pass formation are dominated by lithic-volcanic and lithic-sedimentary grains with minor contributions from quartz and feldspars (Q-17%, F-2%, L-81%). When compared with total lithics, monocrystalline quartz and feldspars account for a small percentage of grains (Qm-4%, F-2%, Lt-94%). These data suggest contributions of detritus derived from a magmatic arc to recycled orogen source during deposition of the Mystic Pass formation.

4. U-Pb detrital zircon geochronology from 277 grains of the upper Paleozoic Mystic Pass formation consists mostly of Phanerozoic age grains (64%) with the remaining 36% being Precambrian in age. Four age peak trends occur at: ca. 2000–1800 Ma (Paleoproterozoic), 465–405 Ma (Middle Ordovician–Early Devonian), 365–315 Ma (Late Devonian–Early Pennsylvanian), and 305–290 Ma (Late Pennsylvanian–Early Permian). Also, Detrital zircons from samples of the Mystic Pass formation support existing Mississippian–Permian biostratigraphic ages for these strata.

5. Sandstone modal compositions from the Mystic Pass Formation of the Farewell terrane suggest the involvement of an arc to recycled orogen source during the upper Paleozoic. A comparison of detrital zircon trends with regional Arctic magmatic source areas reveals a range of possible provenance scenarios. A Pennsylvanian–Permian detrital age peak correlates with magmatism involving Uralian orogenesis in northern Siberia and the Skolai arc of the Wrangellia terrane in southern Alaska. Devonian–Mississippian detrital peaks correlate with magmatic sources associated with the Yukon-Tanana terrane and Devonian plutons of the Arctic Alaska-Chukotka microplate. Ordovician–Silurian



zircons may be derived from magmatism related to the Caledonian orogeny or from plutons associated with the Descon Formation of the Alexander terrane. Age peaks between ca. 2.0–1.8 Ga are present in all three detrital zircon samples from the Mystic Pass formation and correlate well with igneous and detrital trends of this age from both the Siberian and Laurentian cratons. Possible tectonic scenarios for upper Paleozoic orogenesis involving the Farewell terrane include arc-continent or continent-continent collision, which could involve elements of both Laurentian and Siberian affinities or inter-oceanic island arcs within the western Uralian Seaway during the Late Paleozoic.

## APPENDIX A:

Measured stratigraphic section of the Mystic Pass formation

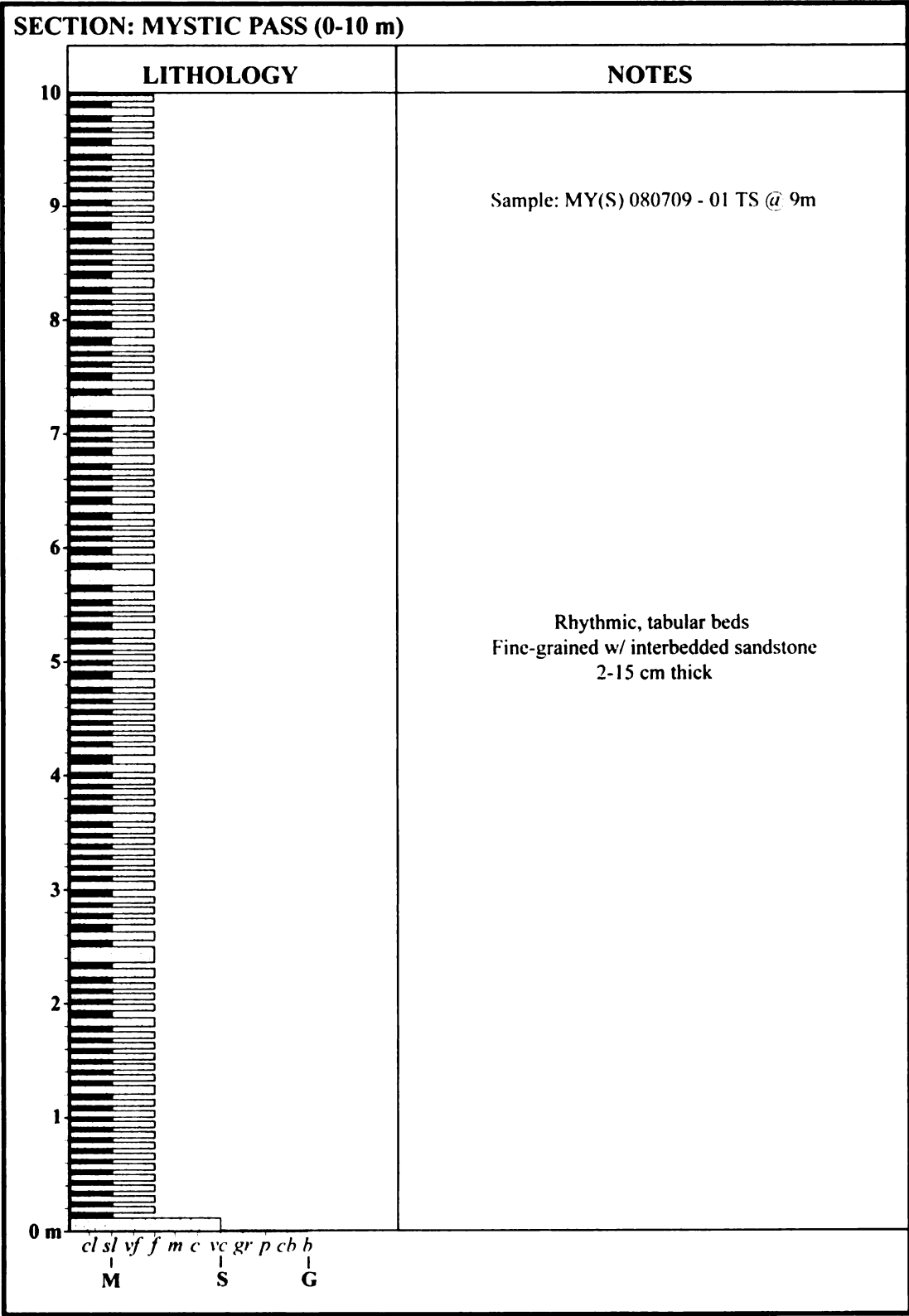


**Figure A1.** Measured stratigraphic sections of the Mystic Pass formation.

Figure A1 continued

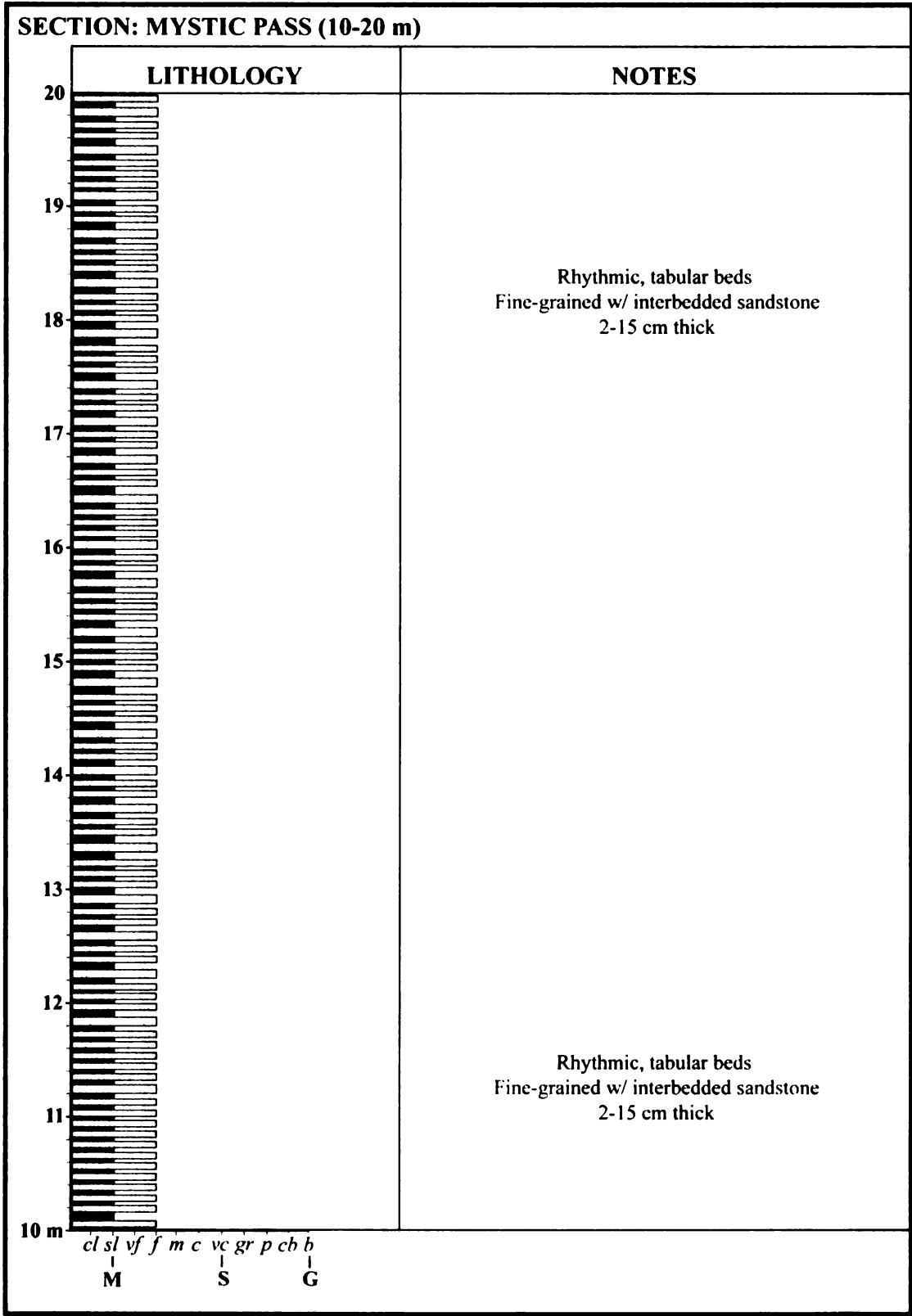


Figure A1 continued

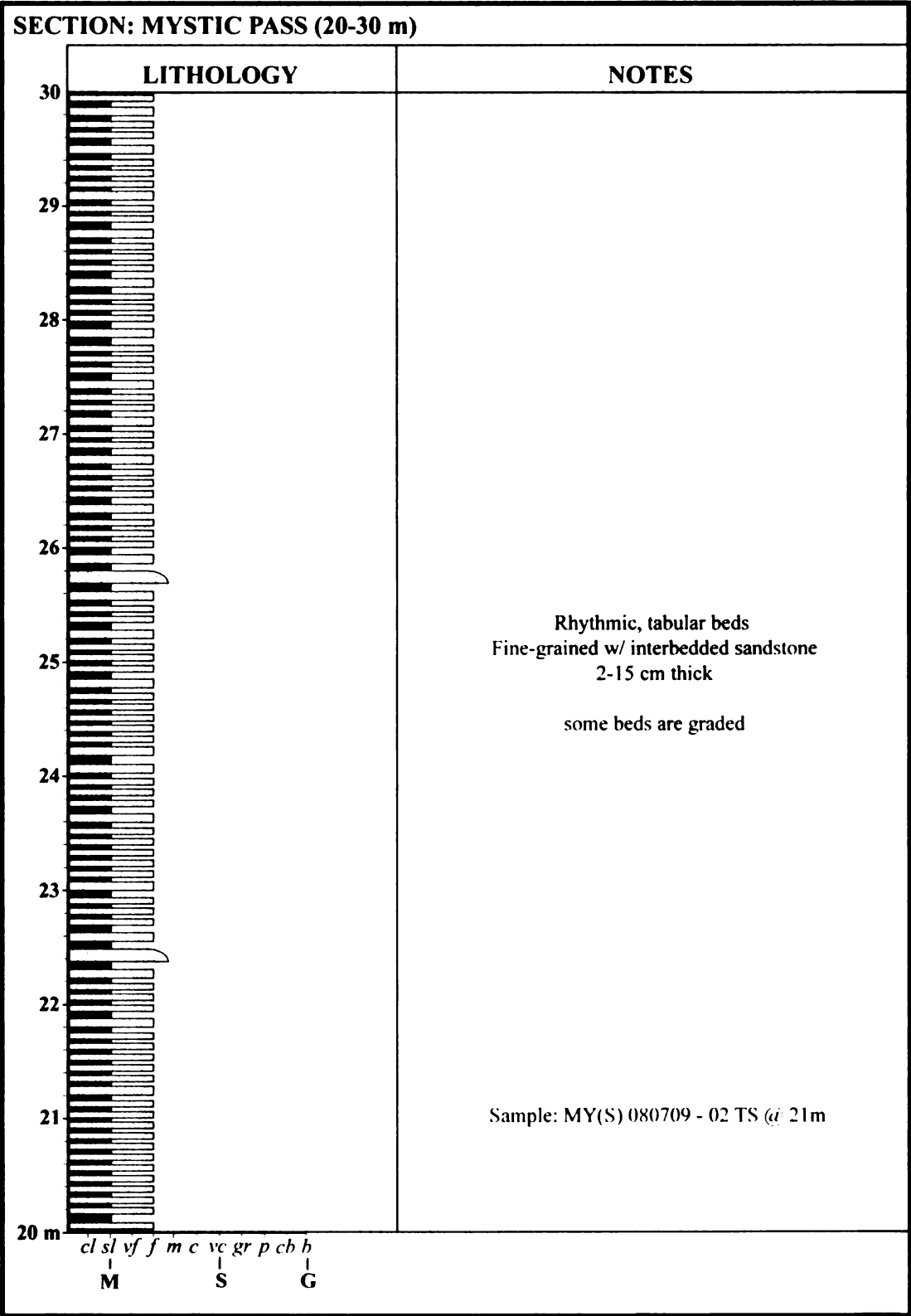


Figure A1 continued

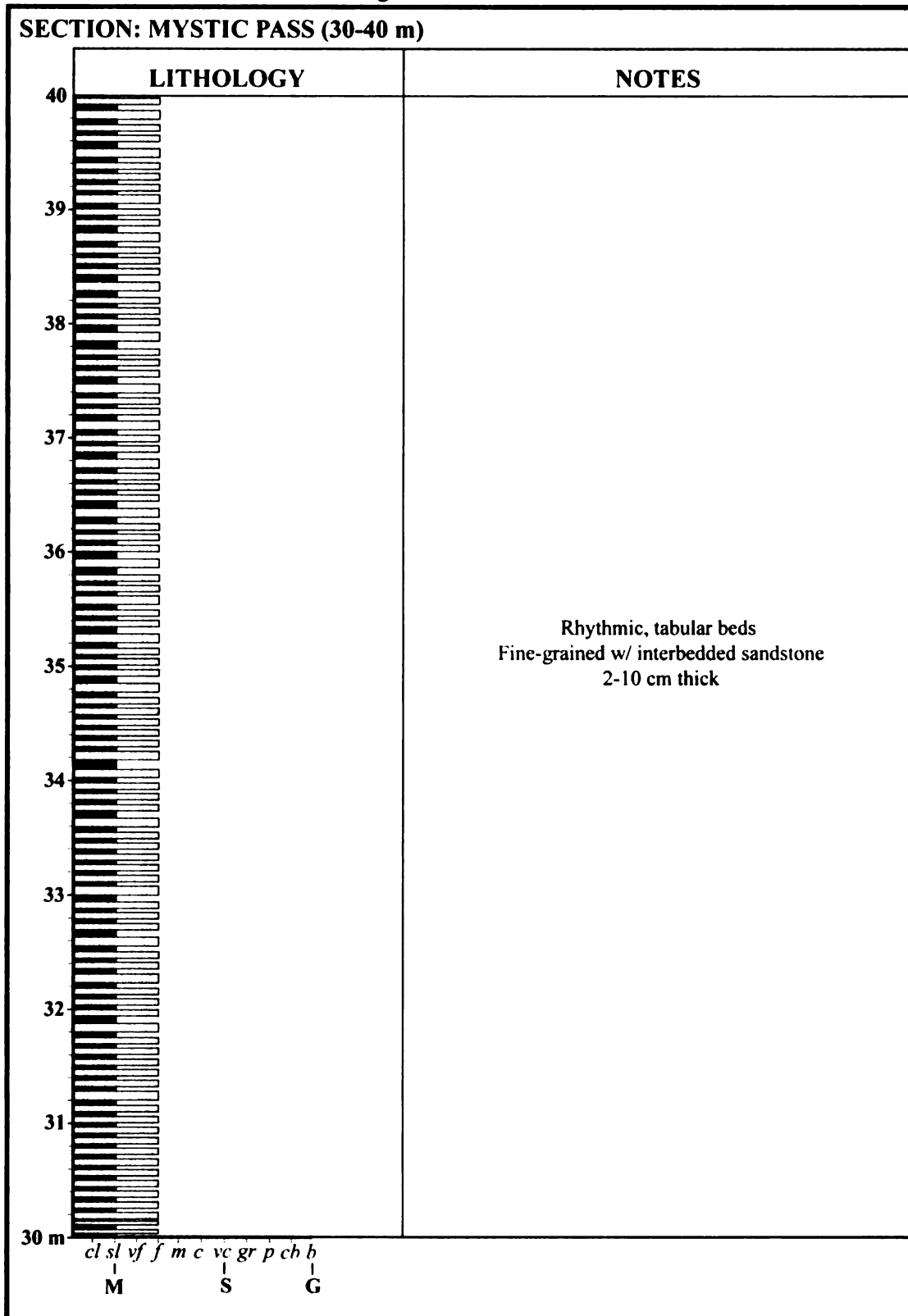




Figure A1 continued

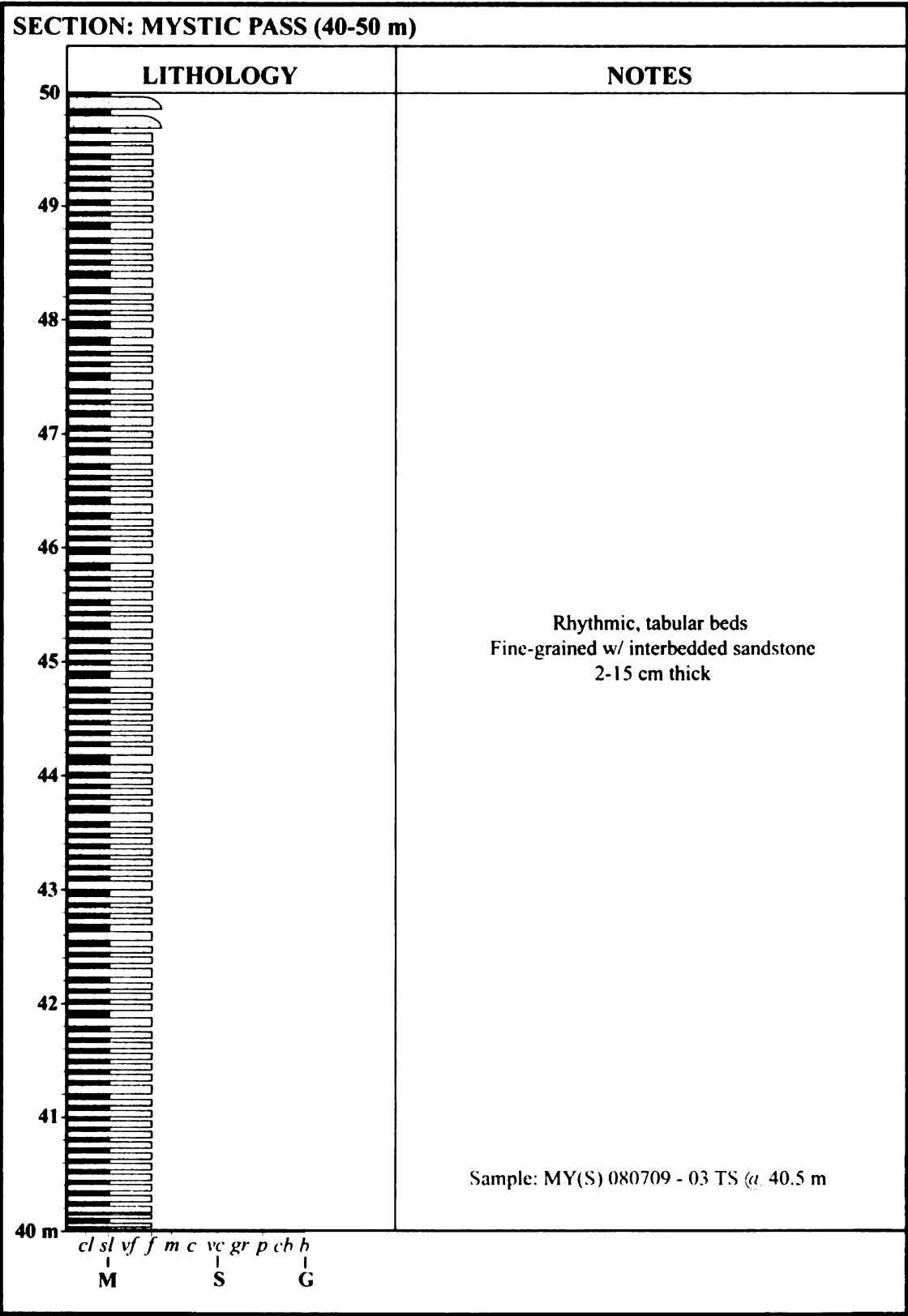


Figure A1 continued

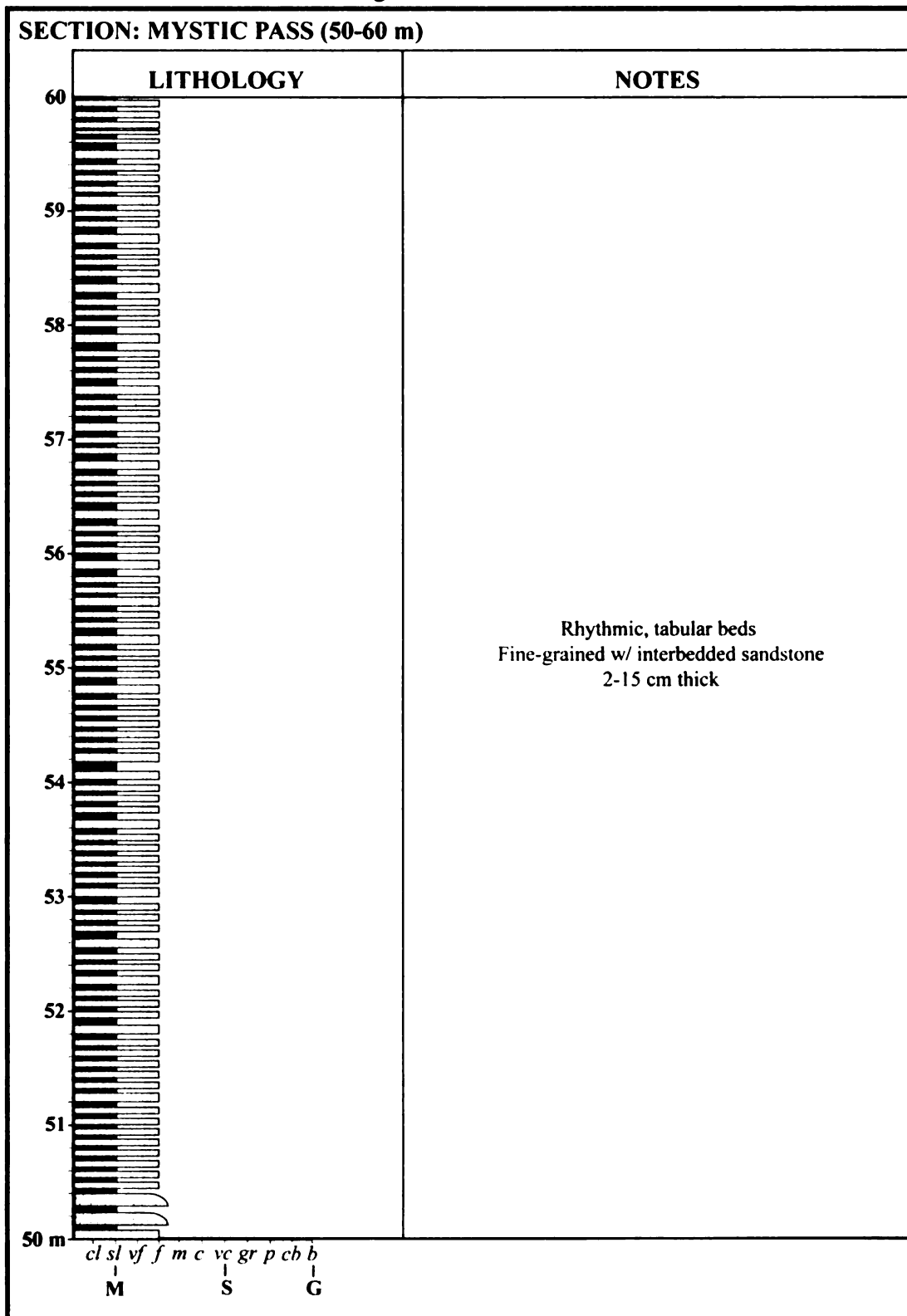


Figure A1 continued

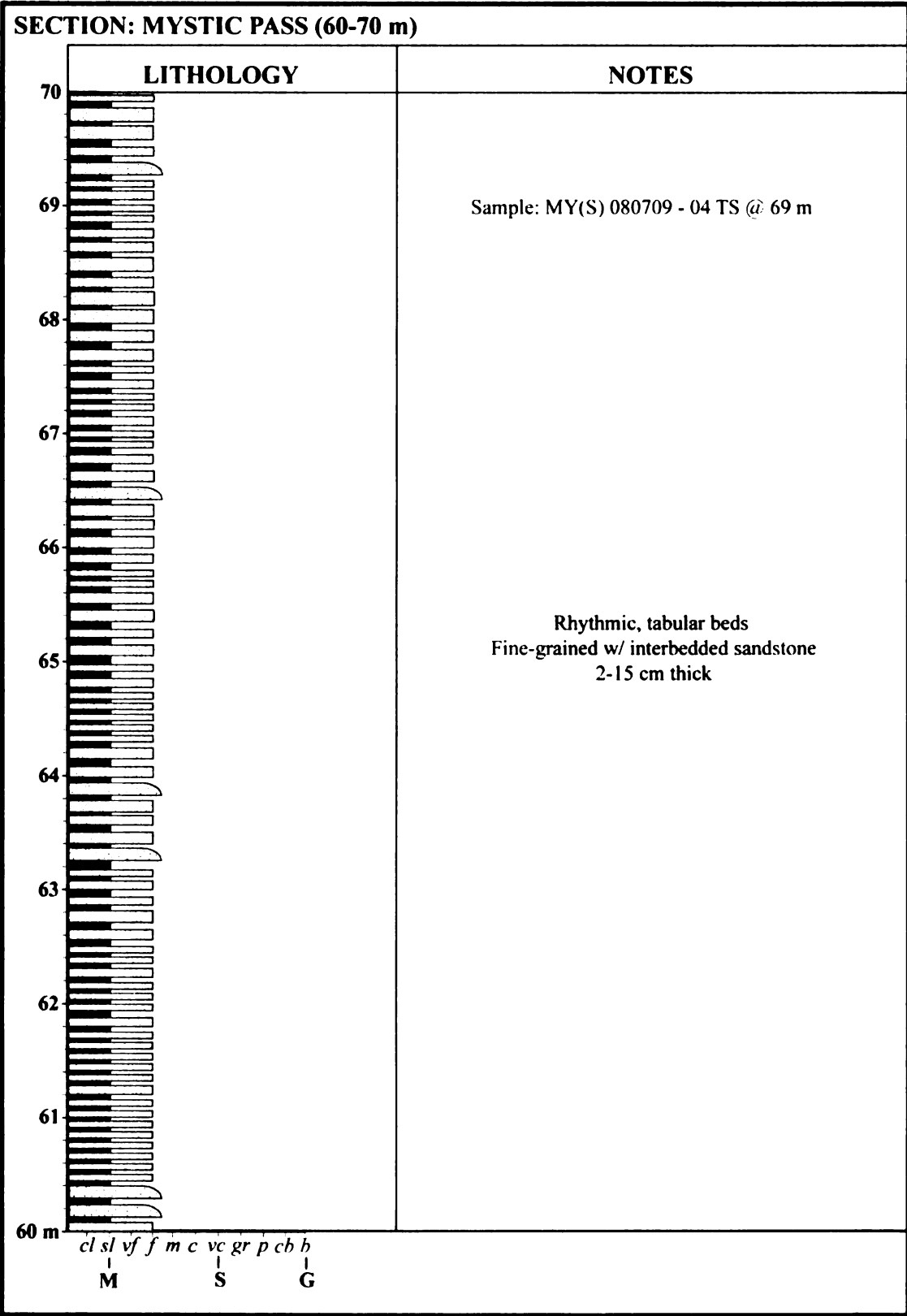


Figure A1 continued

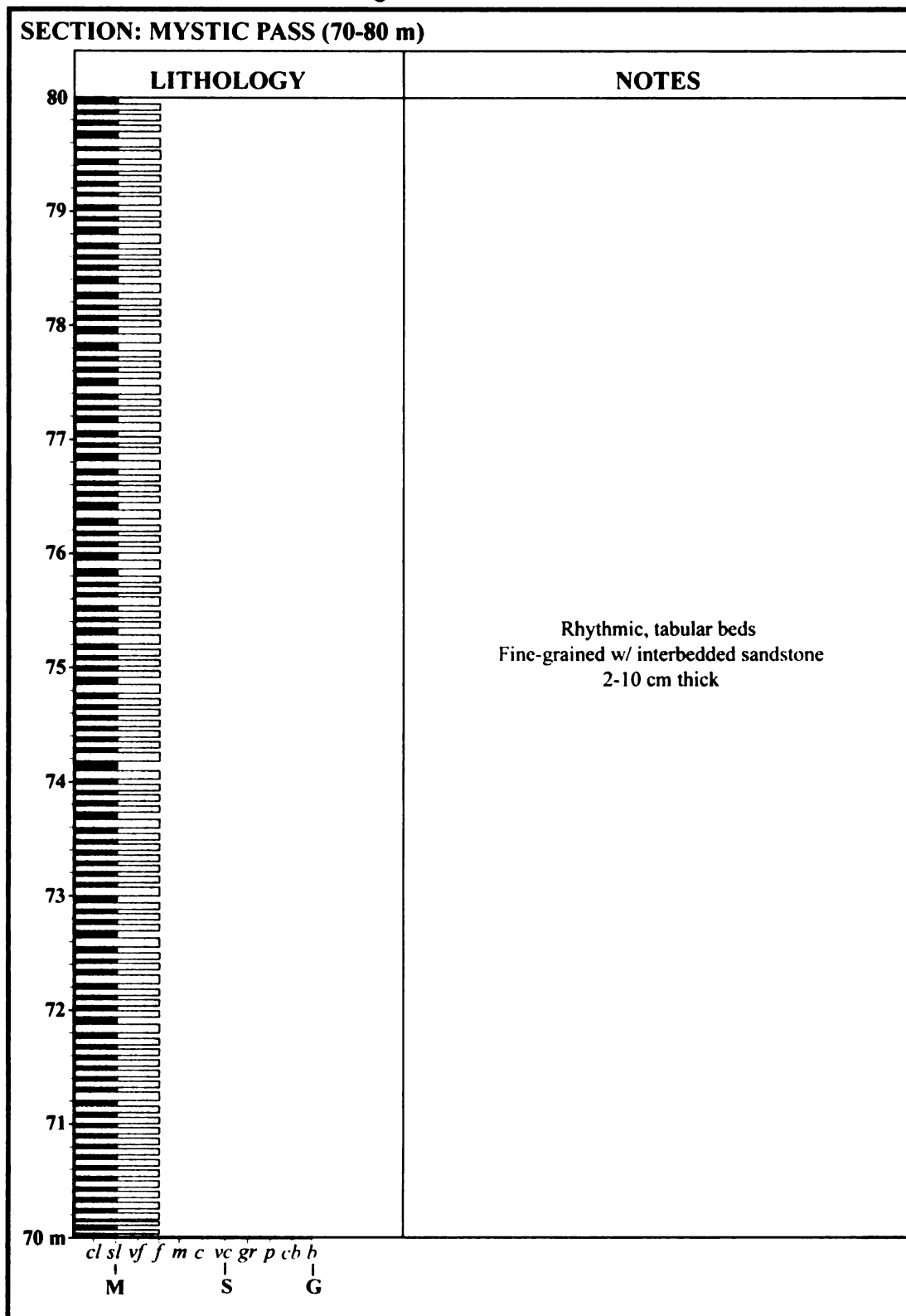


Figure A1 continued

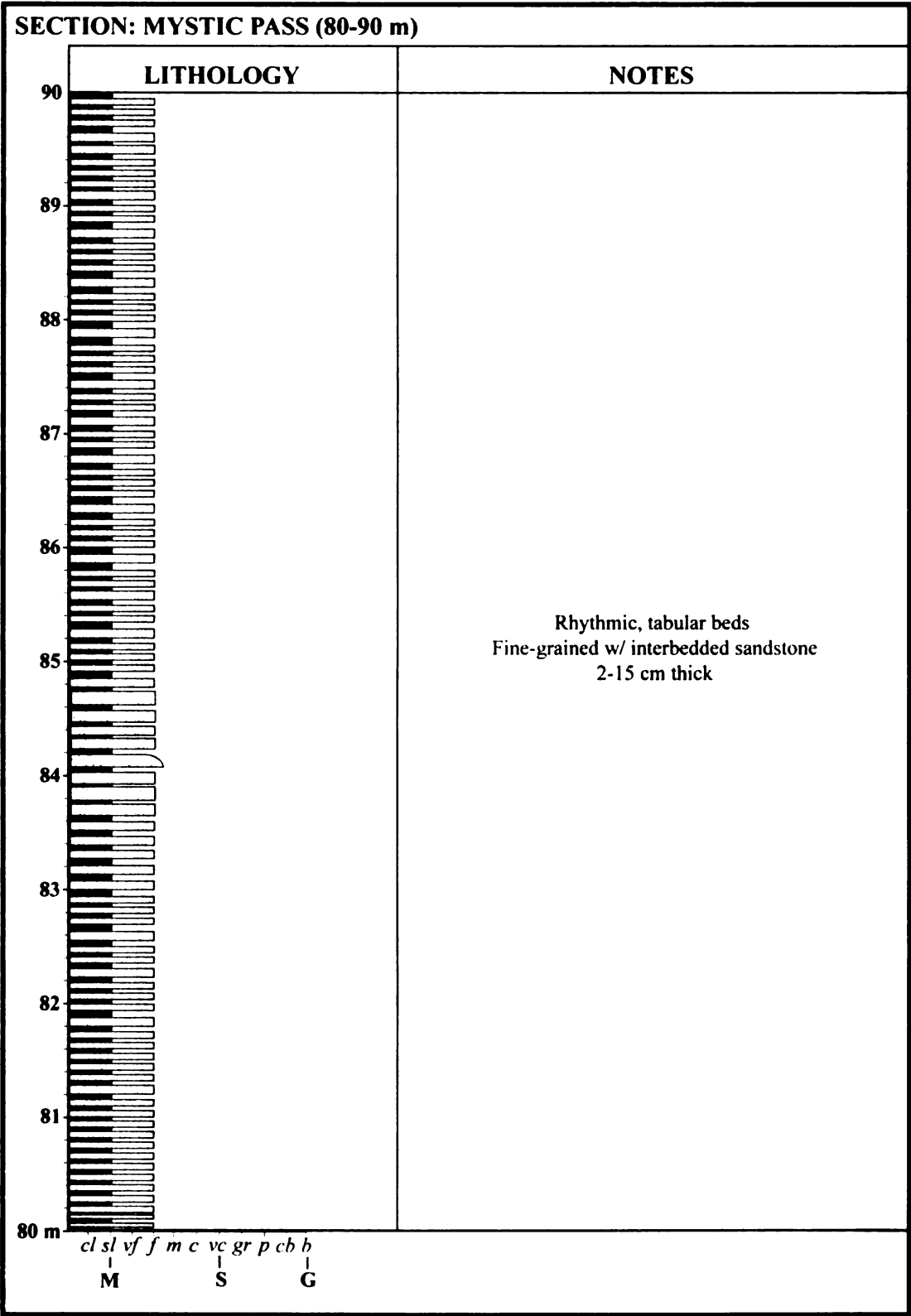


Figure A I continued

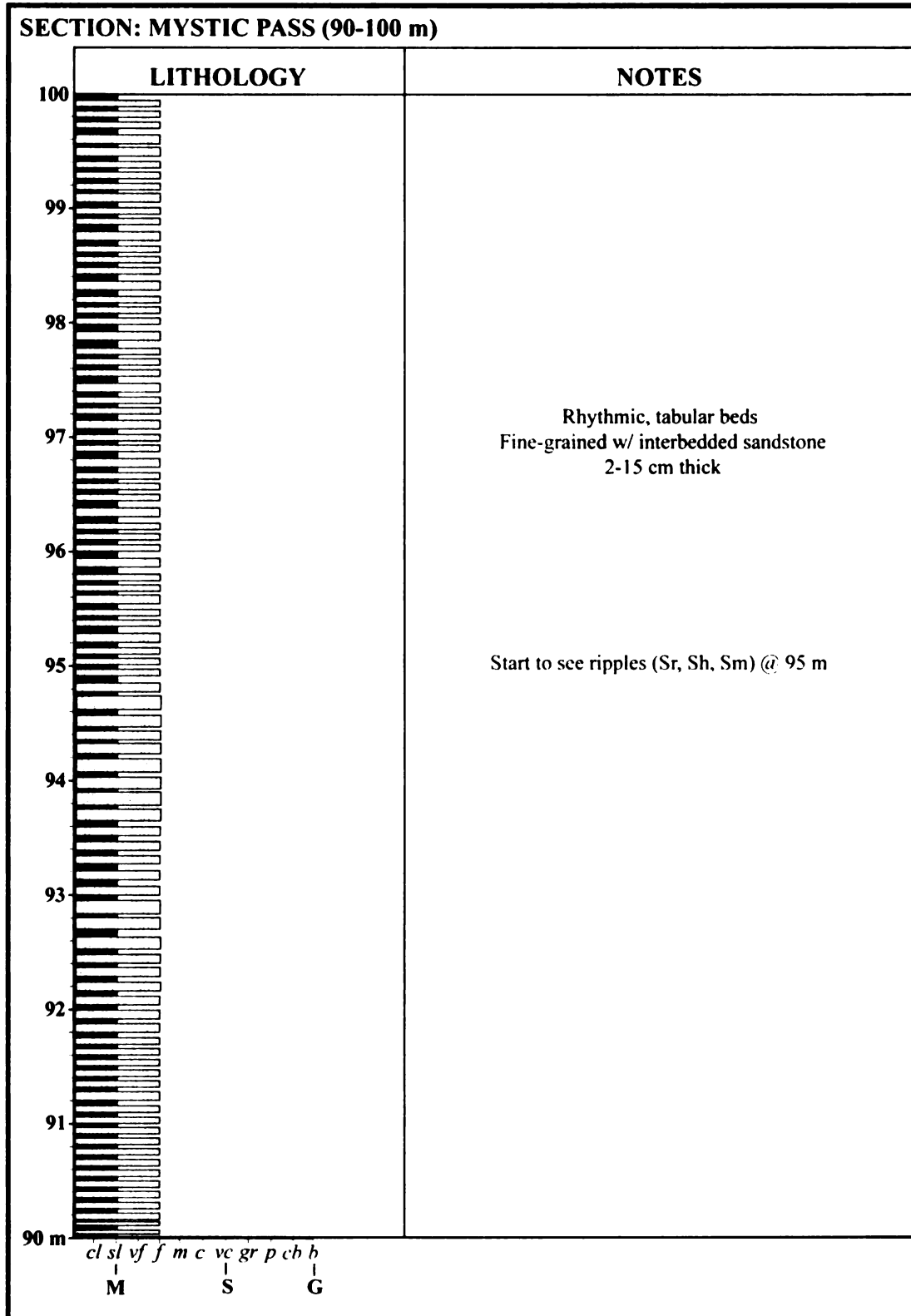


Figure A1 continued

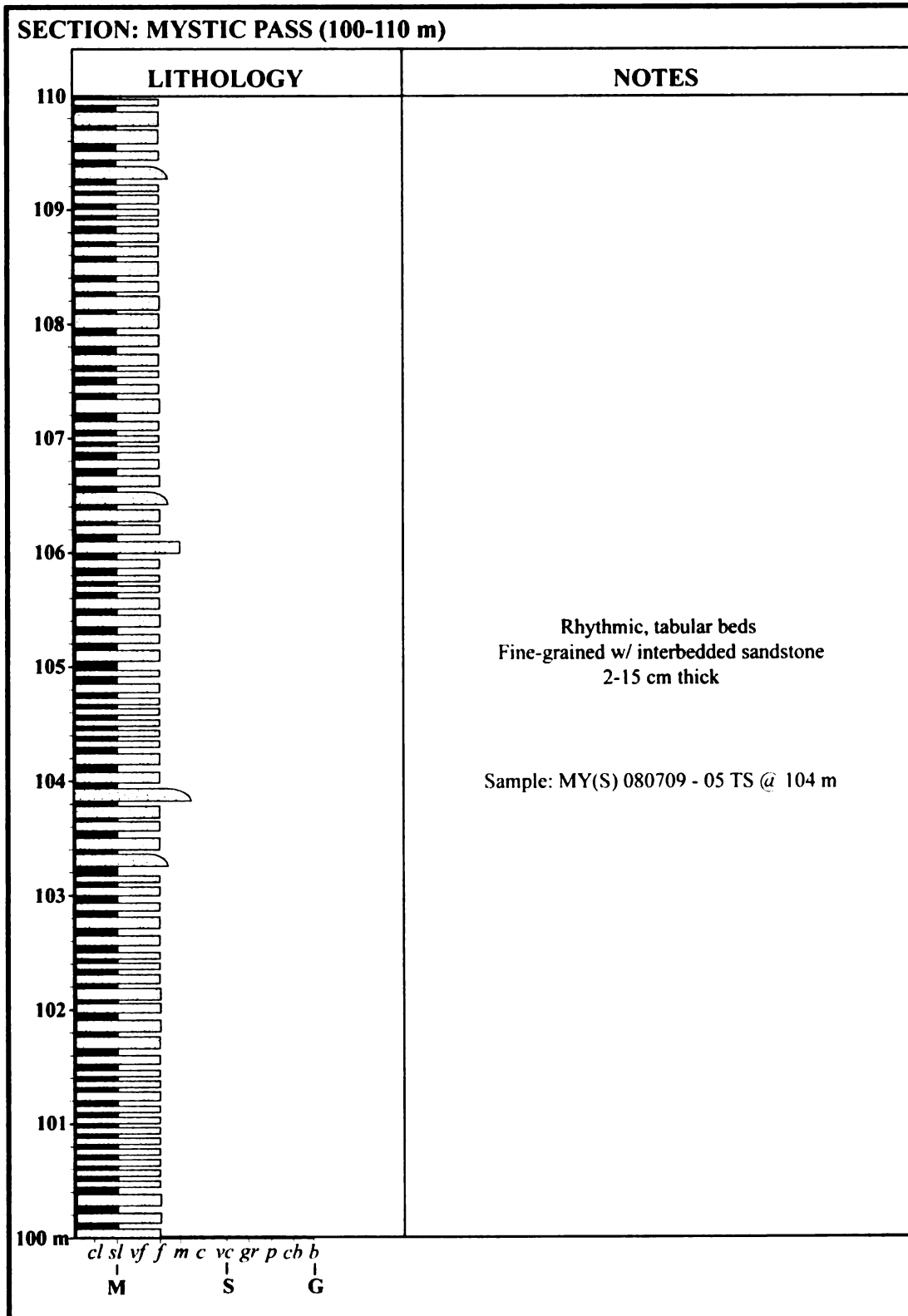




Figure A1 continued

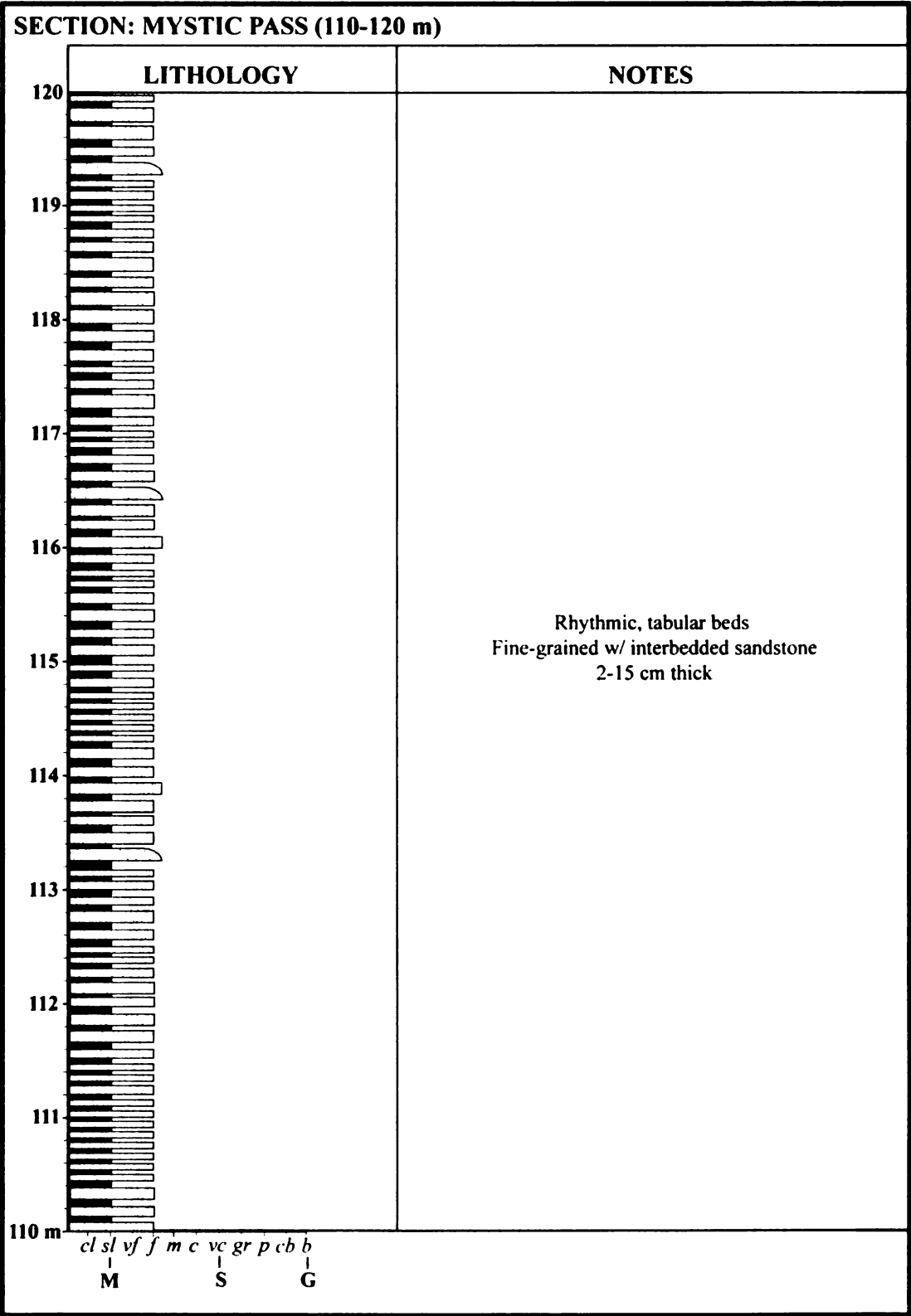
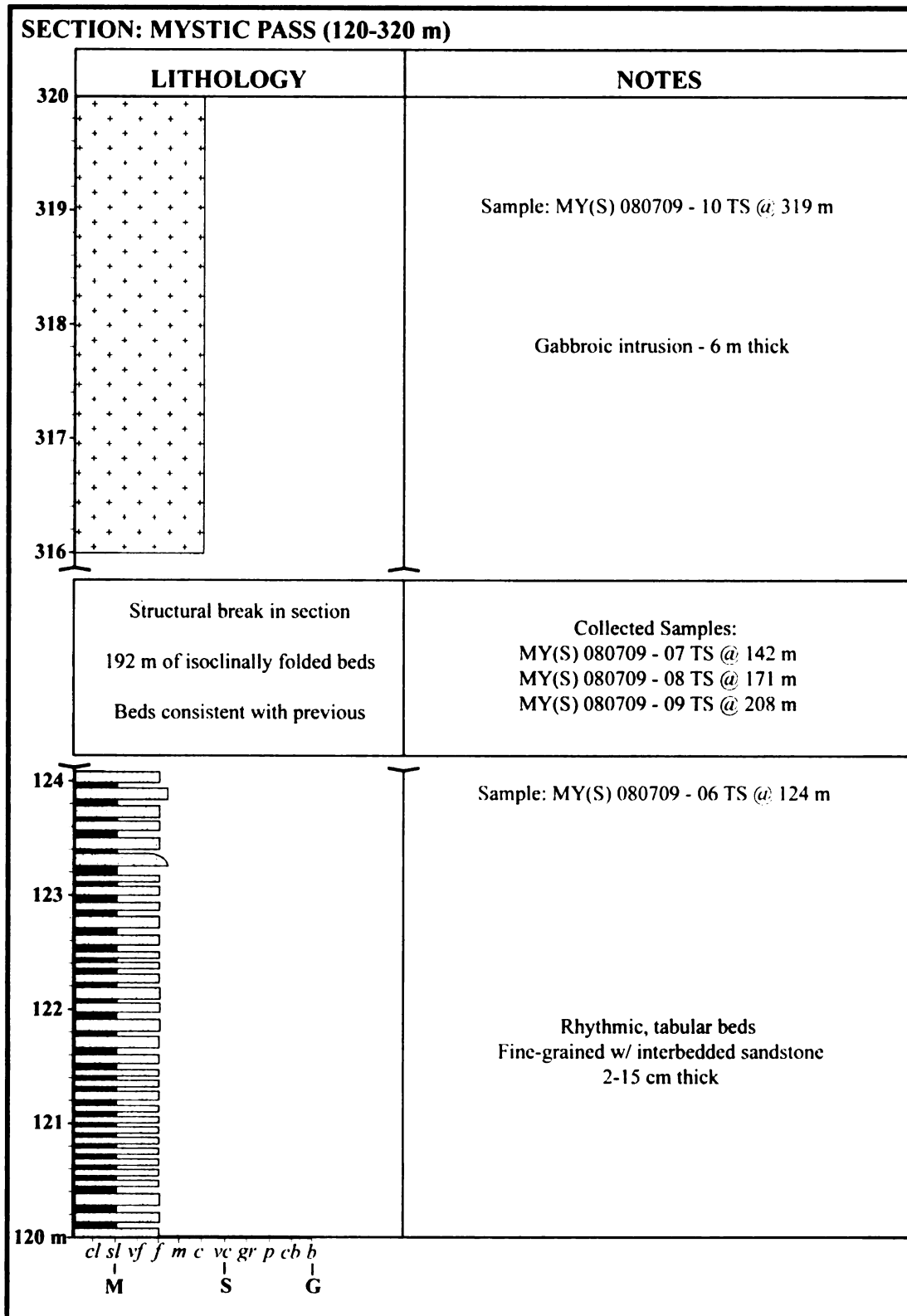
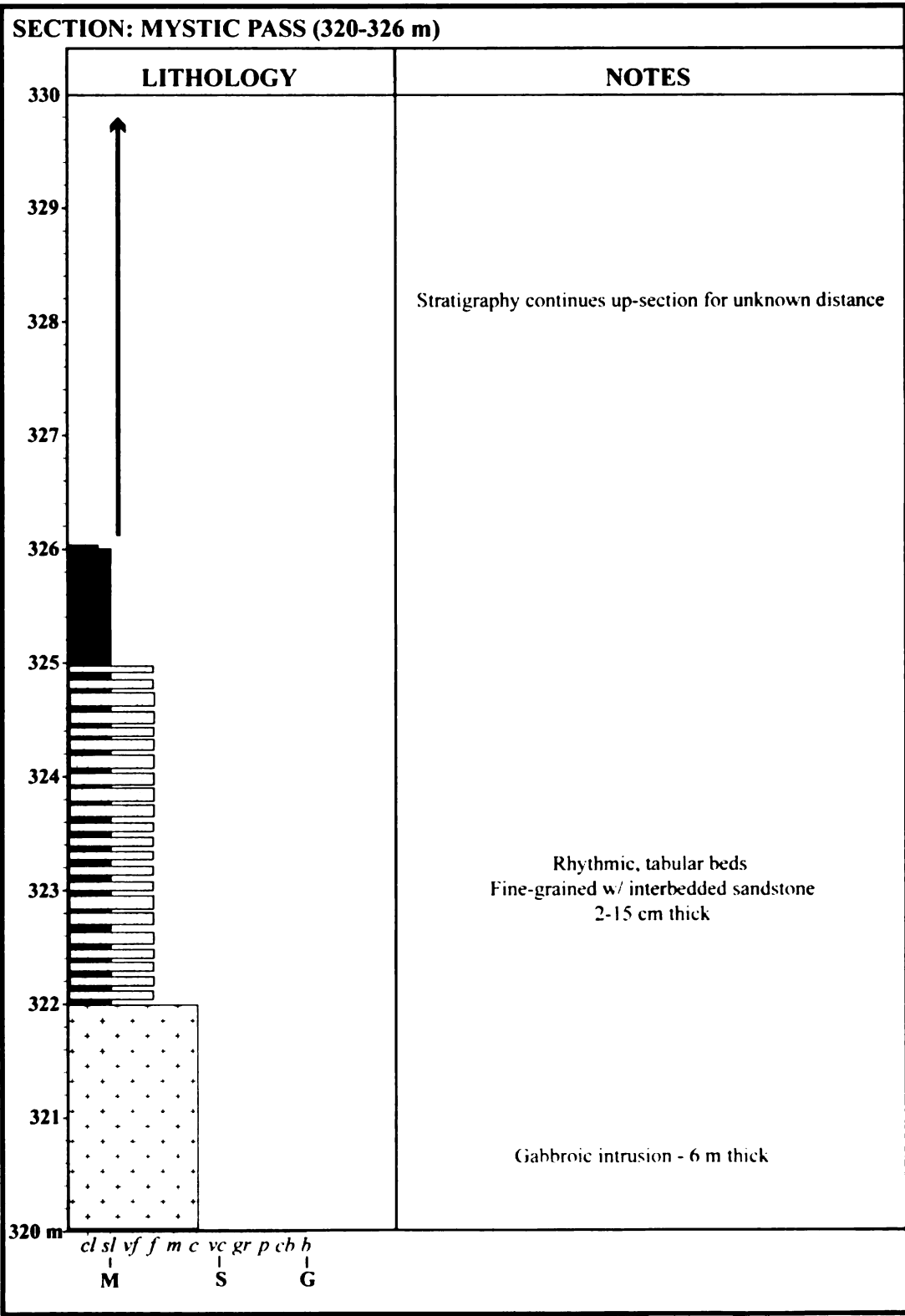


Figure A1 continued



**Figure A1 continued**



**APPENDIX B:**  
**Raw point-count data**

**Table B1.** Raw point-count data from sandstones of the Mystic Pass formation.

<b>Raw point-count data table</b>									
<b>Sample</b>	<b>Qm</b>	<b>Qp</b>	<b>P</b>	<b>K</b>	<b>C</b>	<b>Lv</b>	<b>Lm</b>	<b>Ls</b>	<b>Total</b>
<b>MYN 080709-01</b>	2	2	2	4	13	362	1	14	400
<b>MYN 080709-02</b>	5	4	12	5	45	304	2	23	400
<b>MYN 080709-03</b>	5	3	13	10	41	316	0	12	400
<b>MYN 080709-04</b>	7	1	10	5	39	327	0	11	400
<b>MYN 080709-05</b>	9	3	12	11	25	319	0	21	400
<b>MYN 080709-07</b>	11	3	12	6	56	292	0	20	400
<b>MYN 080709-08</b>	11	3	6	9	26	318	0	27	400
<b>MYN 080709-09</b>	18	2	7	13	109	226	0	25	400
<b>MYN 080709-10</b>	10	3	6	0	67	241	0	73	400
<b>MYN 080709-11</b>	22	4	1	2	85	243	0	43	400
<b>MYN 080709-12</b>	15	0	5	0	88	245	10	37	400
<b>MYN 080709-13</b>	18	2	3	1	78	237	1	60	400
<b>MYN 080709-15</b>	9	1	1	4	46	247	3	89	400
<b>MYN 080709-16</b>	11	2	3	1	74	231	0	78	400
<b>MYN 080709-17</b>	11	0	1	0	85	219	0	84	400
<b>MYN 080709-18</b>	9	0	2	1	83	218	0	87	400
<b>MYN 080709-19</b>	19	1	1	3	105	208	0	63	400
<b>MYN 080709-20</b>	22	2	7	2	92	223	0	52	400
<b>MYN 080709-21</b>	24	0	12	4	46	253	0	61	400
<b>MYN 080709-22</b>	8	0	5	1	61	230	0	95	400
<b>MYN 080709-23</b>	24	2	5	6	46	244	0	73	400
<b>MYN 080709-24</b>	14	1	3	0	38	268	0	76	400
<b>MYN 080709-25</b>	10	0	5	5	33	286	0	61	400
<b>MYN 080709-26</b>	30	4	7	4	34	249	0	72	400
<b>MYN 080709-28</b>	18	2	2	3	38	253	0	84	400
<b>MYS 080709-04</b>	10	1	1	1	5	316	0	66	400
<b>MYS 080709-07</b>	13	0	3	0	33	265	0	86	400
<b>MYS 080709-08</b>	4	0	4	0	19	280	0	93	400
<b>01 DZ</b>	24	1	2	5	18	269	0	81	400
<b>03 DZ</b>	19	2	3	2	19	231	0	124	400
<b>05 DZ</b>	27	5	10	2	43	245	0	68	400

## APPENDIX C:

### Analytical results of U-Pb detrital zircon isotope ratios and age data

**Appendix 3.2** Measured isotopic ratios and age data reported for detrital zircon samples from the Mystic Pass Formation. All uncertainties are reported at the 1 sigma level, and include only measurement errors. Systematic errors would increase the uncertainty of clusters of ages by 1-2%. U concentration and U/Th are calibrated relative to our Sri Lanka zircon and are accurate to ~20%. Common Pb correction is from  $^{204}\text{Pb}$ , with composition interpreted from Stacey and Kramers (1975) and uncertainties of 1.0 for  $^{206}\text{Pb}/^{204}\text{Pb}$ , 0.3 for  $^{207}\text{Pb}/^{204}\text{Pb}$ , and 2.0 for  $^{208}\text{Pb}/^{204}\text{Pb}$ . U/Pb and  $^{206}\text{Pb}/^{207}\text{Pb}$  fractionation is calibrated relative to fragments of a large Sri Lanka zircon of  $563.5 \pm 3.2$  Ma (2-sigma). U decay constants and composition as follows:  $^{238}\text{U} = 9.8485 \times 10^{-10}$ ,  $^{235}\text{U} = 1.55125 \times 10^{-10}$ ,  $^{238}\text{U}/^{235}\text{U} = 137.88$

**Table C1.** Analytical results of U-Pb detrital zircon isotope ratios and age data from the Mystic Pass formation.

**Sample: MYS 080209-01**

Sample: MYS 080209-01																			
Sample #	U (ppm)	206Pb/204Pb	U/Th	206Pb* ± 207Pb* (%)	Isotope ratios				Apparent ages (Ma)				Best age ± (Ma)	Conc (%)					
					206Pb* ± 207Pb* (%)	238U (%)	206Pb* ± 207Pb* (%)	error corr.	206Pb* ± 207Pb* (Ma)	235U (Ma)	207Pb* ± 206Pb* (Ma)								
-1	231	8092	1.5	18.80	4.5	0.425	4.6	0.058	0.7	0.15	363.4	2.4	359.9	13.9	337.2	102.9	363.4	2.4	107.8
-3	108	4914	1.3	18.23	13.5	0.417	13.7	0.055	2.4	0.17	345.8	7.9	353.8	40.9	406.5	303.2	345.8	7.9	85.1
-4	101	23901	1.6	8.64	1.1	5.416	1.6	0.339	1.3	0.76	1883.5	20.5	1887.4	14.1	1891.7	19.3	1891.7	19.3	99.6
-5	118	34987	0.6	8.57	0.8	5.583	3.1	0.347	3.0	0.97	1919.9	50.6	1913.4	27.1	1906.4	14.0	1906.4	14.0	100.7
-6	113	31003	1.9	8.74	1.5	5.364	2.2	0.340	1.7	0.75	1887.0	27.0	1879.1	19.0	1870.4	26.6	1870.4	26.6	100.9
-7	314	86268	2.5	8.06	0.5	6.372	1.0	0.373	0.8	0.85	2041.8	14.8	2028.5	8.7	2014.9	9.1	2014.9	9.1	101.3
-8	437	9232	1.1	18.49	2.2	0.416	4.3	0.056	3.7	0.86	350.3	12.7	353.5	13.0	374.4	50.4	350.3	12.7	93.6
-9	84	3951	1.4	21.80	17.7	0.344	17.8	0.054	1.6	0.09	341.3	5.4	300.0	46.2	-9.6	430.6	341.3	5.4	-3552.7
-10	219	11692	1.8	17.95	3.8	0.537	3.9	0.070	1.0	0.27	436.0	4.4	436.7	14.0	440.7	84.6	436.0	4.4	98.9
-12	185	8200	2.5	18.93	7.2	0.497	7.3	0.068	1.1	0.16	425.2	4.7	409.4	24.6	321.0	163.9	425.2	4.7	132.5
-13	103	3126	0.7	18.88	9.5	0.402	9.8	0.055	2.4	0.24	345.3	7.9	343.0	28.6	327.3	216.8	345.3	7.9	105.5
-14	229	28782	4.9	14.08	1.2	1.630	1.3	0.167	0.6	0.43	993.0	5.1	982.0	8.2	957.4	24.0	993.0	5.1	103.7
-15	218	27037	2.7	12.20	1.1	2.471	1.4	0.219	0.8	0.62	1274.8	9.8	1263.5	9.9	1244.2	21.1	1244.2	21.1	102.5
-16	229	16434	1.6	15.08	1.9	1.237	2.6	0.135	1.8	0.68	818.0	13.5	817.6	14.4	816.6	39.1	818.0	13.5	100.2
-17	202	6825	1.0	19.31	7.8	0.379	8.0	0.053	1.8	0.22	332.9	5.8	325.9	22.3	276.4	178.9	332.9	5.8	120.5
-18	44	11873	0.8	8.98	2.6	5.018	3.4	0.327	2.2	0.64	1822.1	34.5	1822.3	28.9	1822.5	47.8	1822.5	47.8	100.0
-19	124	5619	1.5	18.62	13.7	0.497	13.9	0.067	2.4	0.17	419.0	9.9	409.9	47.0	359.2	310.4	419.0	9.9	116.6
-20	186	8480	2.2	18.26	3.9	0.563	4.5	0.075	2.3	0.51	463.3	10.2	453.2	16.5	402.3	87.0	463.3	10.2	115.2
-21	153	6829	2.3	17.66	4.3	0.629	5.8	0.081	3.9	0.68	499.8	18.9	495.7	22.7	476.5	94.2	499.8	18.9	104.9
-22	145	6039	1.0	18.41	7.0	0.406	7.3	0.054	1.7	0.24	340.3	5.7	345.9	21.3	383.7	158.6	340.3	5.7	88.7
-23	75	680	0.5	16.62	12.5	0.441	13.0	0.053	3.6	0.28	334.1	11.9	371.3	40.4	610.0	270.1	334.1	11.9	54.8
-24	396	31370	4.4	16.24	1.6	0.892	2.8	0.105	2.3	0.81	644.1	13.8	647.7	13.3	660.0	34.8	644.1	13.8	97.6
-25	143	5107	2.9	17.72	6.2	0.549	6.3	0.071	1.0	0.17	439.3	4.4	444.1	22.6	469.4	137.1	439.3	4.4	93.6
-26	118	27217	2.4	8.77	1.2	5.346	2.5	0.340	2.2	0.87	1886.1	35.7	1876.2	21.4	1865.3	22.3	1865.3	22.3	101.1
-27	384	13924	0.8	19.12	2.4	0.381	3.1	0.053	2.0	0.64	332.0	6.5	327.9	8.8	298.7	54.7	332.0	6.5	111.1
-28	164	48823	3.2	6.13	0.9	9.582	4.2	0.426	4.1	0.97	2288.0	79.0	2395.5	38.7	2488.2	15.9	2488.2	15.9	92.0
-30	123	4365	0.7	17.27	9.6	0.413	10.3	0.052	3.8	0.37	325.1	12.0	351.1	30.7	526.6	210.9	325.1	12.0	61.7
-31	88	23374	2.4	8.59	1.7	5.633	2.0	0.351	1.0	0.49	1938.6	16.0	1921.1	16.8	1902.3	30.6	1902.3	30.6	101.9
-32	282	52076	3.6	8.48	0.6	5.639	2.6	0.347	2.6	0.97	1919.4	42.4	1922.1	22.6	1925.0	11.0	1925.0	11.0	99.7



Table C1 continued

-33	153	5857	0.8	17.54	9.4	0.490	9.6	0.062	1.7	0.18	389.5	6.5	404.7	32.0	492.3	208.1	389.5	6.5	79.1
-34	158	38493	2.1	8.72	0.6	5.440	1.7	0.344	1.6	0.94	1906.9	26.5	1891.2	14.6	1874.0	10.1	1874.0	10.1	101.8
-35	263	10258	0.9	18.96	5.8	0.389	6.2	0.054	2.2	0.35	336.3	7.2	334.0	17.7	317.8	132.1	336.3	7.2	105.8
-37	194	46761	1.1	9.32	0.6	4.717	1.5	0.319	1.3	0.91	1783.4	20.9	1770.3	12.3	1754.8	11.0	1754.8	11.0	101.6
-39	98	3300	1.9	21.59	8.6	0.339	8.6	0.053	1.0	0.12	333.1	3.4	296.1	22.2	14.3	206.2	333.1	3.4	2323.2
-40	122	24677	2.6	8.69	1.0	5.251	3.3	0.331	3.1	0.95	1843.4	49.5	1860.9	27.8	1880.5	18.5	1880.5	18.5	98.0
-41	33	8215	1.4	8.37	2.9	6.073	3.7	0.369	2.2	0.60	2022.4	37.9	1986.4	32.0	1949.2	52.7	1949.2	52.7	103.8
-42	96	15304	2.2	8.87	1.5	4.723	2.1	0.304	1.4	0.68	1710.4	21.2	1771.3	17.5	1843.8	27.8	1843.8	27.8	92.8
-43	141	9656	2.4	18.94	11.6	0.522	12.0	0.072	2.9	0.24	446.3	12.5	426.4	41.7	319.9	264.4	446.3	12.5	139.5
-44	491	24819	1.9	17.95	1.6	0.517	1.7	0.067	0.5	0.28	419.7	1.9	422.9	5.9	440.7	36.3	419.7	1.9	95.2
-45	68	37444	1.1	3.93	0.6	23.388	1.1	0.666	0.9	0.82	3290.9	23.2	3243.2	10.7	3213.9	10.0	3213.9	10.0	102.4
-46	905	163347	2.0	9.28	0.3	4.757	1.2	0.320	1.1	0.96	1791.0	17.7	1777.3	9.8	1761.2	5.7	1761.2	5.7	101.7
-47	248	11051	0.9	19.43	6.7	0.408	6.8	0.057	1.5	0.22	360.1	5.3	347.2	20.1	261.6	153.0	360.1	5.3	137.7
-51	178	6288	0.9	18.16	7.5	0.425	7.6	0.056	0.9	0.11	351.0	2.9	359.6	22.9	415.2	168.3	351.0	2.9	84.5
-52	302	52103	2.1	9.85	5.3	2.877	6.3	0.206	3.4	0.54	1205.1	37.4	1375.9	47.6	1651.9	98.7	1651.9	98.7	73.0
-53	569	27454	14.8	18.38	2.5	0.484	5.1	0.064	4.4	0.87	402.9	17.3	400.6	16.9	387.4	55.9	402.9	17.3	104.0
-56	96	3385	0.6	22.40	19.1	0.318	19.3	0.052	2.3	0.12	324.6	7.4	280.3	47.2	-74.7	470.9	324.6	7.4	-434.3
-57	74	4899	2.6	18.53	17.3	0.578	17.7	0.078	3.5	0.20	482.1	16.5	463.1	65.8	370.2	392.8	482.1	16.5	130.2
-58	107	4153	0.7	19.50	10.1	0.445	10.4	0.063	2.8	0.27	393.3	10.7	373.7	32.7	254.0	232.0	393.3	10.7	154.8
-59	148	5594	0.9	19.97	8.2	0.387	8.2	0.056	0.7	0.09	351.9	2.4	332.4	23.3	198.2	190.4	351.9	2.4	177.5
-60	50	14116	1.2	8.56	1.9	5.672	2.5	0.352	1.7	0.66	1944.6	28.2	1927.1	22.0	1908.3	34.3	1908.3	34.3	101.9
-61	181	7859	2.3	19.27	8.0	0.491	11.2	0.069	7.9	0.70	428.0	32.7	405.7	37.6	280.7	183.0	428.0	32.7	152.5
-62	192	60281	2.2	5.92	0.5	11.476	2.0	0.493	1.9	0.97	2582.0	41.0	2562.6	18.5	2547.3	7.9	2547.3	7.9	101.4
-63	121	4371	1.6	20.14	11.6	0.385	11.8	0.056	2.0	0.17	352.4	7.0	330.4	33.2	178.5	271.1	352.4	7.0	197.4
-64	73	2674	1.3	19.27	15.1	0.424	15.4	0.059	2.7	0.18	371.2	9.8	359.0	46.5	280.4	348.1	371.2	9.8	132.4
-65	101	28457	1.7	5.28	0.5	13.184	4.5	0.505	4.5	0.99	2634.2	96.5	2692.9	42.4	2737.2	8.2	2737.2	8.2	96.2
-68	134	32174	4.3	8.04	1.2	6.514	1.9	0.380	1.4	0.75	2075.7	24.7	2047.8	16.3	2019.7	21.6	2019.7	21.6	102.8
-69	233	12020	2.4	17.91	3.9	0.540	4.2	0.070	1.5	0.36	437.0	6.3	438.4	14.9	446.0	87.0	437.0	6.3	98.0
-70	349	17780	1.0	18.87	5.3	0.398	5.6	0.054	1.8	0.32	341.7	5.9	340.0	16.1	328.7	119.6	341.7	5.9	104.0
-71	208	54250	1.9	7.82	0.5	6.664	3.8	0.378	3.8	0.99	2067.3	67.0	2067.9	33.8	2068.5	9.6	2068.5	9.6	99.9
-72	624	39320	3.7	14.73	2.2	0.919	4.8	0.098	4.2	0.88	604.2	24.4	662.1	23.3	864.5	46.3	604.2	24.4	69.9
-74	648	30272	2.3	17.58	1.4	0.564	2.7	0.072	2.3	0.86	447.6	9.9	454.1	9.8	487.1	30.1	447.6	9.9	91.9
-75	55	16462	2.3	8.01	1.8	6.302	3.4	0.366	2.9	0.85	2010.6	49.3	2018.7	29.5	2027.0	31.7	2027.0	31.7	99.2

Table C1 continued

-76	218	9610	1.6	17.83	5.6	0.429	6.4	0.056	3.2	0.50	348.5	10.8	362.8	19.5	455.4	123.4	348.5	10.8	76.5
-77	176	35825	1.2	8.96	0.8	4.795	4.0	0.312	3.9	0.98	1748.5	59.8	1784.1	33.4	1825.8	13.7	1825.8	13.7	95.8
-78	298	6534	2.1	19.81	3.3	0.398	3.8	0.057	1.9	0.49	358.6	6.6	340.3	11.1	216.8	77.0	358.6	6.6	165.5
-79	209	7286	2.7	19.94	7.1	0.368	7.3	0.053	1.8	0.24	334.1	5.7	318.0	20.0	201.7	165.5	334.1	5.7	165.6
-80	85	20401	1.8	9.23	1.3	4.407	2.6	0.295	2.2	0.86	1666.0	32.6	1713.7	21.5	1772.5	24.5	1772.5	24.5	94.0
-82	176	58276	1.2	6.44	1.7	9.692	4.2	0.453	3.8	0.92	2407.4	76.7	2406.0	38.4	2404.7	28.2	2404.7	28.2	100.1
-83	320	13695	0.9	19.01	5.4	0.406	5.4	0.056	0.9	0.17	351.5	3.1	346.3	16.0	311.4	122.2	351.5	3.1	112.9
-85	186	9790	1.9	18.31	7.5	0.506	7.6	0.067	1.1	0.14	419.6	4.4	416.0	25.9	396.0	168.8	419.6	4.4	106.0
-86	233	44994	1.5	9.51	0.4	4.556	1.7	0.314	1.6	0.97	1761.2	25.0	1741.3	14.0	1717.5	7.9	1717.5	7.9	102.5
-88	102	5387	1.4	21.74	13.7	0.405	13.8	0.064	1.5	0.11	398.8	5.7	345.0	40.3	-3.0	331.5	398.8	5.7	-13332.1
-89	206	10696	3.6	16.19	9.0	0.584	11.1	0.069	6.6	0.59	427.7	27.2	467.2	41.8	666.6	193.1	427.7	27.2	64.2
-92	55	19931	1.1	4.83	1.1	16.465	3.2	0.577	3.0	0.94	2936.0	71.6	2904.2	30.9	2882.3	18.0	2882.3	18.0	101.9
-93	173	35466	5.7	8.52	0.8	5.705	1.6	0.352	1.3	0.84	1945.9	22.2	1932.2	13.6	1917.4	15.1	1917.4	15.1	101.5
-94	407	17895	1.2	18.16	2.5	0.487	3.2	0.064	2.0	0.63	400.4	7.8	402.5	10.7	414.8	55.9	400.4	7.8	96.5
-95	155	32099	2.8	7.73	0.6	7.130	2.0	0.400	2.0	0.96	2167.8	36.3	2127.8	18.2	2089.4	9.7	2089.4	9.7	103.8
-96	434	17639	4.0	18.44	2.9	0.410	3.3	0.055	1.5	0.47	343.7	5.1	348.5	9.7	380.5	65.7	343.7	5.1	90.3
-97	143	37621	2.3	8.64	1.0	5.618	1.9	0.352	1.6	0.86	1944.7	27.6	1918.8	16.5	1891.0	17.7	1891.0	17.7	102.8
-98	218	7694	3.3	18.69	6.8	0.381	6.8	0.052	0.8	0.11	324.1	2.5	327.4	19.0	350.7	152.8	324.1	2.5	92.4
-100	222	11681	1.3	18.19	5.8	0.542	5.9	0.071	1.0	0.16	444.9	4.1	439.6	21.1	411.5	130.6	444.9	4.1	108.1
-101	174	7440	2.2	18.35	5.5	0.554	5.6	0.074	0.9	0.16	458.9	3.9	447.9	20.3	392.0	124.4	458.9	3.9	117.0
-102	291	10815	2.3	18.03	5.6	0.573	5.9	0.075	1.6	0.28	465.6	7.4	459.7	21.6	430.5	125.3	465.6	7.4	108.1
-104	127	21476	1.5	9.59	0.8	4.342	1.3	0.302	0.9	0.74	1701.4	13.8	1701.5	10.3	1701.6	15.6	1701.6	15.6	100.0
-105	88	1629	1.2	19.16	21.3	0.407	21.5	0.057	2.5	0.12	354.3	8.7	346.4	63.2	293.6	492.3	354.3	8.7	120.7

Table C1 continued

Sample: MYS 080903-03																			
Sample #	U (ppm)	206Pb/204Pb	U/Th	206Pb* ± 207Pb* (%)	Isotope ratios				Apparent ages (Ma)				Conc (%)						
					207Pb* ± 235U* (%)	206Pb* ± 238U (%)	± error corr.	206Pb* ± 238U* (Ma)	± 207Pb* ± 235U (Ma)	± 206Pb* ± 207Pb* (Ma)	± Best age (Ma)								
-1	983	39404	5.6	19.17	0.9	0.339	1.9	0.047	1.6	0.89	296.8	4.8	296.4	4.8	292.9	19.7	296.8	4.8	101.3
-2	83	5648	2.8	18.17	7.4	0.536	7.9	0.071	2.8	0.36	440.3	12.0	435.9	28.1	413.2	165.9	440.3	12.0	106.6
-3	1347	46381	5.7	18.98	0.6	0.341	2.6	0.047	2.5	0.97	295.8	7.3	298.1	6.7	315.4	14.2	295.8	7.3	93.8
-4	1450	62001	6.8	19.03	0.9	0.345	2.5	0.048	2.4	0.94	299.8	6.9	300.9	6.6	309.2	19.5	299.8	6.9	97.0
-5	94	6790	3.0	19.10	6.3	0.503	6.7	0.070	2.2	0.32	434.5	9.0	414.0	22.7	301.6	144.3	434.5	9.0	144.1
-6	154	8904	3.4	18.62	5.4	0.504	5.7	0.068	1.7	0.29	424.2	6.8	414.1	19.3	358.2	122.5	424.2	6.8	118.4
-6C	992	45707	5.9	19.06	0.8	0.347	2.2	0.048	2.0	0.92	302.2	6.0	302.6	5.7	305.9	19.1	302.2	6.0	98.8
-7	1149	54171	5.4	18.97	0.8	0.342	4.4	0.047	4.3	0.98	296.6	12.6	298.9	11.4	316.9	17.7	296.6	12.6	93.6
-8	1087	59298	6.2	19.13	0.9	0.345	1.9	0.048	1.6	0.87	301.8	4.8	301.3	4.9	297.4	21.5	301.8	4.8	101.5
-9	1346	99452	6.1	18.99	0.6	0.346	2.3	0.048	2.2	0.97	299.7	6.5	301.4	6.0	314.2	12.9	299.7	6.5	95.4
-11	1262	32059	4.5	19.34	1.1	0.346	1.3	0.048	0.8	0.61	305.2	2.4	301.4	3.5	272.1	24.4	305.2	2.4	112.2
-13	82	2714	1.4	22.97	19.6	0.320	19.6	0.053	1.0	0.05	334.9	3.4	282.0	48.3	-136.7	488.4	334.9	3.4	-245.0
-14	2414	56167	3.0	18.41	3.6	0.309	4.1	0.041	2.0	0.49	260.8	5.1	273.6	9.9	384.3	81.3	260.8	5.1	67.9
-15	149	31049	2.1	12.70	0.9	2.206	1.6	0.203	1.4	0.84	1191.9	14.8	1182.9	11.3	1166.3	17.5	1166.3	17.5	102.2
-16	1040	21372	5.7	19.33	1.1	0.331	2.9	0.046	2.6	0.92	292.8	7.6	290.7	7.2	273.3	25.1	292.8	7.6	107.2
-17	1423	32677	5.2	18.95	0.6	0.332	1.9	0.046	1.8	0.96	288.0	5.2	291.4	4.9	318.6	12.6	288.0	5.2	90.4
-18	197	34538	4.3	8.52	0.4	5.567	2.5	0.344	2.4	0.99	1905.2	40.3	1910.9	21.3	1917.2	6.4	1917.2	6.4	99.4
-19A	364	14520	2.0	18.00	1.8	0.578	2.5	0.075	1.7	0.70	468.9	7.9	463.1	9.3	434.6	39.7	468.9	7.9	107.9
-19B	95	15016	1.8	9.36	1.3	4.402	1.5	0.299	0.8	0.52	1685.8	11.4	1712.7	12.4	1745.7	23.4	1745.7	23.4	96.6
-19C	1840	45339	2.5	19.02	1.2	0.305	1.9	0.042	1.5	0.80	266.0	4.0	270.6	4.6	310.7	26.3	266.0	4.0	85.6
-20	1831	45389	4.1	19.00	0.6	0.349	1.5	0.048	1.3	0.91	302.8	3.9	304.0	3.8	313.1	13.6	302.8	3.9	96.7
-21	142	10624	3.5	18.35	4.5	0.537	5.1	0.071	2.5	0.49	445.1	10.7	436.6	18.2	391.7	100.2	445.1	10.7	113.6
-21A	2316	65820	3.3	18.88	0.4	0.308	2.9	0.042	2.8	0.99	266.4	7.4	272.7	6.8	327.0	9.3	266.4	7.4	81.5
-22A	1188	35907	7.6	19.10	0.7	0.352	1.9	0.049	1.8	0.93	307.1	5.3	306.4	5.0	300.7	15.5	307.1	5.3	102.1
-23	1043	51995	8.5	19.24	0.8	0.345	1.6	0.048	1.4	0.86	302.8	4.2	300.7	4.3	284.1	19.0	302.8	4.2	106.6
-24	1170	49328	6.2	19.19	1.0	0.339	1.9	0.047	1.6	0.84	297.0	4.7	296.3	4.9	290.7	24.0	297.0	4.7	102.2
-26	1297	73002	5.2	19.06	0.6	0.345	1.4	0.048	1.3	0.92	300.3	3.9	300.9	3.7	305.8	12.8	300.3	3.9	98.2
-27	1070	63499	6.1	19.07	0.7	0.354	3.6	0.049	3.5	0.98	308.5	10.6	308.0	9.5	304.6	15.8	308.5	10.6	101.3
-28A	2138	61337	2.9	18.64	1.0	0.322	1.2	0.044	0.7	0.53	275.0	1.8	283.8	3.1	356.7	23.7	275.0	1.8	77.1

Table C1 continued

-29	1167	57819	6.9	19.26	1.2	0.343	3.4	0.048	3.2	0.94	301.8	9.5	299.6	8.9	282.2	26.3	301.8	9.5	107.0
-30	2019	75361	4.2	19.03	0.9	0.342	2.1	0.047	1.8	0.89	297.1	5.4	298.5	5.4	309.1	21.6	297.1	5.4	96.1
-32	1224	53204	6.1	19.10	0.7	0.348	1.9	0.048	1.7	0.93	303.8	5.1	303.5	4.9	301.4	15.7	303.8	5.1	100.8
-33	1736	39799	2.8	18.63	0.8	0.324	2.6	0.044	2.5	0.95	276.3	6.7	285.1	6.5	357.8	18.3	276.3	6.7	77.2
-34	1918	55475	3.1	18.56	0.8	0.319	2.4	0.043	2.3	0.94	271.2	6.1	281.2	6.0	365.6	18.7	271.2	6.1	74.2
-35	1476	68390	4.1	19.15	0.8	0.340	1.3	0.047	1.0	0.77	297.3	2.9	297.1	3.3	295.5	18.6	297.3	2.9	100.6
-36	223	91312	36.4	7.79	2.9	5.964	3.4	0.337	1.8	0.52	1872.2	28.6	1970.5	29.7	2075.5	51.4	2075.5	51.4	90.2
-37	206	20332	2.7	17.85	1.5	0.594	2.0	0.077	1.3	0.64	477.3	5.9	473.1	7.6	452.8	34.3	477.3	5.9	105.4
-38	2939	71961	2.7	18.87	0.4	0.286	1.4	0.039	1.3	0.96	247.6	3.2	255.4	3.1	328.1	8.9	247.6	3.2	75.5
-41	172	75287	2.4	8.78	0.4	5.253	1.8	0.334	1.8	0.97	1859.3	29.0	1861.2	15.7	1863.3	7.6	1863.3	7.6	99.8
-42	79	30120	1.4	8.16	1.1	6.124	2.3	0.362	2.1	0.89	1993.9	35.2	1993.6	20.1	1993.3	18.7	1993.3	18.7	100.0
-43	221	10980	1.6	17.22	7.7	0.528	8.0	0.066	2.0	0.24	412.0	7.8	430.7	28.0	532.1	169.8	412.0	7.8	77.4
-43A	128	29890	1.5	9.91	0.6	4.109	1.8	0.295	1.7	0.94	1668.8	24.7	1656.2	14.6	1640.2	11.2	1640.2	11.2	101.7
-44	1564	58734	4.9	19.15	0.7	0.325	2.6	0.045	2.5	0.96	284.5	7.0	285.7	6.5	295.3	15.9	284.5	7.0	96.4
-45	1599	48493	5.6	19.00	0.7	0.342	2.6	0.047	2.5	0.96	296.4	7.4	298.3	6.8	313.3	17.0	296.4	7.4	94.6
-46	88	22339	1.8	8.76	0.7	4.755	2.3	0.302	2.1	0.95	1702.3	32.0	1777.0	18.9	1865.9	13.0	1865.9	13.0	91.2
-47	1354	45562	6.6	18.96	1.1	0.342	2.1	0.047	1.8	0.84	296.6	5.2	299.0	5.5	317.7	25.7	296.6	5.2	93.3
-48A	2481	43829	2.9	18.87	0.6	0.289	1.8	0.040	1.7	0.94	250.4	4.3	258.1	4.2	328.7	14.5	250.4	4.3	76.2
-49	1369	38874	3.4	19.07	0.8	0.328	2.5	0.045	2.4	0.95	285.7	6.7	287.8	6.3	304.8	18.0	285.7	6.7	93.8
-51	151	9579	2.0	18.70	5.0	0.489	5.4	0.066	2.2	0.40	413.9	8.7	404.1	18.1	348.6	112.9	413.9	8.7	118.7
-52	216	11789	2.5	18.34	3.5	0.508	4.1	0.068	2.1	0.51	421.4	8.6	417.1	14.1	393.2	79.6	421.4	8.6	107.2
-53	2929	52090	2.8	18.98	0.4	0.269	1.6	0.037	1.5	0.97	234.5	3.5	242.0	3.4	315.0	8.3	234.5	3.5	74.4
-54	126	45481	1.3	5.25	0.2	13.616	2.2	0.519	2.2	1.00	2693.9	48.3	2723.4	20.8	2745.3	3.5	2745.3	3.5	98.1
-55	1595	40001	1.9	18.91	0.9	0.339	3.4	0.047	3.3	0.96	293.3	9.4	296.7	8.8	323.2	20.8	293.3	9.4	90.8
-56	136	45784	1.2	9.05	0.5	4.672	1.2	0.307	1.1	0.91	1724.7	16.9	1762.3	10.3	1807.1	9.3	1807.1	9.3	95.4
-57	220	66898	5.1	8.50	0.3	5.571	1.8	0.343	1.8	0.99	1903.2	29.1	1911.6	15.4	1920.8	4.9	1920.8	4.9	99.1
-58A	158	7616	2.1	18.80	4.2	0.495	4.4	0.068	1.2	0.28	421.4	5.0	408.6	14.7	337.0	95.0	421.4	5.0	125.0
-56	115	9638	5.5	19.05	13.9	0.508	14.1	0.070	1.9	0.14	437.1	8.2	417.0	48.2	307.2	318.8	437.1	8.2	142.2
-57	93	25701	2.3	8.64	0.6	5.369	1.2	0.336	1.1	0.88	1869.2	17.7	1879.9	10.6	1891.7	10.5	1891.7	10.5	98.8
-59	1266	64742	6.1	18.98	1.0	0.337	2.1	0.046	1.8	0.88	292.6	5.2	295.2	5.3	315.9	22.6	292.6	5.2	92.6
-60	1304	57510	9.1	18.97	1.3	0.339	2.7	0.047	2.4	0.89	293.9	6.9	296.5	7.0	317.1	28.5	293.9	6.9	92.7
-62	438	27332	3.8	18.23	3.1	0.526	4.0	0.069	2.6	0.64	433.0	10.7	428.9	14.0	406.7	68.8	433.0	10.7	106.5
-63	263	12771	3.9	18.11	5.1	0.563	5.6	0.074	2.3	0.42	459.9	10.3	453.5	20.5	420.9	113.7	459.9	10.3	109.3

Table C.I continued

-64	1414	65974	7.6	18.89	1.1	0.333	2.8	0.046	2.5	0.92	287.8	7.2	292.1	7.0	326.4	23.9	287.8	7.2	88.2
-65	1056	38836	8.1	19.08	0.8	0.340	3.3	0.047	3.2	0.97	296.3	9.3	297.1	8.5	302.9	17.8	296.3	9.3	97.8
-67	1477	65019	3.1	19.11	1.6	0.332	3.7	0.046	3.4	0.90	290.2	9.6	291.4	9.5	300.4	36.4	290.2	9.6	96.6
-68	1488	60169	6.8	19.12	1.3	0.334	4.8	0.046	4.6	0.96	292.2	13.2	292.9	12.2	298.4	29.5	292.2	13.2	97.9
-69	1074	52060	8.9	19.12	1.3	0.338	3.5	0.047	3.2	0.93	295.0	9.3	295.4	8.9	298.9	29.2	295.0	9.3	98.7
-70	243	12314	2.8	18.39	4.5	0.493	5.1	0.066	2.5	0.48	410.9	9.8	407.2	17.2	386.7	100.6	410.9	9.8	106.2
-71	1154	50278	7.9	19.06	1.4	0.339	2.5	0.047	2.0	0.82	295.3	5.8	296.4	6.3	305.8	32.2	295.3	5.8	96.6
-72	1689	55155	4.6	19.27	1.7	0.337	5.5	0.047	5.3	0.95	296.7	15.3	294.9	14.2	280.2	38.0	296.7	15.3	105.9
-73	1366	56169	5.9	19.27	1.3	0.317	3.6	0.044	3.3	0.93	279.1	9.0	279.3	8.7	280.5	30.8	279.1	9.0	99.5
-74	223	11146	4.1	18.21	6.0	0.540	6.5	0.071	2.3	0.36	443.9	10.0	438.2	23.0	408.6	134.7	443.9	10.0	108.6
-75	490	25157	2.2	18.07	1.2	0.533	2.9	0.070	2.7	0.91	435.2	11.2	433.7	10.4	425.7	27.6	435.2	11.2	102.2
-76	1111	22718	6.5	19.36	1.1	0.333	2.5	0.047	2.3	0.90	294.4	6.5	291.7	6.4	270.2	25.7	294.4	6.5	108.9
-77	144	5156	1.9	18.25	11.0	0.427	11.2	0.057	2.0	0.18	354.7	6.9	361.2	34.1	403.4	247.9	354.7	6.9	87.9
-78	1155	35958	6.7	19.26	1.2	0.339	3.8	0.047	3.6	0.94	298.1	10.4	296.3	9.7	281.6	28.3	298.1	10.4	105.9
-79	341	13229	2.1	19.29	4.8	0.362	5.9	0.051	3.3	0.57	318.2	10.4	313.5	15.8	278.3	110.5	318.2	10.4	114.3
-80	125	6594	2.6	20.15	14.4	0.458	14.8	0.067	3.5	0.24	417.7	14.2	382.9	47.3	177.3	337.1	417.7	14.2	235.6
-81	61	3961	4.4	18.03	20.6	0.508	21.0	0.066	3.9	0.19	414.5	15.7	417.1	71.8	431.0	463.3	414.5	15.7	96.2
-82	1052	43075	6.9	19.14	1.5	0.338	4.5	0.047	4.3	0.95	295.9	12.4	295.9	11.7	295.8	33.6	295.9	12.4	100.0
-83	68	2145	3.1	22.47	13.5	0.396	14.0	0.065	3.9	0.28	403.5	15.2	339.0	40.5	-83.0	331.4	403.5	15.2	-486.2
-84	180	28659	2.3	8.76	0.5	5.111	3.2	0.325	3.2	0.99	1813.3	49.8	1837.9	27.1	1865.7	8.3	1865.7	8.3	97.2
-85	212	10113	6.7	18.60	4.2	0.538	5.2	0.073	3.0	0.58	451.5	13.3	437.0	18.6	361.3	95.9	451.5	13.3	125.0
-86	1452	63903	5.6	19.14	1.1	0.338	5.5	0.047	5.3	0.98	295.3	15.4	295.3	14.0	295.9	24.8	295.3	15.4	99.8
-87	276	16420	1.8	18.76	3.4	0.461	4.5	0.063	3.0	0.67	392.0	11.6	384.7	14.5	341.5	76.0	392.0	11.6	114.8
-88	1216	49948	6.2	19.30	1.3	0.343	4.0	0.048	3.8	0.94	302.2	11.1	299.4	10.4	277.7	30.8	302.2	11.1	108.8
-89	1263	58591	8.0	19.28	1.6	0.347	5.8	0.049	5.6	0.96	305.6	16.6	302.5	15.1	279.3	36.4	305.6	16.6	109.4
-90	68	3473	1.7	20.86	31.5	0.391	31.7	0.059	4.2	0.13	370.3	15.1	335.0	90.8	96.7	761.0	370.3	15.1	383.1
-91	137	7462	4.3	18.30	6.9	0.516	7.1	0.068	1.5	0.21	427.1	6.1	422.6	24.5	398.0	155.7	427.1	6.1	107.3
-92	145	9397	2.3	18.65	6.3	0.502	7.5	0.068	4.0	0.54	423.3	16.5	412.8	25.3	354.8	142.0	423.3	16.5	119.3
-93	190	11268	2.7	17.84	6.7	0.550	8.2	0.071	4.8	0.58	443.4	20.4	445.3	29.7	454.9	149.4	443.4	20.4	97.5
-94	236	15195	2.7	17.80	2.6	0.598	4.0	0.077	3.0	0.76	479.5	14.1	476.1	15.2	459.9	57.1	479.5	14.1	104.3
-95	157	7806	1.5	18.20	6.4	0.590	7.1	0.078	3.2	0.44	483.7	14.7	471.1	26.9	409.9	143.3	483.7	14.7	118.0
-96	1447	45417	7.5	19.25	1.7	0.333	7.4	0.046	7.2	0.97	292.7	20.6	291.6	18.7	283.2	38.5	292.7	20.6	103.3
-97	159	8582	2.7	19.28	9.0	0.445	9.9	0.062	4.1	0.42	389.5	15.6	374.0	31.0	279.1	206.6	389.5	15.6	139.6

Table C1 continued

-98	134	47278	2.0	8.13	0.4	6.150	5.3	0.362	5.3	1.00	1993.9	90.2	1997.3	46.1	2000.8	7.7	2000.8	7.7	99.7
-99	361	25376	2.9	18.02	2.4	0.505	5.5	0.066	4.9	0.90	411.9	19.5	415.1	18.6	432.6	54.0	411.9	19.5	95.2
-100	1022	54537	5.0	19.00	1.7	0.329	6.1	0.045	5.8	0.96	285.8	16.2	288.8	15.2	312.6	39.5	285.8	16.2	91.4
-101	248	16266	1.9	17.82	4.1	0.560	5.1	0.072	3.1	0.60	450.4	13.4	451.5	18.6	457.2	90.3	450.4	13.4	98.5
-102	180	6013	1.2	20.87	4.9	0.344	6.5	0.052	4.4	0.67	327.4	14.0	300.4	17.0	95.0	115.1	327.4	14.0	344.8
-103	245	13340	3.6	18.03	3.2	0.526	4.0	0.069	2.4	0.61	429.1	10.2	429.4	14.1	431.1	71.3	429.1	10.2	99.5
-104	1084	46220	6.4	19.34	2.0	0.310	5.6	0.043	5.2	0.94	274.4	14.0	274.1	13.4	271.9	44.7	274.4	14.0	100.9
-105	279	23816	1.8	18.00	5.0	0.601	7.8	0.078	6.0	0.76	486.8	28.0	477.7	29.8	434.0	112.2	486.8	28.0	112.2

Table C1 continued

Sample: MYS 080709-05																			
Sample #	U (ppm)	206Pb / 204Pb	U/Th	Isotope ratios				Apparent ages (Ma)				Best age ± (Ma)	Conc (%)						
				206Pb* ± 207Pb* (%)	235U* ± 206Pb* (%)	238U (%)	± error 206Pb* (%)	238U* (Ma)	± 207Pb* (Ma)	± 206Pb* (Ma)									
-1	110	35789	2.9	5.916	0.6	11.490	2.1	0.493	2.0	0.96	2583.7	42.7	2563.7	19.6	2548.0	10.4	2548.0	10.4	101.4
-2	541	73442	3.6	5.962	0.2	10.045	1.4	0.434	1.4	0.99	2325.1	26.8	2438.9	12.8	2535.2	3.2	2535.2	3.2	91.7
-3	19	5121	1.7	7.055	3.1	8.253	3.1	0.422	0.4	0.13	2270.9	7.9	2259.2	28.1	2248.6	53.2	2248.6	53.2	101.0
-4	84	17340	1.0	9.889	1.7	4.165	2.8	0.299	2.3	0.79	1684.8	33.4	1667.1	23.3	1644.8	32.1	1644.8	32.1	102.4
-5	19	2917	0.6	9.338	3.2	4.565	3.4	0.309	1.1	0.33	1736.8	17.1	1743.0	28.5	1750.4	59.2	1750.4	59.2	99.2
-6	251	17514	2.7	15.384	1.0	1.192	2.3	0.133	2.1	0.90	804.7	15.8	796.7	12.8	774.4	21.0	804.7	15.8	103.9
-7	127	5254	1.3	18.173	8.3	0.548	8.4	0.072	1.3	0.15	449.4	5.5	443.5	30.2	413.3	186.0	449.4	5.5	108.7
-8	102	24089	1.1	8.308	0.8	6.181	2.2	0.372	2.0	0.93	2040.9	35.4	2001.8	18.9	1961.7	13.7	1961.7	13.7	104.0
-9	813	177275	11.5	5.679	0.3	12.557	6.3	0.517	6.3	1.00	2687.2	137.5	2647.0	59.0	2616.4	4.7	2616.4	4.7	102.7
-11	167	6593	1.5	19.555	5.7	0.447	6.1	0.063	2.3	0.37	396.1	8.8	375.0	19.2	247.0	130.9	396.1	8.8	160.3
-12	174	14774	0.8	8.736	0.6	5.222	2.3	0.331	2.2	0.96	1842.5	35.5	1856.2	19.6	1871.5	11.1	1871.5	11.1	98.4
-13	240	65360	1.8	5.470	0.5	13.713	2.5	0.544	2.4	0.98	2800.3	54.3	2730.1	23.2	2678.5	9.0	2678.5	9.0	104.5
-14	79	2774	1.1	19.583	13.0	0.400	13.0	0.057	1.1	0.08	356.2	3.6	341.6	37.8	243.7	299.9	356.2	3.6	146.2
-15	334	65501	2.3	8.713	0.2	5.455	3.4	0.345	3.4	1.00	1909.4	56.0	1893.6	29.1	1876.3	2.9	1876.3	2.9	101.8
-16	118	19312	2.4	8.699	0.8	4.990	2.1	0.315	1.9	0.92	1764.4	29.7	1817.6	17.7	1879.2	15.2	1879.2	15.2	93.9
-17	31	1189	1.2	15.760	10.9	0.524	14.3	0.060	9.4	0.65	374.8	34.0	427.7	50.1	723.3	231.1	374.8	34.0	51.8
-18	380	68579	1.8	7.797	0.5	6.427	1.4	0.363	1.3	0.93	1998.5	22.1	2035.9	12.1	2074.1	8.7	2074.1	8.7	96.4
-19	327	69669	19.3	8.624	0.4	5.248	1.4	0.328	1.4	0.96	1829.7	21.7	1860.4	12.1	1894.8	6.8	1894.8	6.8	96.6
-20	293	13300	2.5	17.569	2.5	0.540	3.3	0.069	2.1	0.65	428.7	8.8	438.2	11.7	488.4	55.4	428.7	8.8	87.8
-21	72	14661	2.4	8.562	1.1	5.264	2.0	0.327	1.7	0.83	1823.1	26.6	1863.0	17.3	1907.8	20.5	1907.8	20.5	95.6
-22	33	1450	2.1	20.846	31.2	0.400	31.4	0.061	3.2	0.10	378.7	11.9	341.8	91.4	97.8	755.3	378.7	11.9	387.1
-23	67	2529	1.5	19.563	8.0	0.398	8.3	0.056	2.4	0.29	354.1	8.4	340.2	24.0	246.1	183.4	354.1	8.4	143.9
-24	418	18402	2.9	18.316	1.5	0.461	2.3	0.061	1.8	0.77	383.3	6.6	385.0	7.3	395.7	32.6	383.3	6.6	96.8
-25	893	30376	1.0	18.829	1.7	0.390	2.8	0.053	2.1	0.78	334.2	7.0	334.1	7.8	333.5	39.4	334.2	7.0	100.2
-26	108	4005	1.1	19.686	5.7	0.406	6.0	0.058	1.9	0.31	363.6	6.7	346.3	17.7	231.6	132.6	363.6	6.7	157.0
-27	135	6672	2.2	17.746	4.0	0.613	4.7	0.079	2.6	0.55	489.7	12.3	485.6	18.3	466.2	88.0	489.7	12.3	105.1
-28	159	4703	2.2	19.545	5.5	0.391	5.9	0.055	2.1	0.35	347.6	7.1	335.0	16.9	248.3	127.5	347.6	7.1	140.0
-29	558	98617	5.8	8.481	0.1	5.352	2.3	0.329	2.3	1.00	1834.7	37.2	1877.3	20.0	1924.7	2.1	1924.7	2.1	95.3
-30	156	32802	3.3	8.740	0.4	4.998	2.5	0.317	2.4	0.98	1774.1	38.0	1819.0	21.1	1870.8	8.0	1870.8	8.0	94.8



Table C1 continued

-31	415	15590	19.5	18.330	2.2	0.467	3.1	0.062	2.2	0.70	388.2	8.1	389.0	10.1	394.0	50.2	388.2	8.1	98.5
-32	213	6567	1.5	19.638	4.1	0.342	4.6	0.049	2.2	0.47	306.9	6.6	298.9	12.0	237.3	94.4	306.9	6.6	129.3
-33	252	11104	2.7	18.011	3.1	0.495	3.6	0.065	1.9	0.54	404.2	7.6	408.5	12.2	433.2	68.4	404.2	7.6	93.3
-34	380	112210	5.6	4.994	0.4	14.658	2.6	0.531	2.6	0.99	2745.5	57.1	2793.3	24.5	2828.0	6.0	2828.0	6.0	97.1
-35	309	45366	5.3	9.060	0.5	3.872	0.9	0.254	0.8	0.86	1461.3	10.6	1607.9	7.6	1805.7	8.8	1805.7	8.8	80.9
-36	429	79633	2.4	8.620	0.2	5.348	0.6	0.334	0.5	0.92	1859.2	8.7	1876.5	5.0	1895.6	4.3	1895.6	4.3	98.1
-37	153	5871	2.4	17.819	3.3	0.596	4.6	0.077	3.2	0.70	478.5	14.9	474.9	17.4	457.1	72.5	478.5	14.9	104.7
-38	88	19601	4.7	8.244	0.9	5.943	1.4	0.355	1.1	0.79	1959.9	18.8	1967.5	12.3	1975.5	15.4	1975.5	15.4	99.2
-39	76	16939	1.0	8.488	0.8	5.485	2.0	0.338	1.8	0.91	1875.2	29.2	1898.2	16.9	1923.4	14.5	1923.4	14.5	97.5
-40	116	12157	2.0	14.297	1.9	1.443	2.8	0.150	2.1	0.75	898.6	17.8	906.8	17.0	926.7	38.7	926.7	38.7	97.0
-42	93	22614	1.1	8.526	0.7	5.527	1.9	0.342	1.7	0.92	1895.1	28.5	1904.8	16.3	1915.3	13.4	1915.3	13.4	98.9
-43	158	4796	1.1	17.579	9.2	0.434	9.3	0.055	1.4	0.15	347.0	4.6	365.9	28.5	487.2	203.1	347.0	4.6	71.2
-44	115	19255	2.2	8.781	0.7	5.182	1.7	0.330	1.5	0.91	1838.5	24.7	1849.7	14.4	1862.3	12.7	1862.3	12.7	98.7
-45	94	22163	1.3	8.601	0.7	5.510	1.6	0.344	1.4	0.91	1904.7	23.5	1902.2	13.5	1899.5	11.8	1899.5	11.8	100.3
-46	463	39363	5.3	14.570	0.6	1.387	1.8	0.147	1.7	0.94	881.8	14.2	883.5	10.9	887.8	13.3	881.8	14.2	99.3
-47	382	104400	2.4	5.722	0.3	12.498	1.7	0.519	1.7	0.99	2693.5	37.3	2642.6	16.1	2603.8	4.2	2603.8	4.2	103.4
-48	45	1871	4.0	18.229	13.3	0.410	13.5	0.054	1.9	0.14	340.4	6.3	349.0	39.8	406.4	299.7	340.4	6.3	83.8
-49	204	58684	0.8	7.887	0.3	6.358	1.4	0.364	1.4	0.98	1999.7	23.5	2026.5	12.2	2054.0	4.6	2054.0	4.6	97.4
-50	367	14602	1.3	18.178	2.4	0.463	2.6	0.061	1.1	0.41	382.1	4.0	386.5	8.4	412.7	53.4	382.1	4.0	92.6
-51	317	8933	1.3	18.831	3.4	0.364	3.6	0.050	1.1	0.31	312.9	3.4	315.3	9.8	333.3	77.7	312.9	3.4	93.9
-52	211	8069	3.3	19.439	7.2	0.385	7.4	0.054	1.5	0.21	340.9	5.1	330.8	20.8	260.7	165.4	340.9	5.1	130.7
-53	371	15564	2.4	18.484	1.7	0.465	2.1	0.062	1.2	0.56	390.2	4.4	388.0	6.7	375.2	38.6	390.2	4.4	104.0
-54	39	1280	3.9	21.498	18.6	0.332	18.6	0.052	1.5	0.08	324.9	4.9	290.7	47.2	24.5	449.1	324.9	4.9	1326.4
-56	294	13130	1.7	18.260	2.9	0.480	3.2	0.064	1.3	0.41	397.4	5.1	398.1	10.5	402.6	64.9	397.4	5.1	98.7
-57	680	19643	0.9	18.528	1.1	0.426	2.5	0.057	2.2	0.89	359.0	7.8	360.5	7.6	369.9	25.3	359.0	7.8	97.1
-58	229	7279	2.5	18.712	4.3	0.368	4.4	0.050	1.1	0.25	313.8	3.3	317.9	12.0	347.6	96.3	313.8	3.3	90.3
-59	56	1600	0.8	22.673	22.1	0.319	23.8	0.052	8.9	0.37	329.3	28.4	280.9	58.5	-104.8	549.2	329.3	28.4	-314.2
-63	360	59155	3.5	8.630	0.3	4.936	2.4	0.309	2.4	0.99	1735.7	36.9	1808.5	20.6	1893.4	5.5	1893.4	5.5	91.7
-64	399	43954	2.4	12.760	0.5	2.009	2.8	0.186	2.8	0.98	1099.2	28.0	1118.5	19.1	1156.2	10.1	1156.2	10.1	95.1
-65	327	14479	1.3	18.492	1.5	0.431	2.5	0.058	2.1	0.81	362.0	7.3	363.7	7.7	374.3	33.0	362.0	7.3	96.7
-66	506	62731	1.9	12.515	0.2	2.197	1.8	0.199	1.7	1.00	1172.0	18.7	1180.0	12.2	1194.6	3.4	1194.6	3.4	98.1
-67	94	4836	2.0	17.076	3.1	0.593	3.3	0.073	1.1	0.34	456.6	4.9	472.5	12.4	550.8	67.4	456.6	4.9	82.9
-68	310	11874	2.2	18.725	2.6	0.395	3.0	0.054	1.4	0.47	337.0	4.6	338.1	8.5	346.0	59.3	337.0	4.6	97.4

Table C1 continued

-69	229	3707	1.5	17.491	14.2	0.407	14.7	0.052	3.6	0.24	324.9	11.3	347.0	43.2	498.2	315.2	324.9	11.3	65.2
-70	40	14334	0.6	5.413	1.0	12.858	2.5	0.505	2.3	0.92	2634.4	50.4	2669.3	23.8	2695.9	15.9	2695.9	15.9	97.7
-71	512	97942	2.1	8.681	0.2	5.234	1.6	0.330	1.6	0.99	1836.2	25.9	1858.2	14.0	1883.0	4.3	1883.0	4.3	97.5
-72	93	21261	1.3	7.835	0.7	6.644	2.0	0.378	1.9	0.94	2064.9	32.8	2065.2	17.5	2065.5	12.3	2065.5	12.3	100.0
-73	93	2429	2.1	17.644	6.7	0.512	6.8	0.066	1.2	0.17	409.0	4.7	419.7	23.3	478.9	147.8	409.0	4.7	85.4
-74	115	29902	1.8	8.739	0.7	5.113	2.0	0.324	1.9	0.94	1809.5	29.4	1838.2	16.9	1870.9	12.6	1870.9	12.6	96.7
-75	523	16103	2.5	15.703	5.2	0.661	6.6	0.075	4.1	0.61	467.7	18.4	515.1	26.9	731.1	111.2	467.7	18.4	64.0
-76	423	91091	7.6	8.474	0.2	5.670	1.1	0.348	1.1	0.99	1927.1	17.9	1926.7	9.4	1926.3	2.8	1926.3	2.8	100.0
-77	617	74555	2.8	8.720	0.2	5.216	3.1	0.330	3.1	1.00	1837.9	49.5	1855.3	26.5	1874.8	4.5	1874.8	4.5	98.0
-78	99	6010	1.7	17.791	4.8	0.623	5.3	0.080	2.3	0.44	498.6	11.2	491.9	20.7	460.6	105.7	498.6	11.2	108.3
-79	209	8857	1.1	18.657	4.2	0.396	4.4	0.054	1.5	0.34	336.6	4.9	338.8	12.8	354.2	94.3	336.6	4.9	95.0
-81	137	49119	1.5	5.155	0.3	14.669	1.9	0.548	1.9	0.99	2818.6	43.1	2794.0	18.1	2776.3	4.4	2776.3	4.4	101.5
-82	252	13139	3.5	17.867	3.7	0.564	4.3	0.073	2.1	0.49	454.6	9.3	454.0	15.7	451.1	83.1	454.6	9.3	100.8
-85	309	103023	3.7	5.396	0.5	13.566	2.3	0.531	2.3	0.97	2745.5	50.8	2719.9	22.1	2700.9	8.8	2700.9	8.8	101.6
-86	123	25845	2.2	8.739	0.5	5.375	2.1	0.341	2.1	0.98	1890.0	33.8	1880.9	18.1	1870.8	8.5	1870.8	8.5	101.0
-87	194	6946	1.5	20.614	3.6	0.360	3.8	0.054	1.0	0.26	337.7	3.3	312.0	10.1	124.3	85.7	337.7	3.3	271.7
-88	68	17560	1.3	8.612	0.9	5.500	1.5	0.344	1.2	0.78	1903.7	19.1	1900.6	12.8	1897.3	16.7	1897.3	16.7	100.3
-89	256	12105	3.4	18.482	4.8	0.534	5.3	0.072	2.3	0.44	445.8	10.1	434.6	18.7	375.5	107.2	445.8	10.1	118.7
-90	219	8412	1.4	18.835	7.8	0.436	7.9	0.060	1.3	0.17	372.9	4.8	367.4	24.5	332.8	177.7	372.9	4.8	112.1
-91	55	13313	0.9	7.959	1.4	6.114	2.8	0.353	2.4	0.86	1948.7	40.4	1992.3	24.4	2037.9	25.3	2037.9	25.3	95.6
-92	346	79689	2.5	6.585	0.8	9.071	1.3	0.433	1.1	0.83	2320.1	21.6	2345.2	12.3	2367.1	12.9	2367.1	12.9	98.0
-94	183	12777	1.5	15.304	1.8	1.136	2.9	0.126	2.2	0.78	765.4	16.1	770.5	15.4	785.4	37.5	765.4	16.1	97.5
-95	86	2841	1.3	19.440	12.2	0.367	12.5	0.052	2.5	0.20	325.5	7.9	317.6	34.1	260.7	281.8	325.5	7.9	124.9
-96	111	8638	1.9	15.126	3.1	1.222	3.5	0.134	1.5	0.43	811.0	11.3	810.7	19.3	809.9	65.4	811.0	11.3	100.1
-97	59	12396	1.8	8.788	0.9	5.046	1.5	0.322	1.2	0.81	1797.6	18.5	1827.1	12.4	1860.9	15.5	1860.9	15.5	96.6
-98	106	5068	2.5	19.186	8.4	0.493	8.5	0.069	1.2	0.14	427.4	5.0	406.7	28.6	290.7	193.1	427.4	5.0	147.0
-99	187	36741	1.8	8.693	0.6	5.430	1.5	0.342	1.4	0.92	1897.8	23.2	1889.5	13.2	1880.5	11.0	1880.5	11.0	100.9

#### APPENDIX D:

Mystic subterrane at Sheep Creek, eastern McGrath quadrangle

## EXPLANATION

Additional field work was conducted in the eastern McGrath quadrangle in the western Alaska Range (Figure D1). Field work in this area was focused on map unit PDs (Permian–Devonian siliciclastics) of Bundtzen et al. (1997) which may be correlative with upper Paleozoic siliciclastic rocks (i.e., Mystic Pass formation and Mt. Dall conglomerate) in the western McGrath quadrangle. Bundtzen et al. (1997) assigns PDs as belonging to the Sheep Creek Formation and correlates the Mt. Dall conglomerate of the western Talkeetna quadrangle with a limestone-chert conglomerate identified as being the stratigraphic top of the PDs map unit in the eastern McGrath quadrangle. The following is a brief summary of the work done in the Sheep Creek area of the eastern McGrath quadrangle which includes one detrital zircon sample and approximately 160 m of measured stratigraphic section from the Sheep Creek Formation. Measured stratigraphy is not discussed, but is reported in Appendix F (Figure F1).

## DETRITAL ZIRCON GEOCHRONOLOGY

Sample **09PH160A** was collected from a lens of matrix-supported pebble conglomerate on St. Johns Hill (Figure D2) north of the Denali Fault and mapped as belonging to unit PDs (Bundtzen et al., 1997). Clasts are angular and consist mostly of dark gray chert 2 to 5 cm in diameter with minor occurrences of limestone clasts. The matrix is fine-grained and dominated by quartz veins. GPS coordinates were not taken during sample collection. Geochronologic analyses were conducted at the Arizona LaserChron Center (see Chapter 3 for explanation of methods). Analytical data are

reported in Table E1.

Detrital age spectra (Figure D3) from this sample include a total of 75 grains of which 20% are Phanerozoic and 80% are Precambrian. One Phanerozoic detrital age peak is present at ca. 440 Ma while several Precambrian age peaks occur at ca. 682, 1175, 1425, 1652, and 1816 Ma. The three youngest grains occur at 430, 434, and 435 Ma with a calculated weighted mean age (WMA) of  $435.6 \pm 4.1$  Ma. The youngest age peak occurs at ca. 440 Ma.

Like other Mystic subterrane detrital zircon trends, this sample contains a Phanerozoic age peak between ca. 465–405 Ma and a Precambrian age peak between ca. 2.0 and 1.8 Ga. However, this sample is different from other Mystic subterrane samples in that its youngest peak is substantially older (approx. 440 Ma) and therefore does not contain detrital trends at ca. 300 and 350 Ma. Furthermore, sample 09PH160A contains a significant portion (~27%) of zircons between 1.8 and 1.0 Ga, which are sparsely seen (<7%) in other Mystic subterrane samples. Disparities in detrital trends could suggest that: 1) this sample was collected from Mystic subterrane strata older than any other Mystic subterrane samples or 2) rocks from which this sample was collected are not actually part of the Mystic subterrane and may belong to older portions of the Farewell terrane (i.e., the Dillinger subterrane) or to a different terrane altogether.

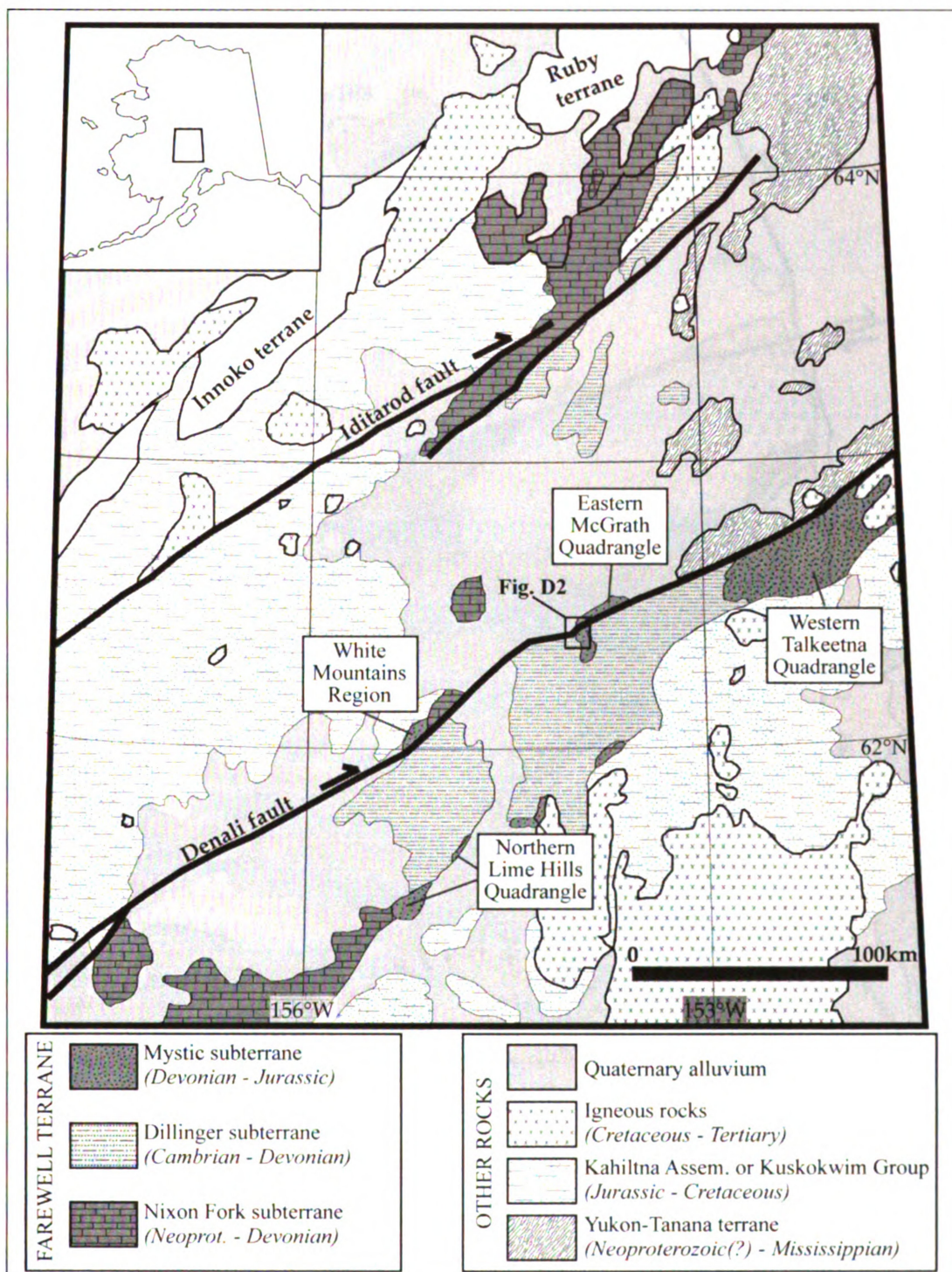


**Figure D1.** Generalized geologic map showing the regional area of interest and the distribution of exposed portions of the Farewell terrane. The majority of Farewell exposures are in the Alaska Range south of the Denali fault, but crop out as far North as the Kuskokwim Mountains north of the Iditarod fault. Note the small box in the eastern McGrath quad. shows the field area in Figure D2. Modified from Bradley et al., 2003.



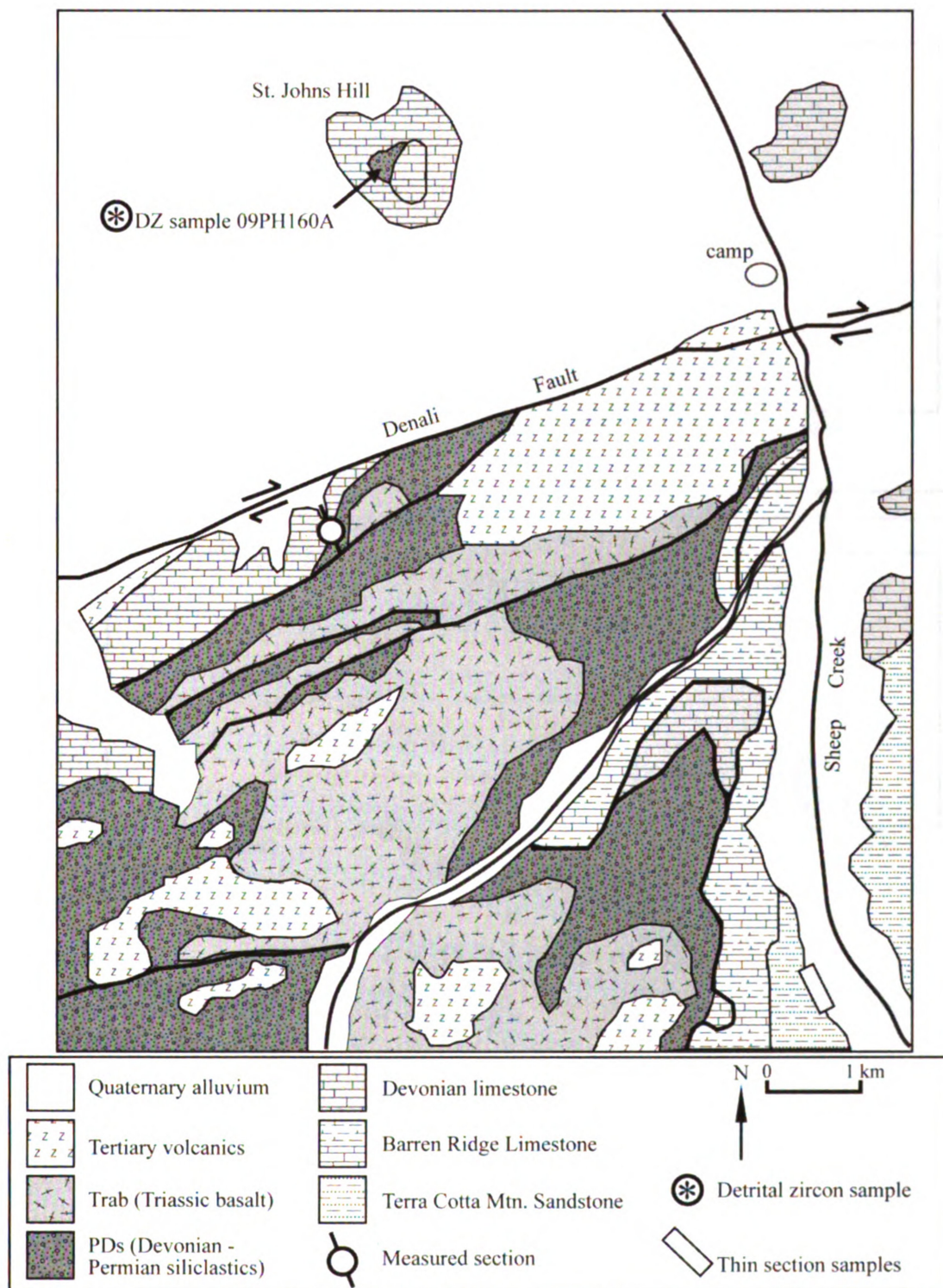


**Figure D2.** Geologic map showing the field area (Sheep Creek) in the eastern McGrath quad. Field work in this area was primarily focused on map unit PDs, which may be correlative with the Mystic Pass formation. In addition to work done for this study (see text), samples were collected for thin section and detrital zircon analyses from the Terra Cotta Mtn Sandstone (white box) for future studies. Modified from Bundtzen et al. (1997).

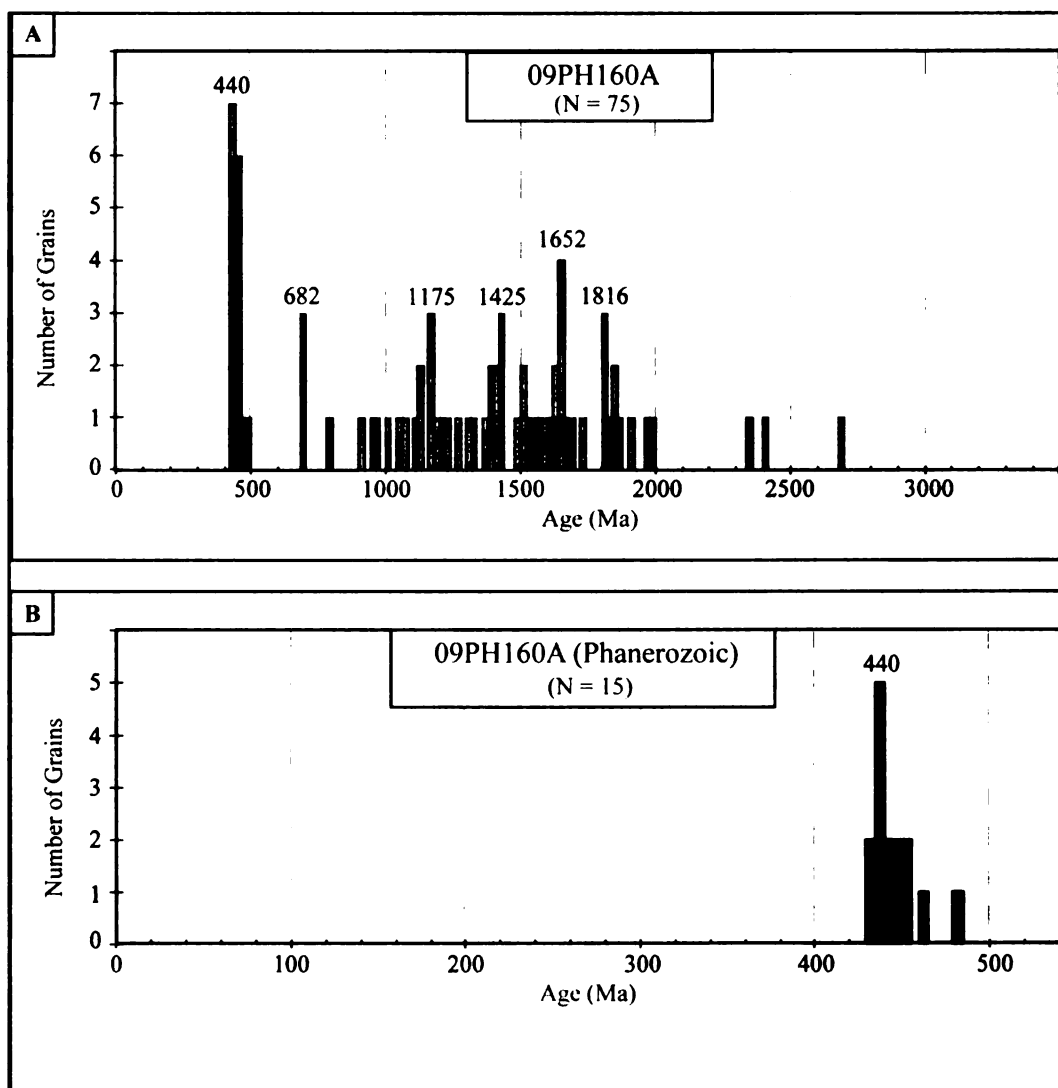


**Figure D3.** Detrital zircon age spectra from Mystic subterranean strata (map unit PDs) in the eastern McGrath quadrangle. A) Age distributions for all 75 grains analyzed. B) Age distributions for Phanerozoic aged grains only. See text for sample details and location.



## APPENDIX E:

### Analytical results of U-Pb detrital zircon data (Sheep Creek Fm.)

**Appendix E.** Measured isotopic ratios and age data reported for detrital zircon samples from the Sheep Creek Formation. All uncertainties are reported at the 1 sigma level, and include only measurement errors. Systematic errors would increase the uncertainty of clusters of ages by 1-2%. U concentration and U/Th are calibrated relative to our Sri Lanka zircon and are accurate to ~20%. Common Pb correction is from  $^{204}\text{Pb}$ , with composition interpreted from Stacey and Kramers (1975) and uncertainties of 1.0 for  $^{206}\text{Pb}/^{204}\text{Pb}$ , 0.3 for  $^{207}\text{Pb}/^{204}\text{Pb}$ , and 2.0 for  $^{208}\text{Pb}/^{204}\text{Pb}$ . U/Pb and  $^{206}\text{Pb}/^{207}\text{Pb}$  fractionation is calibrated relative to fragments of a large Sri Lanka zircon of  $563.5 \pm 3.2$  Ma (2-sigma). U decay constants and composition as follows:  $^{238}\text{U} = 9.8485 \times 10^{-10}$ ,  $^{235}\text{U} = 1.55125 \times 10^{-10}$ ,  $^{238}\text{U}/^{235}\text{U} = 137.88$

**Table E1.** Analytical results of U-Pb detrital zircon isotope ratios and age data from the Sheep Creek Formation.

Sample: 09PH160A																			
Sample #	U (ppm)	206Pb/204Pb	U/Th	206Pb*		207Pb*		Isotope ratios		Apparent ages (Ma)						Best age ± (Ma)	Conc (%)		
				206Pb*	207Pb*	235U*	238U (%)	±	206Pb*	± error	206Pb*	±	235U (Ma)	±	207Pb* (Ma)			±	206Pb* (Ma)
-1	230	17132	3.5	11.343	0.4	2.833	1.6	0.233	1.6	0.97	1350.7	19.4	1364.4	12.3	1386.0	7.4	1386.0	7.4	97.5
-3	92	3131	1.9	8.573	0.7	5.687	1.7	0.354	1.5	0.9	1951.7	25.4	1929.4	14.5	1905.5	13.0	1905.5	13.0	102.4
-4	701	7918	38.0	18.284	1	0.539	2.3	0.072	2.1	0.91	445.3	9.0	437.99	8.2	399.7	21.7	445.3	9.0	111.4
-6	92	12381	2.1	10.685	0.6	3.331	1.4	0.258	1.3	0.89	1480.3	16.6	1488.4	11.0	1499.9	12.2	1499.9	12.2	98.7
-7	95	19348	2.3	9.655	0.7	4.324	1.5	0.303	1.3	0.87	1705.2	19.7	1698	12.4	1689.0	13.6	1689.0	13.6	101.0
-8	48	8998	1.0	9.078	1.9	4.943	2.4	0.325	1.5	0.6	1816.3	23.2	1809.6	20.6	1802.0	35.4	1802.0	35.4	100.8
-9	233	6154	1.2	18.509	2.6	0.540	2.7	0.073	0.8	0.29	451.3	3.4	438.56	9.6	372.2	58.1	451.3	3.4	121.3
-10	180	3473	1.6	19.054	3.4	0.528	3.6	0.073	1.2	0.33	453.9	5.2	430.43	12.8	306.5	78.3	453.9	5.2	148.1
-12	93	2909	4.2	20.437	9.1	0.466	9.2	0.069	0.8	0.08	430.3	3.2	388.18	29.6	144.4	215.0	430.3	3.2	297.9
-14	255	10176	2.3	16.005	1.6	0.965	2.1	0.112	1.4	0.66	684.4	9.2	685.88	10.7	690.6	34.4	684.4	9.2	99.1
-15	98	13302	0.8	9.861	0.7	4.115	2.1	0.294	2	0.95	1663.0	28.8	1657.3	16.9	1650.0	12.2	1650.0	12.2	100.8
-17	63	6566	4.0	12.077	1.9	2.487	2.2	0.218	1.2	0.52	1270.4	13.3	1268.2	16.0	1264.6	36.7	1264.6	36.7	100.5
-18	102	19709	1.7	8.864	0.9	5.077	2.8	0.326	2.7	0.95	1820.8	42.1	1832.2	23.7	1845.2	16.1	1845.2	16.1	98.7
-21	223	8327	1.6	17.904	3	0.541	3.4	0.070	1.8	0.51	437.9	7.5	439.3	12.3	446.5	65.8	437.9	7.5	98.1
-22	282	33902	1.7	8.989	0.4	4.719	1.3	0.308	1.2	0.95	1729.1	18.4	1770.6	10.7	1819.9	7.6	1819.9	7.6	95.0
-23	430	51913	2.3	11.460	0.6	2.858	1.1	0.238	0.9	0.83	1373.9	10.9	1370.9	8.0	1366.2	11.2	1366.2	11.2	100.6
-26	104	11745	2.1	11.826	1	2.609	2	0.224	1.7	0.86	1301.8	20.5	1303.2	14.8	1305.4	19.9	1305.4	19.9	99.7
-27	65	8614	1.7	10.628	0.8	3.443	1.7	0.265	1.5	0.88	1517.3	20.4	1514.2	13.5	1509.9	15.1	1509.9	15.1	100.5
-28	356	8935	1.5	18.236	3	0.529	3.4	0.070	1.7	0.5	436.1	7.2	431.3	12.1	405.5	66.5	436.1	7.2	107.5
-29	175	24287	2.5	9.038	0.3	5.034	1.5	0.330	1.4	0.97	1838.2	22.6	1825	12.3	1809.9	6.1	1809.9	6.1	101.6
-30	42	5056	0.9	10.326	2.3	3.802	2.6	0.285	1.3	0.51	1615.0	19.3	1593.1	21.2	1564.2	42.4	1564.2	42.4	103.2
-31	573	4838	2.0	17.622	3.3	0.559	3.9	0.072	2.1	0.53	445.2	8.8	451.2	14.2	481.7	73.4	445.2	8.8	92.4
-35	39	3004	1.5	6.442	0.7	9.417	1.5	0.440	1.3	0.87	2350.4	25.1	2379.5	13.5	2404.4	12.5	2404.4	12.5	97.8
-36	107	2469	1.3	19.304	5.6	0.530	5.6	0.074	0.9	0.17	461.2	4.2	431.66	19.9	276.7	127.6	461.2	4.2	166.7
-40	33	3449	2.2	6.676	0.8	9.130	1.8	0.442	1.6	0.88	2359.8	31.5	2351.1	16.5	2343.5	14.4	2343.5	14.4	100.7
-43	289	31667	2.5	11.067	0.6	3.135	1.3	0.252	1.1	0.88	1446.8	14.9	1441.3	10.0	1433.1	11.7	1433.1	11.7	101.0
-44	166	36543	0.9	5.411	0.2	13.265	2.2	0.521	2.2	1	2701.6	48.9	2698.7	21.0	2696.4	3.6	2696.4	3.6	100.2
-45	17	3071	0.1	8.261	3.2	6.036	4.1	0.362	2.6	0.62	1989.9	43.7	1981.1	35.8	1971.8	57.3	1971.8	57.3	100.9
-46	635	56086	3.4	13.046	0.3	1.970	1.7	0.186	1.7	0.98	1101.9	17.4	1105.4	11.8	1112.2	6.6	1112.2	6.6	99.1

Table E1 continued

-47	154	14311	1.4	12.437	1.5	2.269	1.9	0.205	1.1	0.61	1200.5	12.3	1202.8	13.0	1207.0	28.9	1207.0	28.9	99.5
-48	128	12814	1.5	8.747	0.6	5.297	2.3	0.336	2.3	0.97	1867.6	36.9	1868.4	20.0	1869.2	10.3	1869.2	10.3	99.9
-49	201	4552	1.2	19.344	4.1	0.497	4.8	0.070	2.4	0.51	434.1	10.2	409.37	16.1	272.0	94.4	434.1	10.2	159.6
-50	78	6203	1.5	10.038	1.1	3.953	2.8	0.288	2.6	0.93	1630.5	37.7	1624.6	22.9	1617.0	19.6	1617.0	19.6	100.8
-51	283	18843	2.0	11.337	0.5	2.939	2.3	0.242	2.2	0.97	1395.2	27.5	1391.9	17.1	1386.9	9.6	1386.9	9.6	100.6
-52	295	15874	3.0	12.675	0.7	2.187	2.2	0.201	2.1	0.95	1181.0	22.6	1176.9	15.3	1169.5	12.9	1169.5	12.9	101.0
-53	244	5214	1.6	18.607	4.6	0.518	5.1	0.070	2.2	0.44	435.4	9.4	423.68	17.7	360.3	103.8	435.4	9.4	120.8
-54	457	22612	96.6	15.218	1.1	1.192	2.8	0.132	2.6	0.92	796.9	19.5	797.01	15.6	797.2	23.0	796.9	19.5	100.0
-55	39	4038	0.9	10.159	1.6	3.890	2.3	0.287	1.7	0.73	1624.6	24.1	1611.6	18.5	1594.7	29.0	1594.7	29.0	101.9
-56	216	6651	1.8	18.288	2.4	0.532	3.7	0.071	2.8	0.76	439.5	11.9	433.08	13.0	399.2	54.3	439.5	11.9	110.1
-57	138	16368	3.1	11.248	0.9	2.918	1.9	0.238	1.6	0.88	1376.5	20.1	1386.6	14.0	1402.2	17.1	1402.2	17.1	98.2
-59	125	9467	2.8	14.117	1.1	1.581	3.4	0.162	3.2	0.95	967.3	29.1	962.86	21.2	952.7	22.1	952.7	22.1	101.5
-60	422	13776	0.9	18.093	1.6	0.539	2.2	0.071	1.5	0.67	440.3	6.3	437.58	7.9	423.1	36.7	440.3	6.3	104.1
-61	67	8300	2.2	10.679	1.8	3.216	3.3	0.249	2.8	0.85	1434.0	36.0	1461.1	25.6	1500.8	33.1	1500.8	33.1	95.5
-62	86	4034	2.1	18.735	6.8	0.573	7.9	0.078	3.9	0.49	483.6	18.0	460.2	29.1	344.8	155.0	483.6	18.0	140.3
-63	193	30498	1.3	10.460	0.5	3.617	2.9	0.274	2.8	0.98	1563.3	39.4	1553.4	23.0	1539.9	10.3	1539.9	10.3	101.5
-65	145	11371	1.0	16.049	2.3	0.960	2.9	0.112	1.8	0.62	683.1	11.6	683.48	14.5	684.7	49.0	683.1	11.6	99.8
-67	53	7882	0.8	8.860	1.2	5.079	2	0.326	1.6	0.79	1820.8	25.0	1832.6	17.0	1846.1	22.5	1846.1	22.5	98.6
-68	56	7642	0.6	11.030	2.2	3.162	2.7	0.253	1.5	0.57	1453.7	19.9	1447.9	20.7	1439.4	41.9	1439.4	41.9	101.0
-69	280	39320	1.9	10.420	0.4	3.553	1.5	0.269	1.5	0.96	1533.2	20.3	1539.1	12.3	1547.2	8.2	1547.2	8.2	99.1
-70	72	7647	3.1	12.928	2.5	2.023	2.8	0.190	1.1	0.4	1119.7	11.5	1123.3	18.9	1130.3	50.7	1130.3	50.7	99.1
-71	934	10106	0.9	17.687	1.1	0.554	2.5	0.071	2.2	0.89	442.4	9.5	447.43	9.0	473.5	24.7	442.4	9.5	93.4
-72	280	27129	2.8	13.380	0.9	1.820	1.3	0.177	1	0.76	1048.6	9.7	1052.8	8.6	1061.5	17.2	1061.5	17.2	98.8
-73	240	9830	2.7	18.501	2.2	0.524	3.2	0.070	2.3	0.72	437.8	9.7	427.6	11.1	373.2	49.2	437.8	9.7	117.3
-74	198	30560	2.8	11.641	0.5	2.775	1.5	0.234	1.4	0.94	1356.7	17.0	1348.7	11.0	1336.0	9.9	1336.0	9.9	101.6
-75	309	36136	3.2	12.574	0.4	2.212	1.8	0.202	1.8	0.97	1184.6	19.0	1184.9	12.6	1185.4	8.4	1185.4	8.4	99.9
-76	61	11200	0.6	9.876	1.6	4.042	2.2	0.289	1.5	0.68	1639.0	21.5	1642.6	17.9	1647.3	29.9	1647.3	29.9	99.5
-78	102	19770	1.6	9.760	0.8	4.166	1.2	0.295	1	0.77	1666.1	14.0	1667.4	10.1	1669.1	14.5	1669.1	14.5	99.8
-79	107	19480	3.0	9.837	0.6	4.019	2.7	0.287	2.6	0.98	1625.0	37.2	1637.9	21.6	1654.6	10.7	1654.6	10.7	98.2
-80	230	19972	3.5	11.190	2.1	2.249	4.2	0.183	3.6	0.87	1080.7	35.9	1196.4	29.3	1412.0	39.8	1412.0	39.8	76.5
-81	202	26521	1.5	11.084	0.5	2.935	1.5	0.236	1.4	0.95	1365.4	17.2	1390.9	11.1	1430.3	8.8	1430.3	8.8	95.5
-82	69	8036	2.1	14.362	1.5	1.510	2.3	0.157	1.7	0.74	941.9	14.6	934.58	13.8	917.4	31.5	917.4	31.5	102.7
-83	99	31062	1.4	8.188	0.6	5.766	2.2	0.342	2.1	0.96	1898.2	34.3	1941.3	18.9	1987.6	11.3	1987.6	11.3	95.5

Table E1 continued

-85	285	33869	2.4	12.905	0.7	2.041	1.9	0.191	1.7	0.92	1126.8	18.0	1129.2	12.9	1133.7	14.5	1133.7	14.5	99.4
-86	64	11338	1.7	9.983	2	4.097	2.2	0.297	1	0.47	1674.6	15.2	1653.7	18.0	1627.3	36.4	1627.3	36.4	102.9
-88	70	9465	1.7	12.640	1	2.179	1.6	0.200	1.2	0.77	1174.1	13.0	1174.4	11.0	1175.1	20.0	1175.1	20.0	99.9
-90	51	9413	1.5	9.945	1	4.131	2.7	0.298	2.5	0.93	1681.0	37.6	1660.4	22.3	1634.3	18.6	1634.3	18.6	102.9
-91	279	18503	4.9	13.666	1.1	1.743	2.4	0.173	2.1	0.89	1027.5	20.3	1024.8	15.5	1018.8	22.4	1018.8	22.4	100.9
-92	167	12968	2.2	12.667	0.8	2.248	2.1	0.206	1.9	0.92	1210.1	21.1	1196.1	14.5	1170.8	15.6	1170.8	15.6	103.4
-93	319	27488	10.5	9.841	0.3	4.090	2.2	0.292	2.1	0.99	1651.1	31.1	1652.3	17.6	1653.8	5.8	1653.8	5.8	99.8
-94	243	25065	2.8	8.961	0.4	5.202	1.7	0.338	1.6	0.97	1877.3	26.2	1852.9	14.1	1825.6	6.7	1825.6	6.7	102.8
-96	377	50204	4.1	12.305	0.5	2.337	1.5	0.209	1.4	0.95	1221.1	15.9	1223.6	10.7	1228.0	9.6	1228.0	9.6	99.4
-97	86	6530	2.5	15.873	1.9	0.985	2.6	0.113	1.7	0.67	692.4	11.2	696.14	12.9	708.3	40.4	692.4	11.2	97.8
-98	80	15488	2.5	9.399	0.8	4.551	1.7	0.310	1.5	0.89	1741.8	23.4	1740.3	14.4	1738.5	14.5	1738.5	14.5	100.2
-99	205	22136	2.9	13.497	1.2	1.789	2.9	0.175	2.6	0.92	1040.2	25.4	1041.4	18.8	1043.9	23.5	1043.9	23.5	99.6
-100	262	20634	2.8	13.998	0.9	1.625	2.2	0.165	2	0.91	984.3	18.4	979.93	13.9	970.0	18.3	970.0	18.3	101.5

**APPENDIX F:**  
**Measured stratigraphic section of the Sheep Creek Fm.**

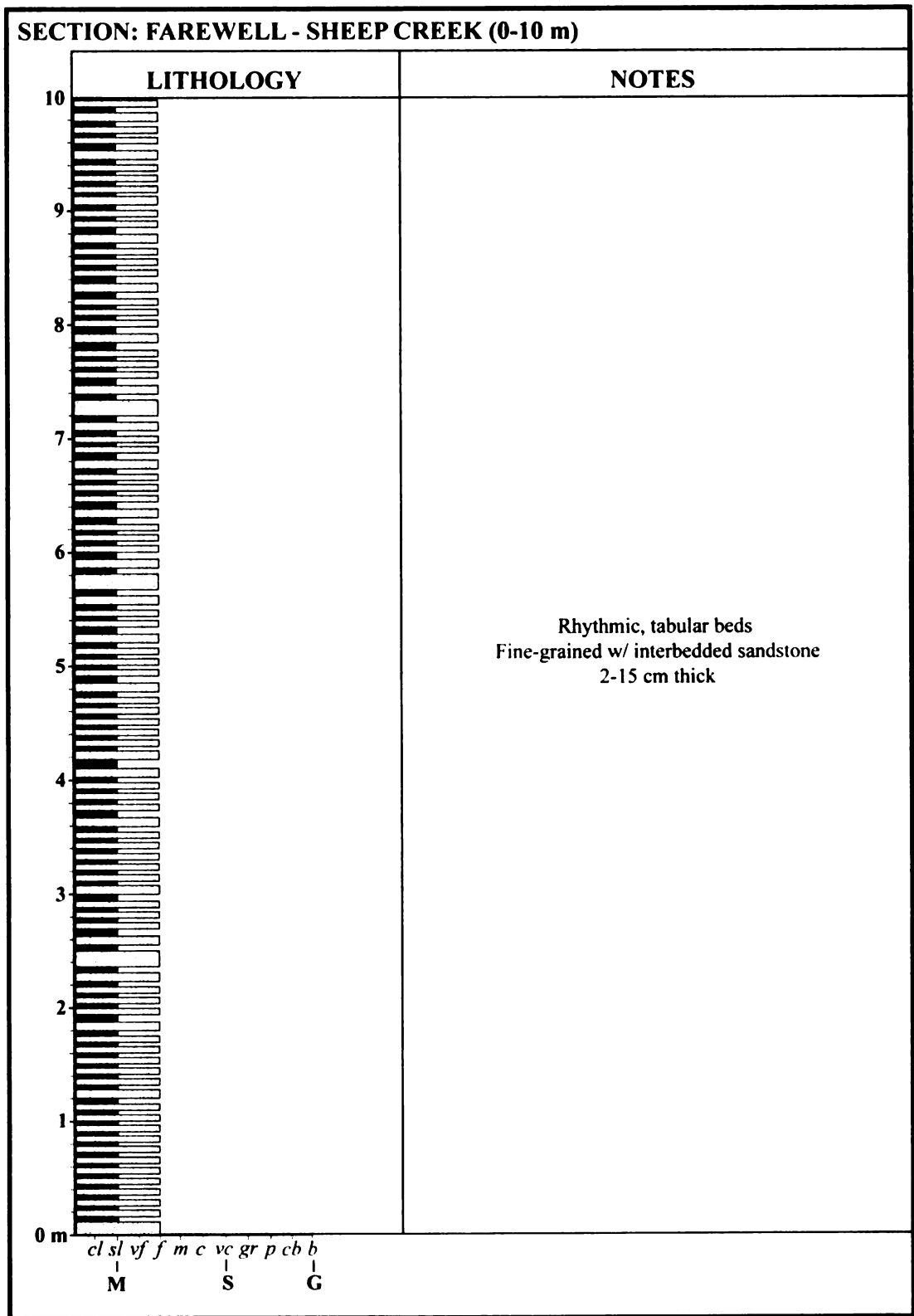


**Figure F1.** Measured stratigraphic sections of the Sheep Creek Formation.

Figure F1 continued

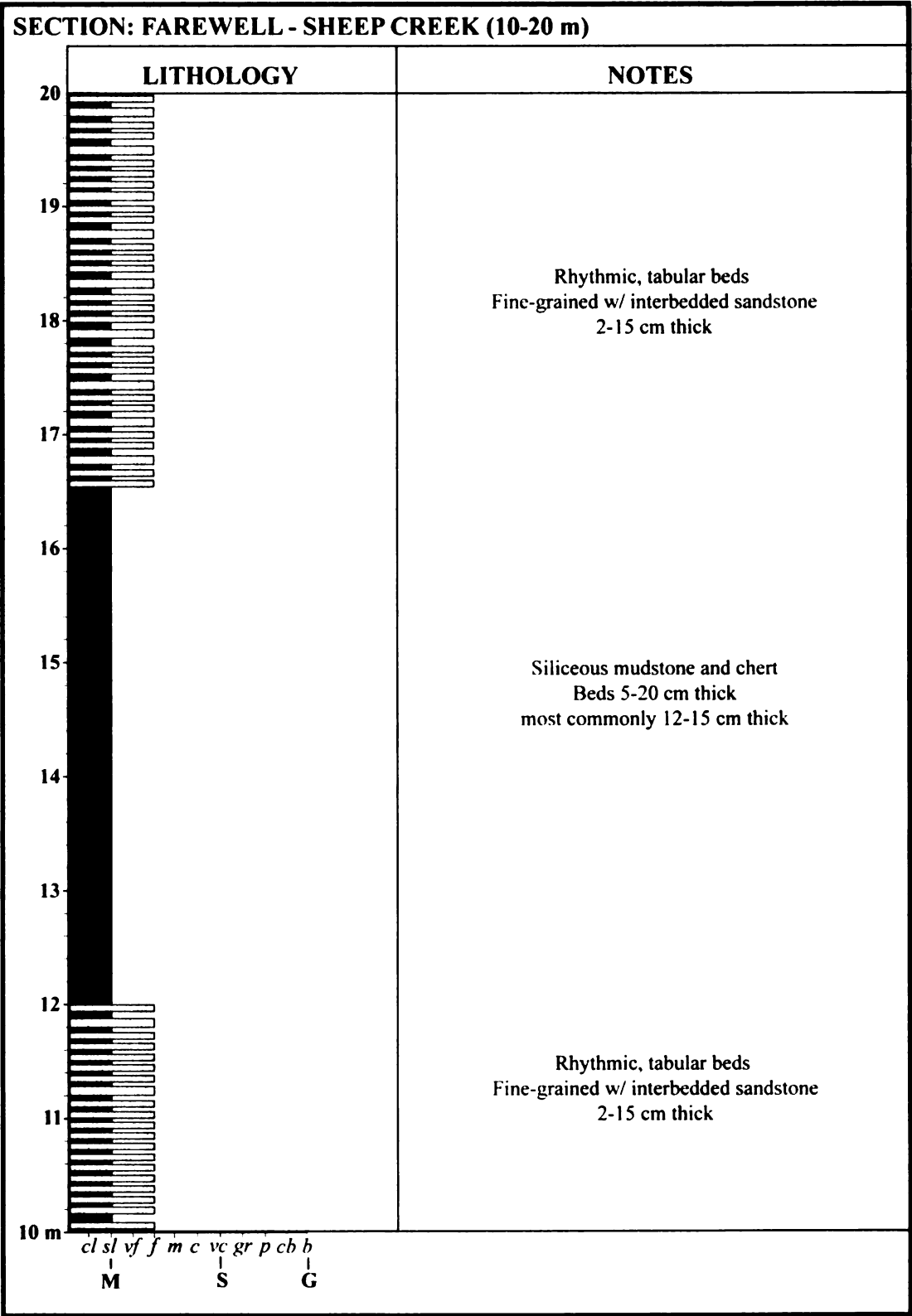


Figure F1 continued

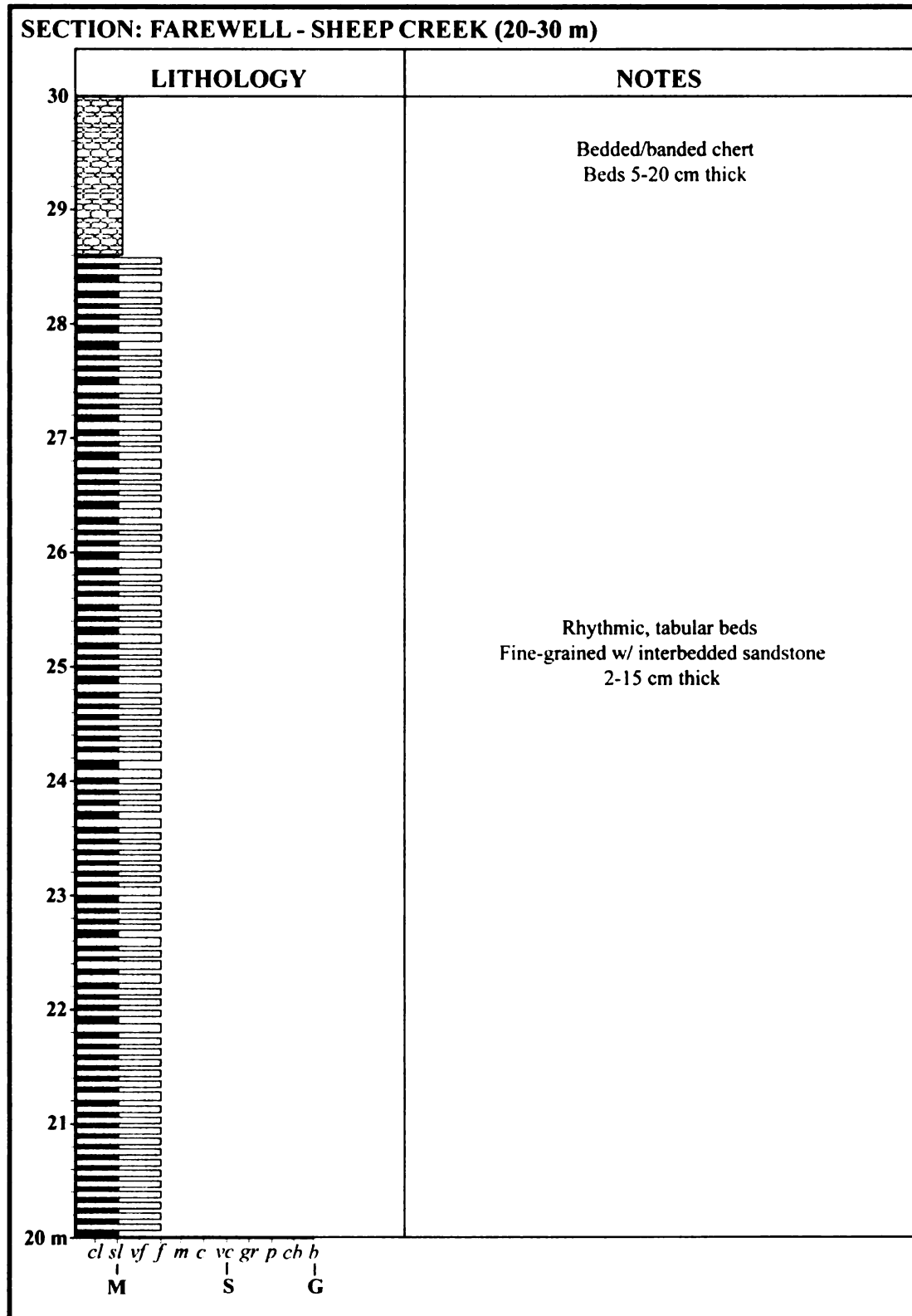




Figure F1 continued

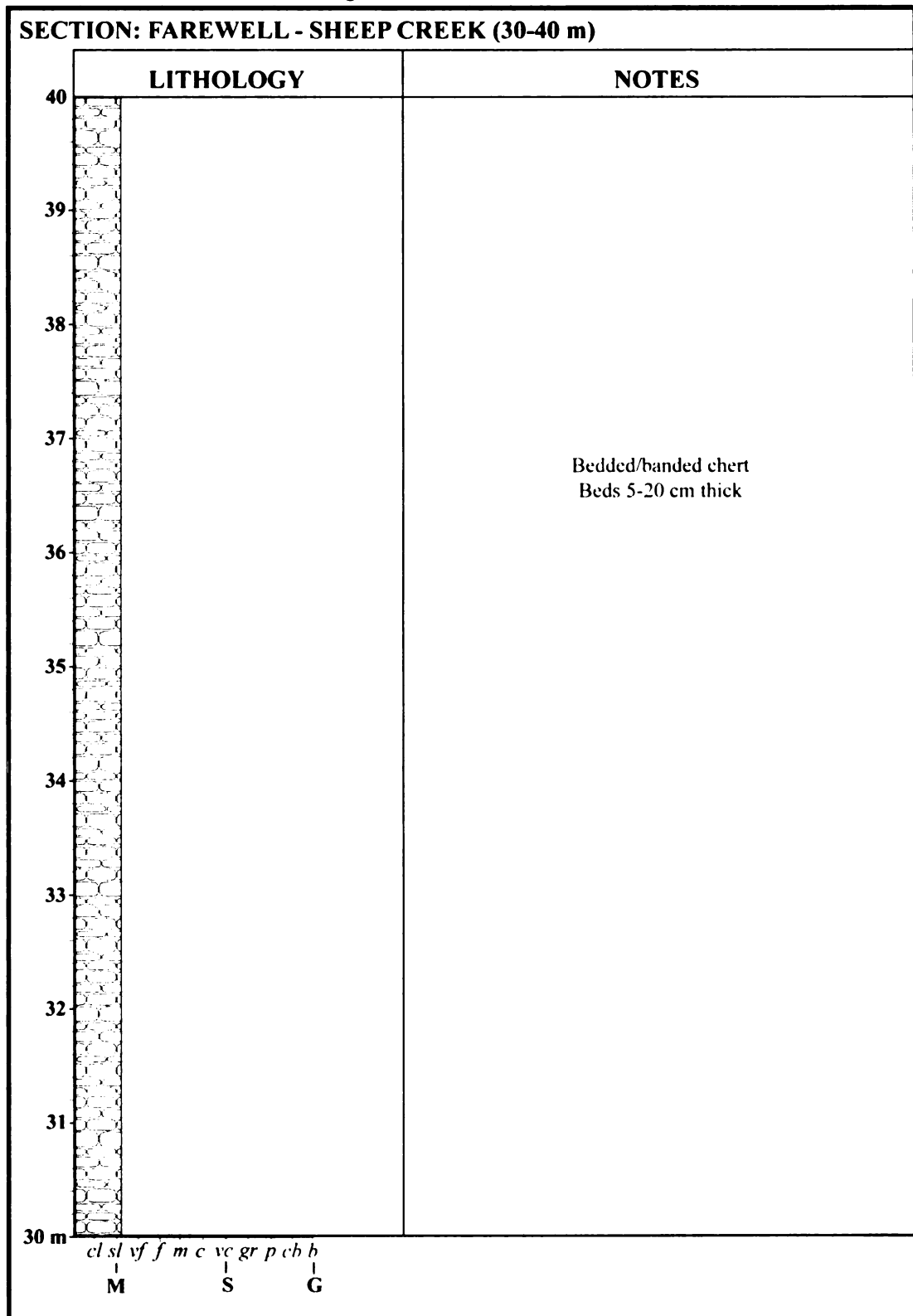


Figure F1 continued

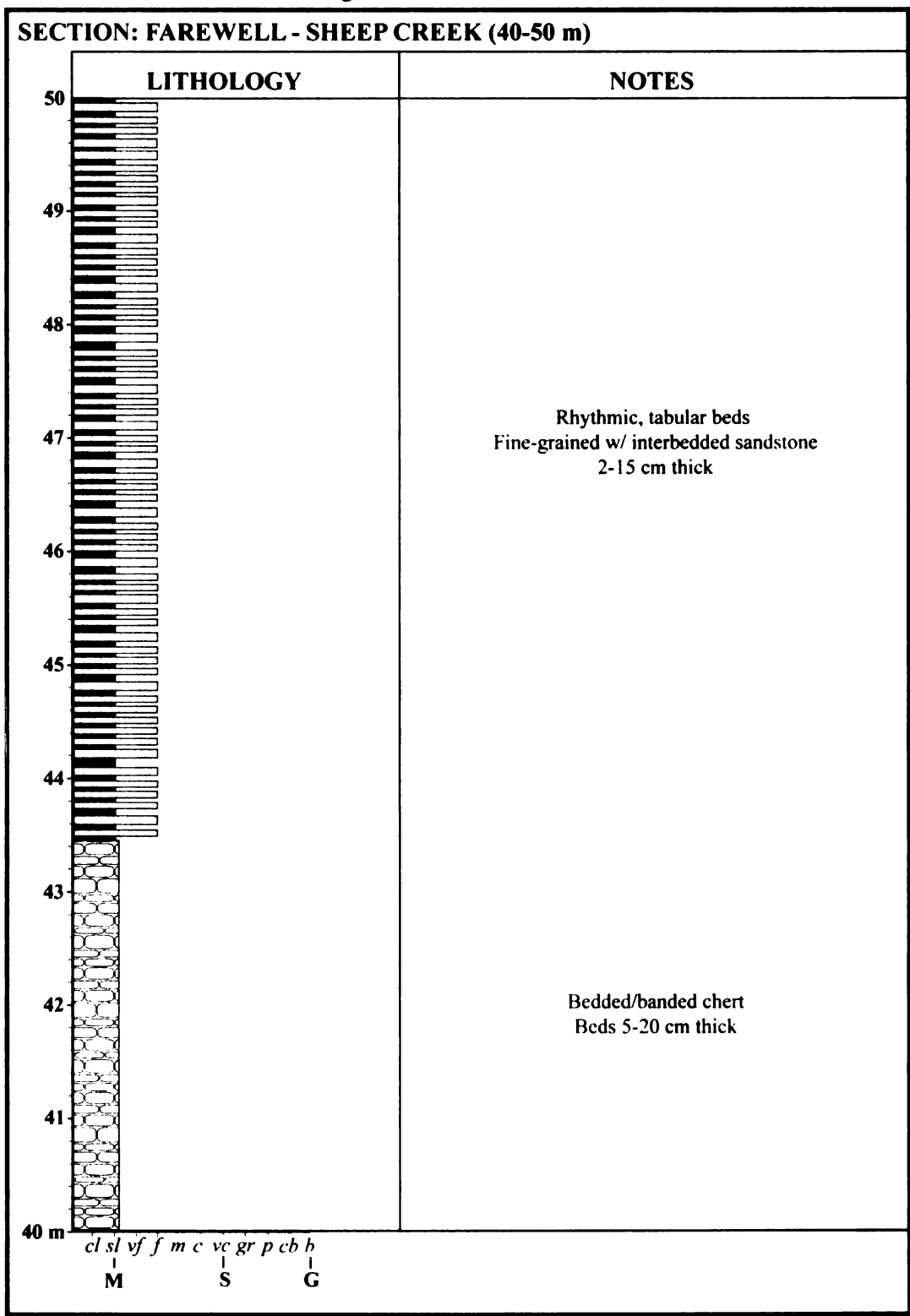


Figure F1 continued

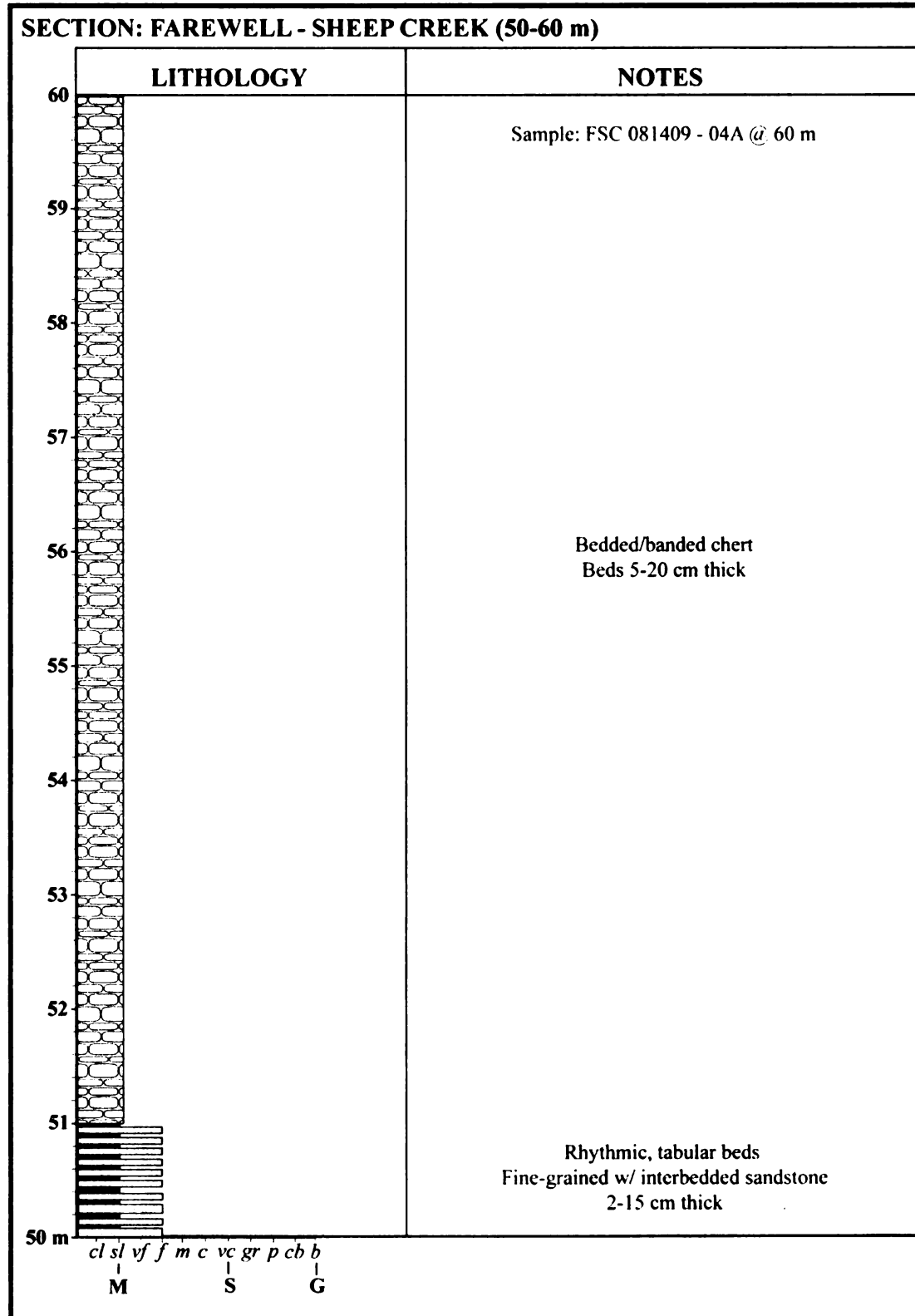


Figure F1 continued

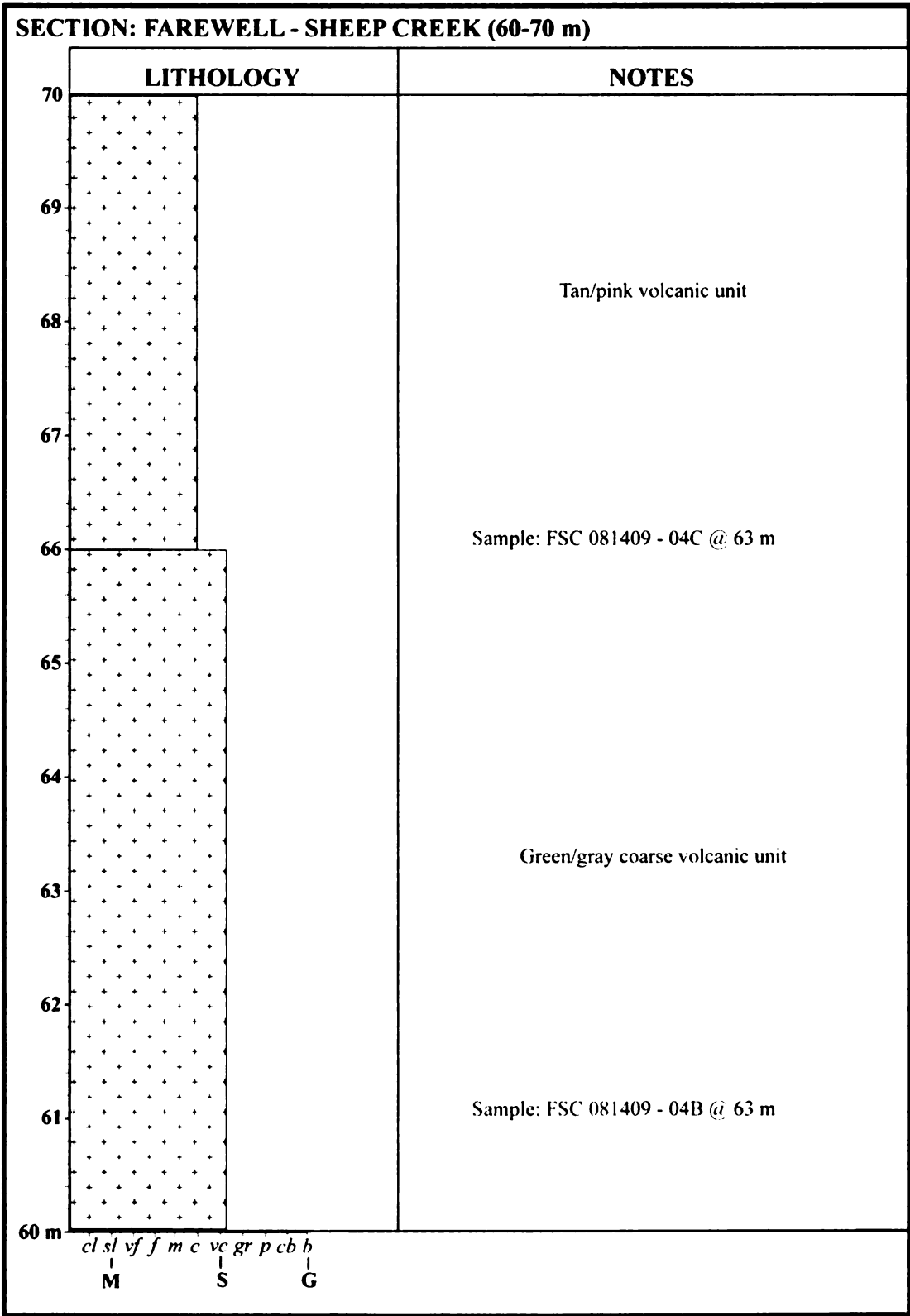


Figure F1 continued

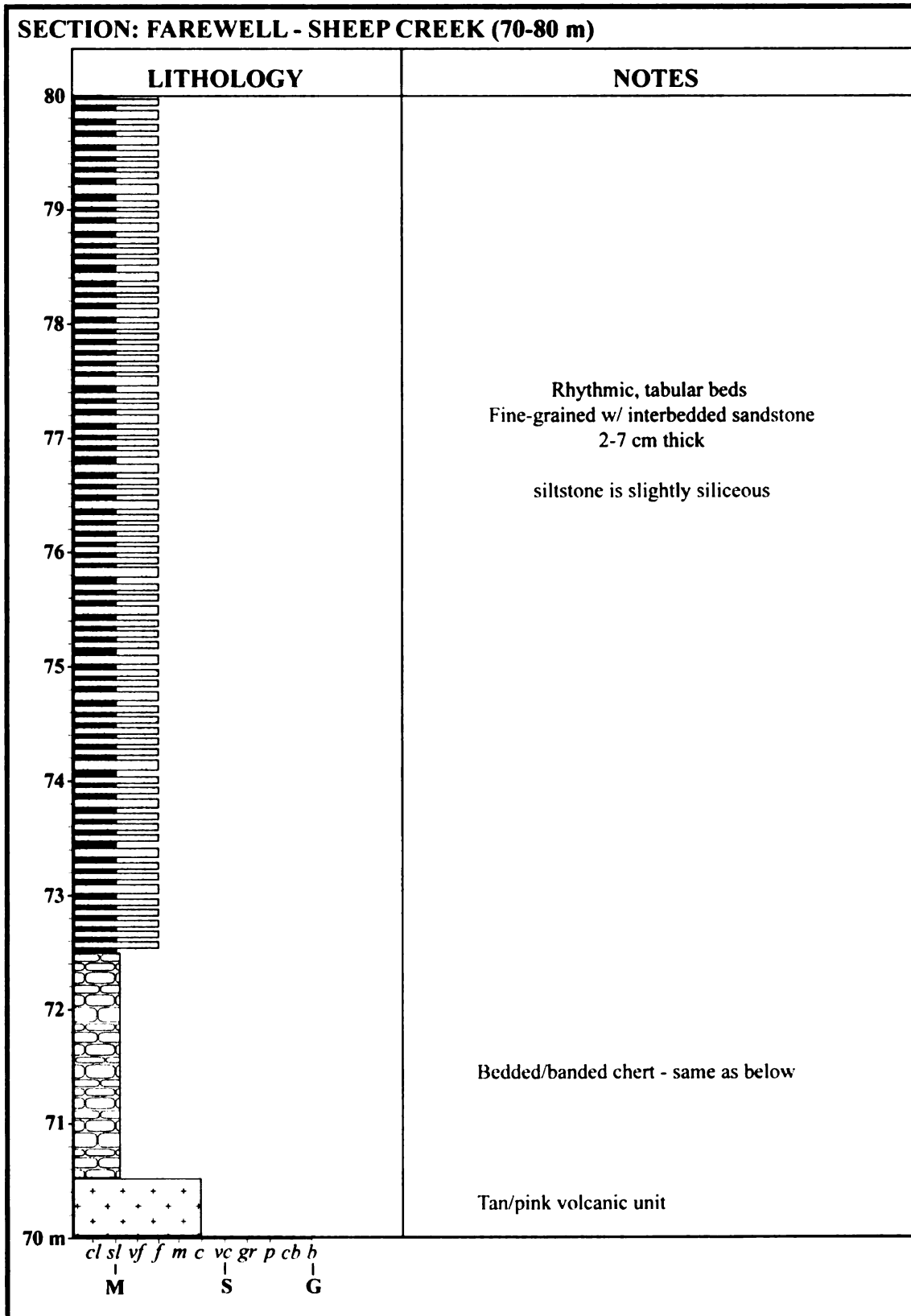


Figure F1 continued

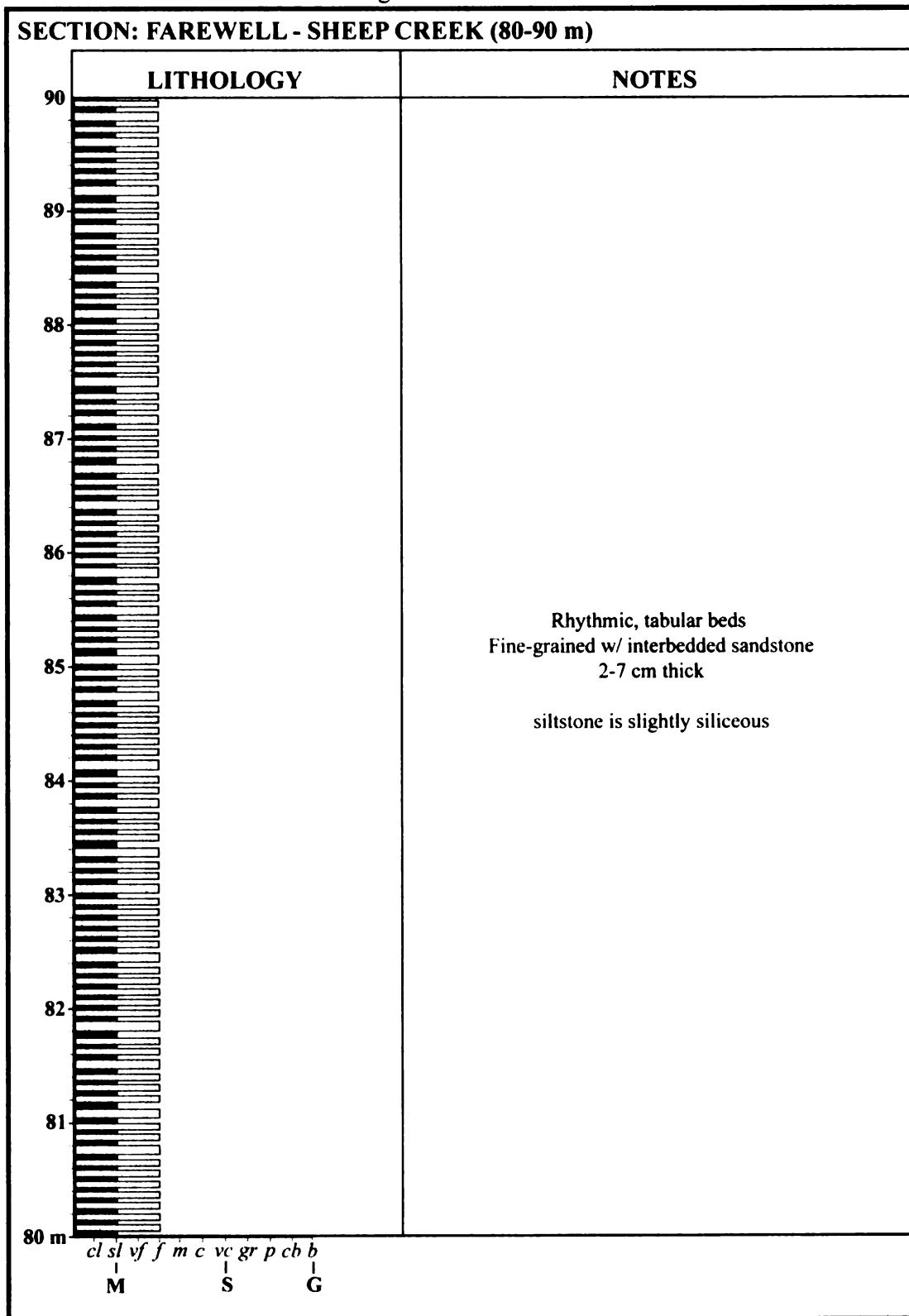
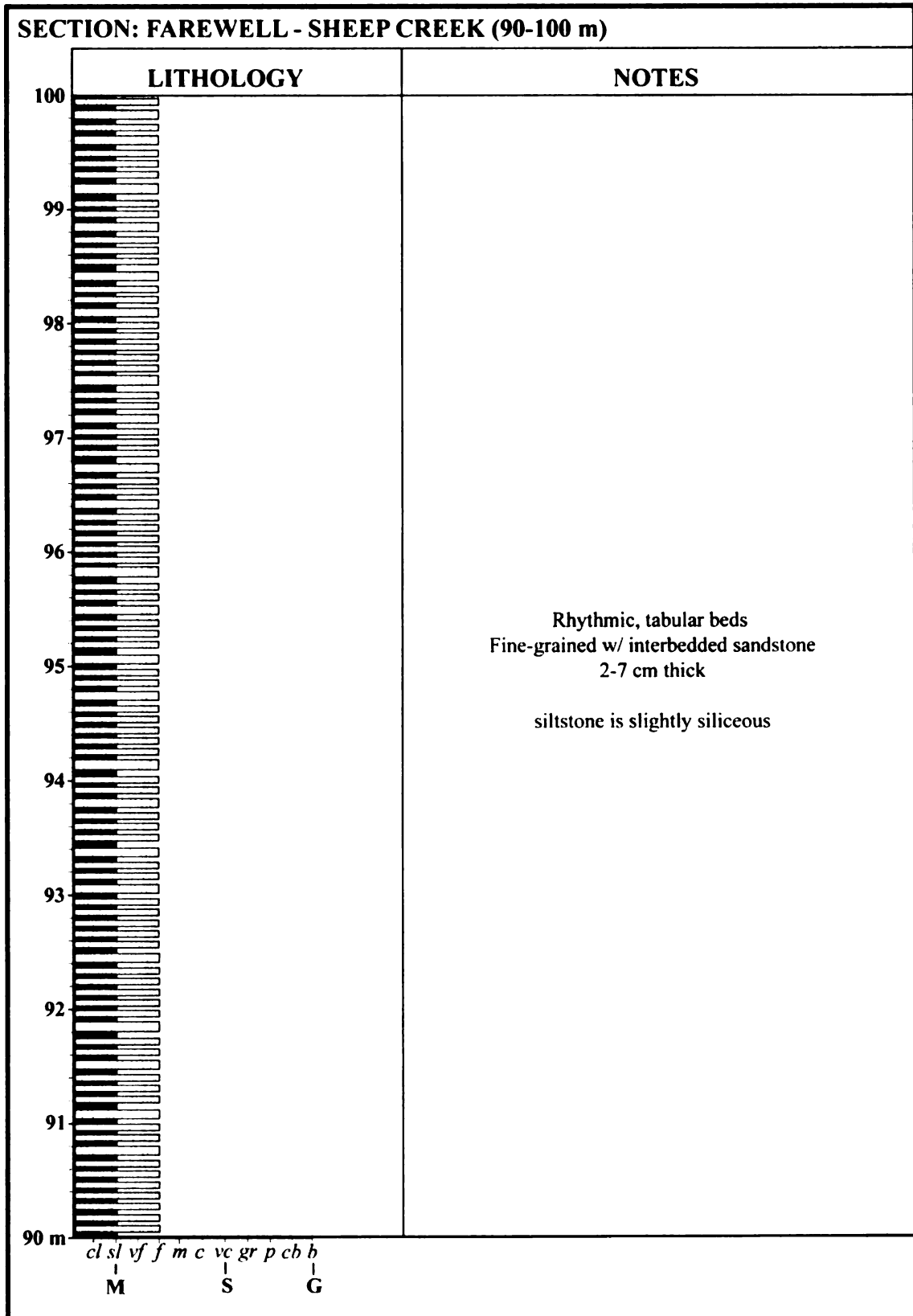


Figure F1 continued



**SECTION: FAREWELL - SHEEP CREEK (100-110 m)**

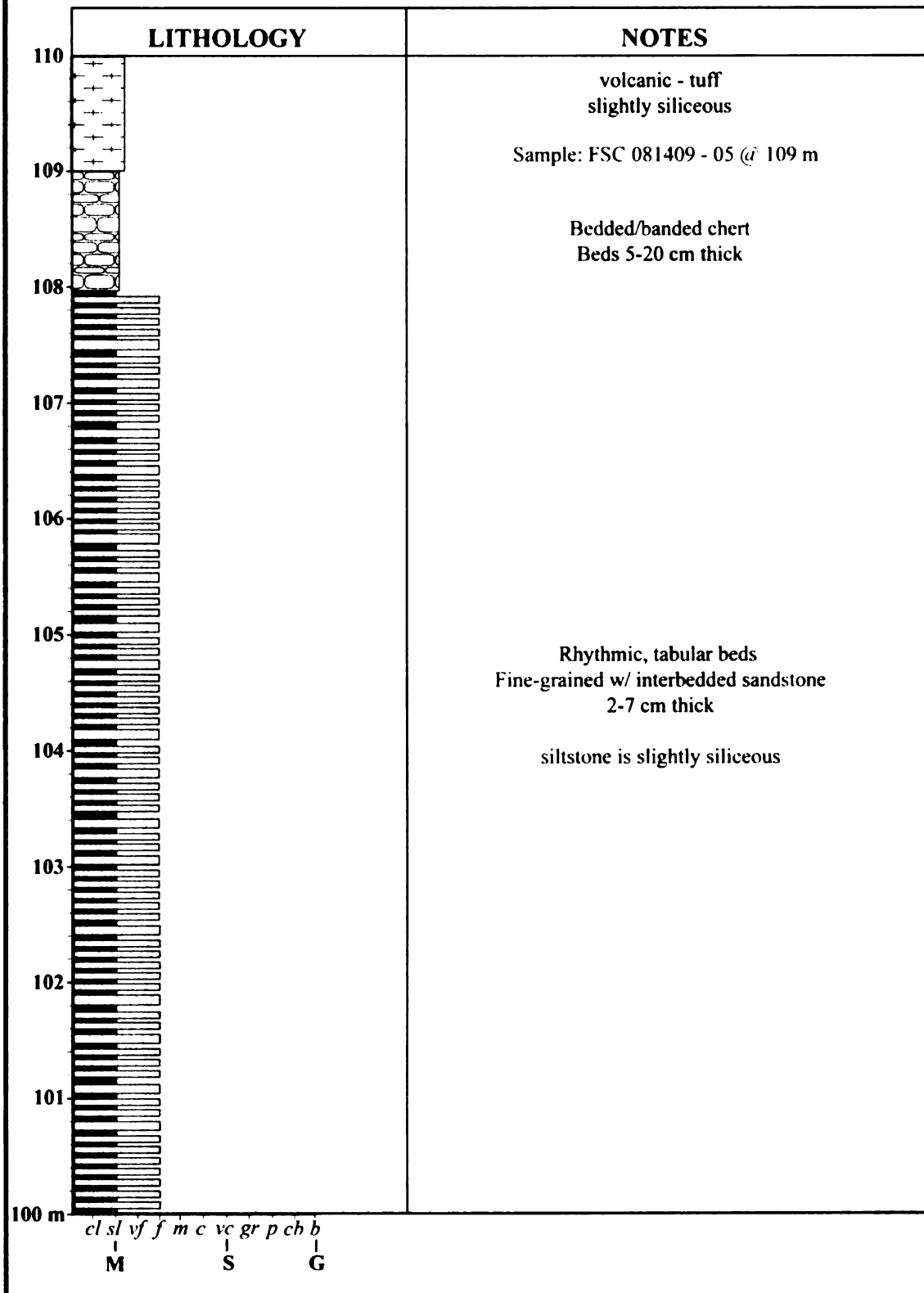




Figure F1 continued

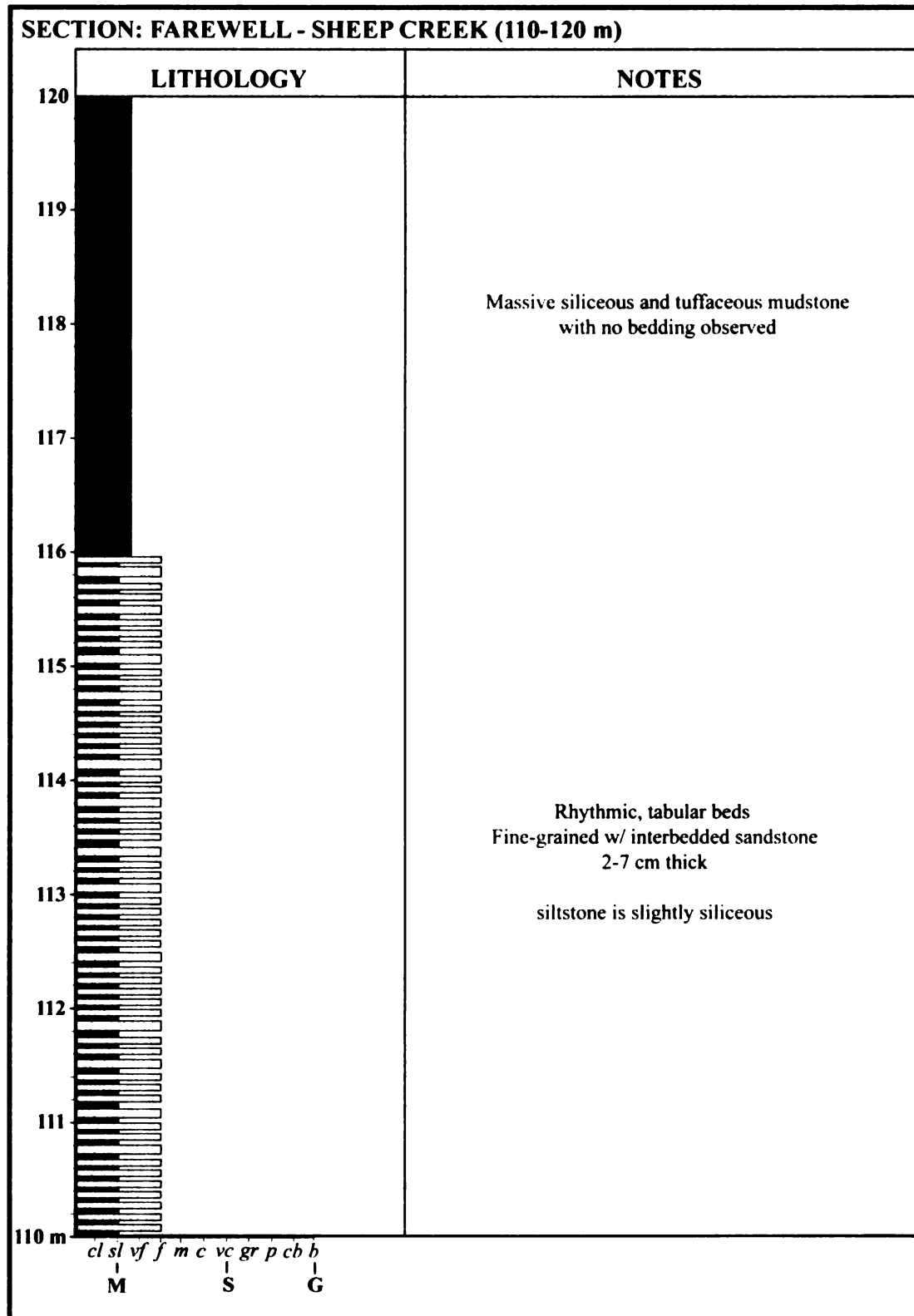


Figure F1 continued

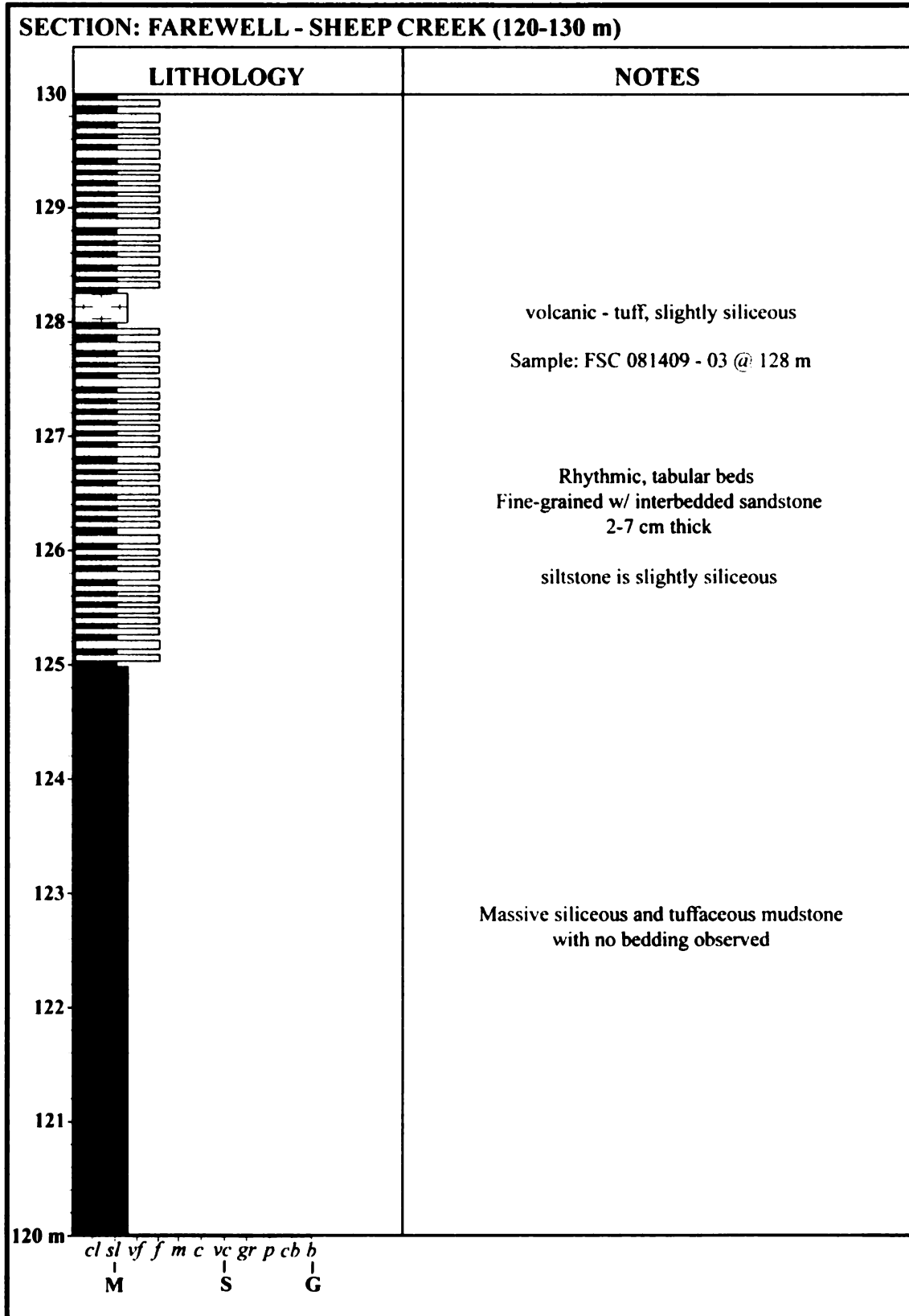


Figure F1 continued

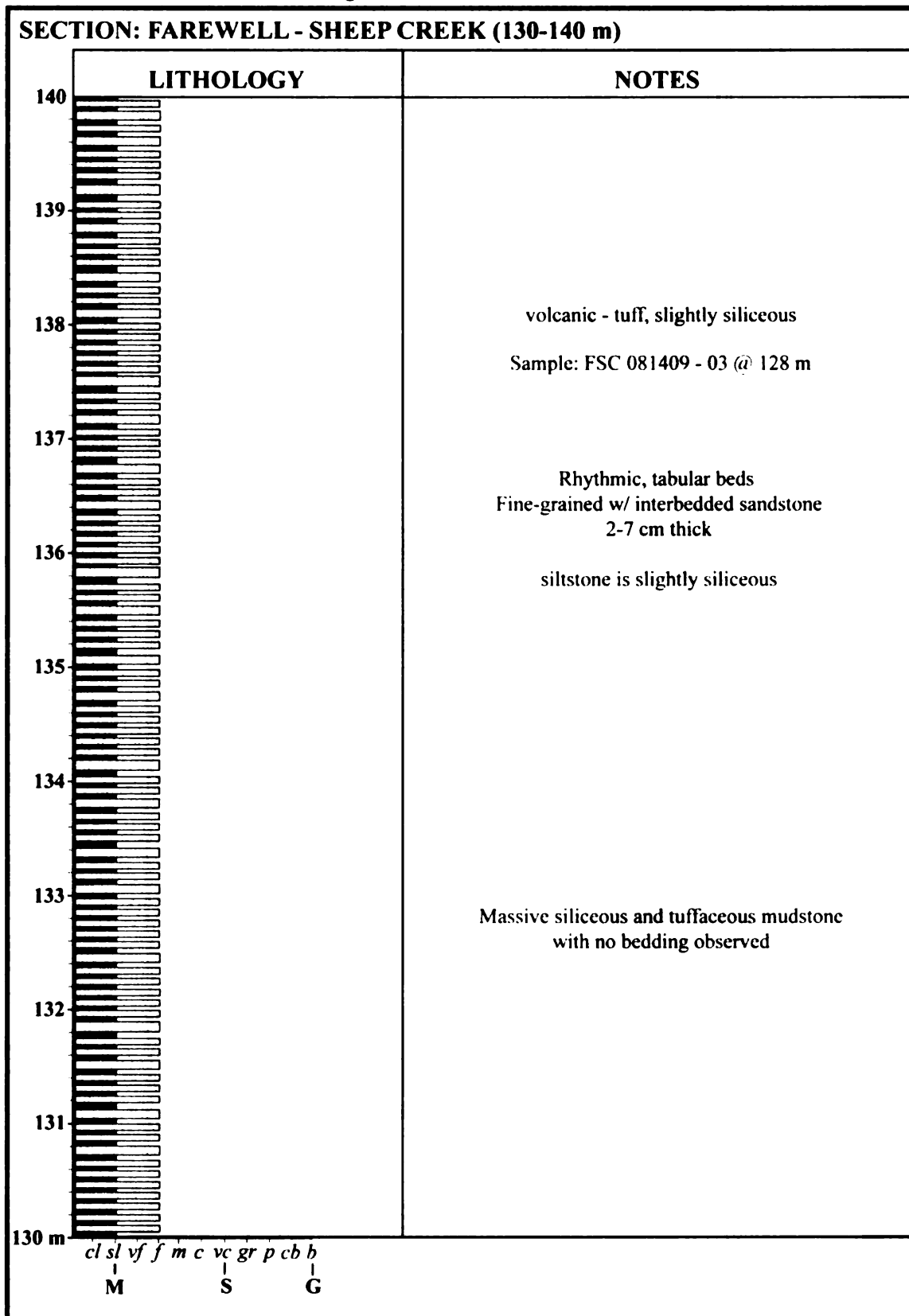


Figure F1 continued

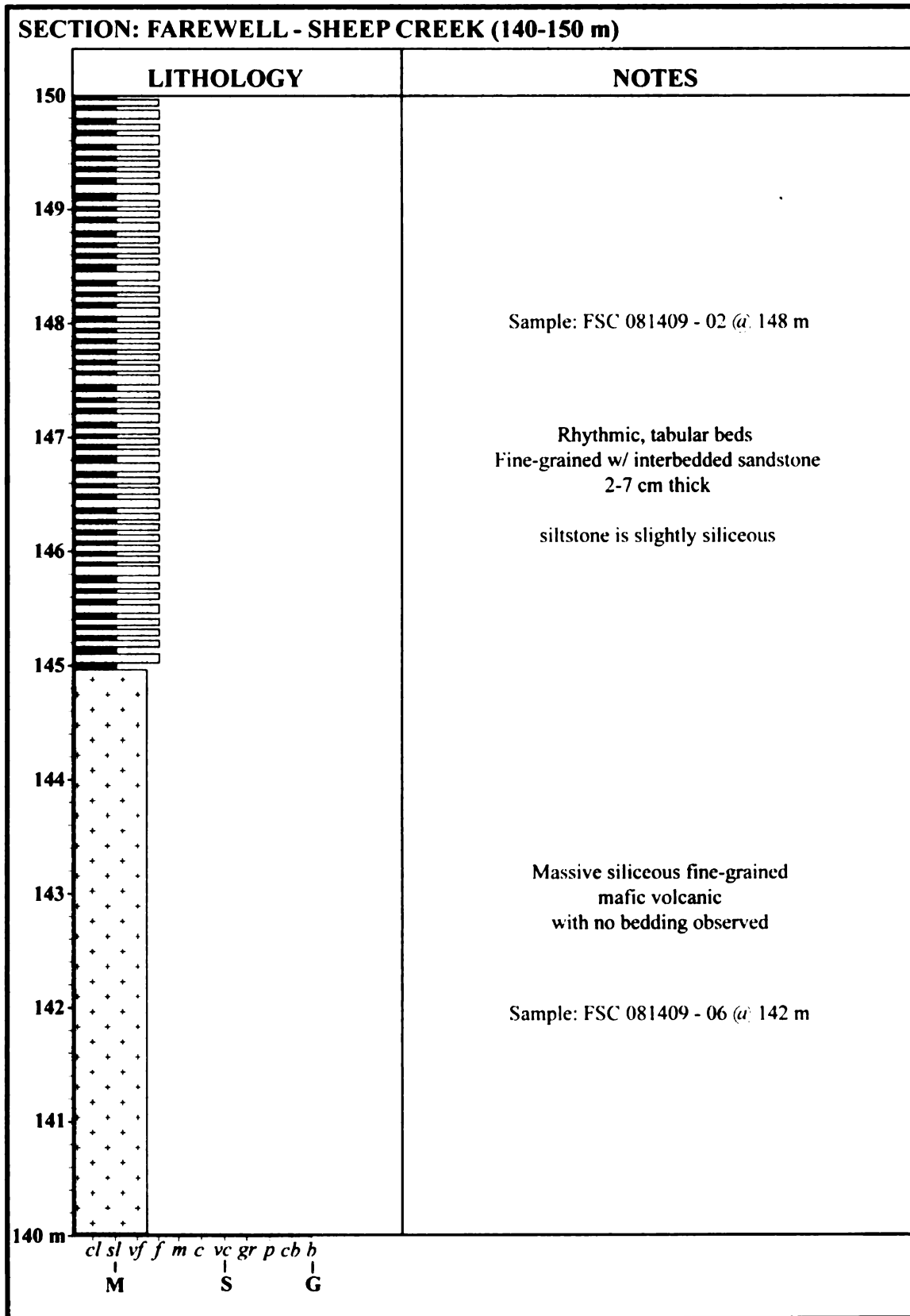
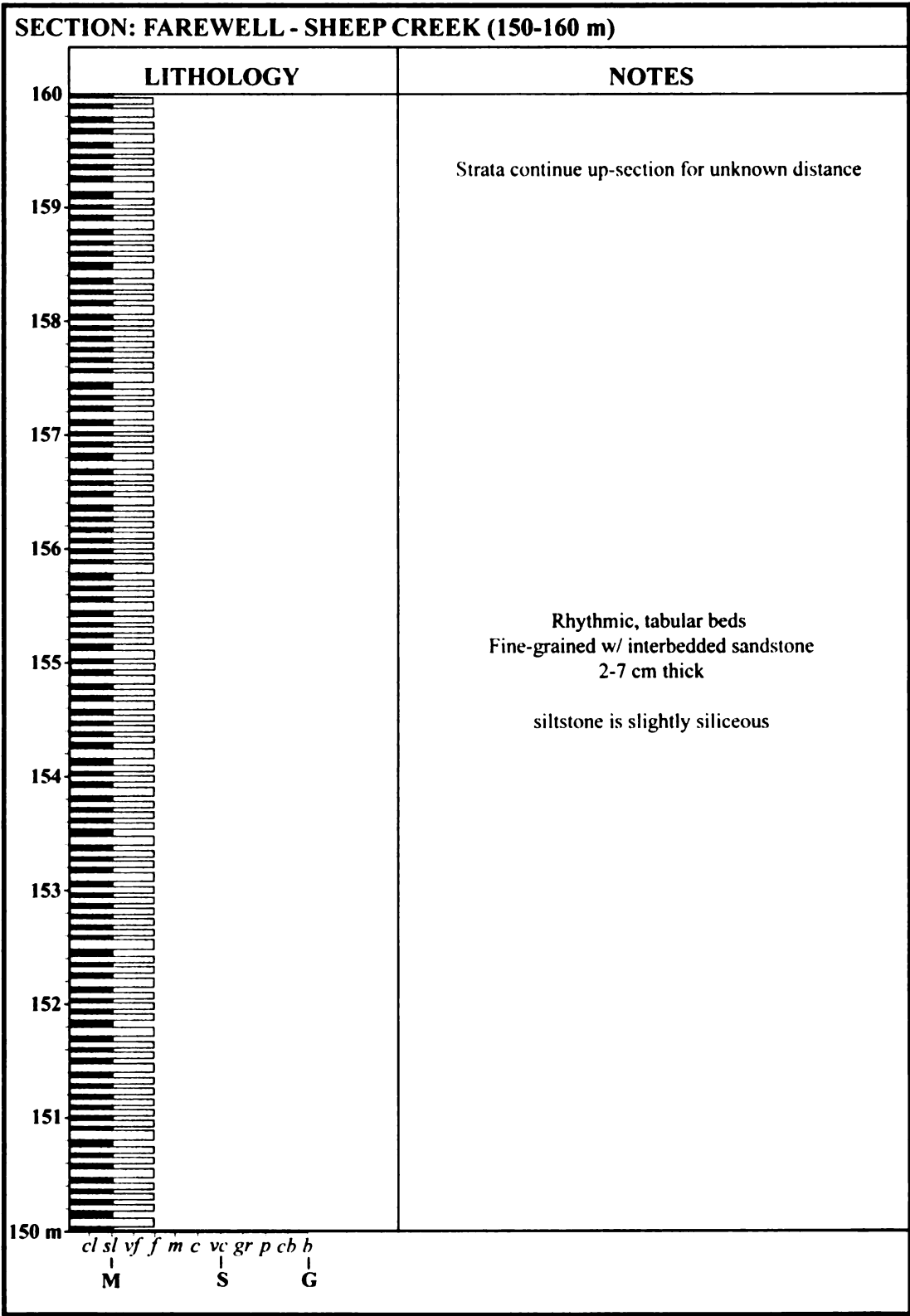


Figure F1 continued





MICHIGAN STATE UNIVERSITY LIBRARIES



3 1293 03063 7494